Cluster analysis of European surface ozone observations for evaluation of MACC reanalysis data

Olga Lyapina

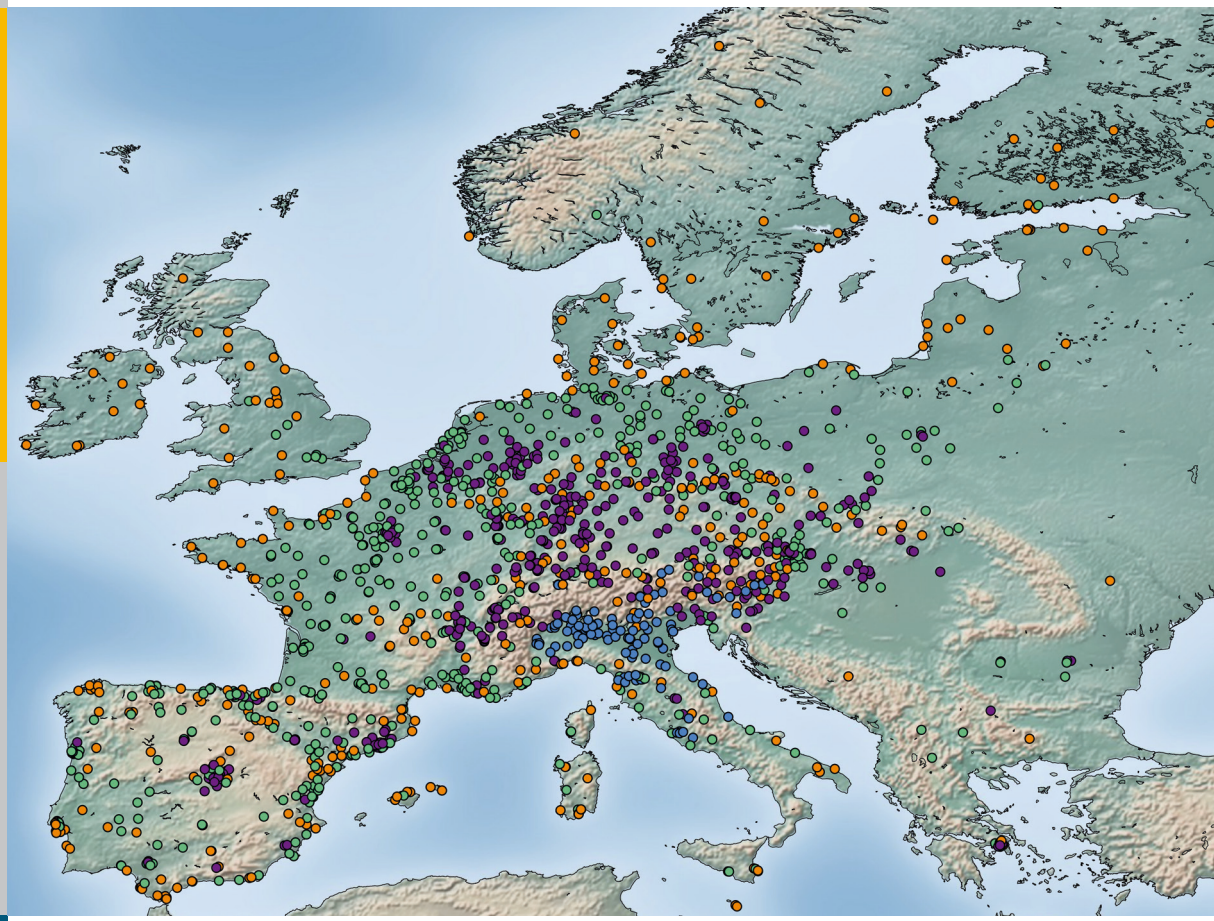

Energie & Umwelt / Energy & Environment
Band / Volume 265
ISBN 978-3-95806-060-9

JÜLICH
FORSCHUNGSZENTRUM

Schriften des Forschungszentrums Jülich
Reihe Energie & Umwelt / Energy & Environment Band / Volume 265

Forschungszentrum Jülich GmbH
Institute of Energy and Climate Research
Troposphere (IEK-8)

Cluster analysis of European surface ozone observations for evaluation of MACC reanalysis data

Olga Lyapina

Schriften des Forschungszentrums Jülich
Reihe Energie & Umwelt / Energy & Environment Band / Volume 265

ISSN 1866-1793 ISBN 978-3-95806-060-9

Bibliographic information published by the Deutsche Nationalbibliothek.
The Deutsche Nationalbibliothek lists this publication in the Deutsche Nationalbibliografie; detailed bibliographic data are available in the Internet at http://dnb.d-nb.de.

Publisher and Distributor: Forschungszentrum Jülich GmbH
Zentralbibliothek
52425 Jülich
Tel: +49 2461 61-5368
Fax: +49 2461 61-6103
Email: zb-publikation@fz-juelich.de
www.fz-juelich.de/zb

Cover Design: Grafische Medien, Forschungszentrum Jülich GmbH

Printer: Grafische Medien, Forschungszentrum Jülich GmbH

Schriften des Forschungszentrums Jülich
Reihe Energie & Umwelt / Energy & Environment, Band / Volume 265

D 5 (Diss., Bonn, Univ., 2014)

ISSN 1866-1793
ISBN 978-3-95806-060-9

The complete volume is freely available on the Internet on the Jülicher Open Access Server (JuSER) at www.fz-juelich.de/zb/openaccess.

Abstract

The high density of European surface ozone monitoring sites offers good opportunities for investigation of the regional ozone representativeness and for evaluation of chemistry climate models. In this thesis we analyze both aspects with close relation of one to another.

As starting point we analyze ozone trends and the seasonal behavior of ozone concentrations at selected individual stations in different regions of Europe. At this step we are interested to find out how the observed long-term trends in surface ozone concentrations are consistent across stations, and would the annual ozone behaviour give any distinctive patterns within Europe. The next analysis is extended to seasonal-diurnal ozone variations, which appear as the main components of ozone time series and therefore allow to describe the ozone behavior more comprehensively. The regional representativeness of European ozone measurements is investigated through a cluster analysis (CA) of ozone air quality data from 1492 European surface monitoring stations (Airbase database). K-means clustering is implemented for 3 sets of properties: (i) seasonal-diurnal variations in absolute mixing ratio units, (ii) normalized seasonal-diurnal variations, and (iii) averaged and normalized seasonal and diurnal variations. Each CA identifies different ozone pollution regimes, and each of them is compared with the output of the multi-year global reanalysis produced within the Monitoring of Atmospheric Composition and Climate (MACC) project.

Recent methods for evaluation of global chemistry-climate models often provide only the comparison of the simulated output mean to individual ozone observations or arbitrarily aggregated sets of observations. This can give general information about the model biases for area, captured by sites, but does not help in the interpretation of these biases.

Our CA approach yields useful information for the evaluation of numerical models, as it allows for a pre-selection of stations and uses clusters as means to stratify the comparison with the respective model output. Comparing the MACC data to cluster results allows to see whether the model is able to capture specifics of each group and how well it describes the various ozone pollution regimes.

The selected parameters for the investigation of ozone representativeness provide several possibilities to distinguish representative groups of ozone over Europe. Relying on the most stable conditions, there are 5 and 4 clusters which adequately describe the seasonal-diurnal ozone European patterns in case of absolute and normalized properties, respectively.

Comparison of the model with observations for individual clusters reveal first of all different overestimation biases, and secondly differences mainly in seasonal ozone behavior. These biases are mostly driven by summertime ozone rather than wintertime, where ozone is generally well predicted. Such biases decrease from more polluted clusters to cleaner ones. Also the seasonal and diurnal cycles are described better for clusters with relatively clean signatures. The best fit is observed for clusters, which stations are influenced more by regional rather than local factors. While

MACC is generally able to capture observed features of diurnal cycles (minima at 6 am and maxima between noon and 3pm), it fails in the description of different seasonal patterns, like spring maximum or July peak, as it always shows broad symmetrical bell-shaped summer maxima.

This thesis shows the usefulness of k-means clustering as an objective classification method for surface ozone measurements stations. Using clusters to preselect observational data for comparison with global models can broaden the observational data that are available for such comparisons and help to make model evaluation more objective.

Contents

CHAPTER 1

1 Introduction

1.1 Tropospheric ozone

Ozone is a molecule consisting of three oxygen atoms. In the atmosphere ozone is a "trace gas" and for the unpolluted troposphere is found in the range of 10-40 parts per billion (ppb) with somewhat higher mixing ratios in the upper troposphere. Ozone reaches a maximum mixing ratio of about 10 parts per million (ppm) in the tropical middle stratosphere (Seinfeld and Pandis, 2006).

The object of the present study is tropospheric ozone. It constitutes only 10% of the total atmospheric ozone, while the remaining 90% reside in the stratosphere and mainly in the altitude range between 20 and 30 km in the so called ozone layer (Seinfeld and Pandis, 2006). Stratospheric ozone has a protective function for life on Earth, absorbing hard UV light ($\lambda \approx$ 240-290 nm), and it exerts a slight cooling effect on the atmosphere (Figure 1.1).

Ozone acts as a strong oxidant, and therefore in the troposphere ozone is a harmful gas, affecting people's health and reducing yields of agricultural plants. It absorbs in the UV spectrum region (up to 340 nm) and partly in the infrared. The last property together with ozone historic evolution contributed to the global warming with positive radiative forcing. In Figure 1.1 the total contribution of ozone to the radiative forcing of the atmosphere in the year 2005 relative to the pre-industrial year 1750 is shown (IPCC, 2007).

Tropospheric ozone is a secondary gas, which is photo-chemically produced in the troposphere from natural and anthropogenic sources: carbon monoxide (CO), methane (CH_4), and non-methane volatile organic compounds (NMVOC), involving reactive nitrogen oxides ($NOx = NO + NO_2$) as catalysts (Logan, 1981; Seinfeld and Pandis, 2006). Ozone precursor concentrations are strongly influenced by anthropogenic activities and to a lesser extent by natural sources. Maximum ozone concentrations are therefore often found near large urban agglomerations during summer ozone pollution episodes (Table 1.1).

Table 1.1. Typical summer daily maximum O_3 concentrations (National Research Council, 1991).

Region	Ozone (ppb)
Urban-suburban	100-400
Rural	50-120
Remote tropical forest	20-40
Remote marine	20-40

However city centers themselves often show low ozone concentrations because of ozone titration by NO freshly emitted from public transport (Klemp et al., 2012) and other sources.

The tropospheric ozone budget is the sum of many processes determining the change in tropospheric ozone concentrations, i.e. photochemical reactions in the atmosphere, long-range transport, dry deposition and stratosphere-troposphere exchange. Photochemical production and destruction of ozone depends on the concentrations of the precursors in the air and on the local meteorological conditions (sunshine, wind). The effectiveness of the dry deposition sink depends not only on meteorological conditions but also on various soil and surface properties, for example vegetation type, leaf area, type of soil, etc. Ozone budget and its photochemical cycle will be considered in more detail in chapter "Theory", section 2.2 "Tropospheric ozone budget".

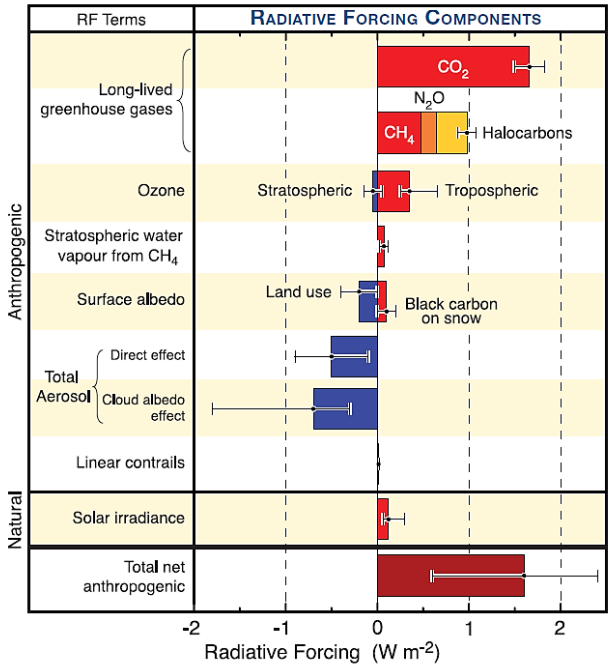

Figure 1.1. Global average radiative forcing (RF) values for the main atmospheric components in 2005 year relative to pre-industrial conditions defined at 1750 year (IPCC, 2007). RF is a measure of the influence on the radiative balance in the Earth-atmosphere system. Positive forcing has warming effect on climate, negative – cooling. RF is expressed in watts per square meter (W m^{-2}).

1.2 Historical ozone evolution and current situation

Among few recorded ozone evidences saved from the 19th century were the measurements from the mountain station Pic du Midi (PDM, 2877 m, French Pyrenees) and the Montsouris station, located now in Paris, and 100 years ago - to the South-West of Paris (1876-1910, 75 m). Their measurement

methods are described in chapter "Theory", section 2.3 "Ozone measurement methods and instruments".

Pic du Midi observations were done using the Schönbein paper method (Marenco et al., 1994). Among the disadvantages of that method were poor standardization, dependence on humidity, wind and exposure times.

The method used at Montsouris was iodine catalyzed oxidation of arsenit (period of measurements: 1876-1909). Uncertainty of the arsenite method is quite high: ± 25%, mainly because of interferences with other oxidants like H_2O_2 and SO_2, the last were obviously coming to Montsouris from Paris, so the data needed to be corrected. That was accomplished by Volz and Kley (1988), where only the sector of the SW-wind was chosen in order to avoid SO_2-influence. Uncertainty of the corrected ozone data at Montsouris is ± 2 ppb.

Old Montsouris and PDM records are shown in Figure 1.2 for the period before 1910. Taking into account uncertainties of mentioned methods one has to be very careful to assess a credible mean value for preindustrial surface ozone concentrations. Based on the extensive discussion in the literature about these historic data (Marenco et al., 1994; Volz and Kley, 1988; Staehelin et al., 1994), it appears that they fall in the range of 10-15 ppb.

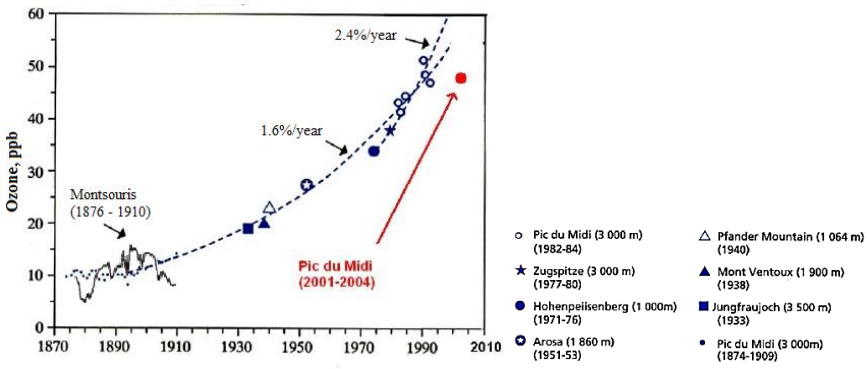

Figure 1.2. Ozone evolution in the free troposphere over Western Europe (Marenco et al., 1994), completed with annual mean ozone concentrations at Montsouris (1876 - 1910) (Volz and Kley, 1988) and mean mixing-ratio at Pic du Midi (PDM) between 2001 and 2004 by Chevalier et al. (2007).

Figure 1.2 also shows other ozone records from European mountain stations during the 20th century (Chevalier et al., 2007). The graph is completed by PDM data from the end of 20th century and beginning of 21st century. During this time PDM ozone concentrations grew from ≈ 10 ppb to ≈ 50 ppb in about 100 years. That fact can be related to the fast industrial growth with associated anthropogenic emissions, which contribute to the formation of tropospheric ozone: nitrogen oxides (NOx), carbon monoxide (CO), methane (CH_4) and non-methane volatile organic compounds (NMVOCs).

To sum up, historic ozone records from the end of the 19th century – beginning of 20th century (Marenco et al., 1994; Volz and Kley, 1988; Bojkov, 1986) typically show ozone concentrations between 10 and 20 ppb, whereas nowadays average surface ozone concentrations in Europe increased to 40-60 ppb (Staehelin et al., 1994; Chevalier et al., 2007; Tilmes et al., 2012). More about historical ozone measurements can be found in chapter "Theory" (section 2.3 "Ozone measurement methods and instruments"). Intensively initiated ozone research was related to the urban smog that appeared in Los Angeles in the middle of 20th century and was described in Haagen-Smit (1952).

The details of the historical evolution of tropospheric ozone concentrations are still unclear and current models fail to reproduce historic ozone trends (RETRO final report, 2007; Parrish et al., 2014; Lamarque et al., 2010). Since the late 1980s there were several European Union legislations regarding air quality, made with a purpose to restrict emissions, particularly ozone precursor gases, as well as to establish a European network of stations for measuring ozone and other species (more in chapter "Theory", section 2.1 "Air pollution control: policies"). On the global level for the period 1990 to 2000 for all components (NOx, CO and VOCs) industrialized regions like the USA and Europe show reductions in emissions, while regions dominated by developing countries show significant growth in emissions (IPCC, 2007; IPCC, 2013).

Tropospheric ozone started to be continuously monitored at few ground stations since the 1970s (for example, Alpine Zugspitze and Hohenpeissenberg). Many more stations appeared in the 1990s all over the world, but especially dense networks of stations were built in Europe and in the USA.

Over Europe surface ozone observations from Hohenpeissenberg, Zugspitze (Germany) and Mace Head (Ireland) show insignificant trends or reductions during summer, while there is an increase during winter (Oltmans et al., 2006). The same tendencies in summer and winter are observed for the German rural background stations during the period 1990-2011, as well as for more polluted (urban, traffic) sites for the same period (chapter "Results and Discussion", section 5.1 "Trend analysis", subsection 5.1.2 "German stations (1990-2011)").

This leads to more detailed investigation of ozone long-term evolution, which will be presented in chapter "Results and Discussion", section 5.1 "Trend analysis". It starts with the analysis of consistency of ozone trends on the Alpine sites Jungfraujoch (3580 m), Sonnblick (3105 m) and Zugspitze (2962 m). As they show similar ozone time series, and comparable ozone trends, it brings to the discussion of representativeness of ozone trends in Central Europe. Other sites from different European regions are included in this analysis to find out consistency of ozone trends across the chosen stations set. The topic of ozone representativeness is opened in the next section 1.3.1.

1.3 Motivation

1.3.1 Representativeness and stations categorization

Ozone concentration levels and variability at an individual station depend on different factors, which are mostly determined by:

1) vicinity to ozone precursor emission sources (anthropogenic: traffic, industries, cities, households, agricultural fields, and natural: biomass burning, forest fires, biogenic VOCs);

2) station altitude and topographic situation, which would determine how easily local emissions can reach the station as well as to what degree the station is exposed to the long range free tropospheric ozone transport;

3) geography of the station, which would imply local climate and meteorological effects (sunshine, vegetation periods, snow cover, wind, soil type, valley flow, land-sea breeze, etc.).

4) vertical air mass exchange, for example mountain-valley flow, mixing of boundary layer and free tropospheric air.

Different ozone stations are affected by these factors in more or less extent, which is reflected in their ozone concentration time series. Due to the variety and large number of European stations one needs to develop objective statistical methods for their classification and the characterization of their representativeness concerning the surrounding area.

Representative area is an area in which air quality has similar characteristics compared to the location of the monitoring station (Spangl et al., UBA report, 2007). Representativeness can also be applied to a network of stations. In that case, it refers to the extent to which the distribution of concentrations across the stations is representative of the concentration distribution in the territory to be covered by the network (Spangl et al., UBA report, 2007). Ozone time series contain several features (parameters), which can be taken for analysis of the representativeness. In this thesis we are mostly concentrating on the representativeness, related to a stations network.

This definition opens several questions, which we tried to answer in the present work. What kind of ozone parameters would divide Europe into representative regions? How to identify the representative regions? Would each representative set of stations characterize some particular continuous geographical area, or vice versa, can one territory be described by several ozone patterns regarding the chosen parameter? How large can the ozone representative areas in Europe be? How many stations would one need in order to obtain a “representative picture” of surface ozone concentrations in Europe? How similar can concentrations at neighboring stations be? Besides we were also interested to find out how the observed long-term trends in surface ozone concentrations are consistent across stations that share similar behaviour in recent years.

We started with the annual ozone trends and the seasonal behavior at selected individual stations in different regions of Europe. In this part of analysis we tried to answer questions: would it be possible to identify different European regions representative of ozone trends and/or of annual cycles? Would the Alpine mountain stations be representative of a general ozone trend in Europe?

If elevated and semi-elevated stations of background rural type are considered, trend similarities as well as consistency of mean annual variations are expected, particularly inside the Central European region. In reality there are many more European stations, which are influenced by local pollution to a greater extent. This is reflected in their time series. As the motivation is to distinguish different representative patterns, we decided to involve in our study all kinds of stations from all over Europe. This included three Alpine stations (Jungfraujoch, Sonnblick and Zugspitze) and several other stations (15 in total) as well as some stations from the German network of the regional air quality data (UBA).

At the next step we extended analysis of representativeness first of all to a larger set of stations, secondly taking seasonal-diurnal variations as the new parameters of representativeness. They appear as the main components of ozone time series and are therefore able to describe the ozone behavior more comprehensively (see section 3.2.2 “Properties for cluster analysis”).

Airbase database, the public regional air quality monitoring network of the European Environmental Agency (EEA) (http://acm.eionet.europa.eu/databases/airbase/; Guerreiro et al., EEA, 2012), provides a categorization of its stations based on the evaluation of the population distribution and emission sources in the proximity of the station. This scheme was given in the Council Decision 97/101/EC (EC Decision, 1997), which was revised and amended by Commission Decision 2001/752/EC (EC Decision, 2001), and finally modified by 2011/850/EU (EC Decision, 2011) as well as described in Mol et al. (2008).

Analysis of the population distribution distinguishes the station type between urban, suburban or rural, while the assessment of emission sources in the surrounding area divides sites into traffic, industrial or background. Such categorization has the disadvantage of being based on subjective assessments by the different station maintainers or regional agencies. Moreover the station information may become outdated, especially this concerns areas with changing anthropogenic environment: for example newly built industries, residential areas, roads or changes to forest areas. This transforms stations from the “background” to “urban”, which would impede objective ozone analysis. Thus, a static category label as given in Airbase may not provide an objective and reproducible classification for use in further statistical analyses.

Instead, this work is based on cluster analysis (CA) applied to the measurement data as a data driven classification of stations to stratify observations across more evenly connected properties.

The main goal at this point is to identify European air quality ozone regimes, when each of them is representative for some group of stations and corresponds to specific patterns of the ozone behavior typical inside the group.

CA has been applied previously to identify different ozone pollution regimes in various geographical regions. Depending on the aim of study, various choices of initial properties and of the clustering technique have been made – modeled daily 8 h ozone maxima: partitional CA (Jin et al., 2011), daily averages of CO, NO_2 and O_3: hierarchical CA (Pires et al., 2008) and percentiles of daily averages: hierarchical CA (Flemming et al., 2005), seasonal-diurnal ozone variations: hierarchical CA (Tarasova et al., 2007), the parameters describing area catchment in 12, 24 and 48 hours: hierarchical CA (Henne et al., 2010). Although Tarasova et al. (2007) already used cluster analysis for a comparison between measurements and model results, this study is the first to apply clustering techniques to quantitatively evaluate a model simulation and identify features in the observational record that can be reproduced by the model.

1.3.2 Model evaluation

A second motivation of present work is related to the evaluation of global chemistry-climate model. Airbase data have not been used frequently in scientific analyses of coarse-scale global model results. Some recent works perform assessment of regional models and their improvement (Solazzo et al., 2012; Nopmongcol et al., 2012; Mailler et al., 2013; Coman et al., 2012; Agudelo et al., 2011). The last one uses ozone measurements from ≈ 30 ground-based Airbase stations of Belgium, Luxembourg, and some small parts of Germany, France and the Netherlands. Data are taken for comparison and improvement of the ozone estimations of the air quality model AURORA, which simulates air pollution in the lower troposphere at urban or regional scale.

Solazzo et al. (2012) and Nopmongcol et al. (2012) have evaluated a regional model or an ensemble of regional models from the Air Quality Model Evaluation International Initiative (AQMEII). They compared model output with the data from European Airbase and North American stations (1400-1500 sites in total). Thunis et al. (2013) proposed performance criteria to evaluate air quality models for O_3 based on measurement uncertainty.

Solberg et al. (EEA, 2009) analyzed Airbase ozone trends during 1995-2005 for European countries and compared them to trends from the EMEP model. Joly and Peuch (2012) explored Linear Discriminant Analysis based on 8 indicators of diurnal cycle and weekend effect for classifying Airbase stations.

Cluster analysis, as described before, is a numerical approach for stations classification, and it may have useful application for model evaluation, helping to test model results on a more physical-chemical basis.

There are studies which provide comparison of several global models and observations, based on the means of several locations (van Loon et al., 2007; Fiore et al., 2009; Stevenson et al., 2006). In Figure 1.3 the model ensemble O_3 mean for year 2000 is compared with ozonesonde observations, taken from Logan (1999), which are located mainly in northern midlatitudes over continental North America, Europe, and Japan. Some of the models generally fit to the band inside standard deviation of observations, but there are also many discrepancies in winter and spring time. The differences between ozone regimes of locations are unknown and somehow hidden behind ozone averages, because the observational cycle as well as each model cycle are the means of 17 sites from the band 30N-90N. Therefore such results are good to establish general biases of models for the area captured by sites, but they will not show how well models predict particular ozone behavior.

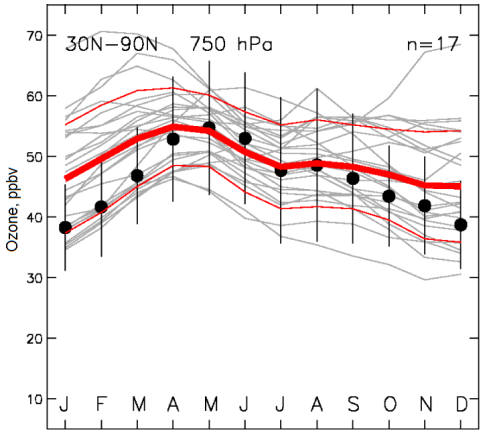

Figure 1.3. Comparison of the annual cycles of ozone observations (black dots with indicated average of the interannual standard deviations at each station) and model ensemble mean (thick red line), sampled for the band 30N-90N and pressure level 750hPa. The gray lines are the results for each model. The thin red lines are the standard deviation of the 26 model ensemble. The panel shows the mean of 17 sites (Stevenson et al., 2006).

Numerical models of atmospheric transport and chemistry (CTMs) have become indispensable tools for the interpretation of measurement data, the analysis of sensitivities towards, for example, emission changes, and the evaluation of potential future air quality changes in the context of climate change. Since 2005, a major European effort is under way to establish an operational system for monitoring and predicting global and European air quality with the help of data assimilation and numerical models (Hollingsworth et al., 2008). This is currently organized in the framework of the Monitoring Atmospheric Composition and Climate (MACC) project (http://www.copernicus-atmosphere.eu/). Evaluation of such models with observational data is crucial in order to detect and remedy errors and to give them credibility for the prediction of future changes. Two related aspects of model-data comparisons can be identified. First, one needs to find out which stations are

representative for the scale of the model, and second, patterns in the observational data should be identified which the models can be expected to reproduce.

In the present work the model data were taken from the MACC reanalysis (Inness et al., 2013). The reanalysis invoked data assimilation of meteorological variables, and trace gas columns of O_3, CO, NO and NO_2 as well as ozone profile information from various satellite instruments. The model system was the European Centre for Medium Range Weather Forecasts (ECMWF) Integrated Forecasting System which was coupled to the Model for Ozone and Related Tracers (MOZART) (Flemming et al., 2009; Stein et al., 2012).

Returning back to the model evaluation, we suggest to test the model output for each of the groups obtained in the CA. Each cluster would be distinguished by some specific ozone features and contain stations with similar ozone regimes. Moreover the mean of each cluster can be representative for all stations, so to evaluate model output on such clusters, or on means of each cluster, is making more sense than to test model on the mean of the complete set of stations with different pollution signatures. Our method allows to see whether the model is able to catch specifics of each group and describe different ozone pollution regimes.

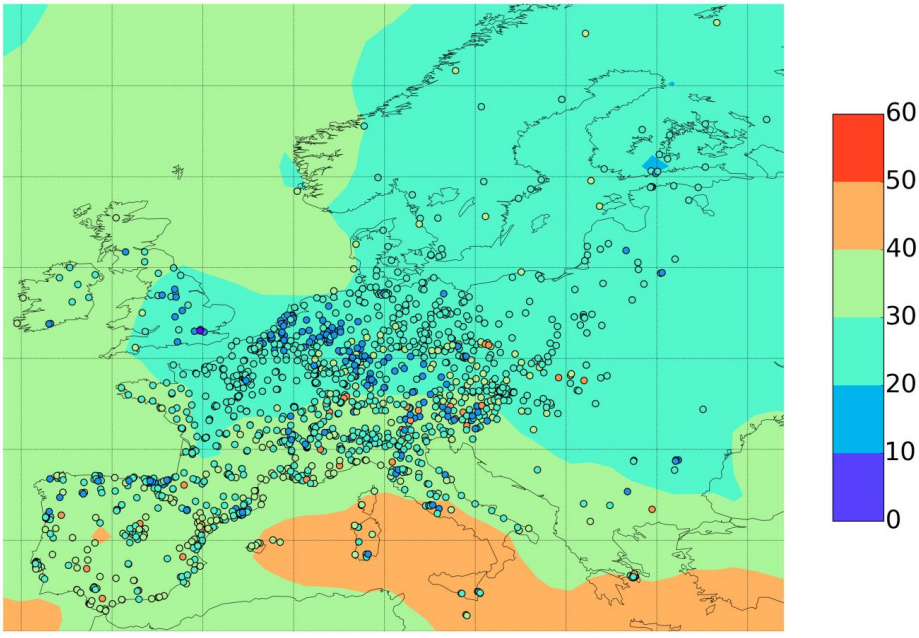

Figure 1.4. Mean MACC and Airbase ozone mixing ratios from reanalysis (1492 locations) for the period 2007 – 2010 (nmol/mol).

If we consider only averages, then it becomes clear that the MACC model predicts ozone unevenly over Europe (Figure 1.4). For the comparison of ozone averages across 2007-2010 period of time the MACC data were extracted from one model level for all grids (59th, approximately 35 m altitude above ground – see MACC description in section 3.3 "MACC model data"). But for the CA as will be said in section 3.3 the MACC data were extracted from pressure levels, corresponding to station altitudes. Therefore the comparison above is not objective, but it fits for a general overview of Airbase and MACC ozone means.

The ozone means of many stations are not predicted by model. The model divides European ozone into Northern part, where the concentrations are lower, and Southern and Mediterranean region, where ozone means are higher. But for Airbase stations the tendency is not the same. On the first look, some areas are already distinguishable by ozone means, for example, Benelux area and Alpine region. CA of ozone stations would help to preselect data and conduct a reasonable model evaluation on obtained groups.

1.4 Objectives of present work

In present work at first we analyze the seasonal and annual ozone trends for individual European stations within the period 1990-2011. For this purpose the 3 Alpine sites Jungfraujoch, Sonnblick and Zugspitze and several selected stations from all over Europe are considered. Then we investigate mean annual ozone variations for these stations for the period 1998-2011. Trend analysis and the differences observed in the annual cycles obtained for different European regions lead to a more thorough analysis of the ozone representativeness.

The regional representativeness of European ozone is investigated through the CA of ozone air quality data. We apply CA to achieve an objective numerical classification of surface ozone measurement sites. Resulting clusters are compared with the output of the multi-year global reanalysis produced within the Monitoring of Atmospheric Composition and Climate (MACC) project (Inness et al., 2013).

To reach this aim ozone records were taken from the AirBase database (http://acm.eionet.europa.eu/databases/airbase/), which contains ozone data for more than 2500 stations of about 35 European countries. It partly covers European Monitoring and Evaluation Program (EMEP) data as well (http://www.emep.int/). The majority of the EMEP as well as Airbase stations are so-called "background" sites, therefore these data should be applicable for evaluation of chemistry transport models at regional and global scales.

Seasonal - diurnal ozone variations were used as the initial parameters for the CA. They appear as typical cycles and represent the ozone concentrations resulting from many factors influencing the particular stations (see section 3.2.2 "Properties for cluster analysis").

We prepared three different sets of input data for the CAs. At first, seasonal - diurnal ozone variations in absolute values are used as a set of properties. Afterwards we apply normalized seasonal - diurnal ozone variations in order to avoid the influence of actual ozone concentrations on the results. This second CA produces different clusters than the first step, but allocates stations to clusters being based on seasonal and diurnal variations themselves regardless of absolute concentrations. The third CA uses normalized seasonal and diurnal cycles, obtained after averaging over 2007-2010 seasonal and diurnal variations respectively.

Output ozone data from the MACC reanalysis (Inness et al., 2013) were sampled at the station locations and evaluated using the same cluster aggregation.

CHAPTER 2

2 Theory

2.1 Air pollution control: policies

The health impact of ozone was the primary reason instigating increased ozone research in the 1960s. Ozone influence on humans depends on the ozone concentration and personal resistance related to health, asthmatic precondition, age, etc. The impact varies from minor respiratory symptoms to severe lung inflammation (Kim et al., 2013).

Much of ozone research was initiated in the US around the 1960s, whereas Europe built a strong "Tropospheric Ozone Research" (TOR) program in the 1980s (Midgley and Reuther, EUROTRAC-2, 2003). After initial regulative attempts on the state or national level, various legislations were introduced under the auspices of European Union policies since the late 1980s (Uekötter, 2003).

EU policies were mainly directed to coordinate an EU strategy through the long-term air quality objectives and measures of air pollutants abatement. There are 2 main directions of those policies: one is establishing limits for emissions of four key air pollutants (nitrogen oxides, sulphur dioxide, non-methane volatile organic compounds and ammonia) from specific sources like industries and transport, and another concerns EU air quality in general and establishes health-based concentration standards and exposure limits for a number of air pollutants.

The first direction imposed limitations of air pollutants emissions and started in 1979 from the UNECE Convention on Long-range Transboundary Air Pollution (LRTAP) (http://www.unece.org/env/lrtap/lrtap_h1.html). This UNECE Convention was extended by eight protocols (1984-1999), each of them related to different pollutants. Among them are *the 1988 Protocol concerning the Control of Nitrogen Oxides*, *the 1991 Protocol concerning the Control of Emissions of Volatile Organic Compounds* and *the 1999 Protocol to Abate Acidification, Eutrophication and Ground-level Ozone*.

Under the LRTAP Convention it was decided to establish a broad scientific co-operation on the reduction of pollution impact. The European Monitoring and Evaluation Program (EMEP) was one of these programs and was assigned to report about emission data (http://www.emep.int/).

The "Exchange of Information Decision" (EoI) was introduced in Council Decision 97/101/EC (EC Decision, 1997). EoI describes the procedures of exchange of information and data from networks and individual air quality monitoring stations within the EU Member States and the public. Since that time all the information from EoI were uploaded to the Airbase database (mentioned in the "Introduction"). The most recent development in this respect is the introduction of electronic data exchange ("e-reporting") as set forward in directives 2004/107/EC (EC Directive, 2004) and

2008/50/EC (EC Directive, 2008). The most recent air quality legislation was made by EU in the Directive 2008/50/EC (EC Directive, 2008), which has merged previous existing legislations (http://www.eionet.europa.eu/aqportal) (see Table 2.1).

Table 2.1. Information on ozone target values, thresholds and long-term objectives (EC Directive, 2008).

	Averaging period	Concentration
Target value for the protection of human health	Maximum daily 8-hour mean	120 μg/m³ not to be exceeded on more than 25 days per year averaged over 3 years (for 2010)
Target value for the protection of vegetation	AOT40*, calculated from 1 h values from May to July	18 000 μg/m³·h averaged over 5 years
Long-term objective for the protection of human health	Maximum daily 8-hour mean within a calendar year	120 μg/m³
Long-term objective for the protection of vegetation	AOT40, calculated from 1 h values from May to July	6 000 μg/m³·h
Information threshold	1 hour average	180 μg/m³
Alert threshold	1 hour average	240 μg/m³

*AOT40 (expressed in (μg/m^3·hours) is calculated by formula $\sum$ ([O_3]-x) t, where t – time, x – a threshold concentration = 80μg/m^3 (40 parts per billion), [O_3] – ozone concentrations above the threshold x. Sum of differences is calculated over a given time period.

According to EC Directive (2008) measurement of ozone precursor substances must include at least nitrogen oxides, and appropriate volatile organic compounds (VOC). An alert threshold for ozone was established as 240 μg/m^3 (averaged over 1 hour). This indicates a level beyond which there is an acute risk to human health from brief exposure. The somewhat lower information threshold is a concentration level beyond which there is a risk to the health of particularly sensitive sections of the population from brief exposure. Target values and long-term objectives are fixed for reducing harmful effects on human health and the environment, to be achieved over a given period. The target value which countries are expected to fulfill by 2010 is defined as the maximum daily 8 hour ozone mean value of 120 μg/m^3. This threshold should not be exceeded on more than 25 days per calendar year averaged over three years. Limit values were also established for the ozone precursors such as nitrogen dioxide, carbon monoxide and some volatile organic compounds.

Figure 2.1 illustrates percentages of German stations that have exceeded or met the target value since 1995. During the past decade, only those 3-year periods, which include the high-pollution year of 2003, are standing out with nearly 60% of stations exceeding the target value. In the most recent period 2010-2012 that was characterized by low ozone pollution, 10 percent of the stations still exceed the target value for the protection of human health (Figure 2.1) **(**Air quality 2012, UBA, 2013**)**.

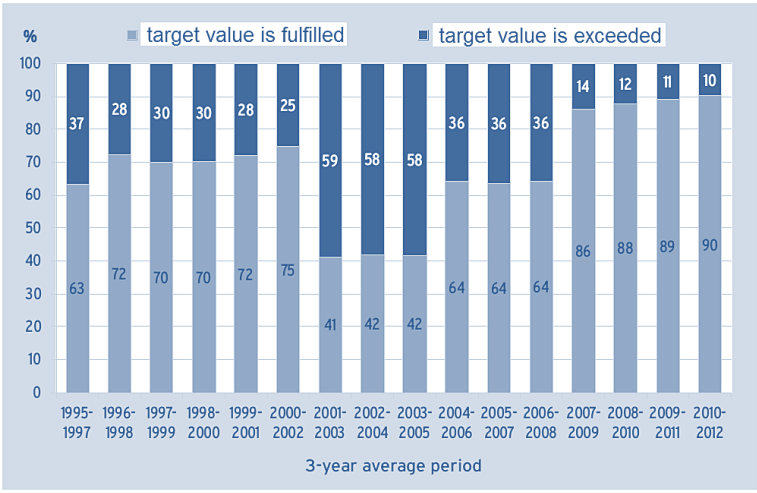

Figure 2.1. Percentage of German ozone measuring stations that have exceeded or met the target value since 1995 (3-year averages) **(**Air quality 2012, UBA, 2013**)**.

2.2 Tropospheric ozone budget

The ozone concentration measured at a certain location and specific point in time results from a multitude of processes that regulate ozone formation, transport and loss (Figure 2.2).

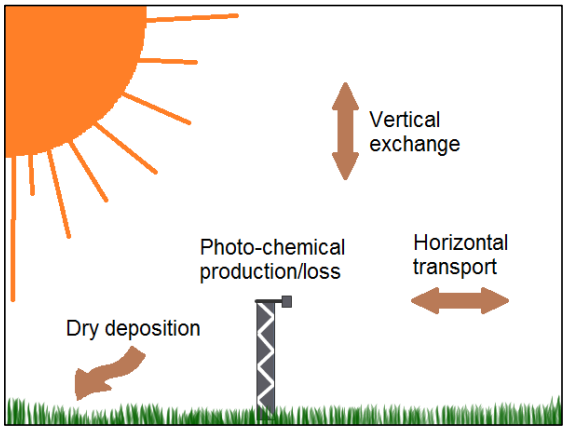

Figure 2.2. Schematic drawing of processes comprising the total ozone local budget.

Ozone production is occurring due to photochemical reactions in the troposphere in presence of anthropogenic and/or natural emissions, but ozone can also be advected to the measurement location from other areas (horizontal transport), and it can be influenced by vertical transport of air masses. Example of the vertical exchange on the global scale is stratosphere-troposphere exchange or STE,

which will be described in following subsection 2.2.2. In present work ozone measurements from ground stations are considered, therefore they are influenced by local scale vertical transport such as mountain-valley flows, mixing of boundary layer and free tropospheric air, inversion blockings (meaning no transport), convective transport, and boundary layer turbulence.

Mountain-valley air mass transport happens on a daily basis. During the night cool air flows down from the mountain into the valley while during the daytime (if it is sufficiently warm), the valley air heats up and creeps up the mountain slope. In the Alpine region there is a coordinated action of different valleys in a mountain range, contributing to the measured ozone at the mountain peak. As consequence, nighttime ozone measurements at mountain sites are generally related to "clean background air" (or "free tropospheric air"), whereas during the day ozone is often coming from the "polluted boundary layer air".

Considering the typical daily cycle of the atmospheric boundary layer (Figure 2.3), convective mixing layer is characterized by turbulent air flow (especially after the midday) due to higher temperature at the ground than in the layer. Stable boundary layer is produced after the sunset and stays during the night, where the temperature is lower than in the upper residual layer, therefore there is no mixing of the air occurring.

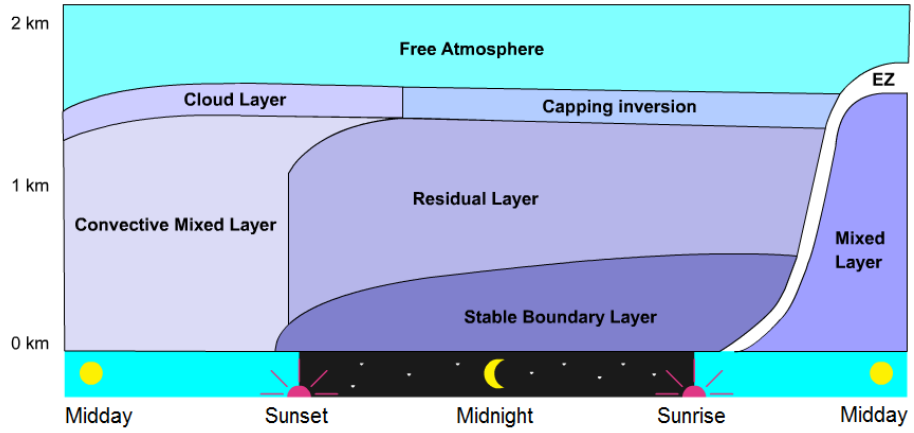

Figure 2.3. Typical daily cycle of the atmospheric boundary layer. EZ – Entrainment zone. (After Stull, 1988).

Ozone is removed during ozone loss reactions, including photolytic destruction as well as dry and wet deposition on the surface of plant leaves and soil.

Ozone production and destruction also depend on the local meteorological conditions and type of climate (sunshine, wind, humidity, length of vegetation period) as well as on the presence of ozone sinks (ex., plants, type of soil).

2.2.1 Ozone photo-chemistry

As it was said in the "Introduction", the photo-chemical cycle of ozone production and destruction in the troposphere involves such precursors as: carbon monoxide (CO), methane (CH4), non-methane volatile organic compounds (NMVOC), and reactive nitrogen oxides (NOx = NO + NO_2) (Logan, 1981; Seinfeld and Pandis, 2006). Concentrations of these species are mainly influenced by emissions from anthropogenic activities (industries, traffic, households and others), but also by natural emissions (forests, biomass burning, wetlands, oceans, lightning) (see Figure 2.4).

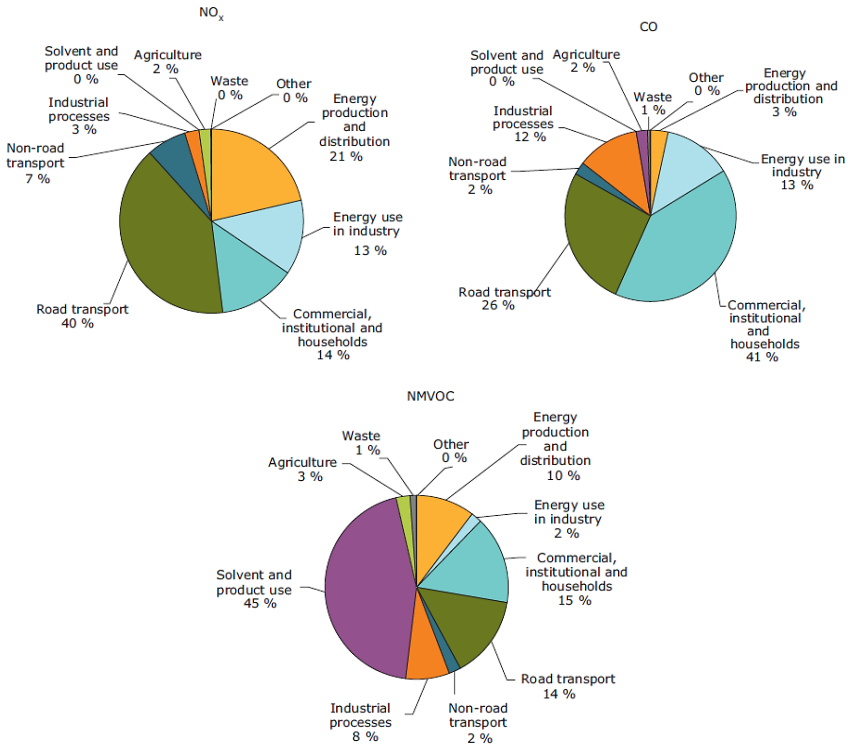

Figure 2.4. Sources of anthropogenic ozone precursor emissions in EU-27 (LRTAP, EEA Technical report No 10, 2013).

The chemistry of ozone in the troposphere has been largely described by Logan (1981). A fundamental discovery was the important role that radicals play in the oxidation of ozone precursors and in the ozone production and loss processes (Levy, 1971; Crutzen, 1973). Worth to mention that different reactions dominate in the stratosphere and troposphere, about 50% of stratospheric ozone can be explained by Chapman cycle (Chapman, 1931).

A characteristic element of tropospheric ozone chemistry is the fast photochemical cycle that inter-converts ozone and NO_2 in the presence of NOx. Under sunlight (i.e. UV radiation) NO_2 is

decomposed within few minutes, followed by ozone production from O_2 and $O(^3P)$. Conversely ozone is quickly destroyed by reaction with NO. The last reaction happens independently of UV light, and is the fastest way of ozone destruction in night and winter time. This cycle is described by reactions:

$NO + O_3 \rightarrow NO_2 + O_2$ (R2.1),

$NO_2 + h\nu \rightarrow NO + O(^3P)$ (R2.2) ($\lambda < 400$ nm),

$O(^3P) + O_2 + M \rightarrow O_3 + M$ (R2.3).

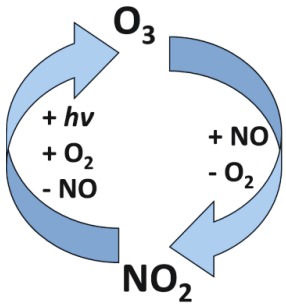

Figure 2.5. Equilibrium reached between NOx and ozone when no other species are present.

Reactions R2.1-2.3 represent a quasi-steady-state cycle, where no additional ozone is produced (Figure 2.5). O_3 achieves a steady concentration, determined by the initial concentration of NO_2, the photolysis rate of NO_2 and the temperature dependent rate constant of the reaction between NO and O_3. The established equilibrium implies no net ozone production as long as we have no other species which can interact with this cycle and shift the equilibrium. The equilibrium is refered as photo-stationary state (Seinfeld and Pandis, 2006) or Leighton relationship (Leighton, 1961). It is somehow hypothetical, because in reality other precursors, particularly VOCs, are always present in the air.

The chemical lifetime of ozone varies and usually is about 3 weeks, depending on the altitude. While in the dry upper troposphere ozone can exist up to several months, in the boundary layer it may last only for a couple of hours due to fast titration with NO emissions (Midgley and Reuther, EUROTRAC-2, 2003).

In the vicinity of roads, agricultural fields, forests and industries NMVOC play a crucial role in the ozone photochemistry, as the most reactive and thus short-living precursors. Most NMVOCs live from several minutes up to 1 month. They play a major role in ozone formation close to emissions sources, while the less reactive precursors CO and CH_4 are important in more remote areas as well as in the upper troposphere. CO is a relatively stable gas and can live in the atmosphere from several

days up to one year. Methane is the longest-living ozone precursor with a lifetime of about 10 years (Midgley and Reuther, EUROTRAC-2, 2003).

For ozone accumulation the presence of VOCs, CO, CH_4 in the air is crucial. The full scheme of photochemical ozone net production, which will be described now, is shown in Figure 2.6.

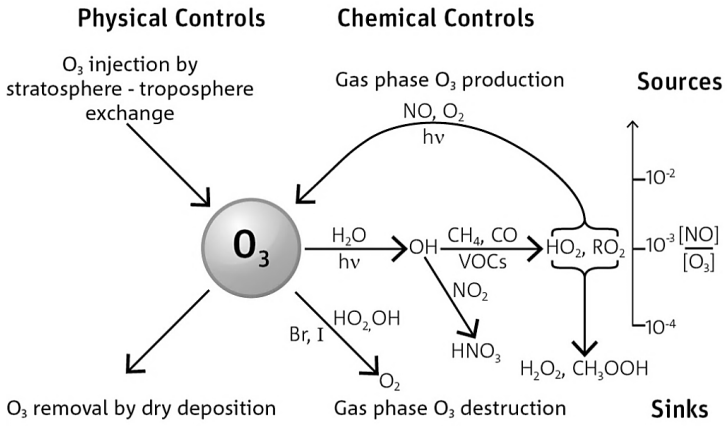

Figure 2.6. The physical and chemical processes controlling tropospheric ozone. Processes indicated in the top half of the figure are sources, and processes in the bottom half of the figure - are the sinks for tropospheric ozone. The key sinks for the short lived radicals produced from tropospheric ozone are also indicated (Galbally and Schultz, GAW Report No. 209, 2013).

The chain of chemical reactions leading to ozone production or loss is started with formation of highly reactive hydroxyl radicals. During ozone photolysis at $\lambda < 320$ nm the electronically excited $O(^1D)$ atom is produced and further reacts with H_2O to generate OH radicals (Seinfeld and Pandis, 2006):

$O_3 + h\nu \rightarrow O_2 + O(^1D) \quad \lambda < 320nm$ (R2.4),

$O(^1D) + H_2O \rightarrow 2OH$ (R2.5).

At larger wavelengths ($320 < \lambda < 400$ nm) ozone decomposition leads to formation of ground-state oxygen atoms $O(^3P)$, which binds with oxygen to form ozone again:

$O_3 + h\nu \rightarrow O_2 + O(^3P)$ (R2.6),

$O(^3P) + O_2 + M \rightarrow O_3 + M$ (R2.3).

90% of the $O(^1D)$ produced in reaction R2.4 are de-excited to more stable atoms $O(^3P)$ by collisions with N_2 or O_2 molecules, and only 10% of the $O(^1D)$ reacts with H_2O to generate OH.

As soon as hydroxyl radicals OH are formed, they initialize oxidation of surrounding compounds and thus change the tropospheric composition due to their high reactivity. It is shown in Crutzen and Zimmerman (1991) that once OH radicals are produced, they increase amount of radicals in

reactions with other species. The OH radical concentration is reasonably independent of altitude (Dentener and Crutzen, 1993). It plays a very important role in the chemistry of the troposphere, destroying pollution gases and performing the cleansing function. OH radicals attack not only hydrocarbons and CO, but also NO_2 in the presence of high NOx (R2.7). The amount of NOx, marked as "high", "enough" or "low" will be explained below. Reaction 2.7 acts as OH sink and produces nitric acid, a main contributor of acid rain (Crutzen and Zimmerman, 1991):

$OH + NO_2 + M \rightarrow HNO_3 + M$ (R2.7).

Therefore in case of high NOx there are less OH radicals available for oxidation of emission gases (VOCs, CO, CH_4). This oxidation results in creation of peroxy radicals RO_2 and HO_2:

$OH + RH + O_2 \rightarrow H_2O + RO_2$ (R2.8),

$OH + CO + O_2 \rightarrow CO_2 + HO_2$ (R2.9).

Formed by reactions R2.8 and R2.9 RO_2 and HO_2 radicals play the role of catalysts in further reactions and they continue oxidation having two possibilities. First, in case of low NOx, they cannot react with NO, instead RO_2 and HO_2 radicals destroy themselves or ozone. This causes chain termination:

1) with HO_2:

$HO_2 + HO_2 \rightarrow H_2O_2 + O_2$ (R2.10),

followed by peroxide destruction:

$H_2O_2 + OH \rightarrow HO_2 + H_2O$ (R2.11)

or peroxide photolysis:

$H_2O_2 + h\nu \rightarrow 2OH$ (R2.12),

2) with ozone:

$HO_2 + O_3 \rightarrow OH + 2O_2$ (R2.13),

3) with RO_2 through hydroperoxide ROOH formation:

$RO_2 + HO_2 \rightarrow ROOH + O_2$ (R2.14),

$ROOH + OH \rightarrow R_{-H}O + H_2O + OH$ (R2.15).

Thus, a low NOx content results in ozone loss (R2.13), and forces HO_2 radicals to terminate with production of substances like H_2O_2 (R2.10) or formaldehyde (R2.14, 2.15 in case if R = CH_3). Hydrogen peroxide plays an important role in the photochemistry of ozone, as it releases OH radicals (R2.12) continuing the chain of reactions towards ozone loss or production dependent on NOx and VOC/CO content.

Two organic peroxy radicals reacting with each other form various oxygenated substances:

$RO_2 + R'O_2 \rightarrow ROH + R'_{-H}O + O_2$ (R2.16).

A temporary termination of radical cycling is the formation of PAN (peroxyacyl nitrate: $RC(O)OONO_2$), balanced by its thermal decomposition:

$RC(O)O_2 + NO_2 \rightarrow RC(O)OONO_2$ (R2.17),

$RC(O)OONO_2 \rightarrow RC(O)O_2 + NO_2$ (R2.18).

The acyl peroxy radical $RC(O)O_2$ is a product of the reaction of aldehyde RCO with OH radicals and O_2. Produced in R2.17 PAN is transported with cold air masses to other areas and then decomposed by warming up, releasing peroxy radicals and NO_2 (R2.18), thus contributing to ozone production in remote areas.

Finally on the second path, in case of enough (medium) NOx concentrations, RO_2 and HO_2 radicals react with NO giving NO_2:

$HO_2 + NO \rightarrow OH + NO_2$ (R2.19),

$RO_2 + NO \rightarrow RO + NO_2$ (R2.20).

The NO_2 is then photolyzed (R2.2) with further ozone production (R2.3). These reactions (R2.19, 2.20) lead to ozone net production, because RO_2 and HO_2 radicals convert NO to NO_2 without destroying ozone. The processes described above are schematically shown in Figure 2.7.

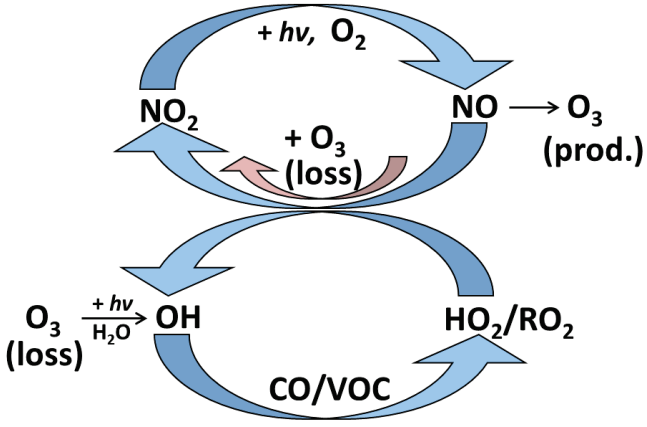

Figure 2.7. The scheme of reactions, included into ozone photochemical cycle.

To sum up the oxidation chain with NOx participation we get:

-a) for HO_2:

$OH + CO + O_2 \rightarrow CO_2 + HO_2$ (R2.9),

$HO_2 + NO \rightarrow OH + NO_2$ (R2.19),

$NO_2 + h\nu \rightarrow NO + O(^3P)$ (R2.2),

$O(^3P) + O_2 + M \rightarrow O_3 + M$ (R2.3),

Net: $CO + 2O_2 \xrightarrow{h\nu, NO_x} CO_2 + \boldsymbol{O_3}$ (R2.21),

(Crutzen, 1973; Crutzen and Zimmerman, 1991).

-b) for RO_2 on the example of CH_3O_2:

$OH + CH_4 + O_2 \rightarrow H_2O + CH_3O_2$ (R2.8),

$CH_3O_2 + NO \rightarrow CH_3O + NO_2$ (R2.20),

$CH_3O + O_2 \rightarrow HCHO + HO_2$ (R2.22),

formaldehyde removal:

$HCHO + h\nu \rightarrow H + HCO$ (R2.23a),

$\rightarrow H_2 + CO$ (R2.23b),

$HCO + O_2 \rightarrow HO_2 + CO$ (R2.24),

$CO + OH \rightarrow CO_2 + H$ (R2.9a),

$2\ H + 2\ O_2 + M \rightarrow 2\ HO_2 + M$ (R2.9b),

$4\ HO_2 + 4\ NO \rightarrow 4\ OH + 4\ NO_2$ (R2.19),

$5\ NO_2 + h\nu \rightarrow 5\ NO + 5\ O(^3P)$ (R2.2),

$5\ O(^3P) + 5\ O_2 + M \rightarrow 5\ O_3 + M$ (R2.3),

Net: $CH_4 + 10\ O_2 \xrightarrow{h\nu, NO_x} CO_2 + \mathbf{5}\ \boldsymbol{O_3} + 2\ OH + H_2O$ (R2.25)

(Crutzen, 1973; Crutzen and Zimmerman, 1991; Chameides et al., 1992).

Thus theoretically one O_3 molecule is produced from one molecule of CO in the first case (R2.21), and 5 O_3 molecules from one molecule of CH_4 with additional 2 OH radicals in the second case (R2.25). The produced O_3 and OH radicals start another oxidation cycle. NOx acts as catalyst. It is not straightforward to estimate the number of ozone molecules formed per precursor molecule. This depends on the exact composition of the precursor mix, which can contain several hundreds of different VOCs, many of which are intermediate products from initial hydrocarbon oxidation reactions, and on the NOx concentration, which controls the balance of ozone production and radical termination reactions.

As a result of intensive photochemistry with present precursors under UV, which is often happening in large cities with plenty emissions, photochemical smog is formed. As was mentioned in the

"Introduction", one of the first such smog episodes appeared in Los Angeles in 1944 (Haagen-Smit, 1952). When concentrated, this smog contains a mixture of pollutants, what causing its brown color.

Terminating reactions reduce ozone yields: when OH radicals are wasted on NO_2 oxidation (R2.7), and when HO_2 and RO_2 radicals react with each other, with ozone or with NO_2 (R2.10 - R2.18). Obviously, not only NOx, but also initial CO and VOCs concentrations play crucial role. One of the most important factors, influencing the yield of ozone during photo-chemical reactions is the ratio of NOx/NMVOC (or NOx/CO) (Logan, 1981; Seinfeld and Pandis, 2006).

Altogether the net ozone production is determined by several factors:

- the sunlight, which makes photochemical reactions possible.
- the ratio NOx/O_3, which predetermines what kind of radical reactions will take place.
- the ratio of VOC and CO to NOx.

It is clear that the sunlight is a condition of initiating and facilitating the reaction chain to produce ozone. In case of low UV light during winter time or during the night, ozone losses are larger than production, because the titration of O_3 by NO prevails over NO_2 photolysis in the cycle:

$NO + O_3 \leftrightarrow NO_2 + O_2$ (R2.1).

Moreover, during the night time, NOx and O_3 are lost in reactions:

$NO_2 + O_3 \rightarrow NO_3 + O_2$ (R2.26),

$NO_2 + NO_3 \rightarrow N_2O_5$ (R2.27).

The ratio NOx/O_3 is important because there are two competing reactions for HO_2 radicals, one with O_3 and another with NO:

$HO_2 + O_3 \rightarrow OH + 2O_2$ (R2.13),

$HO_2 + NO \rightarrow OH + NO_2$ (R2.19).

The first of these reactions (R2.13) interrupts the chain, while the second (R2.19) leads to ozone production. In theory if the ratio $NO/O_3 > 2.5 \cdot 10^{-4}$, then ozone production is favorable if only reactions R2.13 and R2.19 are considered (Crutzen, 1979). Taking into account also the reaction of NO with RO_2 radicals, the ratio NO/O_3 must be higher than $1 \cdot 10^{-3}$ (Galbally et al., 2000). Reaction of NO with CH_3O_2 radicals is:

$CH_3O_2 + NO \rightarrow CH_3O + NO_2$ (R2.20)

and it competes with the reaction of CH_3O_2 radical termination:

$CH_3O_2 + HO_2 \rightarrow CH_3OOH + O_2$ (R2.14).

As derived previously, one CO molecule produces up to one O_3 molecule (R2.21), while one CH_4 may yield up to 5 O_3 (R2.25). Therefore R2.20 is more productive for the net ozone production than

R2.19, and thus determines lower limit of NO concentration for ozone production. In Logan (1981) was established that at NO mixing ratio >= 30 ppt the reaction of the radical CH_3O_2 with NO (R2.20) will dominate over radical termination (R2.14). This amount is usually considered as a crossover point between ozone destruction and production (Seinfeld and Pandis, 2006).

NO of 30 ppt roughly corresponds to 60-100 ppt (or 0.1 ppb) of NOx, so the ozone destruction prevails when NOx is less than 0.1 ppb. NOx concentrations are normally considered together with VOCs/CO to identify ozone production/destruction. At places with high (Amazon, tropical forests) and moderate VOCs/CO (urban traffic or industrial areas) the final ozone amount will depend on both VOCs and NOx concentrations. At other places what drives the net ozone production or destruction is mostly the NOx concentration. The VOCs/NOx and CO/NOx ratios are important in terms of ozone production in case of polluted air, while they play a lesser role in clean air.

The dependence of the ozone production on NOx is not linear. Increase of VOCs or CO leads either to ozone growth or no change. This is because NOx and VOCs or CO compete for OH radicals. They would react mainly with NOx if the VOCs/NOx or CO/NOx ratio is too low and result in slow NO to NO_2 conversion, or would terminate in peroxy-peroxy reactions if these ratios are too high, therefore ozone cannot accumulate. In the middle ground OH radicals react with VOCs or CO producing RO_2 and HO_2 radicals which leads to net ozone production. The optimum ratio of VOCs to NOx is established roughly as 5.5 : 1 (Seinfeld and Pandis, 2006).

In typical rural areas the maximum ozone production can take place at ≈ 1 ppb NOx. And this can happen with plenty of VOCs and CO present. Figure 2.8 shows the ozone formation rate dependencies on NOx and CO. The plotted values result from a simulation run with initial conditions of 1% of water and 50 ppb of ozone. The diamond on the plot is placed in the NOx limited, the star - in the VOC limited regime (Figure 2.8). Reductions of VOC or NOx by a factor three (small symbols) have crucially different effects on the ozone production rate. Reduction of VOC causes either no change in the rate of ozone production or its decrease, while reduction of NOx may bring either enhanced ozone production or destruction.

Typical polluted daytime concentrations of NOx are 70-100 ppb. The maximum ozone production dependent on the initial amounts of NOx and VOC is represented on the ozone isopleth diagram (Figure 2.9). The ozone values are simulated through a large number of chemical reactions varying initial concentrations of NOx and VOCs. Above the ridge line on the plot there is “VOC-limited” regime and below – “NOx-limited”.

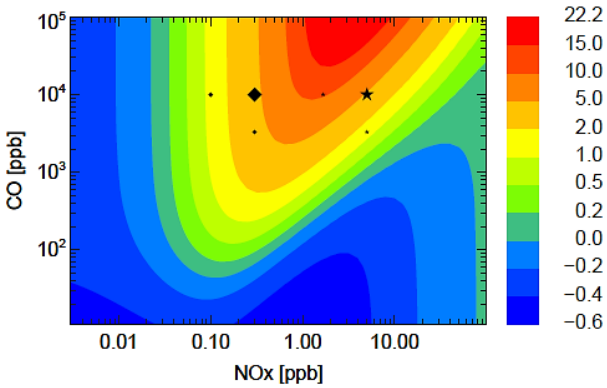

Figure 2.8. Ozone production rate dependence on the NOx and VOC concentrations demonstrated with a simple model case. The color coded isopleths indicate the range of the O_3 production rate (see colorbar) (in ppb/h) (PhD thesis of C. Richter, Forschungszentrum Jülich, 2008).

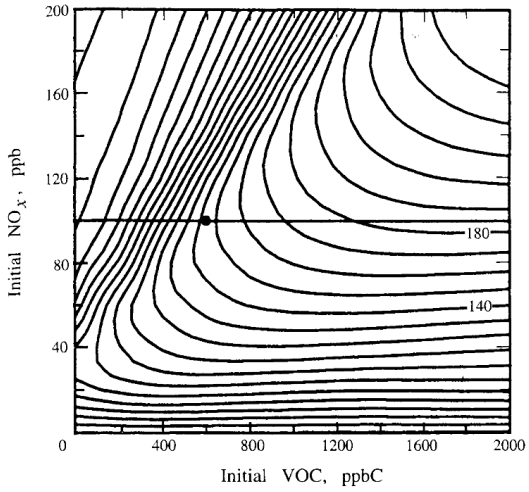

Figure 2.9. Ozone isopleth plot based on the simulations of chemistry along air trajectories in Atlanta over a 14 hour period. Each isopleth is 10 ppb higher in O_3 as one moves upward and to the right. The circle indicates initial conditions in simulations (Jeffries and Crouse, 1990; Seinfeld and Pandis, 2006).

2.2.2 Stratosphere-troposphere exchange

Stratosphere-troposphere exchange or STE is one term of the tropospheric ozone budget. In the literature STE is described primarily as Northern Hemispheric phenomenon which occurs in mid-latitudes in winter and spring-time (Levy et al., 1985; Holton et al., 1995; Harris et al., 1998; Monks, 2000), the nature of this phenomenon is under investigation since the 1970s. In trend and cluster analyses there were data from some mountain stations included, the highest of them are Jungfraujoch (3580 m), Sonnblick (3105 m) and Zugspitze (2962 m) (section 5.1). In comparison to ground-based stations, where ozone is mainly affected by the “surface” processes, elevated stations

are the most exposed to the STE influence. For this reason mountain stations can show different ozone trends and increased ozone concentrations in spring time.
The maximum ozone concentrations are found at 20-30 km altitude forming the so called ozone layer. There is a strong gradient near the tropopause, which induces a diffusion of ozone into the zone of the lower concentrations through the break in the tropopause near subtropical jet stream, which is located in the latitudinal belt 25-40 ºN.
This phenomenon is called "stratospheric intrusion" and is described in several studies (van Velthoven and Kelder, 1996; Baray et al., 1998; Langford, 1999; Stohl et al., 2000). The descending side of a spiral around the subtropical jet captures ozone from the stratosphere and brings it down, and in turn air masses from the troposphere like H_2O, aerosols, etc. are taken by the ascending part of the spiral up and lifted into the stratosphere. Therefore such mass circulation keeps balance in the spiral. Once ozone is included in the tropospheric circulation, it distributes in the troposphere and moves towards the poles. Hence different regions will have unequal stratospheric ozone contribution.

So far it remains difficult to estimate precisely the STE contribution to the global tropospheric ozone budget. In numerical model simulations STE is often diagnosed as a residual term from other known ozone budget terms (Stevenson et al., 2006). Another method is related to mass fluxes assessment (Hsu et al., 2005). It was shown that STE contribution to the local ozone budget can reach 15-25% (Megie et al., 1994), or even 30% over the eastern Mediterranean region (Roelofs et al., 2003).

The occurence of ozone transport with air during STE can be confirmed by the inflow of radionuclides like ^{7}Be, ^{10}Be and ^{210}Pb (Danielsen, 1968; Dibb et al., 1994; Graustein and Turekian, 1996; Koch and Rind, 1998; Zanis et al., 2003), which have stratospheric origin. Stratospheric intrusion is observed also with other tracers like low water vapour at Jungfraujoch, Sonnblick and Zugspitze (Elbern et al., 1997; Stohl et al., 2000).

Zanis et al. (2003) on the example of two isotopes of Be confirmed that less than 10% of ozone at Zugspitze are from the stratosphere. Dibb et al. (1994) found that in spring the stratosphere brings 10–15% of the ozone to the surface, and less in other seasons. Scheel et al. (2002) established that stratospheric intrusions are between 5% in May and 15% in January and October, but potentially those calculations may underestimate stratospheric ozone due to the difficulties of tracing ozone molecules during STE.

2.2.3 Ozone dry deposition

Ozone removal from the troposphere to the Earth's surface without precipitation assistance is called dry deposition. Ozone is destroyed when it comes in contact with the surface: soil and vegetation. Ozone may also be chemically destroyed by reactive gases released from the surface or can be absorbed by plant leaves. The dry deposition of ozone is important, because it is the process by which ozone causes harm to vegetation and reduces crop yields.

The formula for the calculation of dry deposition mass flux assumes that the deposition flux is proportional to the concentration of the considered specie (Seinfeld and Pandis, 2006):

$$F = -v_d \cdot C \quad (2.1),$$

where F is the vertical dry deposition flux – the amount of substance depositing to the surface area per unit time, v_d is a deposition velocity, which is referenced to some specific height above the surface, because the concentration C is a function of altitude. Therefore the flux F is constant up to the reference height. F is negative by convention, so that the velocity v_d is positive.

The value of v_d is determined by dry deposition processes, which consist of three steps: the aerodynamic transport through the atmospheric layer of air down to a very thin layer of stagnant air surrounding the surface, the molecular ozone transport (diffusion) across this thin layer and finally the uptake by the surface (Seinfeld and Pandis, 2006).

Thus the velocity and therefore ozone deposition flux depends on the wind flow conditions and the type of the surface. Ozone is a moderately soluble gas, therefore the moisture on the surface of plants and soil would influence the adhesion and removal of the O_3 molecule. On water, snow and ice surfaces ozone destruction is much slower than on the vegetation or bare soils (Galbally and Roy, 1980; Hauglustaine et al., 1994; Helmig et al., 2007, 2012) (Table 2.2).

Table 2.2. Typical dry deposition velocities for ozone (Hauglustaine et al., 1994).

	continent	ocean	ice/snow
v_d, (cm s^{-1})	0.4	0.07	0.07

2.3 Ozone measurement methods and instruments

Ozone measurements are necessary not only for understanding of ozone changes and trends, but also for verification of atmospheric chemistry-climate models. Both tasks require long-term high-quality data, measured by well-maintained instruments.

2.3.1 Historical measurements

As mentioned in the “Introduction” (section 1.2 “Historical ozone evolution and current situation”) some ozone records are available from surface stations, which used the Schönbein paper method and iodine catalyzed oxidation of arsenit.

For the Schönbein paper method KI and starch are used (Rubin, 2001). The amount of ozone that has reacted with KI is determined after the paper changes its color:

$$2KJ + O_3 + H_2O \rightarrow 2KOH + O_2 + J_2 \quad (R2.27),$$

$$J_2 + starch \rightarrow Blue\ or\ Purple\ color \quad (R2.28).$$

Among the disadvantages of that method are poor standardization, dependence on humidity, wind speed and exposure times.

Iodine catalyzed oxidation of arsenit is based on the oxidation of arsenite in neutral aqueous solution (Volz and Kley, 1988):

$$O_3 + AsO_3^{3-} \xrightarrow{I^-/I_2} O_2 + AsO_4^{3-} \quad \text{(R2.29)}.$$

Unexposed $(AsO_3)^{3-}$ served as a reference: after sampling of the air the remaining arsenite solution was titrated by I_2 solution after the addition of starch and $(NH_4)_2CO_3$:

$$I_2 + AsO_3^{3-} + 2OH^- \rightarrow 2I^- + AsO_4^{3-} + H_2O \quad \text{(R2.30)}.$$

Uncertainty of the arsenite method is quite high: ± 25%, because arsenite can also be oxidized by other molecules like H_2O_2 and SO_2:

$$AsO_3^{3-} + H_2O_2 \rightarrow AsO_4^{3-} + H_2O + H^+ \quad \text{(R2.31)},$$

$$2AsO_3^{3-} + SO_2 \rightarrow 2AsO_4^{3-} + S \quad \text{(R2.32)}.$$

2.3.2 Recent measurement techniques

Ozone absorbs at several wavelength intervals: UV range 100-340 nm (see Figure 2.10), visible spectrum at 550-650 nm, and at some infrared and microwave part of spectrum.

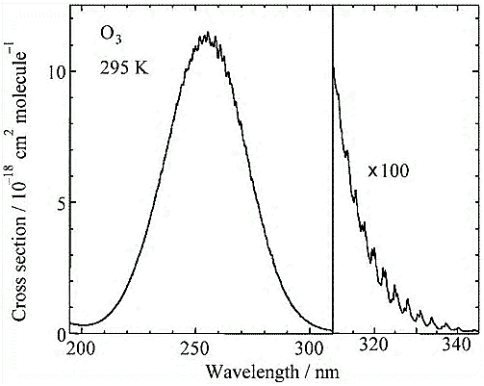

Figure 2.10. Absorption spectrum of ozone in the ultraviolet region (Matsumi and Kawasaki, 2003).

The developed measurement techniques for ozone monitoring can be sorted in two groups: in-situ and remote sensing methods. Their schematic picture is given in Table 2.3.

In-situ methods imply taking ozone samples from the air for the determination of ozone amount by optical, electrochemical or chemical techniques. UV photometry is the most reliable method for surface ozone measurements. It is recommended by the WMO Global Atmosphere Watch program (Galbally and Schultz, GAW Report No. 209, 2013). The electrochemical method is applicable in

balloons/sondes measurements. Another in situ technique is based on the chemiluminescence method. It is based on the reaction of ozone with NO in darkness accompanied with luminescence. Nowadays these instruments are less common due to their lower reliability in comparison to UV photometry, but they are used when fast response times are needed.

Table 2.3. The overview of ozone detection methods (World Meteorological Organization: WMO-No.8, 2008).

method	**in-situ**			**remote sensing**		
	method	instrument	information	method	instrument	information
ground -based	stationary	UV photo-metry	surface ozone	stationary	Dobson spectrometer	total column
	stationary	chemi-luminescence	surface ozone	stationary	Brewer spectrometer	total column
				stationary	lazer-radar LIDAR	total column, vertical profile
distant from ground	sondes, aircraft, zeppelin	electro-chemistry UV photo-metry	vertical profiles, flight path profiles	satellites	UV Backscatter, UV Forward Scanner, infrared radio-meter, etc.	total column, vertical profile

Together with surface ozone observations, there are other types of ozone measurements: columns and vertical profiles. The ozone column gives the information about the total ozone amount in the vertical column of a given radius in the atmosphere. Vertical ozone profiles are the concentrations distribution as a function of altitude.

The remote sensing of ozone is based on the UV light absorption and uses ground or satellite instruments for measuring total ozone columns or ozone distribution with altitude. Ground-based instruments like Dobson and Brewer spectrometers are measuring total ozone column according to the intensity of the UV light passed through the atmosphere. Vertical ozone profiles can be obtained by both in-situ methods like ozonesondes (balloons) measurements, which sample the air during the flight, and remote sensing methods like ground-based radars and spectrometers, as well as satellite instruments.

Table 2.4. Summary of ozone units for ozone content evaluation.

	Units
Partial pressure	millipascal, millibar
Mass mixing ratio	microgram per gram of air ($\mu g\ g^{-1}$)
Volume mixing ratio	ppb, nmol mol^{-1}
Local concentration	molecules cm^{-3}(m^{-3})
Mass density	$\mu g\ cm^{-3}$(m^{-3})
Ozone column	DU (1 Dobson Unit ≈ $2.69 \cdot 10^{16}$ molecules cm^{-2})

Units for reporting of ozone data are given in Table 2.4. The equation below shows the relationships between presented in Table 2.4 ozone measures:

$$p_i = p_{atm} \cdot vmr = p_{atm} \cdot \frac{M_{air}}{M_i} \cdot mmr = \frac{RT}{N_A} \cdot 10^6 \cdot [C_i] = \frac{RT}{M_i} \cdot 10^6 \cdot \rho_i,$$

where p_i – partial pressure, *vmr* - volume mixing ratio, *mmr* - mass mixing ratio, $[C_i]$– local concentration, ρ_i - mass density.

2.3.2.1 UV absorption photometry

In our work we analyze ozone data from surface stations recorded with UV absorption photometric analyzers. This method is based on the ozone absorbtion of the UV light at wavelength = 253.7 nm. The light is emitted from a mercury lamp, which spectral line coincident with absorption maximum of ozone (Figure 2.10). The analyzer consistes of a cell with inlet tube, where the air is coming into the cell, and outlet tube, where the air is leaving the cell after light absorbance (Figure 2.11). Transmitted light reaches the detector and its intensity is recorded.

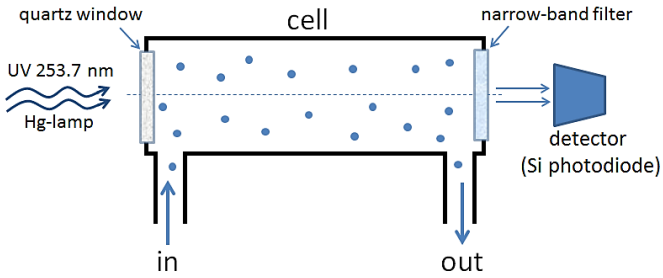

Figure 2.11. The simplified draft of one UV photometric cell.

The analyzer has two parallel cells with simultaneous measurements, one of which is for ambient air and another one for ozone-free air. Then the air streams are swapped to repeat the measurements. Using two cells in the instrument allows avoiding the influence of the light source instability.

Ozone mole fractions are derived from the Beer-Lambert and ideal gas laws, and calculated by the following formula (Galbally and Schultz, GAW Report No. 209, 2013):

$$x = \frac{-1}{2\sigma L_{opt}} \frac{T}{P} \frac{R}{N_A} \ln D \qquad (2.2),$$

where σ is the absorption coefficient of ozone at 253.7 nm (= $1.1476 \cdot 10^{-17}$ $cm^2 molecule^{-1}$) under standard temperature and pressure conditions; L_{opt} – is the optical length of the cell; P and T – are the pressure and temperature at the measurement conditions; N_A is the Avogadro constant, $6.022142 \cdot 10^{23}$ mol^{-1}; R is the gas constant, 8.314472 J mol^{-1} K^{-1};

$D = T1 \cdot T2$, (2.3),

where T1 and T2 are the transmittances of two cells. Transmittance is defined as:

$$T = I_{oz}/I_{ref} \quad (2.4),$$

where I_{oz} is the intensity measured in the cell when containing ambient air, and I_{ref} is the intensity measured in the cell when containing ozone-free air (also called as reference or zero air).

For measuring ambient ozone the GAW program (Galbally and Schultz, GAW Report No. 209, 2013) has adopted and recognized SRP instruments (Standard Reference Photometers), which were manufactured by the National Institute of Standards and Technology (NIST).

Experiments with instrument calibration have shown that the uncertainty in the ozone absorption coefficient at 253.7 nm is ± 2.12% (at 95% level of confidence) (Viallon et al., 2006). Errors of 10 hPa in the pressure measurement correspond to 0.1% error in the ozone measurement. Errors of 3 to 4 °C in temperature convert to an ozone correction of 1%.

The uncertainty of ozone data mostly depends on the measurement technique and the implementation of the measurement itself, as well as on the instrument design and operation. For the reduction of uncertainties station operators have to make weekly checks and maintenance. Among them are sample inlet, instrument alarms and sample air flows, lamp intensities, cell pressure and temperature, zero air and span checks, data recording and some others (Galbally and Schultz, GAW Report No. 209, 2013).

The rules of the uncertainty estimation are described by the Joint Committee for Guides in Metrology (2008). Since such estimates depend largely on the individual analytical set-up, they cannot be given here in general, and data providers must assess the uncertainty of their own specific system.

Galbally and Schultz provide in the GAW Report No. 209 (2013) the uncertainty of ± 1.7 nmol/mol (2 sigma) for the typical background ozone mixing ratio of 30 nmol/mol.

CHAPTER 3

3 Data

3.1 Data for trend analysis

The Airbase database is the public air quality database system of the European Environmental Agency (EEA) (http://acm.eionet.europa.eu/databases/airbase/; Guerreiro et al., EEA, 2012) and collects data from most European regional air quality monitoring networks.

The Airbase network partly covers data from European database EMEP (http://www.emep.int/) as well. The majority of sites of the EMEP and Airbase networks are labelled as "background" stations, therefore these data should be applicable for evaluation of chemistry transport models at regional and global scales.

Under the World Meteorological Organization's Global Atmosphere Watch (WMO GAW) program (www.wmo.int/pages/prog/arep/gaw/gaw_home_en.html) a voluntary network of global stations has been established. It provides information on "background" concentrations. Some of these records date back into the late 1970s. The World Data Centre for Greenhouse Gases (WDCGG) (http://ds.data.jma.go.jp/gmd/wdcgg/) is established under the GAW program to collect, archive and provide data for greenhouse (surface ozone, CO_2, CH_4, CFCs, N_2O, etc.) and reactive gases (CO, NO_X, SO_2, VOC, etc.) in the atmosphere, measured under GAW and other programs. Data from some EMEP stations are also reported to the WDCGG under GAW.

The Federal Environment Agency Umwelt Bundesamt (UBA) represents the national collection of the German regional air quality data (http://www.umweltbundesamt.de/) for O_3, CO, NO_2, SO_2, PM_{10}. At Forschungszentrum Jülich the data are downloaded daily in order to allow for near realtime evaluation of MACC forecast simulations. Quality-controlled and calibrated data are provided to us annually by Stefan Feigenspan (Umweltbundesamt, Dessau-Roßlau, Germany) and they replace the near realtime data.

In addition there is the French network of stations, focused on long-term monitoring of ozone and its main precursors. Until 2008 these stations were in the operation under the Pollution Atmosphérique à Echelle Synoptique (PAES) program (http://paes.aero.obs-mip.fr/), and afterwards they joined the EMEP. Pic du Midi and Puy de Dôme also contribute to the WDCGG GAW program of WMO.

Ozone data used for the trend- and representativeness analysis (chapter "Results and discussion", section 5.1 "Trend analysis") of 15 stations are collected through several networks: EMEP, WDCGG, Airbase, UBA and PAES.

3.2 Data for cluster analysis

Ozone data for the cluster analysis were extracted from the Airbase database (http://acm.eionet.europa.eu/databases/airbase/), as already stated in the "Introduction". It provides hourly integrated ground-based ozone data records, measured by UV photometric analyzers. Geographically, the station network covers all countries from the European Union and the EEA member countries, albeit with varying density. Station altitudes vary from 0 to about 3100 m above sea level. In this study Airbase version 6 data from 2007 to 2010 were used. Atmospheric ozone content was recorded as ozone density in $\mu g \cdot m^{-3}$ units. For the analysis presented here these were converted to number densities (nmol/mol or ppb) using the density of dry air at T_o = 20 ºC and pressure P_o = 101325 Pa. This T_o corresponds to the acknowledged factor = 2 of conversion, suggesting that the mole fraction of 0.5 nmol/mol should be equal to ozone concentration of 1 $\mu g \cdot m^{-3}$. T_o = 20 ºC and P_o = 101325 Pa correspond to the standard settings of commercial ozone analyzers, which automatically convert measurements at actual temperature and pressure to these standard conditions.

3.2.1 Data filtering

In order to ensure that only robust time series of measurements enter the analysis, the data were filtered in 4 steps: filter for data coverage, visual inspection filter, automatic data quality filter, and filter for data coverage applied a second time. All steps are schematically shown at the flow chart in Figure 3.1 (without the last filter for data coverage, which had no effect).

The automatic data quality filtering was tested extensively on many different ozone time series and found to reliably detect obvious errors while removing only very few valid data points. Flagged data points were removed from the time series. All other filters were applied in order to decide if a given station should be removed or retained in the analysis.

The automatic data quality filter flagged "suspicious" data values according to four tests:

1) identify data below a minimum value of zero in order to eliminate non-physical values;

2) flag data above a given threshold, which was taken either as 2.83 times the value of the 95-quantile or 2 times the value of the 99-quantile. For a Gaussian distributed random variable both values should be approximately identical. Even though later it will be shown that the ozone probability density functions are often not Gaussian (see Figure 5.40), this test can be used to define a reasonable upper limit value, because deviations from the normal distribution are mainly at the lowest percentile range of data;

3) flag data, which shows erratic behavior near a missing value. The rationale behind this test is that a visual inspection of measurement time series sometimes indicates that data reporting stopped too late or resumed too early after a calibration procedure or an instrument maintenance or malfunction. On

each side of the missing value, the five nearest (hourly) measurements are tested if they lie in the range of the surrounding values or exhibit abnormal variability;

4) flag data, which did not pass a statistical outlier test (a multi-step low pass filter with a running mean of 240 samples, flagging data that exceed the overall standard deviation of the data set by more than a factor of 8, followed by two variable band width filters and thresholds of 8 and 6 times the standard deviation, respectively).

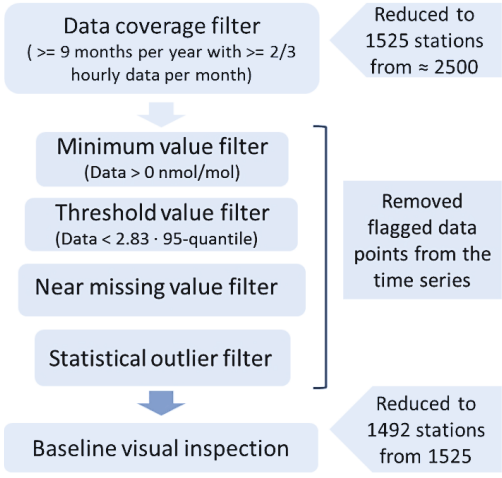

Figure 3.1. The scheme of the Airbase data filtering procedure.

The automatic data quality filter is demonstrated on a chunk of the ozone time series of the Italian station IT1598A (Figure 3.2).

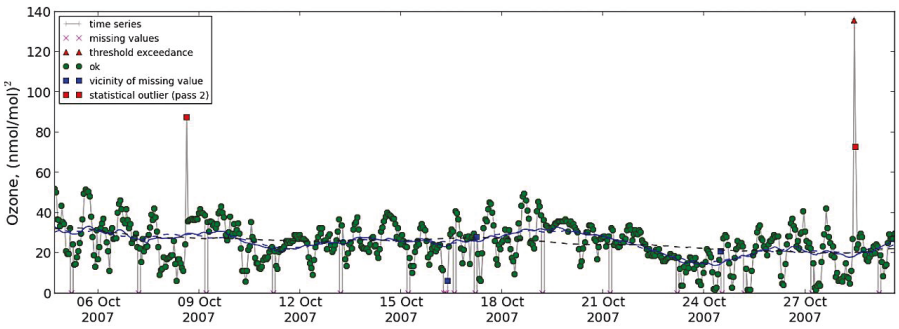

Figure 3.2. A chunk of the ozone time series of the station IT1598A (in nmol/mol) with applied automatic data quality filter. Filter flagged following points: missing values, vicinity of missing value, threshold exceedance, and statistical outliers. Black dashed line is a 240-point smoother; solid and dashed blue lines are smoothers with bandwidths in the interval 10-72 points and are determined automatically from autocorrelation of data.

The criterion for data coverage was that in every year, at least 9 out of 12 months had to contain at least 2/3 of the theoretical maximum hourly values. After first application of this criterion, the original Airbase set of more than 2500 ozone data stations was reduced to 1525 stations. Their time series were then visually inspected for sudden changes in the baseline (this phenomenon is not captured by the automatic data quality filter; see also Solberg et al. (EEA, 2009)). We adopted a conservative approach and flagged only those stations, where baseline shifts were of magnitudes of 5 nmol/mol or greater. The 33 stations which were filtered out at this step are presented in Appendix C. We note that among these stations only one is rural, others are either suburban or urban according to the Airbase classification.

Ozone time series of three removed stations are presented in Figure 3.3, they represent the most common behavior met in the time series baselines. Italian site Colico (Figure 3.3, a) shows the large baseline jump for some period of time in comparison to the whole time series. At the Spanish station Hermanos Felgueroso (Figure 3.3, b) we see a distinct drop of the baseline by 5 nmol/mol or more. Furthermore, the minimum values at this station suggest an offset or a calibration error in the measurements. And on the last picture for Italian Villa Ada the baseline is slowly growing from winter till summerof 2010 and then suddenly drops back (Figure 3.3, c).

Thus, 1492 sites were left, which were then subjected to the data quality filtering procedure described above. Finally, the data coverage test was run again. This step removed no further stations.

The final list of 1492 stations including their station code, location, altitude, and cluster number can be found in Appendix D. This table also contains a brief summary of the data quality filtering. The column “N flag.” combined number of all flagged data points which were below zero, above the calculated threshold, in the vicinity of missing value, or outliers. Typically, 0.5% of data or less were removed based on the automated filtering procedure. Last column “N valid” shows total number of valid data points, which were taken as filtered data set for further calculations and CA analysis.

(a). Background suburban station Colico from Italy, 280 m.

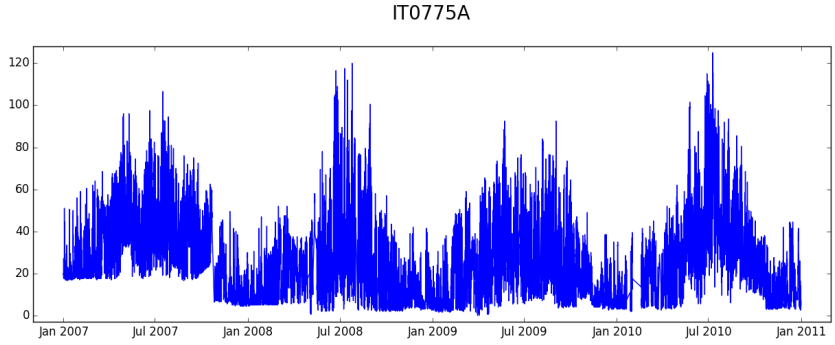

(b). Traffic urban station Hermanos Felgueroso from Spain, 10 m.

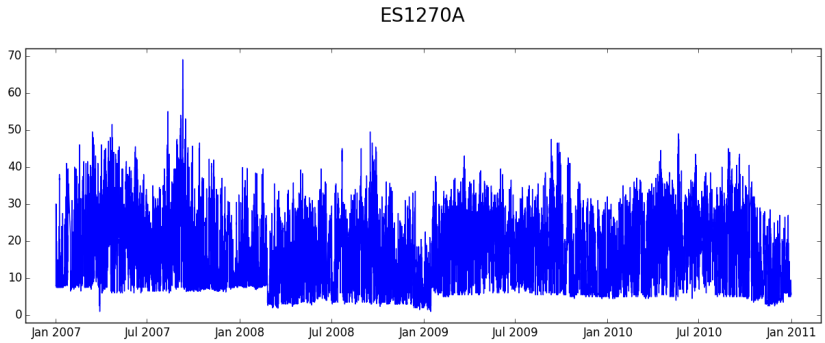

(c). Background urban station Villa Ada from Italy, 50 m.

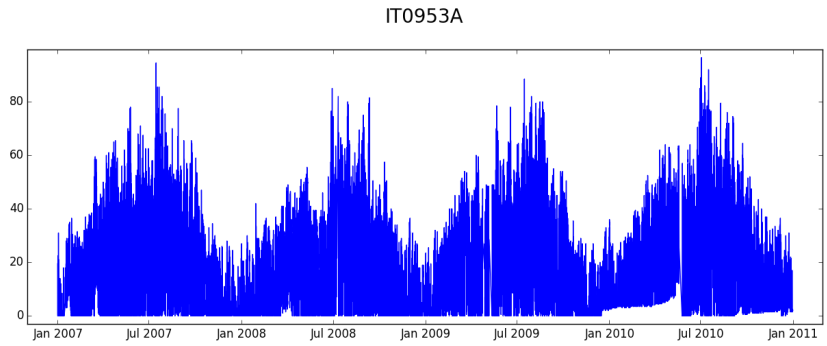

Figure 3.3, (a,b,c). Examples of ozone time series (in nmol/mol) with "wrong" baselines. Such stations were not eligible for the further analysis, as they were removed on the visual inspection filtering step.

3.2.2 Properties for cluster analyses

One of the aims of the present work is to identify air quality ozone regimes over Europe based on the measurements of ozone alone, and we use cluster analysis (CA) as a numerical method to process large amounts of data.

Choice of the appropriate set of properties is important in order to get an objective classification of stations. The data for every station should be converted so, that at the end there is a compact vector representing only essential and crucial information about the data set. To find suitable sets of properties it is necessary to characterize the ozone data set and identify the main components of ozone time series.

In the typical ozone time series there are two types of well distinguished cycles – seasonal and diurnal, which exist due to different conditions of ozone formation and removal in winter/summer and day/night respectively. Depending on the geography of the station (i.e. climate type, local weather changes, etc.) daily and seasonal cycles may vary in shape and amplitude. In the mid-latitude region

of Europe, the daily ozone cycle is especially pronounced in summertime and exhibits a maximum in the afternoon and a minimum during the night. The shape of the seasonal cycle can vary, and may show a maximum in summer or spring, or a combination of both.

Stable sunshine periods in spring or summer facilitate ozone concentration build-up. For example, such increase is noticeable in the time series of Simmerath (NRW, Germany, 572 m) from 3rd to 7th May 2013, followed by a sudden ozone decrease probably related to changed weather conditions (Figure 3.4). Rather rapid decrease in ozone concentrations may happen due to frontal passages. Wind change is another example, when a different air mass with a different chemical history is advected to the station.

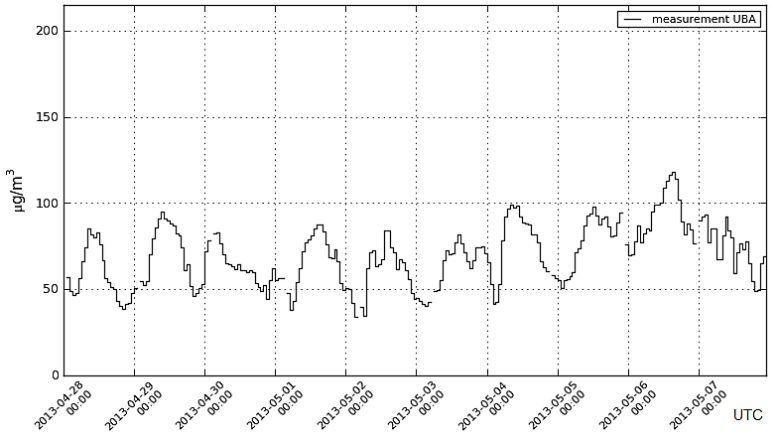

Figure 3.4. Hourly ozone time series of the station Simmerath (NRW, Germany) in April-May 2013.

On the same Figure 3.4 diurnal cycles are well distinguishable. All of them exhibit similar shapes with minima during the night or early morning, and maxima during the day or afternoon time, until weather conditions change after 7th of May 2013.

The seasonal cycle is a robust feature that is generally repeated every year. On the plot for the years 2008-2011 (Figure 3.5) of Simmerath the spring maxima in April are present for 2009-2011 and in May for 2008, while a summer maximum is strongly pronounced only for the year 2010, which is an exception. Simmerath is a rural station relatively remote from anthropogenic emissions. The corresponding typical seasonal cycle is therefore expected to exhibit a maximum in spring.

To sum up, daily and seasonal cycles are the most prominent and characteristic cycles describing typical ozone time series. Therefore we expect that the monthly averaged diurnal variations should be the most appropriate set of properties for the CA.

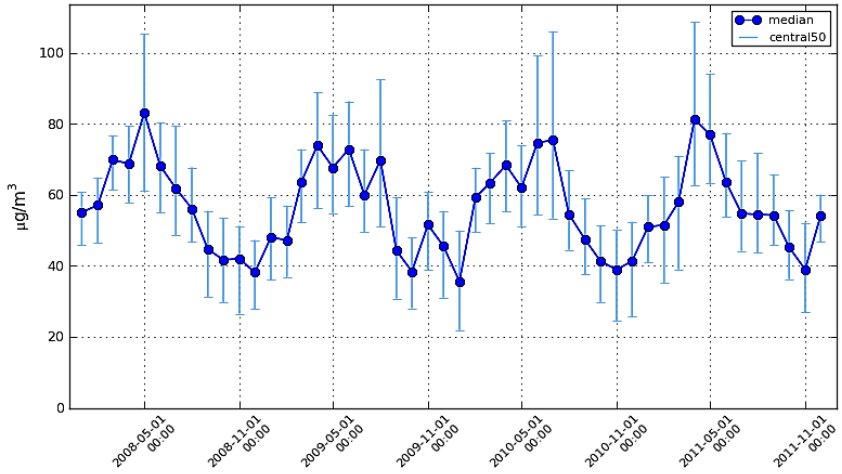

Figure 3.5. Monthly ozone medians (with 25-75 percentiles) of the station Simmerath (NRW, Germany) for the period 2008-2011.

We perform 3 different CA analyses, and each of them is based on a different set of properties. As input for the first CA monthly mean diurnal variations averaged over the four year period 2007 - 2010 (i.e. daily cycle with 3-hourly time step) of the individual ozone time series were used. We used 3-hourly resolution rather than the original hourly resolution in order to match the frequency of the MACC model output (see next section 3.3 "MACC model data"). Thus each station is represented by a vector of dimension 96 (12 months multiplied by 8 time steps per day). The time-averaged data at all stations were arranged into a matrix of dimension 1492 · 96. All entries in this matrix are ozone number concentrations and thus have the same units. As they do not differ vastly in their variances, we did not normalize variables of the matrix prior to applying the CA. Since the interannual variability (trend) of the data sets is usually insignificant and certainly much less than the diurnal or seasonal variability, we also did not detrend the data prior to the CA.

The second CA aimed to consider only the patterns of the seasonal and diurnal ozone cycles. To remove the influence of the ozone mean values we normalized each vector of the original matrix by the total average of this vector. Thus, each new element of every vector in the normalized matrix was computed as:

$$x_{norm} = \frac{x_{abs} - mean}{mean}, \qquad (3.1),$$

where x_{abs} – is the element of the vector in the analogous matrix of absolute values; mean – is the mean of the vector, i.e. the ozone average of the particular station.

The third CA was tested based on the annually averaged diurnal cycle and seasonal cycle. Each vector was represented in 20 dimensions (12 monthly and 8 diurnal means averaged over the period 2007 - 2010).

Further in the text we name each set of properties according to the number of the CA, in which they were used: 96 properties of absolute seasonal-diurnal variations – first set, 96 properties of normalized seasonal-diurnal variations - second, and 20 properties of normalized averaged cycles – third set of properties.

3.3 MACC model data

Model data were taken from the MACC reanalysis (Inness et al., 2013). The reanalysis invoked data assimilation of meteorological variables, and trace gas columns of O_3, CO and NO_2 as well as ozone profile information from various satellite instruments. The model system was the European Centre for Medium Range Weather Forecasts (ECMWF) Integrated Forecasting System which was coupled to the Model for Ozone and Related Tracers (MOZART) (Flemming et al., 2009; Stein et al., 2012). We extracted data for the years 2007-2010 at locations corresponding to the Airbase data. Similar to O_3, also CO, and NOx were provided as number concentrations.

The model output is available on a grid resolution of about $80 \cdot 80$ km^2 with a time step of 3 hours, and a vertical representation of 60 hybrid sigma-pressure levels reaching from the surface to about 60 km altitude. Model data were bi-linearly interpolated to the geographical locations of the 1492 Airbase stations in our analysis including vertical interpolation onto average pressure altitudes.

For comparison with the results from the CA the model output was arranged in a matrix of the same kind as the Airbase observations (order of stations, and the set of properties), and then rows were reordered according to the cluster membership of each station. In case of normalized set of properties the MACC data matrix was also normalized similarly to Airbase data matrix, and then grouped according to the clustering results.

3.4 Initial model-data comparison

The differences of monthly mean ozone concentrations (i.e. MACC means minus Airbase means) for January and July averaged over the period 2007-2010 for all 1492 stations are depicted in Figure 3.6. Here interpolated MACC data to actual locations and altitudes were used. The maximum and minimum biases between model and observations are + 32 to – 26 nmol/mol in January respectively, and + 37 to – 15 nmol/mol in July. The biases between the simulated and observed ozone averages over Europe are partly consistent with Inness et al. (2013) for Northern and Southern Europe, but there the MACC reanalysis data were evaluated based on the smaller data set of EMEP ozone observations.

The model generally shows better performance in winter than in summer. The summertime values are mostly overestimated by the model, often exceeding 20 nmol/mol difference in Great Britain, North

of Spain, Italy, Benelux area and at some stations in Germany. There are only few stations, where summer means are underestimated by the model – these are located along the Mediterranean coast and in mountainous areas (Figure 3.6).

In contrast, winter ozone means tend to be underestimated by –8 nmol/mol on average for Northern and Eastern Europe as well as in parts of Central Europe. In the Alpine region, part of France, Benelux area and part of Germany winter means are overestimated by +8-10 nmol/mol. In the South and West of Europe the positive bias often reaches +16-32 nmol/mol. Spain and Italy together with Sicilia and most of Sardinian stations are standing out as areas with model overestimation in both seasons (Figure 3.6).

MACC and Airbase monthly mean ozone concentrations for January and July averaged over the same period 2007-2010 are shown in Figure 3.7. Only stations of altitudes less than 200 m were taken in this case (822 stations) for reasonable comparison with the model, where the data for all grids were extracted from one pressure level (59^{th}, approximately 35 m altitude above the ground).

Both Airbase and model data exhibit low ozone concentrations in January (between 0 and 40 nmol/mol). As expected from the previous discussion, the model suggests that the lowest wintertime ozone concentrations occur over Central and Eastern Europe and over Finland (Figure 3.7, a). This is not inconsistent with the observational data, albeit the latter also show some low concentrations along the Mediterranean coast and in the Po Valley region. Higher ozone concentrations of 30-40 nmol/mol are simulated for the central and eastern Mediterranean region and over the Atlantic, affecting Ireland and Northern Scotland. There are only few stations in these regions, and most of these tend to measure somewhat lower concentrations than the model suggests. The exception is one station in Western Ireland (Mace Head), which observes higher ozone by 4 nmol/mol than modeled.

In July, the model generates the highest ozone concentrations over Sardinia (60-70 nmol/mol) followed by the Italian Peninsula and the eastern Mediterranean regions (Figure 3.7, b). These hotspots are with a few exceptions not seen in the observations. Moderately elevated concentrations (between 40 and 50 nmol/mol) are found over most of Southern Europe, Germany, and in a belt extending from Poland to the Adriatic coast. Ireland, the United Kingdom, Northern France, the Benelux countries, southern Scandinavia, and most of Eastern Europe are predicted to have ozone concentrations in the 30-40 nmol/mol range, and northern Scandinavia would experience lower concentrations. While there are some stations in Western and Eastern Europe, which seem to agree with the modeled values within the 5 nmol/mol contour intervals, one can also discern quite a few stations, where the model deviates by larger amounts and generally tends to overestimate the ozone concentrations. Over Italy couple of stations do indeed reach the high concentrations predicted by the model, but the majority of stations show lower values.

(a)

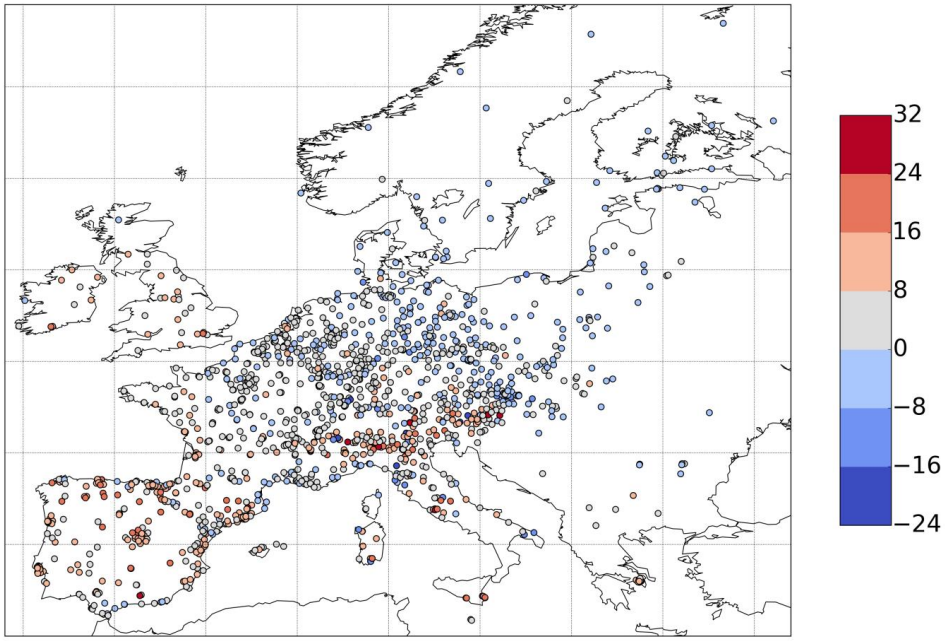

(b)

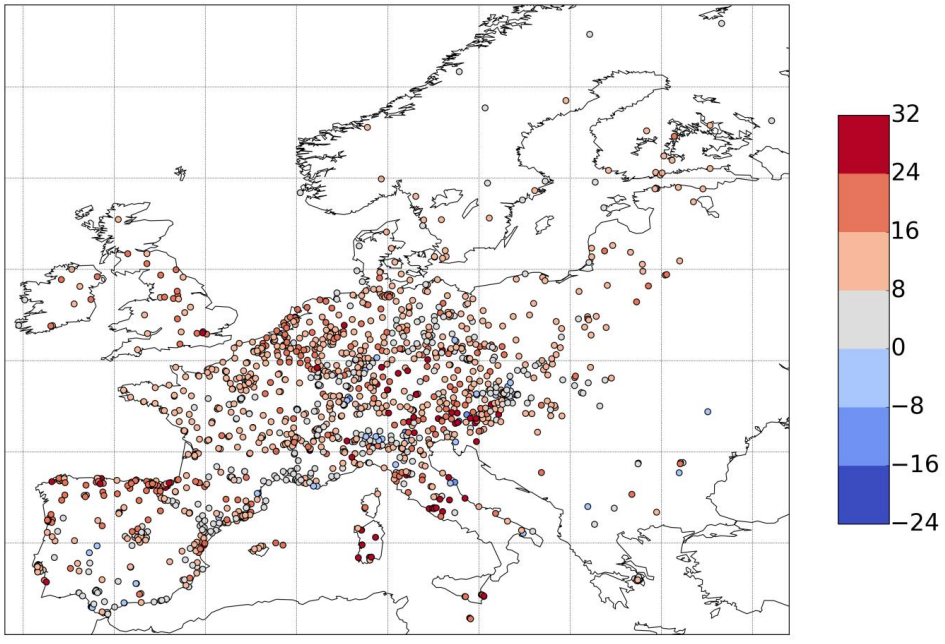

Figure 3.6. Difference between ozone averages of MACC data and Airbase data (1492 locations). January (a) and July (b) for the period 2007 – 2010 (in nmol/mol).

(a)

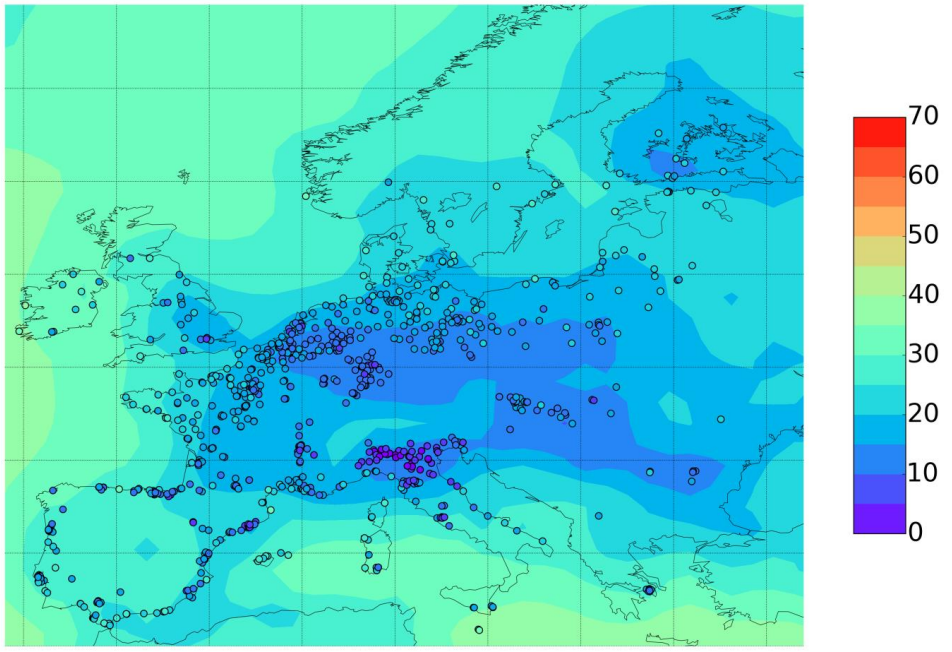

(b)

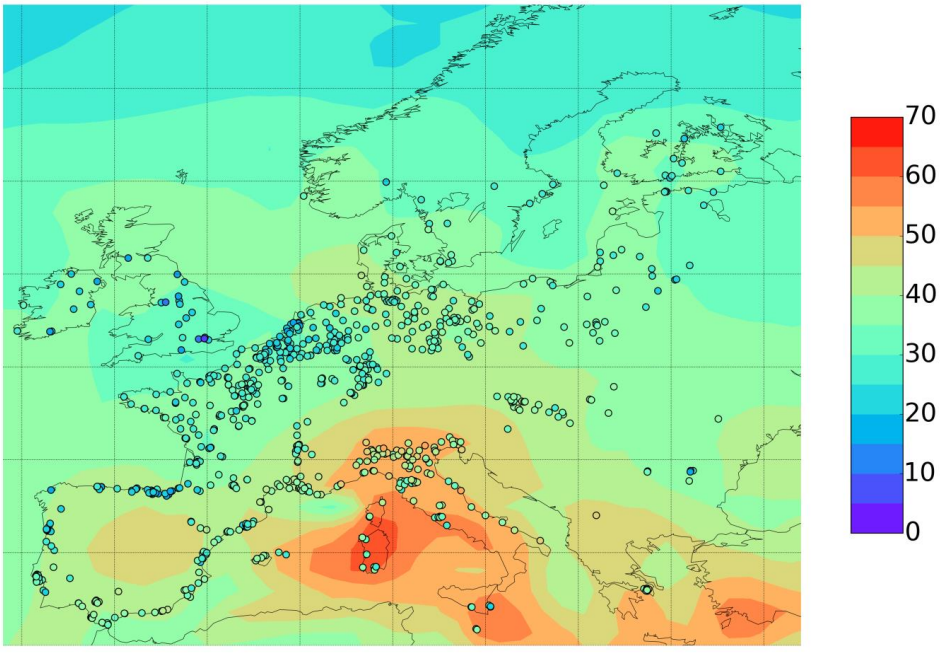

Figure 3.7. Ozone MACC data from reanalysis and Airbase data (822 locations). January (a) and July (b) averages for the period 2007 – 2010 (in nmol/mol).

CHAPTER 4

4 Methodology

4.1 Trend statistics

In the present work the ozone seasonal and annual linear trends were calculated using standard linear regression. The confidence interval of the trend slope is derived from the normal distribution statistics. The maximum length of a time series was 1990-2011, therefore the corresponding number of annual mean points is less than 22. Thus, the sample is not large enough to be normally distributed and the estimation of standard deviation would produce uncertainties. In order to get meaningful evaluation of the error of the trend slope we applied the t-statistics, suitable for small samples.

In this section at first we describe shortly the normal distribution and define the confidence interval of the variable. Afterwards follows t-statistics with definition of the t-distribution and corrected confidence interval formula. At last the linear regression statistics is presented with the equation for the trend slope error estimation and confidence interval computation relying on the t-statistics.

4.1.1 Normal distribution

In theory the normal or Gaussian distribution has a bell-shaped symmetrical curve, the maximum of which is the centrality parameter. It corresponds to the maximum probability and turns out to be the mean of the distribution (Figure 4.1). For a normal random variable X with mean μ and variance σ^2 one standard deviation (or sigma) from the mean in both directions ($\mu \pm \sigma$) describe 2·34.1 % of data, i.e. equal to 68.2% of the area under the bell-curve. Two sigmas ($\mu \pm 2\sigma$) describe (2·34.1 + 2·13.6) % = 95.4% of the distribution, and within 3 sigmas ($\mu \pm 3\sigma$) are 99.7% of the sample.

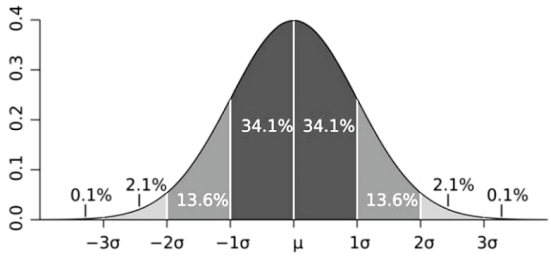

Figure 4.1. Normal (Gaussian) distribution curve. Each band has 1 standard deviation, and the labels indicate the approximate proportion of the area inside a band (http://en.wikipedia.org/wiki/Standard_deviation, by Jeremy Kemp).

The number of sigmas for describing the amount of data is used in the definition of confidence intervals (CI). The CI is the percentage of data around the mean, which is covered by the range $(\mu - z \cdot \sigma, \mu + z \cdot \sigma)$.

The CI indicates a probability of the estimated expectation (i.e. the arithmetic mean of the sample) to fall into this interval. The CI, or area under the curve, is described by the error function:

$$CI = \text{err}\left(\frac{z}{\sqrt{2}}\right) \quad (4.1).$$

Thus, it is possible to calculate the number of sigmas for a given CI. For the 90% confidence interval for any normal distribution 1.644854 sigmas are enough to cover 90% of data. The statistics require only the z number to establish the CI range if the distribution is large enough and with known sigma.

4.1.2 T-statistics

For a normally distributed random variable the size of the sample is sufficiently large. In case of small samples, it is difficult to estimate the standard deviation of the population. This estimation enlarges the uncertainty, which can be taken into account in t-statistics (or Student-distribution) (Gosset, 1908). Smaller distributions of the same mean have broader shapes of bell-curves, thus the confidence interval limits would grow on both sides for the description of the same percentage of data (the same area under the curve).

In the case of small distributions of size n the CI range is $(\mu - t \cdot SE, \mu + t \cdot SE)$, where SE – is a standard error of the statistic; t is a t-score from the normal t-distribution, which has (n-1) degrees of freedom. The t-distribution is described by the formula:

$$t = \frac{\mu - x}{\delta\sqrt{n}} \quad (4.2),$$

where μ is the mean of our initial distribution, x – a random value of this distribution, δ – the standard deviation.

If the value of the CI is given as α, then according to the symmetry of the t- distribution, the t- score would be a $\left(\frac{1+\alpha}{2}\right)$ percentile of this distribution. Therefore each random value x would be described by the CI equal to $(\mu - t_{n-1,(\frac{1+\alpha}{2})} \cdot SE, \mu + t_{n-1,(\frac{1+\alpha}{2})} \cdot SE)$.

T-values for various degree of freedoms and different values α are calculated and listed in special tables of any statistical book.

4.1.3 Linear regression statistics

Trend statistics was done by computing the linear fit with the margin of the slope error. In general case uncertainty of the slope arises from the uncertainties of both parameters x and y (Figure 4.2).

Each of i = 1,…N data points is described by (x_i,y_i). Let us define a linear regression function that provides an optimal fit to the observations:

$f = a \cdot x+b$ (4.3),

where x is the independent variable and f is the dependent variable, which corresponds to y_i of the observations; a is the slope value of the trend:

$$a = \frac{\sum_{i=1}^{N}(x_i - \bar{x})(y_i - \bar{y})}{\sum_{i=1}^{N}(x_i - \bar{x})^2} \quad (4.4);$$

The intercept b is given by:

$$b = \bar{y} - a \cdot \bar{x} \quad (4.5);$$

and average values x and y are:

$$\bar{y} = \frac{1}{N}\sum_{i=1}^{N} y_i \quad (4.6)$$

and

$$\bar{x} = \frac{1}{N}\sum_{i=1}^{N} x_i \quad (4.7),$$

respectively.

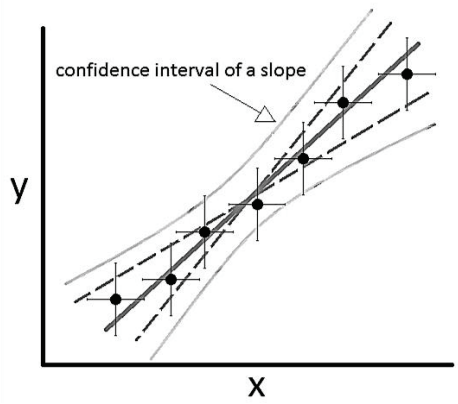

Figure 4.2. Schematic view of the linear fit of a small data sample.

The standard error of the slope SE of the linear regression (Kenney and Keeping, 1962) is:

$$SE = \frac{\sqrt{\frac{1}{N-2}\sum_{i=1}^{N}(f_i - y_i)^2}}{\sqrt{\sum_{i=1}^{N}(x_i - \bar{x})^2}} \quad (4.8).$$

Graphically the confidence interval bands around the regression line have the hyperbolic shape. This arises from the estimation of both errors – the slope and the mean. The standard error of the position of the regression line at the mean $\bar{x}$ is:

$$SE_y = \sqrt{\frac{1}{N(N-2)}\sum_{i=1}^{N}(f_i - y_i)^2} \quad (4.9).$$

Within the limits of the CI the regression line can vary its slope as well as shift along the x-axis to value χ from the mean $\bar{x}$. Therefore to derive an equation of the CI bands, the error SE_y of the position of the regression line at the mean $\bar{x}$ is added to the error of the slope SE, which should be multiplied by the uncertainty of the mean (χ - $\bar{x}$). When summing described errors together, we get an equation for the CI bands, which turn out to have a hyperbolic form:

$$((\tilde{a} \cdot \chi + \tilde{b}) - t_{n-2,(\frac{1+\alpha}{2})} \cdot SE_f, \quad (\tilde{a} \cdot \chi + \tilde{b}) + t_{n-2,(\frac{1+\alpha}{2})} \cdot SE_f),$$

where SE_f is the summarized error of a regression line:

$$SE_f = \sqrt{\frac{1}{(N-2)}\sum_{i=1}^{N}(f_i - y_i)^2 \left(\frac{1}{N} + \frac{(\chi-\bar{x})^2}{\sum_{i=1}^{N}(x_i-\bar{x})^2}\right)} \quad (4.10)$$

and $t_{n-2,(\frac{1+\alpha}{2})}$ is a $0.5 \cdot (1 + \alpha)$ -quantile of the t-distribution with (n-2) degrees of freedom. We note that for the linear fit statistics df = n-2 is used, because two parameters are estimated (a and b) in order to find the best linear regression curve.

In the present work we are more interested to estimate the confidence interval of the slope, because only trend value can give the understanding of ozone changes in time. Trends were computed using the 90% confidence interval ($\alpha = 0.9$). It means that the slope of the trend a in 90% cases would fall into the range:

$$(a - t_{n-2,(\frac{1+\alpha}{2})} \cdot SE, \quad a + t_{n-2,(\frac{1+\alpha}{2})} \cdot SE),$$

where $t_{n-2,(\frac{1+\alpha}{2})}$ is a 0.95-quantile of t-distribution and SE is estimated using formula 4.8.

Some routines on linear trend statistics computation are given in Appendix B.

4.2 Cluster Analysis

Cluster Analysis (CA) is a data driven technique for classifying objects into groups whereby each object is described through a set of input parameters (properties or variables) which are used as criteria for grouping. Clusters are formed so that the similarity between objects inside a cluster is maximized while the dissimilarity is minimized. Initially the concept of “Cluster Analysis” was suggested by Tryon in 1939. Since then it has found applications in statistical processing of large data sets in biology, medicine, computer science, meteorology and atmospheric sciences (Zhang et al., 2007; Lee and Feldstein, 2013; Camargo et al., 2007; Christiansen, 2007; Beaver and Palazoglu, 2006; Dorling and Davies, 1995; Marzban and Sandgathe, 2006) as well as in other fields.

4.2.1 K-means

Several methods for clustering objects into groups have been developed and different choices can be made for the computation of distances between objects or groups of objects. The most commonly used types of clustering are hierarchical and partitional (centroid-based clustering, or simply k-means). Hierarchical clustering progressively splits the data set into more and finer clusters, whereas partitional clustering groups the data into a pre-determined number of clusters. Clusters are non-overlapping groups, such that each object will belong to exactly one cluster.

In the present study we applied partitional clustering, because it allows for estimating the robustness of results and places less emphasis on outlier values than hierarchical clustering.

K-means uses Euclidean metric for the calculation of distances:

$$Edist = \sqrt[2]{\sum_{m=1}^{M}(x_{mA} - x_{mB})^2} \qquad (4.11),$$

where x_A and x_B are two objects of the data set which have M properties (i.e. variables) each. In our case each object is a station, represented by the vector of 96 variables (monthly averaged 3-hourly absolute values) in the 1st CA, 96 normalized variables in the 2nd CA, or 20 variables (normalized averaged seasonal and diurnal cycles) in the 3rd CA, respectively. The k-means algorithm is directed towards minimization of the Euclidean distances between individual objects and cluster centroids.

A centroid is an artificial object that represents its cluster and is the arithmetic mean of all properties of cluster members:

$$c_i = \frac{1}{n_i}\sum_{j=1}^{n_i} x_{ij} \qquad (4.12),$$

n_i – number of objects in i^{th} cluster, c_i – centroid of the i^{th} cluster, x_{ij} – j^{th} object of the i^{th} cluster.

The minization is achieved iteratively in an analysis cycle of three steps. At the initial step of each k-means run, k centroids are defined randomly from the data array. The second step assigns each object to the closest centroid, so that an initial set of clusters is formed. In the third step, each centroid is recalculated, as the mean of the cluster members. Steps 2 and 3 are then repeated until the centroid coordinates don't change anymore. The goodness of the clustering can be assessed with the sum of squared distances (SSD) between objects and corresponding centroids:

$$SSD = \sum_{i=1}^{k}\sum_{j=1}^{n_k} Edist(c_i, x_{ij})^2 \qquad (4.13),$$

where Edist is the Euclidean distance, k is the number of clusters, and n_k the number of objects inside the k^{th} cluster.

K-means requires that the number of clusters k is known for initialization of the algorithm, so prior to the CA we applied a method to determine the optimum value of k for the first CA. Figure 4.3 shows an "elbow" - curve (SSD versus number of clusters k), derived from 50 · 100 independent k-means runs of the first set of properties (96 absolute seasonal-diurnal variations) with varying

number of k from 1 to 100. At k = 6 the curves of the SSD deviate one from another, while at k = 5 they overlap very well. At k = 4 curves are not consistent again, but taking k = 3 for the analysis wouldn't describe variety of ozone regimes. We therefore chose k = 5 for the first CA in order to obtain the maximum number of groups which should still yield reproducible results.

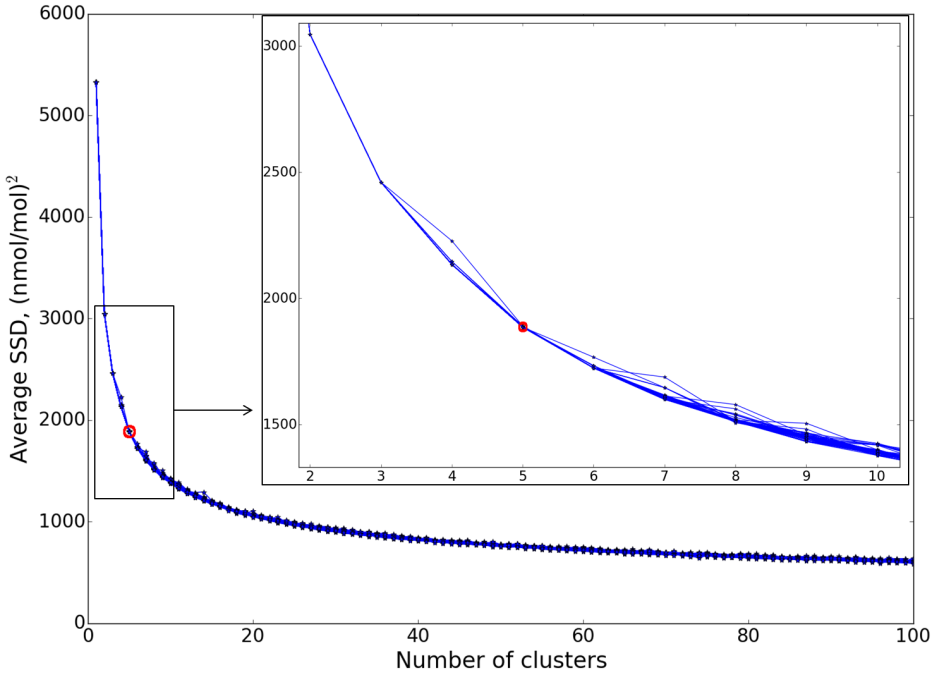

Figure 4.3. Averaged SSD ("elbow"- plot) of 50 · 100 independent k-means runs with varying number of clusters k from 1 to 100, based on the 1st set of properties.

On the contrary, similar "elbow" – curves produced after 50·100 k-means runs of the 2nd set of properties (96 normalized seasonal-diurnal variations) shows the coherency of runs until k = 4 and already big disagreement at k = 5 (Figure 4.4). Third set of properties (20 normalized seasonal and diurnal cycles) is able to achieve reproducible clustering up to k = 4 also, and represent similar "elbow"- curve, as the 2nd set of properties, although showing not so much deviation of curves after k = 5 (Figure 4.5).

The "elbow" plots not only give the appropriate number of clusters to run k-means, but they also provide a preliminary answer on the question of stability of the CA run for the chosen k. The robustness will be discussed in section 5.2.9.

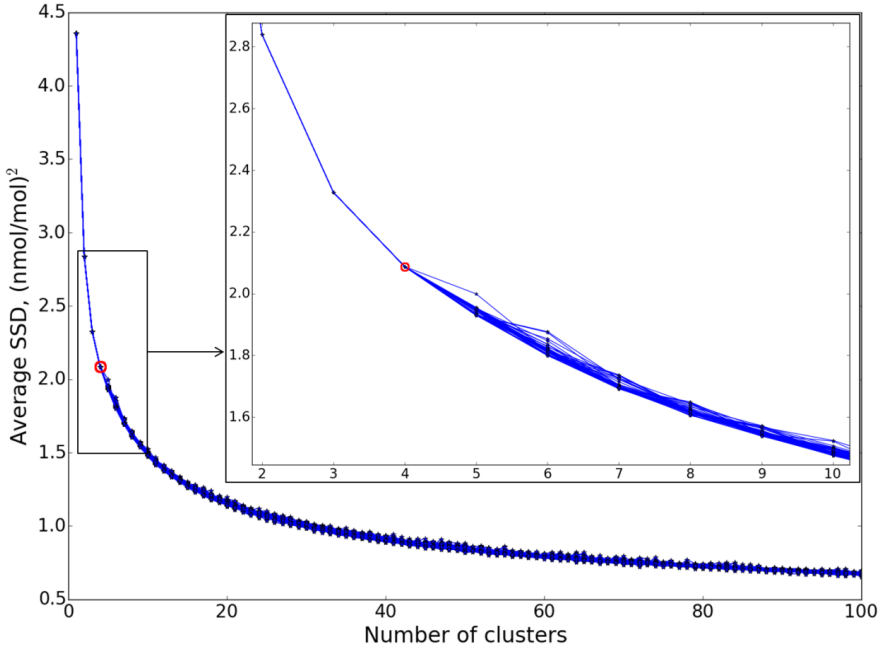

Figure 4.4. Averaged SSD ("elbow"- plot) of 50 · 100 independent k-means runs with varying number of clusters k from 1 to 100, based on the 2nd set of properties.

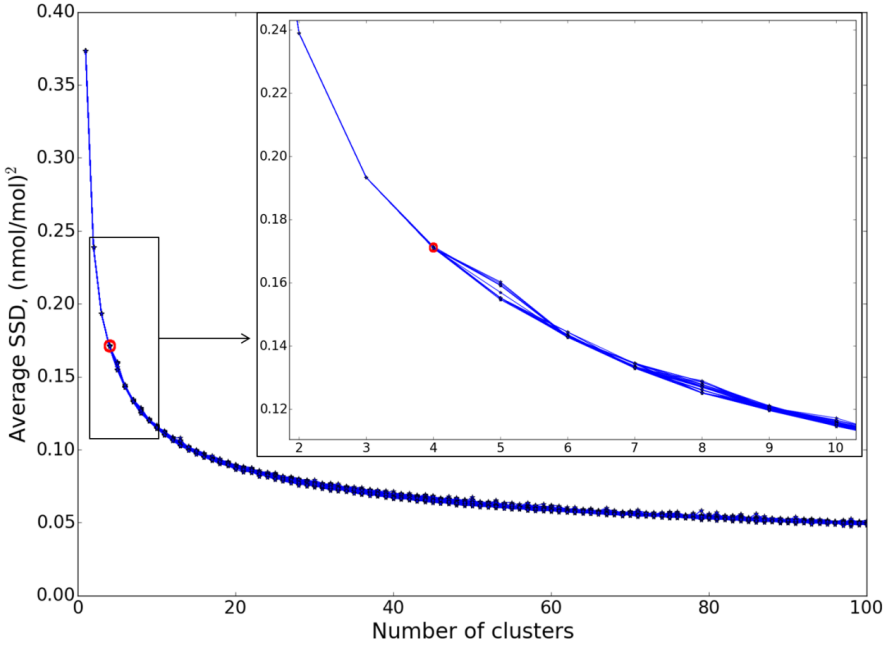

Figure 4.5. Averaged SSD ("elbow"- plot) of 50 · 100 independent k-means runs with varying number of clusters k from 1 to 100, based on the 3rd set of properties.

Routines for k-means algorithm implementation were built on the Pycluster module and its function "kcluster" (Python programming language). The routine is presented in Appendix A. "Kcluster" requires not only the k number but also the iteration number, i.e. amount of times the algorithm is initialized: every time with new randomly generated centroids. Kcluster then only returns the result with the minimum SSD. In the present work we used only one iteration (npass = 1 in "kcluster" function, see Appendix A), which means that centroids are generated randomly only once, then the process is beginning from the assignment of stations to the closest centroids, and is continuing with recalculation of centroids coordinates and next reassignment of stations and so on until centroid coordinates don't change anymore. After all steps are done, the result is given in the output. Here "iteration" means not the number of times centroids are recalculated, but complete step starting from centroids generation till the last assignment of stations to clusters.

The "elbow" plots shown in Figures 4.3, 4.4 and 4.5 are produced with one iteration, as described above. For the actual CAs we have made 100 kmeans runs with fixed conditions (each run with iteration = 1 and fixed k) to choose one single run out of 100 with the minimum SSD. 100 runs with iteration = 1 each would be equal to 1 run with 100 iterations. But 100 runs were made in order to see the SSD changes for every such run. The resulting SSD curve will be discussed in section 5.2.9 "Robustness of the cluster analyses".

4.3 Earth Mover's Distance

In order to quantitatively evaluate the model's ability to reproduce the observed frequency distributions in each cluster, we calculated the Earth Mover's Distance (EMD). Initially the EMD was suggested by Rubner et al. (1998). EMD provides an objective distance measure between two frequency distributions or estimates of probability density functions. It is a true distance measure in the sense that it is positive semidefinite and symmetric and fulfills the triangle inequality. Additionally it has the property of being (asymptotically) proper meaning that the smallest distance is only achieved when the two probability densities are identical.

The formula for EMD according to Rabin et al. (2008) is:

$$D(f||g) = \frac{1}{n_b}\sum_{i=1}^{n_b} |F_X(x_i) - G_X(x_i)| \qquad (4.14),$$

where n_b is the number of bins, $F_{X(xi)}$ and $G_{X(xi)}$ are two cumulative distribution functions of f and g, i.e. two corresponding estimated probability densities obtained from the normalization of the respective frequency distribution histograms.

4.4 Bootstrapping

Bootstrapping is a method for estimation of the accuracy of sample statistics, such as variances, medians, confidence intervals, etc. (Efron and Tibshirani, 1994). In our case we assess the precision of EMD values, calculated as described in the previous subsection from the full sets of Airbase and MACC data, i.e. based on the hourly data of 1492 stations. Bootstrapping belongs to resampling methods, when the parameters are evaluated on the approximating distribution, obtained by random sampling with replacement from the original dataset, so that the final size of the resampled data is preserved. It means that in the randomly generated data some values from the original data set are repeated, while others are absent.

In the present work, for the estimation of the stability of obtained EMD values, new EMD values were calculated on the basis of 10% of initial data (i.e. 149 stations), randomly selected from the full set. To keep the size of the original data set (1492), these 10% of data were repeated 10 times and two other stations out of the chosen 149 were added. To get the statistics of EMD values (5- and 95-percentiles distributions and EMD mean), we performed 10 tests with different randomly generated samples for each test.

CHAPTER 5

5 Results and discussion

5.1 Trend analysis

5.1.1 Alpine stations (1990-2011)

As stated in section 1.3 “Motivation”, trend analysis is the first step of the analysis of European ozone representativeness. To begin the study of the temporal ozone change over Europe we have taken the three Alpine stations Jungfraujoch (JFJ, 3580 m), Sonnblick (SNB, 3105 m) and Zugspitze (ZUG, 2962 m) (see Table 5.1). These mountain stations have measured tropospheric ozone already for more than 2 decades and thus have the longest continuous ozone records in Europe. That they are also the highest stations makes them valuable for studying ozone evolution in the free troposphere and secondly comparable to each other. Mountain stations mostly show “cleaner” ozone due to the relative remoteness of the emission sources. Other Alpine stations are at lower altitudes, or may have shorter time periods of available measurements. For example, the station Hohenpeissenberg, located 40km North from Zugspitze, is only 985 m high, and contains data till 2008. Moreover JFJ, SNB and ZUG are about 150-200 km apart one from another (Figure 5.1), so we expect that data from these three Alpine stations may correspond to the European regional ozone changes, if stations will show the consistency of their trends.

Before presenting the results of the analysis of the temporal ozone change over Europe, it is worth to summarize what was already done in other studies (Chevalier et al., 2007; Cui et al., 2011; Gilge et al., 2010; Tarasova et al., 2009; Logan et al., 2012).

Table 5.1. Information on the three Alpine stations.

station	abbrev.	latitude	longitude	altitude, m	sourse*
Jungfraujoch	JFJ	46.55	7.99	3580	WDCGG
Sonnblick	SNB	47.05	12.96	3105	WDCGG
Zugspitze	ZUG	47.42	10.98	2962	personal communication (H.E. Scheel**)

* see chapter “Data” for the information about the data networks.

** Hans-Eckhardt Scheel, Karlsruhe Institute of Technology, Germany.

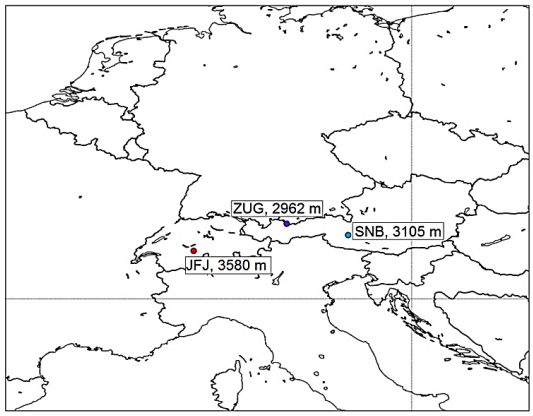

Figure 5.1. Location of the Alpine stations Jungfraujoch (JFJ, 3580 m), Sonnblick (SNB, 3105 m) and Zugspitze (ZUG, 2962 m).

Chevalier et al. (2007) have shown positive linear trends for moving segments of 9 year periods based on annual ozone means, but decreasing from one segment to another. In Table 5.2 their annual trend values are presented. The time period is limited by 2004. Trends for the overall period 1991-2004 are positive at all stations. JFJ trend is approximately 2 times larger than for SNB and ZUG.

Table 5.2. Annual ozone trends and corresponding 95% confidence intervals (in ppb) over the indicated periods at JFJ, SNB and ZUG (Chevalier et al., 2007).

	1991–2000	1992–2001	1993–2002	1994–2003	1995–2004	1991–2004
JFJ	0.92±0.34	0.68±0.38	0.62±0.40	0.54±0.36	0.34±0.38	0.62±0.23
SNB	0.46±0.36	0.46±0.36	0.40±0.39	0.25±0.24	0.12±0.34	0.28±0.23
ZUG	0.38±0.30	0.29±0.33	0.22±0.32	0.30±0.38	0.03±0.39	0.27±0.22

In a similar study (Cui et al., 2011) has considered only the JFJ station. The seasonal 9-year moving trends (Figure 5.2) revealed the reduction of ozone summer and winter trends from ≈ 1 ppb/year for 1990-1999 to no trend for 1998-2007 and then further decrease yielding a negative slope for 1999-2008.

Logan et al. (2012) have analyzed trends based on annual and seasonal ozone means of Alpine sites for 1998-2008 in comparison with trends from the European ozone sondes and MOZAIC aircraft data (http://mozaic.aero.obs-mip.fr) (Figure 5.3). Sondes and aircraft data were taken from altitudes above 2 km, and represent free tropospheric ozone over Hohenpeissenberg/Payerne and Frankfurt/Munich respectively. All annual trends in their study are negative except for Frankfurt/Munich, which showed insignificant trend. For other sites such decline is driven by ozone in all seasons, especially during summer and spring time. JFJ, SNB and ZUG trends for 1998-2008

are about -0.2 ppb/year, which is similar to calculated JFJ trend for 1999-2008 in the work of Cui et al. (2011).

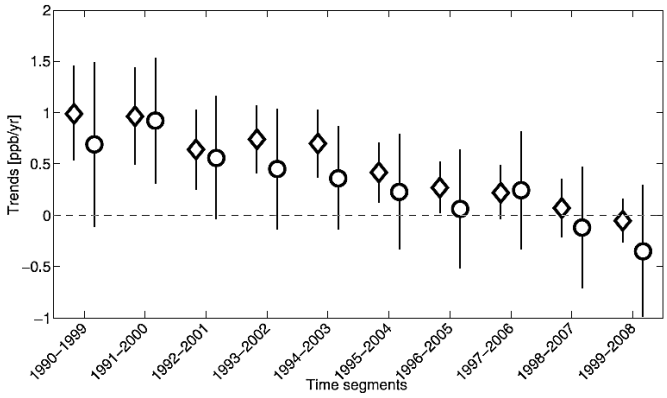

Figure 5.2. Linear ozone trend values of moving 10 year periods in winter (diamonds) and summer (circles) at Jungfraujoch. Vertical lines show 95% confidence intervals (Cui et al., 2011).

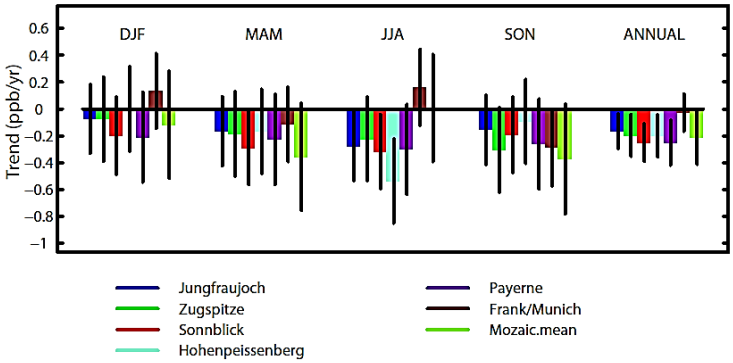

Figure 5.3. Seasonal and annual ozone trends (ppb/year) for sondes, MOZAIC data (681 hPa) and Alpine sites (1998-2008). Two standard errors are shown (Logan et al., 2012).

The studies regarding the European ozone trends of mountain stations are summarized in Table 5.3.

In the present work we took a longer period of time for investigation of ozone annual and seasonal trends: 1990-2011. The results are presented in Table 5.4. Here and further all indicated uncertainty ranges of trend values are capturing the 90% confidence interval, which means that there is 10% probability that the trend value is outside a given range.

Air quality policy measures (see section 2.1 “Air pollution control: policies”) and restriction of emissions led to significant reduction of anthropogenic emissions in the EU-27 (by 48 % for NOx, 59% for nonmethane VOCs, and 64% for CO) in the period 1990-2011 (LRTAP, EEA Technical report No 10, 2013) (Figure 5.4).

Table 5.3. Information on the studies about Alpine stations ozone trends.

Reference	Alpine station	Method	Resulting trends
Chevalier et al., 2007	JFJ, SNB and ZUG	9 year moving annual trends; 1991 - 2004	All positive. Decreasing trend from segment 1991–2000 to segment 1995–2004
Cui et al., 2011	JFJ	9-year moving seasonal trends; 1990 - 2008	Positive till segment 1997-2006, then zero trend and negative for 1999-2008
Logan et al., 2012	JFJ, SNB and ZUG	Annual trends; 1998-2008	Negative
Gilge et al., 2010	JFJ, SNB and ZUG	Annual trends; 1995-2008	Slightly positive or no change
Tarasova et al., 2009	JFJ	Annual trends; 1991-2001 and 1997-2006	Positive for 1991-2001, nearly no change for 1997-2006

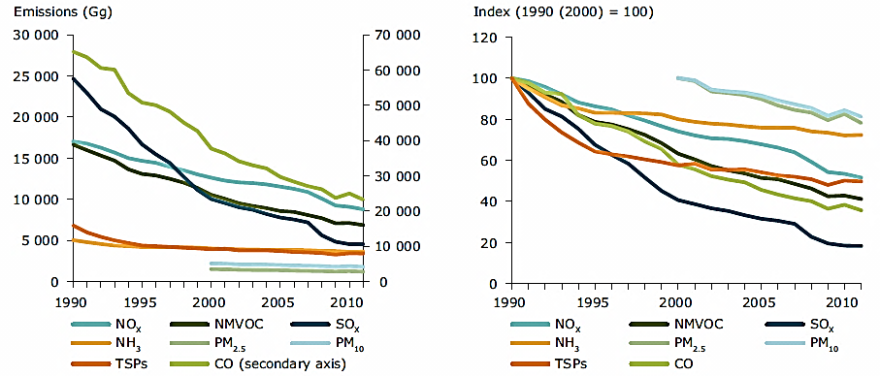

Figure 5.4. EU-27 emission trends for the main air pollutants and substances (EEA Technical report No 10, 2013).

The increase of ozone concentration in winter and slight decrease or no change in summer is observed on the ozone time series of SNB and ZUG for the period 1990-2011. For JFJ all seasons present positive trends, though the strongest in winter and weakest in summer time (Figure 5.5). Such results are consistent with the previously reported seasonal trends (Oltmans et al., 2006; Cui et al., 2011; Gilge et al., 2010). The seasonal ozone changes are explained first of all by a general increase of baseline ozone over Europe (Oltmans et al., 2006) and by the reduction of emissions since the early 1990s (Figure 5.4).

(a)

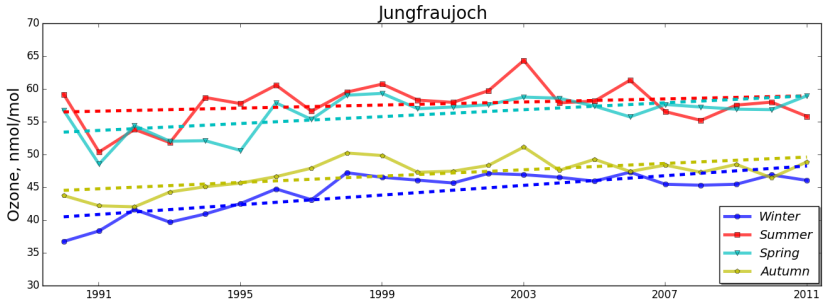

(b)

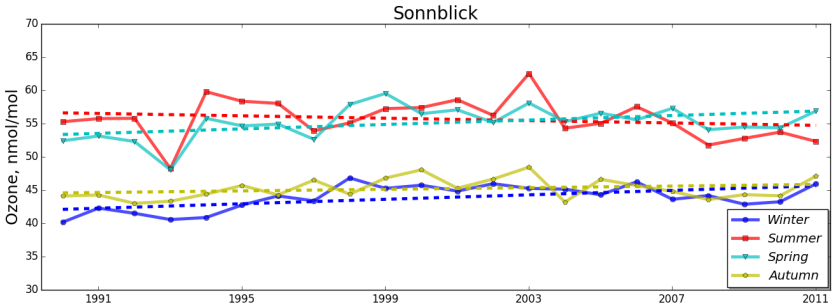

(c)

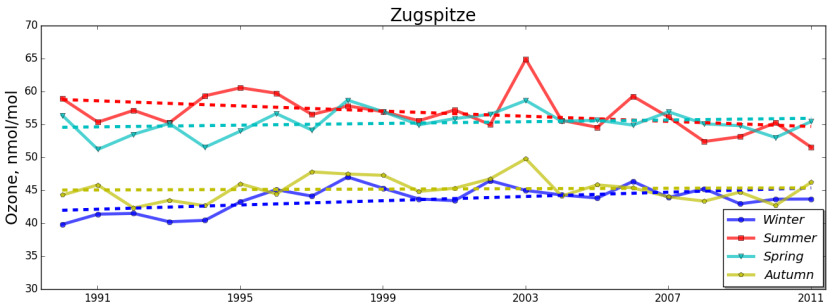

Figure 5.5, (a,b,c). Seasonal means of Jungfraujoch, Sonnblick and Zugspitze (1990-2011).

Baseline ozone is observed in the air which was not affected by freshly released emissions. As discussed in Cui et al. (2011), winter ozone is more influenced by the baseline air due to less vertical air mass exchange and better exposure to the free troposphere, while summer ozone is mainly dependent on the boundary layer ozone production. In the first case, it results in increase of winter ozone, because of positive baseline ozone trend and decreased ozone titration due to fewer emissions. In summer time, in contrast, less anthropogenic emissions would lead to the decrease of photochemical ozone production. But in summer ozone from the boundary layer also can be balanced with ozone coming from the free tropospheric air during the air mass exchange. This is

especially possible at mountainous sites. Because of these two factors summer ozone trend can vary from negative to positive. The last is observable only for the highest Alpine station JFJ, where the summer ozone slope is positive, but small and thus insignificant, while for lower sites ZUG and SNB there are ozone decline and insignificant change respectively (Table 5.4).

Table 5.4. Ozone seasonal trends for 1990-2011 and corresponding 90% CI, in nmol/mol per year.

	Jungfraujoch		Sonnblick		Zugspitze	
trend value, nmol/mol per year	winter	summer	winter	summer	winter	summer
	0.3691 ±0.1159	0.1168 ±0.1785	0.1679 ±0.0941	-0.0893 ±0.1775	0.1614 ±0.1008	-0.1948 ±0.1598
	annual		annual		annual	
	0.2382 ±0.1158		0.0952 ±0.1052		0.0031 ±0.0871	

On the seasonal means (Figure 5.5) there are two time-segments standing out on each plot, with a transition in the middle, when ozone noticeably stops to increase. We calculated slopes of trends for winter and summer time for two periods: 1990-1997 and 1998-2011, their trend values are given on the bar-plot (Figure 5.6).

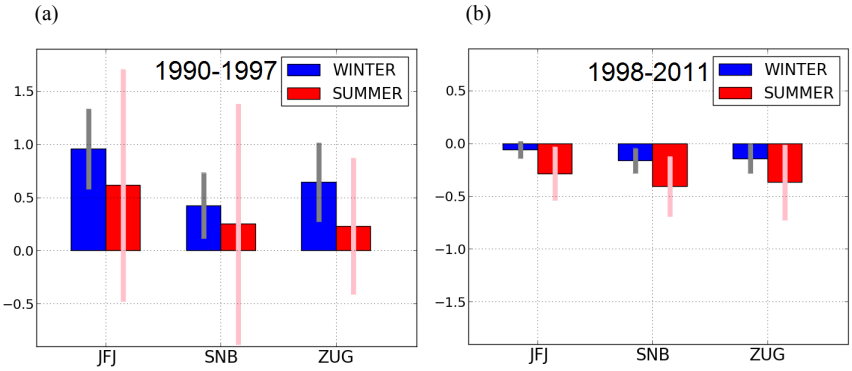

Figure 5.6, (a,b). Seasonal trends of Jungfraujoch, Sonnblick and Zugspitze for 1990-1997 and 1998-2011, in nmol/mol per year.

Indeed for all seasons we observe ozone growth during the first period of time (1990-1997), although insignificant in summer, and ozone decline - during the second period (1998-2011). Ozone decrease in 1998-2011 is mainly driven by summer time ozone, their trends are significant and negative winter time trends are quite small. This result is similar to annual trends values as shown in Logan (2012) for these stations, but for the period 1998-2008.

There are larger differences in the trends for the early period, which could point to problems with the measurement quality. To explain these differences with local emission changes alone is difficult.

Frequency distributions built from the hourly data of each station (not shown) have asymmetrical / skewed shapes with the maxima around 45-50 nmol/mol and a range of concentrations from 25 to 80 nmol/mol, therefore the tail of the curve is shifted towards higher concentrations. EMD values were obtained after comparing these frequency distributions for each pair of sites, and for 3 periods: 1990-1997, 1998-2011 and complete 1990-2011 (Table 5.5). Values are indicating little difference between the distributions. There were nearly no differences between all 3 sites for the earliest period, while it has grown because of JFJ for the later period, as its concentrations became generally higher than for SNB and ZUG. For the total period 1990-2011 JFJ shows more distinction from other Alpine sites still, and as also seen from monthly means (Figure 5.14), it had slightly lower ozone before 1998 and then higher afterwards in comparison to SNB and ZUG.

Table 5.5. EMD values for each pair of Alpine stations (see text).

	1990-1997		1998-2011		1990-2011	
	SNB	ZUG	SNB	ZUG	SNB	ZUG
JFJ	0.008	0.009	0.022	0.024	0.013	0.012
SNB	-	0.01	-	0.004	-	0.005

5.1.2 German stations (1990-2011)

The broader set of stations from the German Umweltbundesamt (UBA data network for ozone and other pollutants – see chapter "Data") is taken to consider trends over the larger territory for stations of different types. The UBA data was used together with metadata on station types and area types from Airbase. Most stations are at low altitudes, except for Schauinsland (1205 m), Schwarzwald Süd (920 m), Tiefenbach/Altenschneeberg (755 m) and Garmisch-Partenkirchen (735 m), which are mainly located close to the Alpine region. Data for NO_2 and O_3 were extracted and corresponding stations are shown on the maps (Figure 5.7).

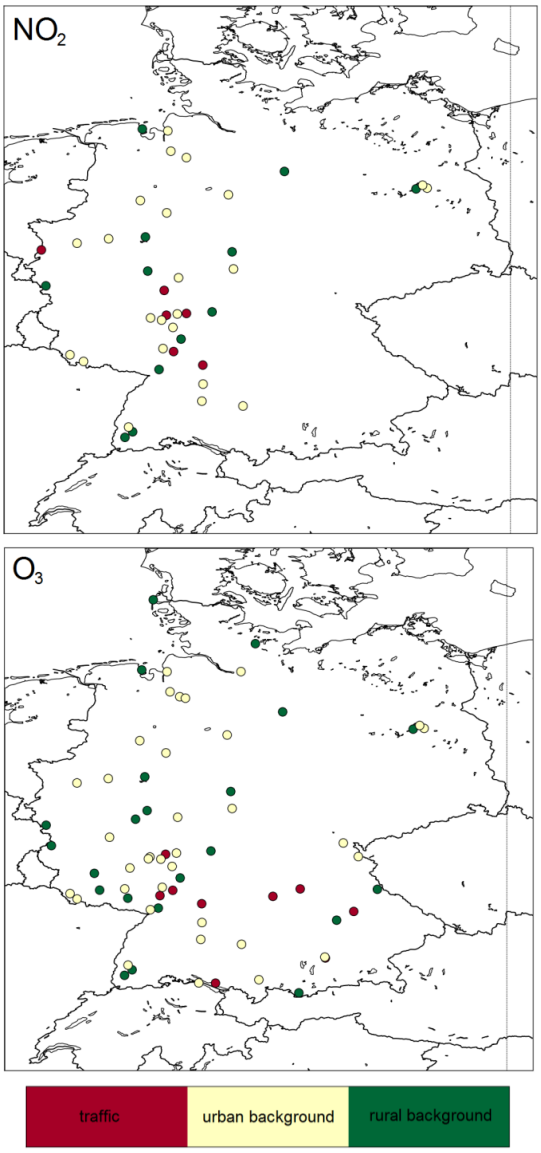

Figure 5.7. Map of German stations (UBA) used in this study with colors, corresponding to the station type (taken from Airbase). The sets of stations overlap, and contain 66 O_3 stations, and 41 NO_2 stations. O_3 stations: 22, 35, and 9 stations of rural background, urban background and traffic type respectively, NO_2 - 12, 23, and 6 stations correspondingly.

NO_2 annual means show continuous decrease during 1990-2011, as expected from the emissions reduction policies (Figure 5.8). The strongest decrease is observed for urban stations, the smallest for rural.

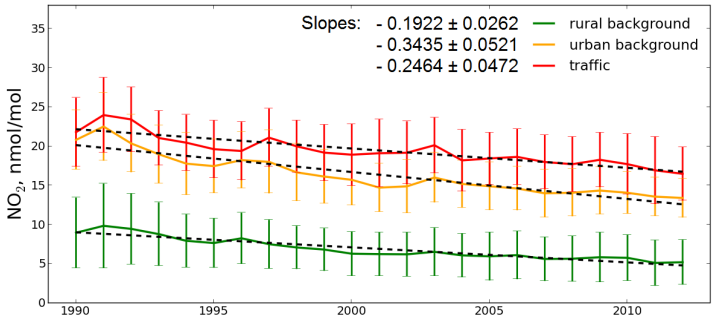

Figure 5.8. NO_2 annual means (1990-2011) with standard deviation. Slope values are in nmol/mol per year.

Ozone annual means show a pronounced increase for polluted sites (urban and traffic), while for rural stations the trend is small and not significant (Figure 5.9).

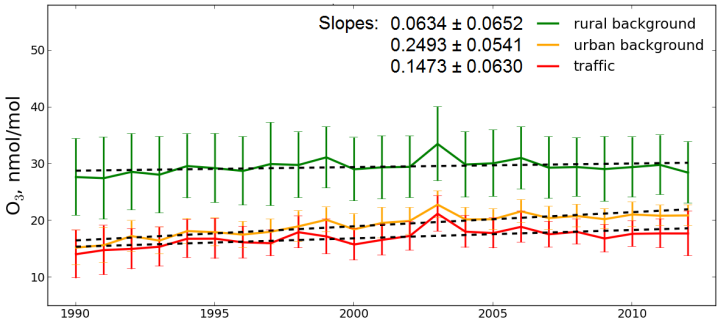

Figure 5.9. O_3 annual means (1990-2011) with standard deviation. Slope values are in nmol/mol per year.

Winter ozone trends show nearly the same growth for all 3 types of stations, which is in accordance with the winter NO_2 decline at all station types (Figure 5.10, b). Comparable ozone growth of the same order of magnitude was also observed for the Alpine stations JFJ, SNB and ZUG in winter time, and is explained by less ozone titration by NOx. In contrast, summer time ozone is more dependent on local photochemistry and intensive vertical mixing processes. The urban and traffic sites exhibit insignificant summer ozone trends, but visually slightly positive, while rural stations show a negative trend (Figure 5.10, a). This corresponds to NO_2 decrease for all stations, though more pronounceable for polluted sites.

(a)

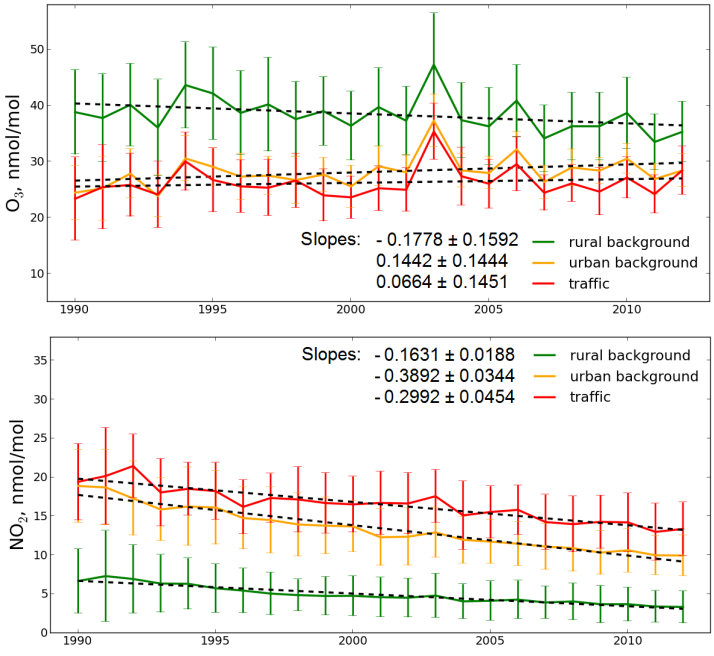

(b)

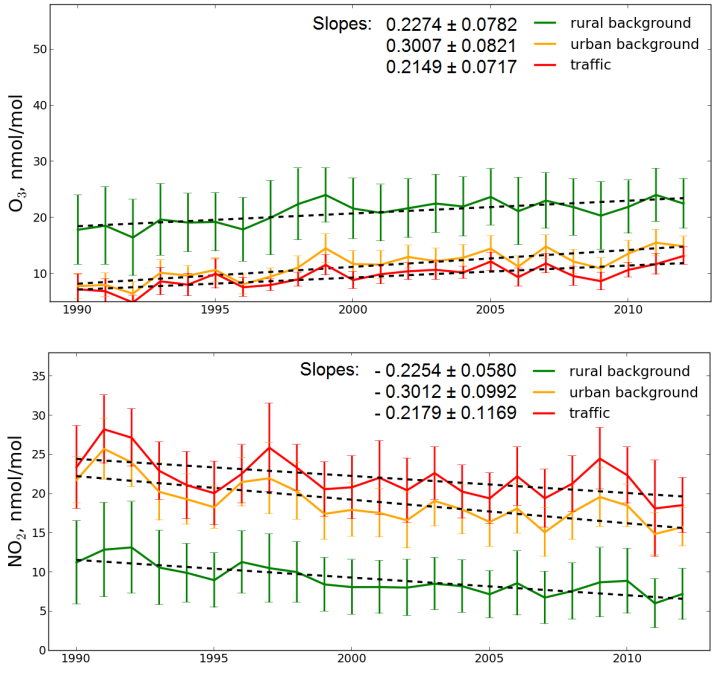

Figure 5.10, (a,b). O_3 and NO_2 seasonal means (1990-2011) with standard deviation: a – summer, b – winter. Slope values are in nmol/mol per year.

Similarly for SNB and ZUG we observed slightly negative ozone trends, for the highest station JFJ the ozone trend is insignificant due to stronger influence from the free troposphere air. If for rural stations with moderate NOx concentrations the ozone decline can also be explained by the drop of emissions, then in the case of urban and traffic stations with high NOx the insignificant ozone trend would correspond neither to baseline ozone changes like for JFJ nor to linear dependence between emissions and ozone.

As was mentioned in section "Tropospheric ozone budget" (chapter "Theory"), ozone production may have no change or decrease with the amount of VOCs decreasing, but is not linearly dependent on NOx (Figures 2.8, 2.9). From both figures we may see that if NOx concentrations decrease, O_3 production can either grow or shrink, dependent on the initial NOx and VOC/CO. At some VOC/CO concentrations on both plots decrease of high NOx leads to ozone growth, and further decrease of NOx results in ozone decline. This is consistent with the summer ozone trends for polluted stations, where NOx concentrations are elevated, and for relatively clean rural stations, where NOx is present in lesser amounts.

Hence despite general NOx emissions reductions since 1990s, the ozone trend at individual stations will depend on the station type, vicinity of traffic, industries, and on the ratio of VOCs to NOx concentrations.

5.1.3 Selected European stations (1998-2011)

In this section we analyze the representativeness of the three Alpine sites discussed above by comparing their monthly means and mean annual variations with data from other European background stations. We found several additional sites which fulfill the following requirements:

- temporal coverage:
  - continuously recorded data at least for 1998-2011 (the second time period, to compare with JFJ, SNB and ZUG). Exception were two stations: Iraty (1999-2010) and Great Dun Fell (2000-2011), which had no data for some years, but they were added in order to provide coverage over a larger region;
- spatial coverage:
  - semi - elevated or elevated stations (i.e. far from the local pollution sources);
  - relatively distant from each other stations in order to cover large area (to see how far the ozone pattern of high mountain stations can be still representative).

The list of stations fulfilling these requirements is presented in Table 5.6 and their locations are shown in Figure 5.11. Ozone data are given in nmol/mol. We note that most of these sites are listed in Airbase and classified there as background rural. The Airbase station classification was described in subsection 1.3.1 "Representativeness and stations categorization".

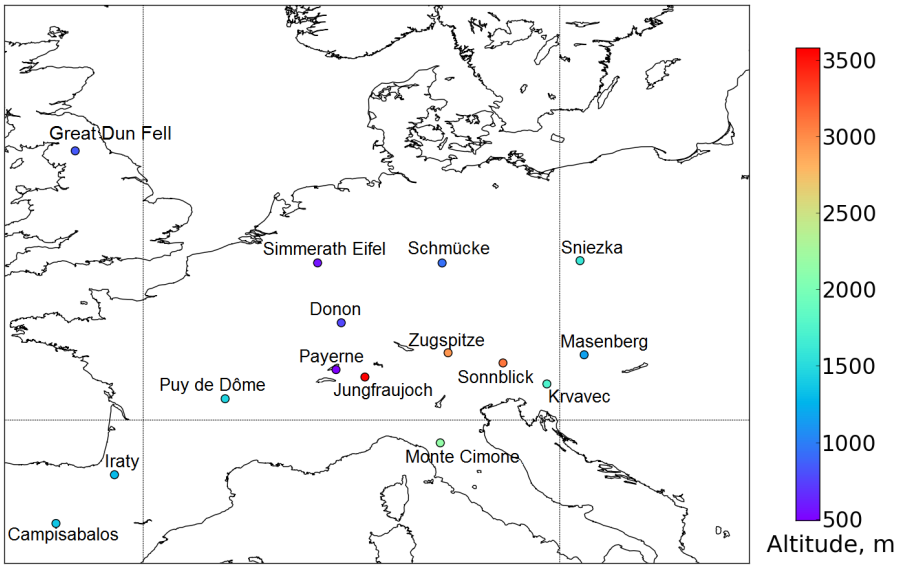

Figure 5.11. Map of the 15 European stations, chosen for the extended analysis of ozone trends.

At first we performed a trend analysis of annual mean values of the selected stations in the period 1998-2011. The resulting annual trend values are presented in Figure 5.12 and Table 5.7.

As discussed above, the three benchmark Alpine sites all show ozone decline after 1998. Almost all other stations confirm these negative ozone trends, though only slope values for Iraty and Great Dun Fell (Western Europe) as well as Masenberg and Donon (Central Europe) are significant. SNZK and PDD yield slightly positive trends which are, however, not significant.

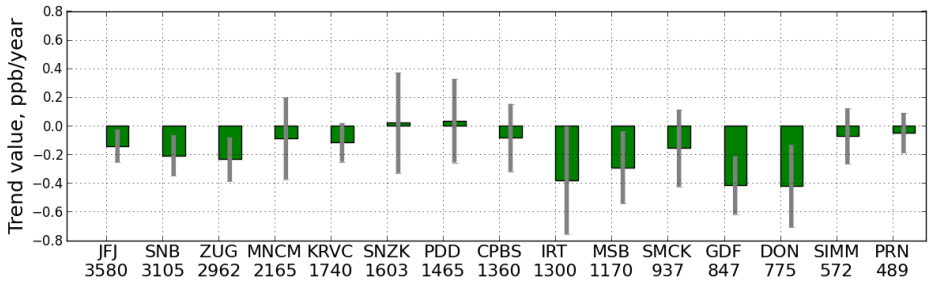

Figure 5.12. Annual mean trend values of 15 stations (1998-2011), errorbars correspond to 90% CI. Exception: IRT: 1999-2010 and GDF: 2000-2011.

Table 5.6. List of 15 European stations for analysis of the representativeness and trends.

station	abbrev.	lat.	lon.	alt., m	missing data inside 1998-2011	station type (Airbase)	source*
Jungfrau-joch	JFJ	46.55	7.99	3580		-	WDCGG
Sonnblick	SNB	47.05	12.96	3105		background rural	WDCGG
Zugspitze	ZUG	47.42	10.98	2962		background rural	personal communication
Monte Cimone	MNCM	44.18	10.7	2165		-	WDCGG (not in Airbase)
Krvavec	KRVC	46.3	14.54	1740		background rural	EMEP
Sniezka	SNZK	50.73	15.73	1603	beginning of 1998	background rural	EMEP
Puy de Dôme	PDD	45.77	2.95	1465	sum. 1998 and win. + spr. of 1999	background rural	PAES+EMEP
Campisa-balos	CPBS	41.28	-3.14	1360		-	EMEP (not in Airbase)
Iraty	IRT	43.03	-1.04	1300	all 1998 and 2011	background rural	EMEP
Masenberg	MSB	47.35	15.88	1170		background rural	EMEP
Schmücke	SMCK	50.65	10.77	937	all 2004	background rural	EMEP
Great Dun Fell	GDF	54.68	-2.45	847	all 1998 and 1999, beginning of 2000	background rural	EMEP
Donon	DON	48.5	7.13	775	all 2005, end of 2008	-	PAES+EMEP (not in Airbase)
Simmerath Eifel	SIMM	50.65	6.28	572	end of 2011	background rural	UBA
Payerne	PRN	46.81	6.94	489		background rural	EMEP

* see chapter “Data” for the information about the data networks.

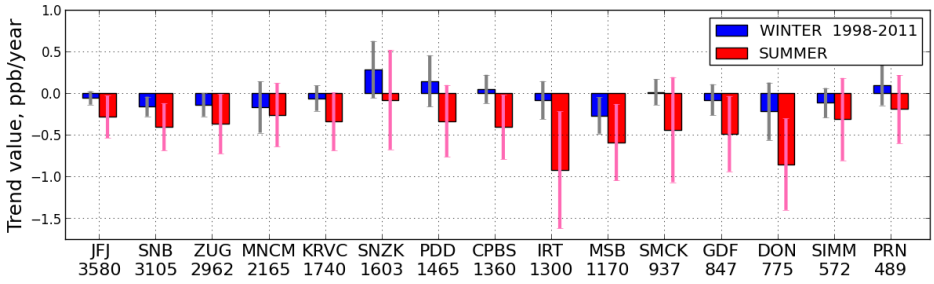

Figure 5.13. Seasonal mean trend values of 15 stations (1998-2011), errorbars correspond to 90% CI. Exception: IRT: 1999-2010 and GDF: 2000-2011.

A trend analysis of seasonal mean values underlines that the decrease of ozone trends during 1998-2011 is mostly driven by summertime ozone: trends are negative for most of the stations and usually are more pronounced than in winter (Figure 5.13).

Table 5.7. Annual mean trends and corresponding 90% CI (nmol/mol per year). Statistically significant trends are in bold.

station	trend for 1990-1997	trend for 1998-2011*
JFJ	**0.5870 ± 0.5799**	**-0.1410 ± 0.1143**
SNB	0.3362 ± 0.5409	**-0.2095 ± 0.1410**
ZUG	**0.3262 ± 0.2810**	**-0.2344 ± 0.1526**
MNCM		-0.0888 ± 0.2855
KRVC		-0.1175 ± 0.1356
SNZK		0.0202 ± 0.3505
PDD		0.0345 ± 0.2920
CPBS		-0.0838 ± 0.2361
IRT		**-0.3801 ± 0.3765**
MSB		**-0.2916 ± 0.2512**
SMCK		-0.1565 ± 0.2689
GDF		**-0.4154 ± 0.2025**
DON		**-0.4217 ± 0.2873**
SIMM		-0.0726 ± 0.1935
PRN		-0.0504 ± 0.1401

* for IRT: 1999-2010 and for GDF: 2000-2011.

This analysis shows that ozone trends are quite consistent within Europe, and one cannot identify different regions in Europe with respect to ozone trends. To proceed with the analysis we took ozone monthly means to estimate possibly existing differences between stations of different regions. Monthly means of JFJ, SNB, and ZUG (Figure 5.14) exhibit very good correlation, therefore in order to compare them with data from other stations, we take the mean of these three stations to avoid conglomeration of graphs. Further they are called as Alpine set.

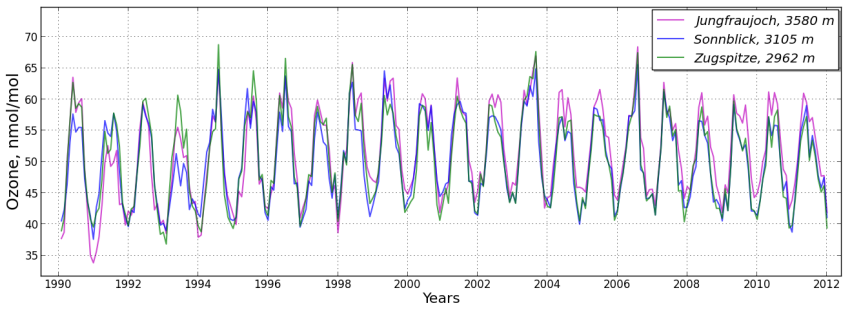

Figure 5.14. Monthly means of Jungfraujoch, Sonnblick and Zugspitze (1990-2011).

At first, we compare stations from the Alpine region and surroundings (Figure 5.15). Here we see quite coherent ozone monthly means of the Alpine set and Krvavec, as well as Monte Cimone with the exception of some of their summer peaks, especially during the period 2004-2007.

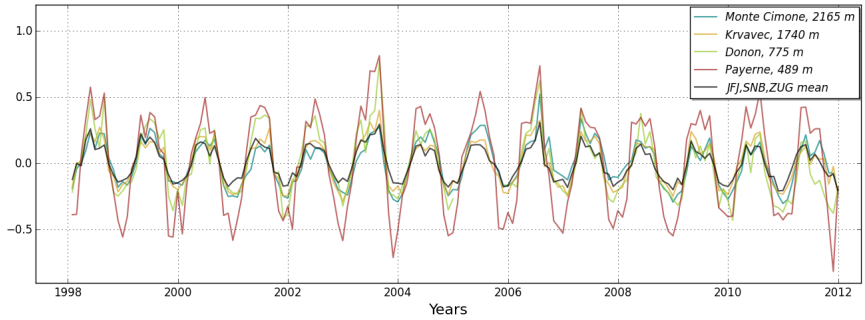

Figure 5.15. Comparison of normalized monthly means of stations from the Alpine region and surroundings (1998-2011).

Payerne's variability of ozone data is consistent with other time series, but the spring-summer maxima are spikier, although their shapes are generally similar. Payerne's normalized seasonal variability is much larger (Figure 5.15) than for high-mountain stations. Donon (775 m) is more like Payerne before 2004, but becomes more similar to the Alpine set and Monte Cimone after 2007. Donon and Payerne often show spiky maxima, but in general their monthly means correlate with the other stations (Figure 5.15).

Secondly, we considered the stations, which are remote to the North and North-West from Alpine region (Figure 5.16, a,b,c): Great Dun Fell and Simmerath. Generally there is some consistency between each pair of monthly means (Figure 5.16, a).

Simmerath presents a more variable seasonal pattern, but its minima and maxima are always coherent with Alpine set. The spikiness is possibly related to local influences, which can happen due to the relatively low altitude of the Simmerath station (572 m). In contrast, British Great Dun Fell presents a quite different ozone profile: it partly correlates with Simmerath, partly with the Alpine set in their seasonal shapes. Great Dun Fell exhibits strong spring maxima and summer minima, features which are also marked for the station Mace Head, located on the west coast of Ireland (Derwent et al., 2013).

The spring maximum has been described by Monks (2000) as a Northern Hemispheric phenomenon which occurs in mid-latitudes in the boundary layer and the lower free troposphere on the western edge of Europe (see also section 2.2.2 "Stratosphere - troposphere exchange"). Scheel et al. (1997) concluded that the annual maximum is shifted from spring to late summer in the northwest to southeast direction within Europe.

(a)

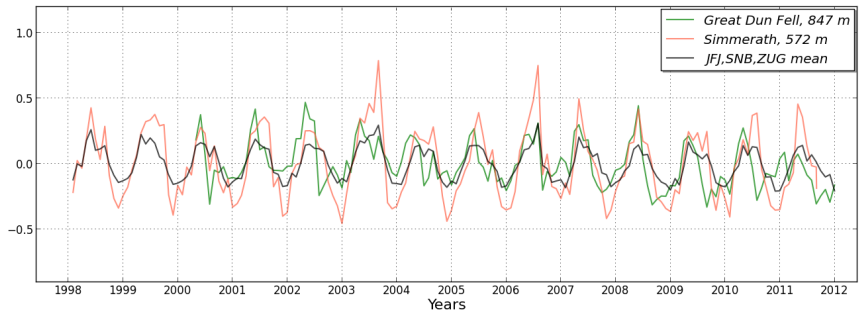

(b)

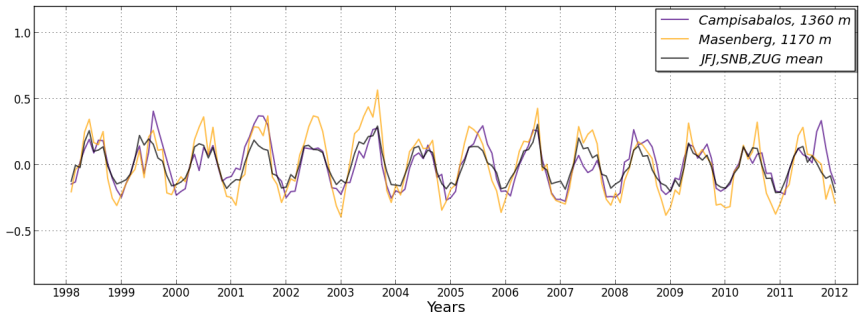

(c)

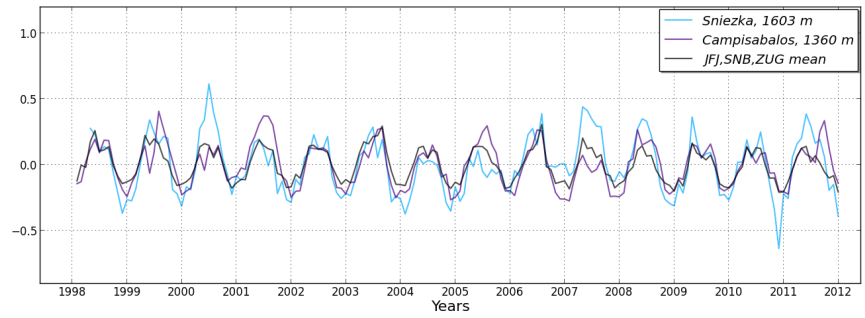

Figure 5.16, (a,b,c). Comparison of normalized monthly means of stations remote from Alpine region (1998-2011). In case of GDF: 2000-2011.

Stations taken from South-West to East (Spain – Poland, Spain - Austria): Campisabalos, Masenberg and Sniezka share quite good consistency with each other and with the Alpine set (Figure 5.16, b, c). Though summer maxima amplitudes and shapes are not always similar, the seasonality is in general correlating at these sites.

Note that the Eastern European station Masenberg has more pronounced spring maxima than the Western site Campisabalos in the years 1998, 2000, 2005, 2009 and 2011. The Polish station Sniezka exhibits somewhat different seasonal cycles (Figure 5.16, c), which are not always consistent with other sites. Some discrepancies in ozone behavior at Sniezka are appearing in the

summers of 2000, 2007, 2008 and 2011 (strong maximum), though seasonal amplitudes are generally in agreement with Campisabalos and Alpine set.

Comparing the Central European stations Masenberg, Schmücke, Simmerath with the Alpine set (Figure 5.17, a) we notice good correlation between their monthly means. Specific peculiarities of some years are visible in the time series of all these stations. Alpine stations have more obvious summer peaks in 2003 and 2006 (heat waves), while more spring maxima in other years. Other stations show noticeably increased amplitudes of the seasonal cycle in these two years in comparison to other years (see for example Donon and Payerne in Figure 5.15). There is furthermore good consistency among the stations, which are the most remote from each other: Monte Cimone, Campisabalos, Masenberg, and Simmerath (Figure 5.17, b).

At last, among western sites Iraty and Puy de Dome both exhibit rather consistent monthly means, but for each station the shape of the seasonal cycle varies from year to year. Their "western signature" is obvious due to the presence of spring maxima (Figure 5.18), and even summer heat waves of 2003 and 2006 seemingly have not influenced them much. Campisabalos, on the contrary, has more pronounced summer maxima every year and steady cycles, which are similar for some years to those of IRT and PDD, but mostly resemble Central European ozone pattern (Figure 5.16, Figure 5.17, b).

(a)

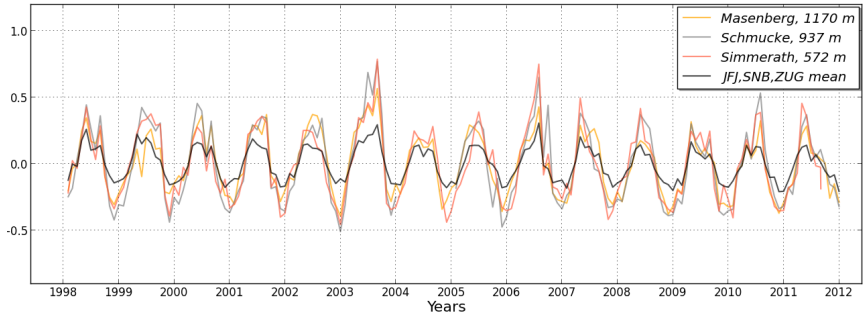

(b)

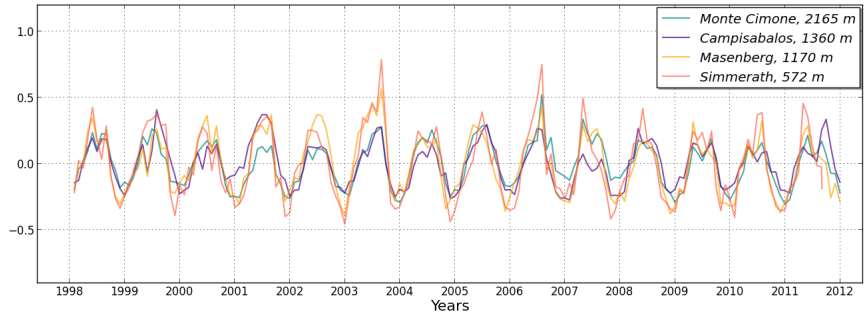

Figure 5.17, (a,b). Comparison of normalized monthly means of Central European stations (1998-2011) (Schmücke has no data for 2004).

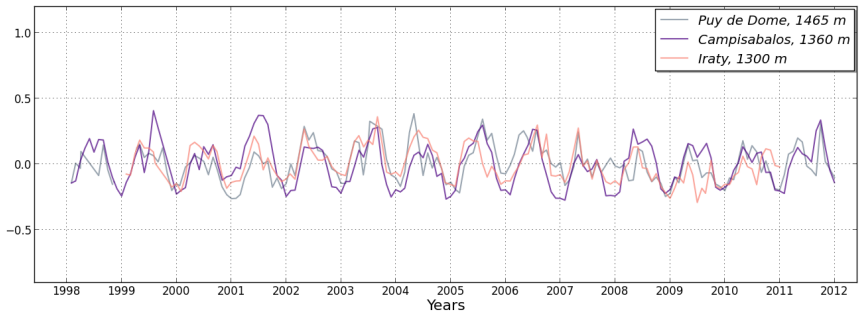

Figure 5.18. Comparison of normalized monthly means of western stations (1998-2011). In case of IRT: 1999-2010.

It is worth to mention that spiky maxima and sudden minima for IRT and PDD are often due to missing data for these stations, which have frequent small gaps in their data sets.

For the numerical comparison between data sets we took the normalized seasonal cycles calculated for the available periods of time for each station (Figure 5.19, a,b,c). All cycles are grouped in comparison to those of Alpine stations, which represent slight maxima in April, and JFJ also shows a small peak in July. In general the cycle amplitude is decreasing from the first group (a) to the third (c). In the first figure (Figure 5.19, a) there are only Central European stations, located to the North and East from Alpine region, which represent similar shapes of their cycles. Two exceptions are Sniezka, which doesn't have a summer maximum, and Payerne, which shows a large seasonal amplitude with a broad June-July maximum. This group is reflecting generally similar patterns of seasonality. The differences like amplitude and spring maxima are related to the altitude of stations, therefore we see the change from the smooth cycles of Alpine sites to the convex cycles of lower stations.

The high altitude southern stations Monte Cimone, Krvavec and Campisabalos (Figure 5.19, b) exhibit very similar cycles and reproduce features of JFJ, SNB and ZUG cycles especially well in spring and autumn. The only difference is a stronger summer maximum in July and therefore a slightly larger seasonal amplitude. Spanish Campisabalos also has a noticeable minimum in May, similar to the western sites Iraty and PDD, which express the same feature (Figure 5.19, c). But in contrast to Campisabalos, they exhibit no summer maxima, therefore only April shows the highest ozone concentrations for Iraty and PDD. At last, British Great Dun Fell, which was already discussed, shows a specific seasonal profile with a pronounced spring maximum and summer minimum continuing till winter. It is therefore different from all other European cycles (Figure 5.19, c) and only partially similar to western stations.

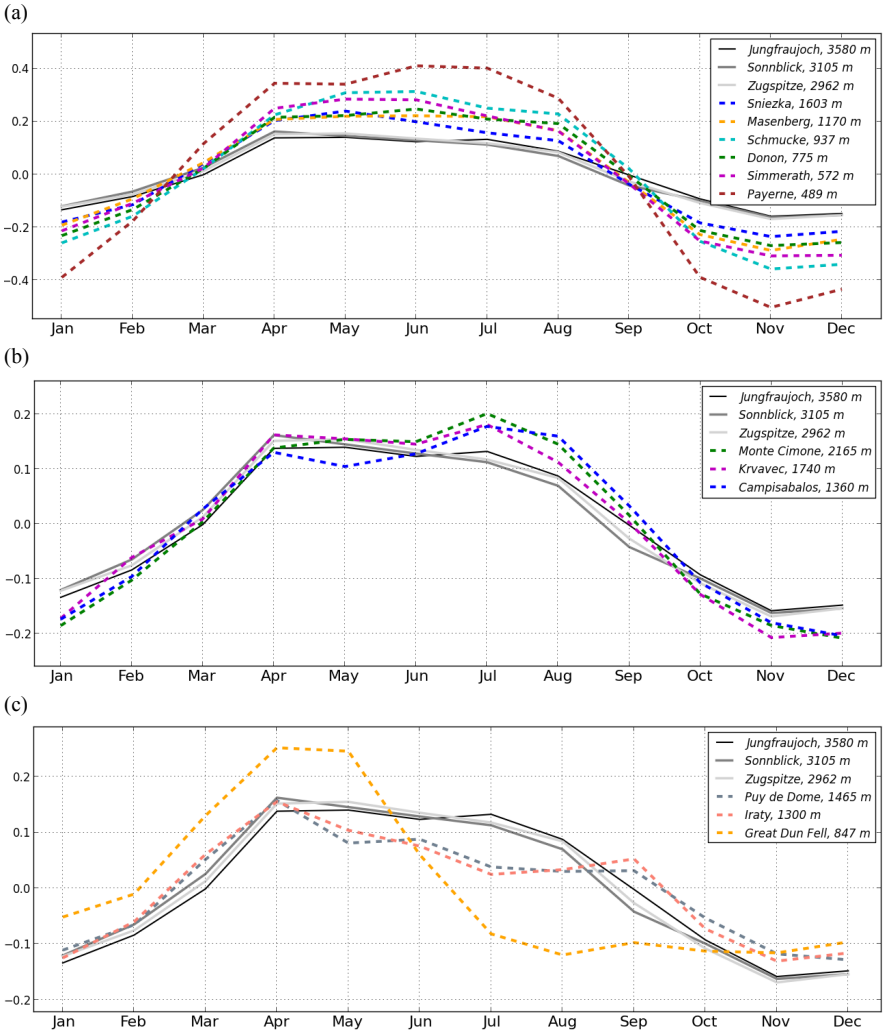

Figure 5.19, (a,b,c). Normalized seasonal cycles of 15 European stations.

The numerical comparison of the normalized seasonal cycles is given in Table 5.8, where each value is the Euclidean distance between pairs of cycles. Sites in the same group are marked with the same color. The smallest values are expected for JFJ, SNB and ZUG, but also within groups between some stations, for example Monte Cimone and Krvavec, Monte Cimone and Campisabalos, PDD and Iraty, Masenberg and Donon. Even though the seasonal pattern of the Central European sites is similar to the shapes of the Alpine set, their seasonal cycles distances are larger, while Southern Monte Cimone, Krvavec and Campisabalos, as well as western PDD and Iraty are closer to the Alpine set.

Table 5.8. Correlations (Euclidean distances) between normalized seasonal cycles of station pairs (see text).

	JFJ	SNB	ZUG	MNCM	KRVC	SNZK	PDD	CPBS	IRT	MSB	SMCK	GDF	DON	SIMM	PRN
JFJ		0.07	0.05	0.13	0.11	0.22	0.16	0.13	0.17	0.29	0.48	0.4	0.31	0.39	0.81
SNB			0.03	0.17	0.13	0.21	0.15	0.17	0.16	0.29	0.49	0.35	0.32	0.39	0.81
ZUG				0.15	0.11	0.19	0.17	0.15	0.17	0.27	0.47	0.37	0.3	0.37	0.79
MNCM					0.07	**0.16**	0.27	0.07	0.28	0.2	0.37	0.5	0.21	0.3	0.7
KRVC						**0.15**	0.25	0.1	0.25	0.2	0.39	0.46	0.22	0.3	0.71
SNZK							0.34	0.21	0.33	0.11	0.29	0.46	0.13	0.19	0.61
PDD								0.24	0.05	0.42	0.6	**0.33**	0.44	0.51	0.93
CPBS									0.24	0.25	0.42	0.5	0.26	0.36	0.74
IRT										0.41	0.6	**0.32**	0.43	0.51	0.92
MSB											0.22	0.55	0.08	0.12	0.53
SMCK												0.73	0.18	0.14	**0.36**
GDF													0.59	0.61	1.02
DON														0.12	0.51
SIMM															0.44

Euclidean distances show that Sniezka is rather similar not to the neigbouring station Schmucke, but to the more southern stations Masenberg and Donon, moreover also to the mediterranean stations Monte Cimone and Krvavec. Great Dun Fell and especially Payerne show big distances to all other stations, with only Schmucke being relatively close to Payerne, and PDD and Iraty – to Great Dun Fell. Yet the seasonal cycles are quite different for these pairs.

To summarize, with two exceptions ozone concentrations at all stations considered in this analysis have negative linear trends after 1998 which are driven by summertime ozone. According to the analysis of seasonal cycles and interannual variability there are three geographical areas of different ozone behavior – Western, Southern and Central Europe. Stations in the first region generally exhibit a springtime maximum, ozone data from the second region shows a summertime maximum, while Central European stations may exhibit both of them. Within each region, the stations generally show a rather consistent pattern of seasonal cycles and interannual variability, and at nearly all of them there are pronounced summer peaks in the years of European heat waves in 2003 and 2006. There are two exceptions to this: Great Dun Fell (Great Britain), which does not fit with the pattern of any other station, and Campisabalos (Spain), which shows a combination of Western and Southern patterns.

Thus we conclude that Alpine stations represent regional patterns of tropospheric ozone over large parts of Europe, or more specifically Central Europe. Certain patterns of seasonal and interannual behavior appear also for stations in Western and Southern Europe. The differences of mean annual variations obtained for 3 European regions lead to a deeper analysis of the ozone representativeness.

5.2 Cluster analysis

To repeat from section 3.2.2 “Properties for cluster analyses”, we name our different CAs and corresponding sets of properties according to the order, in which they were made:

- first CA, or 1st CA – based on 96 properties of seasonal - diurnal ozone variations (absolute values) or first set of properties (96 abs PR);
- second CA, or 2nd CA – based on 96 properties of seasonal - diurnal ozone variations (normalized values) or second set of properties (96 norm PR);
- third CA, or 3rd CA – based on 20 properties of seasonal and diurnal ozone averaged cycles (normalized values) or third set of properties (20 norm PR).

The stations that were analyzed in the previous section 5.1 "Trend analysis" measured different ozone levels, and varied in the shape of seasonal cycles and their amplitudes. All 12 stations are relatively elevated and most of them are background rural sites implying low pollution levels. But there are much more European stations, which are influenced by local pollution to a greater extent, and this should be reflected on their time series. Based on this, one may expect various ozone profiles all over Europe, therefore on the local scale the statement about representativeness of Alpine stations is not correct.

As described in the "Introduction", one of the aims of the present work is to identify European air quality ozone regimes, based on the available data sets from all over Europe, so that each regime would be representative for some group of stations and correspond to specific patterns of the ozone behavior typical inside the group. The main focus is shifted from the temporal ozone evolution to the spatial distribution of different ozone pollution patterns over Europe.

Secondly, the obtained in the CAs groups are then further used for the evaluation of MACC model output.

5.2.1 Geographical distribution and cluster allocation of stations

5.2.1.1 First CA

The spatial distribution of the 1492 Airbase stations and their cluster number obtained after the 1st CA are shown in Figure 5.20. Evidently, the five clusters do not simply represent different regions in Europe, although the members of cluster 1 (CL1) and cluster 2 (CL2) are concentrated in the Benelux and Ruhr region and in the Po Valley region, respectively. CL1 extends from Slovenia to Great Britain through the Netherlands, but also includes stations from France, Italy, Spain and Eastern Europe. Besides the Northern Italian stations CL2 also consists of a few stations in the Alpine region, the North-Western Balkans and in Spain. The third cluster (CL3) is much larger in its spatial extension and contains stations from almost all over Europe, including Scandinavia. The fourth cluster (CL4) spreads all over Europe with increased density along the Mediterranean coast and in the mountainous areas to the North and East of the Alps, the Bohemian Massif, and the Carpathian Mountains. Finally, the smallest cluster (CL5) largely overlaps with the mountainous regions of the Alps, the Pyrenees, Spain, and the Carpathians.

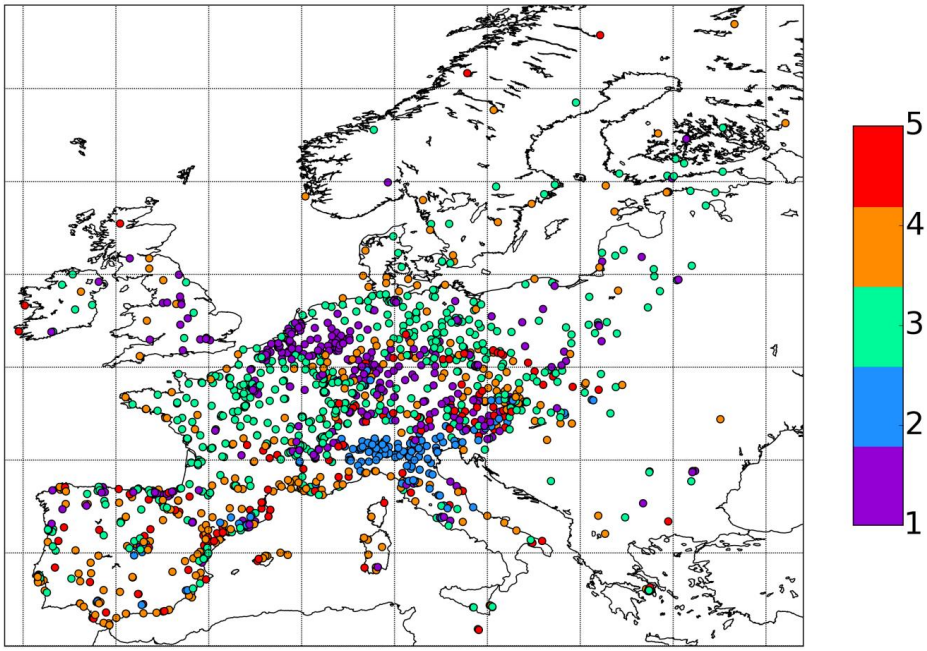

Figure 5.20. Map of 1492 Airbase stations clustered in 5 groups, 1st CA.

Table 5.9 presents a qualitative interpretation of the five clusters and Figure 5.21 shows the distribution of station altitudes for each cluster. The cluster descriptions were derived based on the geographical and altitude distribution together with some information on the expected pollution type and level, which was obtained from the station descriptions in Airbase (see next section 5.2.2 "Comparison with the Airbase station classification scheme").

Table 5.9. Cluster statistics and description based on the Airbase classification, geographical location and altitude range of clusters. 1st CA.

cluster	cluster description	number of stations
1	urban, traffic	382
2	urban/suburban, industrial, Po Valley	155
3	background, moderately polluted	524
4	rural, remote, coastal, background, middle-elevated	304
5	rural, background, elevated	127

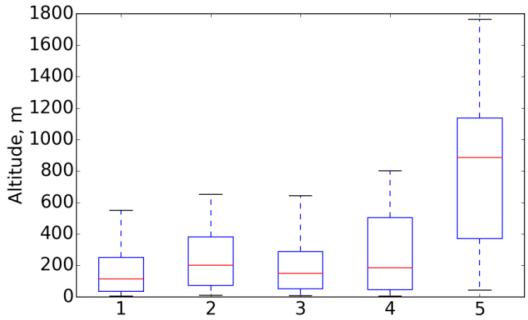

Figure 5.21. The 5-25-50-75-95 percentile distributions of station altitudes in the clusters. 1st CA.

5.2.1.2 Second and third CA

The 2nd and 3rd CAs show similar allocations of stations to clusters. A comparison of those runs is given in Table 5.10. There are 88.3% of stations (i.e. 1317 out of 1492) assigned to the same cluster in these CAs (diagonal values of Table 5.10). For this reason analogous maps of the 1492 Airbase stations and their allocations to clusters look nearly the same for the 2nd and 3rd CA, with some minor differences (Figure 5.22, 5.23).

Interestingly, the first cluster of the 3rd CA contains a few more stations than in the 2nd CA, capturing not only the stations from the Po Valley and middle Italy, but also partly the South of Pyrenees. Additionally the 2nd cluster has fewer stations in Spain in the 3rd CA.

Table 5.10. Contingency table with number of stations for each cluster: 2nd CA (96 norm PR, rows) vs 3rd CA (20 norm PR, columns).

cluster	CL1	CL2	CL3	CL4
CL1	**97**	11	0	0
CL2	24	**377**	55	0
CL3	0	51	**475**	25
CL4	0	0	9	**368**

The 1st cluster of the 2nd and 3rd CAs corresponds to the 2nd cluster of the 1st CA, but it is not containing stations from the Alpine region. The 2nd cluster is much larger and spreads over the Benelux and Ruhr regions in the Center of Europe, capturing partly France, Switzerland and Eastern Europe, so it is partially overlapping with the 1st cluster from the 1st CA.

The 3rd cluster extends all over Europe and has several stations in Scandinavia. This cluster contains the highest number of stations. The 4th cluster includes high-mountain stations from the Alpine region and the Pyrenees, from the mountainous areas to the North and East of the Alps, the Bohemian Massif, and the Eastern part of the Carpathian Mountains. Moreover it includes low-

altitude stations from Spain, France, Great Britain, Scandinavia and the Mediterranean coast. Geographically it is a mix of stations from nearly all clusters of the 1st CA.

In Table 5.11 the comparison between the 1st CA and 2nd CA results are presented. Tables 5.12 and 5.13 give information about the size and description of each cluster, while Figure 5.24 shows the altitude range.

With the help of these tables and the geographical representation we come to the conclusion that the clusters from different CAs have some common features. For example, the 1st "Po Valley" cluster of the 2nd CA contains fewer stations, which are mostly concentrated in the North of Italy, than the 2nd cluster of the 1st CA, and it contains fewer stations of higher altitudes. The second cluster has the majority of stations, which were assigned to the first cluster in the 1st CA, and moreover captures also stations of the 2nd and 3rd clusters of the 1st CA. However, it appears as more elevated agglomeration. The 3rd cluster shares 326 stations out of more than 500 with the 3rd cluster of the 1st CA, resembling it also geographically and in altitude. It is the largest cluster in all CAs. The 4th cluster is containing both high and low altitude stations. It includes completely the 5th cluster and has some stations from 4th and 3rd clusters of the 1st CA. Therefore on average the 4th cluster is semi-elevated with the mean altitude 433 m for the 2nd CA and 415 m for the 3rd CA.

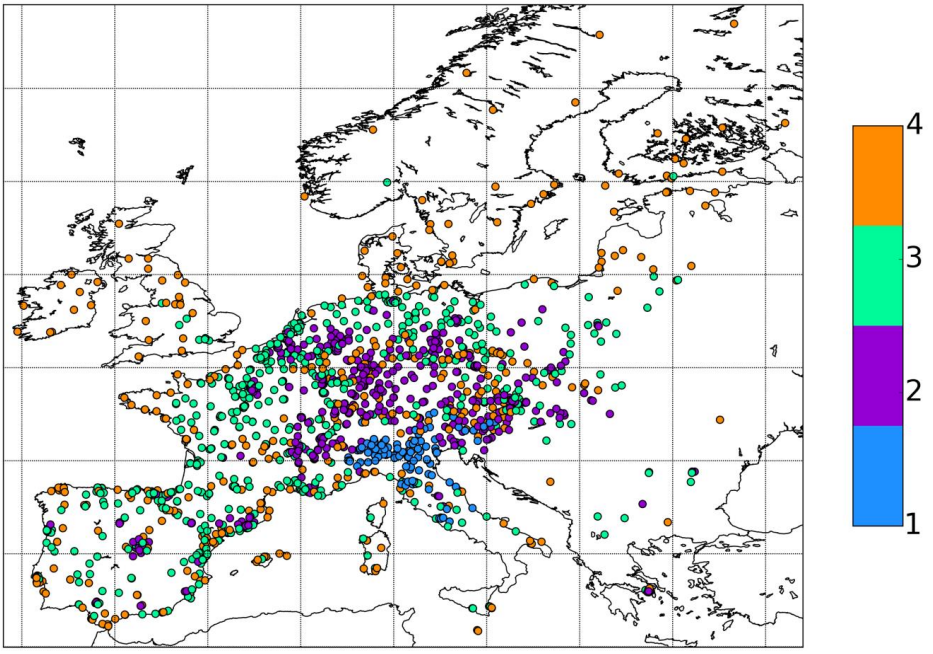

Figure 5.22. Map of 1492 Airbase stations clustered in 4 groups, 2nd CA.

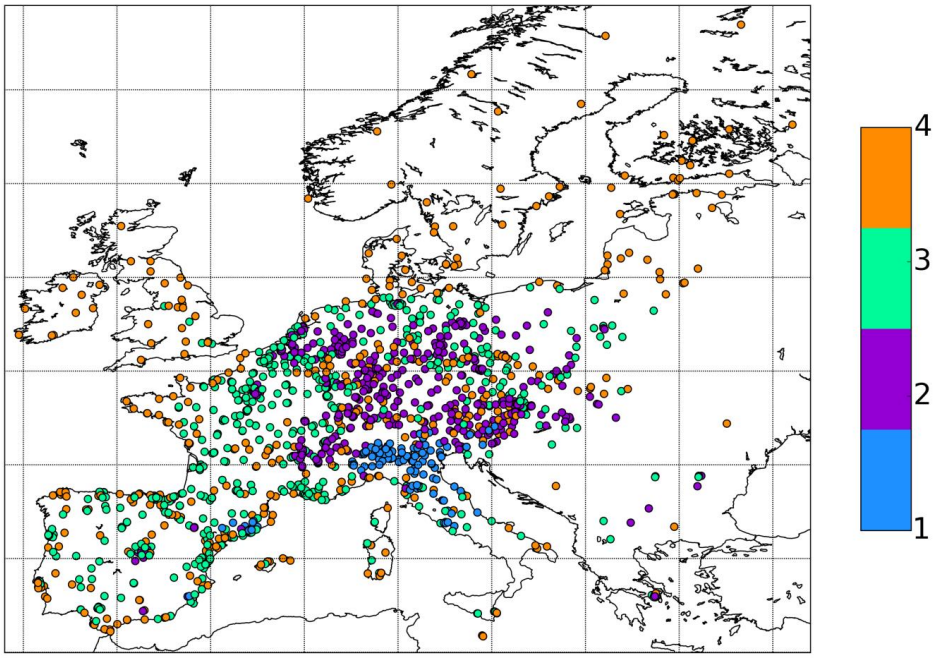

Figure 5.23. Map of 1492 Airbase stations clustered in 4 groups, 3rd CA.

Table 5.11. Contingency table with station distribution in clusters: 1st CA (96 abs PR, rows) vs 2nd CA (96 norm PR, columns).

cluster	CL1	CL2	CL3	CL4
CL1	23	**251**	88	20
CL2	**85**	**67**	3	0
CL3	0	135	**326**	63
CL4	0	3	134	**167**
CL5	0	0	0	**127**

Table 5.12. Cluster statistics and description based on the Airbase classification, geographical location and altitude range of clusters. 2nd CA.

cluster	cluster description	number of stations
1	Po Valley, urban, traffic	108
2	urban/suburban, industrial, traffic	456
3	moderately polluted (urb., sub., rur.), industrial, traffic	551
4	rural, remote, coastal, background, middle -elevated, industrial	377

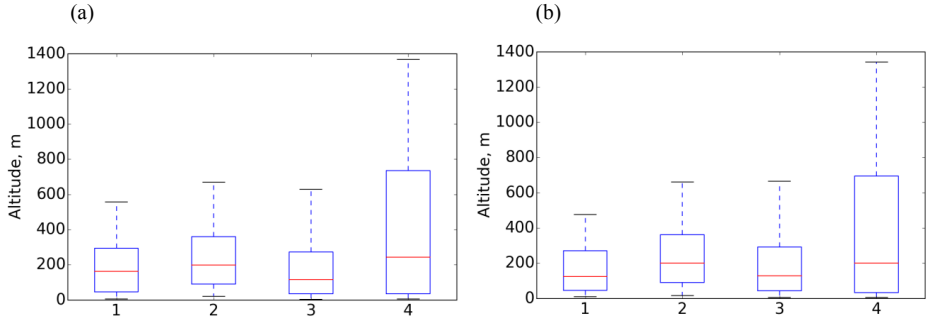

Figure 5.24 (a,b). The 5-25-50-75-95 percentile distributions of station altitudes in clusters. (a) 2nd and (b) 3rd CA.

Table 5.13. Cluster statistics and description based on the Airbase classification, geographical location and altitude range of clusters. 3rd CA.

cluster	cluster description	number of stations
1	Po Valley, urban, traffic	121
2	urban/suburban, traffic	439
3	moderately polluted (urb., sub., rur.), industrial, traffic	539
4	rural, remote, coastal, background, middle-elevated, industrial	393

5.2.2 Comparison with the Airbase station classification scheme

According to the Airbase classification ("Introduction", section 1.3.1 "Representativeness and stations categorization") stations are marked as either "urban", "suburban" or "rural" depending on the area type and as "traffic", "industrial" or "background" according to the station type. A comparison of this classification with the results of the 1st, 2nd and 3rd CAs is given in Tables 5.14, 5.15 and 5.16. Each row in there corresponds to one of the Airbase clusters and shows the number of stations related to each of 9 Airbase classification pairs.

Most of the stations that we retained in our data filtering procedure (chapter "Data", section 3.2.1 "Data filtering") are background stations, which could indicate that there are no local pollution sources in the vicinity and measured concentrations should ideally be representative for a larger area (and hence suitable for the evaluation of numerical models), except when local orographic effects confound the analysis. There is a relatively even split between rural, suburban, and urban background stations. Industrial and traffic stations constitute about 10-15% each and are concentrated in the suburban and urban environments, respectively.

For the 1st CA CL1 has a significant contribution of urban background and urban traffic stations. CL2 represents predominantly urban and suburban background stations, but 15% of stations show

traffic or industrial influences. CL3 has a similar percentage (≈ 35%) of urban stations, classified as "background" in the Airbase database, but it also has large contributions of rural and suburban stations (both are ≈ 50% in CL3), therefore we assume that CL3 is moderately polluted. CL4 and CL5 consist mainly of rural background stations, whereby CL4 has the higher share (15%) of industrial stations. CL5 is the least polluted cluster with ≈ 81% of the stations being characterized as "rural background" in the Airbase database.

According to the pollution level the five clusters of the 1st CA could be ranked as follows: CL1 would be the most polluted, followed by CL2 and CL3. CL4 and CL5 might be considered relatively clean.

For the 2nd and 3rd CAs the tables are quite similar (Tables 5.15, 5.16). For the 2nd CA CL1 consists of 52% urban background stations and 10% traffic stations of suburban and urban area types, while CL2 has ≈ 65% of both suburban and urban background stations and ≈ 10% of industrial and 15% of traffic stations. Therefore both CL1 and CL2 are polluted, but relying only on this information it is difficult to estimate which is in higher extent. CL1 has a greater portion of stations characterized as "urban" in the Airbase database, while CL2 has industrial stations and more traffic ones. There is no such distinction between CL1 and CL2 (3rd CA) as they are showing similar percentage ratios of all types of stations with the only difference that CL1 retains ≈ 10% more urban background stations than CL2. CL3 has nearly equal amounts of rural, suburban and urban background stations, but still has ≈ 10% of stations of each traffic and industrial types. Finally CL4 predominantly consists of rural stations (≈60%) with 15% of background urban and 10% of industrial stations in the 2nd CA.

The level of pollution can be assessed as the highest at CL1 and CL2, followed by the moderately polluted CL3 and the relatively clean CL4 (2nd and 3rd CAs).

Table 5.14. Contingency table, showing the distribution of stations in clusters (rows) and in Airbase classification groups (columns). Abbreviations: Bac – background, Ind – industrial, Trf – traffic, Rur – rural, Sub – suburban, Urb – urban. 1st CA.

CL	BacRur	BacSub	BacUrb	IndRur	IndSub	IndUrb	TrfRur	TrfSub	TrfUrb	total
1	30	78	134	3	22	11	6	13	85	382
2	22	45	64	2	6	3	1	3	9	155
3	117	147	184	12	20	11	1	4	28	524
4	135	53	50	16	22	10	0	3	15	304
5	103	12	1	5	3	1	0	0	2	127
total	407	335	433	38	73	36	8	23	139	1492
		Bac	1175		Ind	147		Trf	170	
		Rur	453		Sub	431		Urb	608	

Table 5.15. Contingency table, showing the distribution of stations in clusters (rows) and in Airbase classification groups (columns). 2nd CA.

CL	BacRur	BacSub	BacUrb	IndRur	IndSub	IndUrb	TrfRur	TrfSub	TrfUrb	total
1	14	25	56	0	1	0	0	1	11	108
2	46	136	154	6	29	11	6	10	58	456
3	129	140	162	17	30	15	2	10	46	551
4	218	34	61	15	13	10	0	2	24	377
total	407	335	433	38	73	36	8	23	139	1492
		Bac	1175		Ind	147		Trf	170	
		Rur	453		Sub	431		Urb	608	

Table 5.16. Contingency table, showing the distribution of stations in clusters (rows) and in Airbase classification groups (columns). 3rd CA.

CL	BacRur	BacSub	BacUrb	IndRur	IndSub	IndUrb	TrfRur	TrfSub	TrfUrb	total
1	14	26	53	0	8	1	0	5	14	121
2	42	136	159	7	19	7	7	6	56	439
3	133	137	154	15	31	17	1	9	42	539
4	218	36	67	16	15	11	0	3	27	393
total	407	335	433	38	73	36	8	23	139	1492
		Bac	1175		Ind	147		Trf	170	
		Rur	453		Sub	431		Urb	608	

5.2.3 Cluster representatives

5.2.3.1 First CA

Table 5.17 lists the five stations which have the smallest Euclidian distance to the respective cluster centroid, and which should therefore be "typical" for each cluster. The time series (hourly ozone concentrations) for each of these stations are shown in Figure 5.25 and their seasonal and diurnal cycles are shown in Figure 5.26.

Table 5.17. Stations closest to the cluster centroids (information from the Airbase database). 1st CA.

CL	station ID	station type	station area type	longitude	latitude	alt., m
1	DENW096	background	suburban	6.43	51.15	78
2	IT0950A	background	urban	11.89	43.46	260
3	FR34062	background	urban	1.33	47.59	70
4	DEBW037	background	suburban	8.41	48.47	750
5	AT80503	background	rural	9.93	47.53	1020

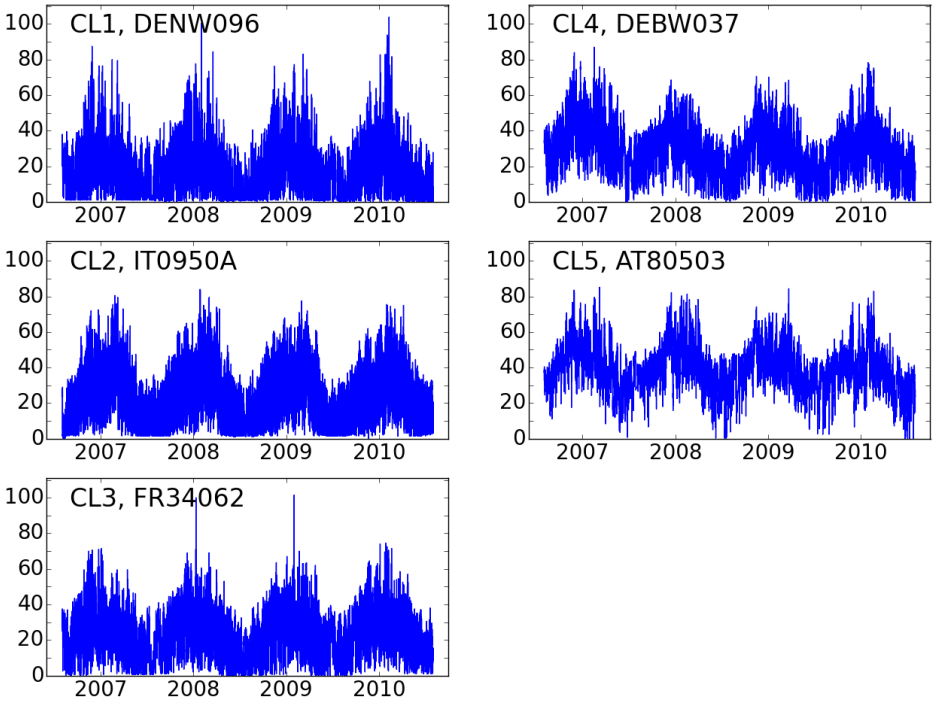

Figure 5.25. Time series of the stations representing the clusters (in nmol/mol). 1st CA.

As seen from Figure 5.25, the time series of stations from the predominantly urban and suburban clusters 1, 2 and 3 exhibit high ozone variability. Ozone destruction by titration with NO at these stations is quite apparent during wintertime but also happens during summer. In contrast, the station representing CL4 shows low ozone concentrations only in winter time, while the station that illustrates CL5 has nearly no ozone titration throughout the year. Clearly, ozone data from the mountain station AT80503 (CL5) exhibits the least variability among these time series. Stations in CL5 usually have low diurnal variability (Figure 5.45) as well as larger average concentrations (Figure 5.35).

Much of the high-frequency variability at the suburban site (CL1) is caused by local pollution sources, which cannot be resolved in a coarse scale CTM. In contrast, the remote site (CL5), where ozone concentration changes are often influenced by large-scale weather patterns, exhibits less variability, so that this time series is expected to be reproduced in a coarse scale CTM. Obviously, characterizations such as “urban”, “rural” or “remote” can at best be qualitative and they will often depend on a subjective judgment when analyzing the observations.

As we may see from Figure 5.26 the seasonal and diurnal cycles of representative stations are different in their average ozone concentrations as well as the shape of the cycle, but their amplitudes are comparable except for CL5 and CL2. 5- and 95-percentiles of the seasonal and diurnal cycles are

calculated from the hourly values (i.e. retaining diurnal variability), but nevertheless they show not much distinction between clusters except probably for CL2. For example, "typical" station of CL5 has the highest mean, the highest level of 5- as well as 95-percentiles, while representative of CL1 has the lowest values of these quantities. This proves that the 1st CA distinguishes clusters mainly by the average ozone concentrations, and only to a lesser extent by seasonal-diurnal amplitudes and variability.

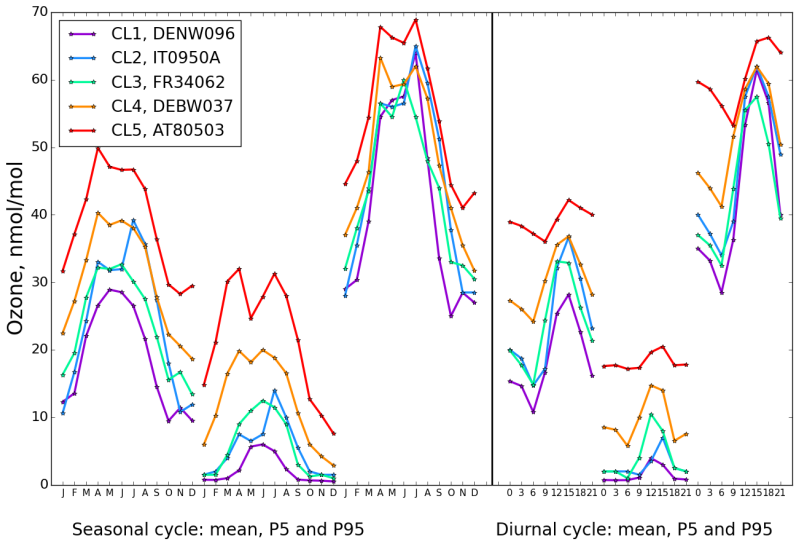

Figure 5.26. Mean seasonal and diurnal cycles, and their 5- and 95-percentiles. Stations nearest to cluster centers. 1st CA.

5.2.3.2 Second and third CAs

The representative stations from the 2nd and 3rd CAs share 3 stations in common (representatives of CL1, 3 and 4), confirming high resemblance of these analyses. Tables 5.18 and 5.19 show the description of representative stations together with the information about the station classification taken from the Airbase database. In this case the CL4 representative is not a high mountain station, but at a lower altitude. Nevertheless it is characterized as "background rural".

The representatives of CL2 do not coincide, but they show similar time series with ozone reaching zero in winter and the level of ≈ 10 nmol/mol in summer, with the maxima at ≈ 100 nmol/mol in 2010 for both stations (Figure 5.27).

Interestingly, one of the representative stations, namely FR34041 is also the "typical" station of CL3 for the previous analysis (1st CA) (Tables 5.17, 5.18, 5.19), as discussed above. This is not unexpected, given that in the contingency Table 5.11 CL3 has the highest number of stations, allocated to CL3 in all CAs (319 locations in common for 1st CA and 2nd CA results).

Similar to the results from the 1st CA the variability for representative stations is reduced in order CL1 → CL2 → CL3 → CL4. The first two representative stations (CL1 and 2) show the highest ozone titration during the winter and pronounced seasonal cycles. In contrast, CL3 exhibits less ozone titration in summer and at the same time flatter summer maxima. Finally the representative station of CL4 has the lowest variability throughout all periods, nearly no low ozone concentrations are observed. The variability changes among the representative stations, but the mean ozone concentrations are nearly at the same level. This is one of the differences in comparison to the 1st CA.

Table 5.18. Stations closest to the cluster centroids (information from the Airbase database). 2nd CA.

CL	station ID	station type	station area type	longitude	latitude	alt., m
1	IT1214A	background	urban	11.79	45.04	3
2	DEBW112	background	suburban	8.9	48.65	463
3	FR34041	background	urban	1.51	48.44	145
4	DESH013	background	rural	11.22	54.41	2

Table 5.19. Stations closest to the cluster centroids (information from the Airbase database). 3rd CA.

CL	station ID	station type	station area type	longitude	latitude	alt., m
1	IT1214A	background	urban	11.79	45.04	3
2	DEBW023	background	suburban	7.63	47.59	275
3	FR34041	background	urban	1.51	48.44	145
4	DESH013	background	rural	11.22	54.41	2

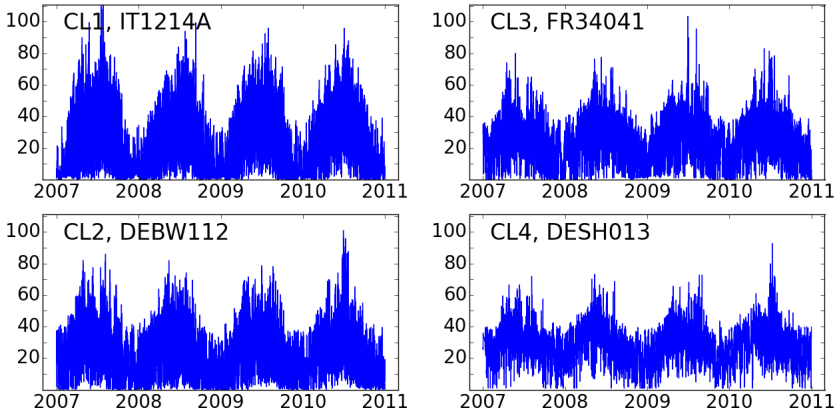

Figure 5.27. Time series of the stations representing the clusters (in nmol/mol). 2nd CA.

To compare amplitudes of seasonal - diurnal cycles, we plot the stations representing the 2nd CA in the same coordinates as the 2nd set of properties, i.e. in the 96 – dimensional vector with normalized

values (12 monthly averaged diurnal variations, represented for 8 hours of a day: 0, 3, 6, 9, 12, 15, 18, 21 hours) (Figure 5.28). In this case seasonal and diurnal cycles, which are especially pronounced in summer time, are proportional to each other. For example, station DESH013 of CL4 with the lowest seasonal amplitude has at the same time the lowest diurnal amplitude. The amplitudes grow from CL4, 3, 2 to CL1. The corresponding plot of the 3rd CA looks very similar to Figure 5.28 and is therefore not shown.

Considering mean seasonal and diurnal cycles of these stations with corresponding cycles of 5- and 95- percentiles also in absolute values (Figure 5.29), we notice that not only amplitudes are changing for these stations, but also the magnitude of the difference (95-5)-percentiles. The lowest amplitudes correspond to the lowest variability, and the highest amplitudes to the highest variability. In contrast to the 1st CA (Figure 5.26), the average concentrations are not very different in this case.

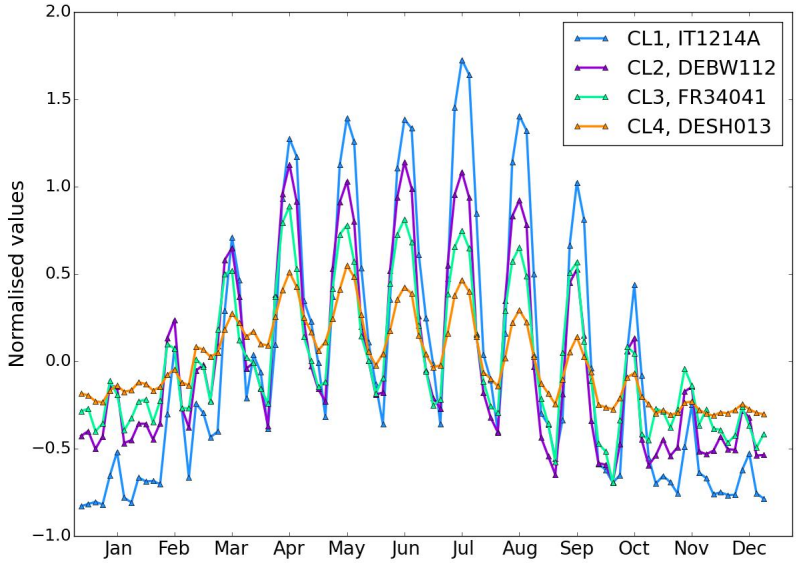

Figure 5.28. Cluster representatives in 96 normalized seasonal-diurnal variations coordinates. 2nd CA.

Another representation of seasonal and diurnal cycles of "typical" stations is given in Figures 5.30 and 5.31. They also show 5- and 95- percentiles of each monthly mean and hourly mean, and as they are calculated from the hourly values, they retain the diurnal variability.

For the station DESH013 of CL4 the variability is the least and reaches 40 nmol/mol in summer time or at 15 o'clock. For the station FR34041 of CL3 the maximum variability is ≈ 50 nmol/mol, for DEBW112 of CL2 it is ≈ 60 nmol/mol, and finally for IT1214A of CL1 the variability reaches ≈ 70 nmol/mol.

5.2.3.3 Difference in clustering of absolute and normalized properties

From the above analysis we conclude that the 1st CA groups stations mainly according to ozone average concentrations, whereas the dominant clustering criteria in the 2nd and 3rd CAs are amplitudes of diurnal and seasonal cycles and ozone variability.

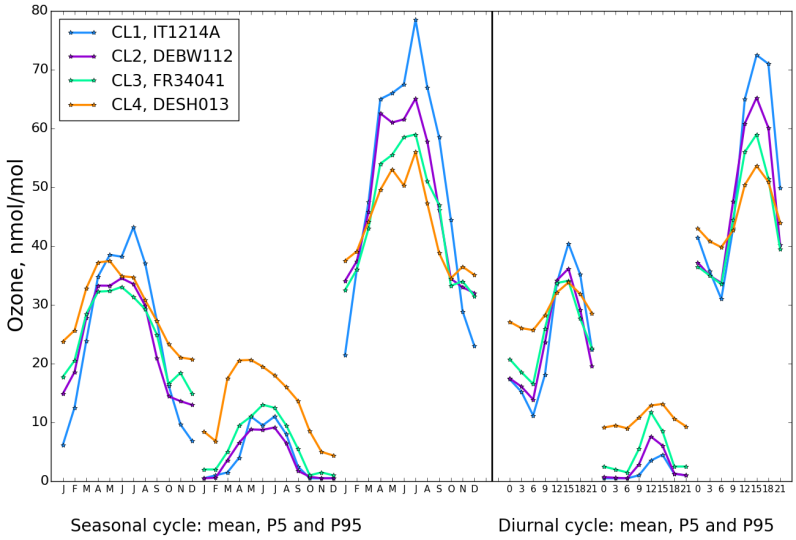

Figure 5.29. Mean seasonal and diurnal cycles, and their 5- and 95-percentiles. Stations nearest to cluster centers. 2nd CA.

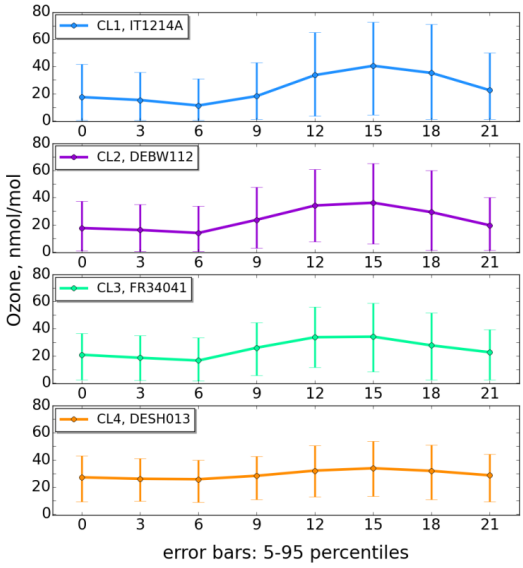

Figure 5.30. Averaged diurnal cycles of stations nearest to cluster centers. The error bars denote 5- and 95-percentiles. 2nd CA.

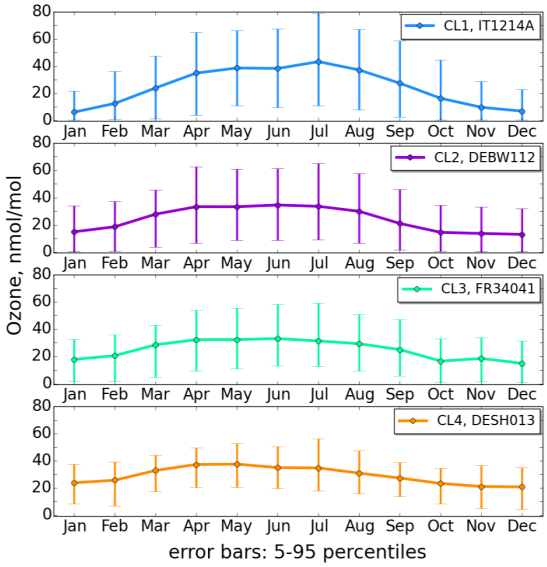

Figure 5.31. Averaged seasonal cycles of stations nearest to cluster centers. The error bars denote 5- and 95-percentiles. 2nd CA.

To test this conclusion we plot the distributions of ozone 5-percentiles, means and 95-percentiles in clusters (Figure 5.32). Each distribution was made on the basis of 3 corresponding values for each station, computed from the complete data set of each location.

We note that 5-percentiles distributions increase from CL1 (average 5-percentile is 1 nmol/mol) to CL5 (average 5-percentile is 19 nmol/mol). Thus they have similar tendency as the means. Moreover the 95-percentiles distributions are also increasing from CL1 (average 95-percentile is 46 nmol/mol) to CL5 (average 95-percentile is 59 nmol/mol) except for CL2 (average 95-percentile of 59 nmol/mol). Therefore, the differences between the average 95- and 5-percentiles in clusters CL1 to CL5 are: 45, 57, 47, 46, 40 nmol/mol, i.e. there is no relation between the values. Thus we see again that ozone means are increasing from cluster to cluster while there is no clear pattern with respect to variability.

The same picture of distributions of means and 5- and 95-percentiles for the 2nd CA is illustrated in Figure 5.33. For the 3rd CA it is very similar, so we don't provide it. Averages of distributions of means are increasing in order: CL2, CL1, CL3 and CL4, while the differences between average 95- and 5-percentiles in clusters are decreasing from CL1 to CL4: 58, 49, 47, 40 nmol/mol. Here we confirm, that the 2nd CA distinguishes clusters by short-term variability. Higher ozone mean for CL4 is probably a consequence of the analysis, as the least titration and least variability can only be observed for remote and elevated locations, and the latter contribute to the higher ozone average of CL4.

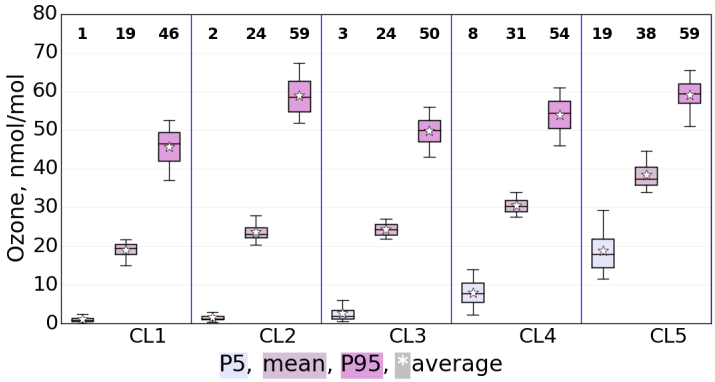

Figure 5.32. Distributions of ozone 5-percentiles, means and 95-percentiles in clusters. 1st CA.

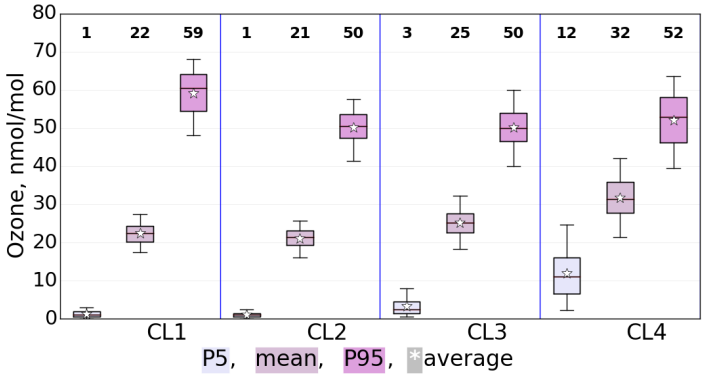

Figure 5.33. Distributions of ozone 5-percentiles, means and 95-percentiles in clusters. 2nd CA.

5.2.4 Comparison of Airbase ozone data with MACC model results

Figure 5.34 presents an initial comparison of the 5-25-50-75-95- percentiles distributions from the 3-hourly Airbase and MACC data sets for the period 2007 - 2010. The mean and median volume mixing ratios averaged over the entire set of 1492 stations are 25 nmol/mol and 24 nmol/mol for Airbase, and 34 nmol/mol and 33 nmol/mol for MACC, respectively. Thus the central percentile and the mean of the model data are 8 nmol/mol higher than those of the measurement data.

As mentioned in section 3.3 “MACC model data”, for comparison of different parameters (means, seasonal and diurnal amplitudes) between the MACC model and Airbase observations in clusters, the model output were interpolated to the locations of the sites and arranged in a matrix of the same kind as the Airbase observations (order of stations, and the set of properties) and then grouped into CLs according to the Airbase clustering results.

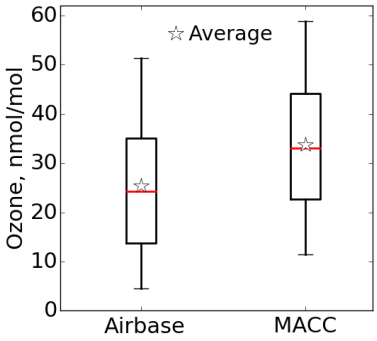

Figure 5.34. Percentiles (5-25-50-75-95) of 3-hourly ozone mixing ratios for 1492 stations, Airbase vs MACC.

When plotting distributions of station-mean values as box and whisker plots for individual clusters of the 1st CA (Figure 5.35) some patterns begin to emerge. With the exceptions of CL2 and CL3, which show quite similar distributions, the distributions of the observed (Airbase) values are rather distinct for each cluster and increase from CL1 to CL5. In comparison, the MACC distributions are generally broader and exhibit a high bias of 5-12 nmol/mol except for CL5. MACC distributions also show increasing values from CL3 to CL5, but only little difference among clusters 1 to 3.

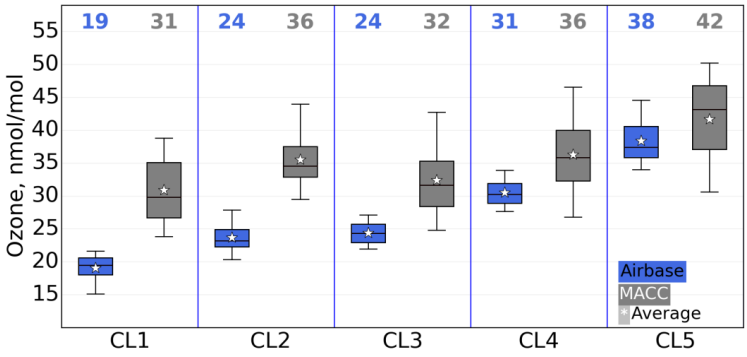

Figure 5.35. Percentiles (5-25-50-75-95) of ozone means in clusters, Airbase vs MACC. Upper values indicate the mean of each cluster. 1st CA.

Obviously, the model does not capture the differences among the somewhat more polluted sites very well. This is consistent with the distributions of simulated CO and NOx concentrations (there are too few observations available to make a meaningful comparison) shown in Figure 5.36. While the MACC model clearly indicates a separation between clusters 1-3 and 4-5, there is relatively little difference among the distributions for CL1, 2, and 3. These results are not surprising given that ozone concentrations in CL1-CL3 are more likely influenced by local, small-scale pollution sources, which the model cannot simulate correctly with its grid point distance of approximately 80 km. It is

however reassuring to see that the simulated mean values of ozone precursors are higher in those clusters that have been labeled more polluted according to the Airbase characterization tags.

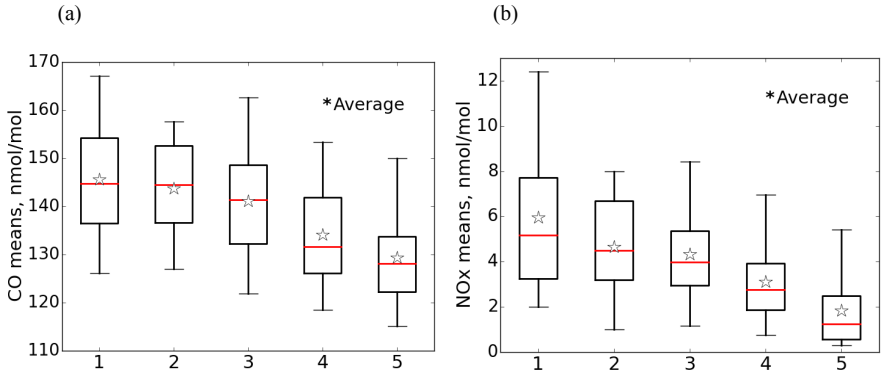

Figure 5.36, (a,b). Percentiles (5-25-50-75-95) of modeled CO (a) and NOx (b) means in clusters. 1st CA.

Figure 5.37 shows the distributions of mean ozone mixing ratios in the clusters of the 2nd CA.

The MACC distributions of mean values are again broader than the observations and the model overestimates all clusters with the highest bias of 14 nmol/mol for CL1 and the lowest 4 nmol/mol for CL4. The distribution of observed ozone means of CL4 is broader, than in the 1st CA. This can be explained by the mix of stations of various altitudes. For other clusters, the distributions are relatively narrow, but still nearly twice broader than those of the 1st CA, except for CL1 (Figure 5.35).

MACC model distributions of CO and NOx concentrations (Figure 5.38) are reflecting the pollution of the first 2 clusters and somewhat intermediate pollution conditions for CL3. CL4 as relatively clean is described by the lowest CO and NOx concentrations.

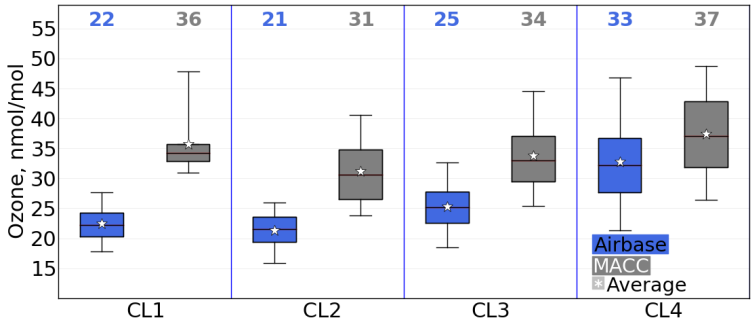

Figure 5.37. Percentiles (5-25-50-75-95) of ozone means in clusters, Airbase vs MACC. Upper values indicate the mean of each cluster. 2nd CA.

The discussion about CL1 and CL2 in section 5.2.2 “Comparison with Airbase station classification scheme” hasn't brought to conclusion whether CL1 is more polluted than CL2 or vice versa. To remind, CL1 has more background urban stations than CL2, and contains some traffic urban stations (Table 5.15). CL2 has less background urban locations, but more traffic urban and industrial urban sites. Therefore the level of emissions for CL2 is expected to be higher than for CL1, and this is consistent with simulated CO and NOx concentrations (Figure 5.38). Figure 5.33 shows similar ozone mean levels of both clusters and the same zero-level of 5-percentiles distribution, confirming strong ozone titration in both clusters. But 95-percentiles distributions are ≈ 8 nmol/mol higher for CL1, and this is an indication of more intensive photochemical ozone production during summer time. Seemingly stations of CL2 have also plenty of precursor emissions for ozone production.

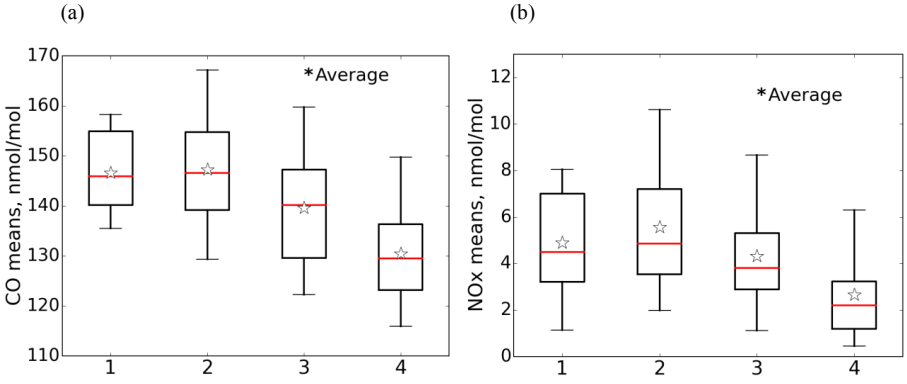

Figure 5.38, (a,b). Percentiles (5-25-50-75-95) of modeled CO (a) and NOx (b) means in clusters. 2nd CA.

The reason for these differences could be the geographical location of the cluster members: CL1 is concentrated in the North Italian Po Valley, while CL2 is spread over wide areas in Central and Eastern Europe, i.e. we can expect warmer temperatures and more sunshine at stations in CL1 compared to CL2.

5.2.5 Frequency distributions of ozone in clusters

5.2.5.1 First CA

The frequency distributions of the observed and modeled 3-hourly surface ozone values for the period 2007-2010 are presented for Airbase and MACC data for each cluster of the 1st CA in Figure 5.40 and seasonal frequency distributions in Figure 5.39.

From both pictures we may conclude that in the Airbase data the three clusters with more urban characteristics (CL1, CL2 and CL3) contain a significant number of values of very low concentrations, which are caused by ozone titration during the winter time in the presence of large amounts of NOx from traffic and industries. Airbase winter distributions reveal peaks at low ozone

mixing ratios with frequencies decreasing from CL1 to CL4, though the last is showing nearly no ozone titration.

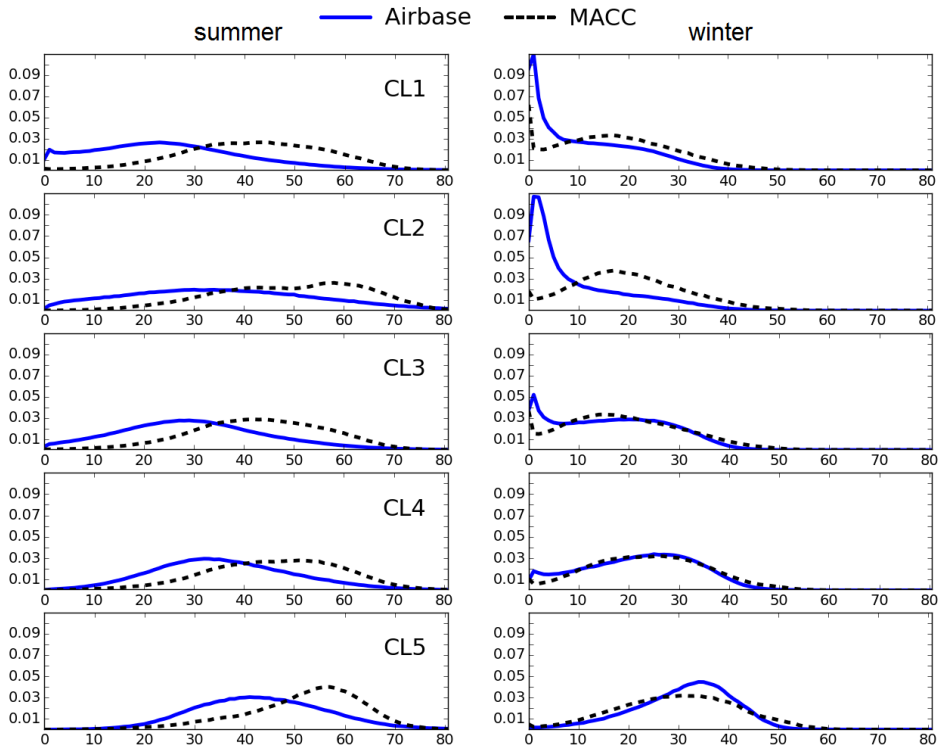

Figure 5.39. Normalized frequency distributions of 3-hourly ozone values in clusters (2007-2010), summer (left) and winter (right), Airbase vs MACC, 1st CA.

For clusters CL1, CL3 and CL4 the low ozone values are predicted to some extent by the MACC model, but not for CL2 (Po Valley). The probability for low ozone concentrations is equal to zero in CL5 for both seasons (Figure 5.39).

MACC exhibits quite a good fit to CL4 and CL5 winter ozone concentrations and predicts winter values in general better than summer ones. During summer the measured ozone data are almost normally distributed (except for CL1), which is not seen for the MACC summer values. The model summer curves exhibit a high bias and contain two maxima for CL2 and CL4 (Figures 5.39, 5.40).

Winter ozone determines the general asymmetry of most of the frequency distributions (Figure 5.40), which can actually be represented by a superposition of two gamma distributions (not shown); only CL4 and CL5 exhibit an almost Gaussian shape. In contrast, the frequency distributions from the MACC model are all more or less symmetric, and they show much fewer values with very low concentrations (although a small peak can be found in the frequency distributions for CL1 and CL3).

The MACC frequency distribution of CL5 has a broader maximum than the Gaussian distribution of the corresponding Airbase data. As explained above this is caused by summer time ozone (Figure 5.39).

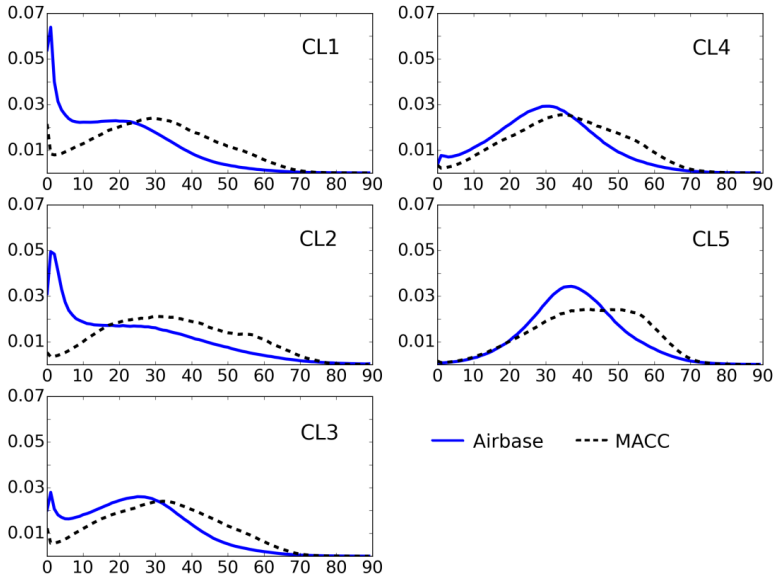

Figure 5.40. Normalized frequency distributions of 3-hourly ozone values in clusters (2007-2010), Airbase vs MACC. 1st CA.

In order to quantitatively evaluate the model's ability to reproduce the observed frequency distributions in each cluster, we calculated the Earth Mover's Distance (EMD, described in chapter "Methodology") (Table 5.20). EMD is an objective distance measure between two frequency distributions or probability density functions. As expected from Figures 5.39 and 5.40, EMD calculates the largest difference between the model and observations for CL1 and CL2, while the model shows greater skill in capturing the frequency distributions of CL4 and CL5 and to a lesser extent also CL3 (Table 5.20). This is again consistent with the previous characterizations of CL3 as "background, moderately polluted" and of CL4 and CL5 as (mostly rural) background stations (Table 5.9).

From CL1 to CL5 the EMD values for summer are decreasing, thus model prediction of observations improves in that order. We note that in the same order the level of pollution of clusters is decreasing while mean ozone concentrations are increasing. The winter EMD values are smaller than summer ones, and show no dependence from CL1 to CL5. In general the model describes winter ozone relatively well with the only exception of CL2, where MACC isn't predicting low concentrations (Table 5.20, Figure 5.39).

Table 5.20. EMD values for each cluster between Airbase and MACC data (2007-2010). 1st CA.

cluster	summer	winter	all
1	0.181	0.068	0.126
2	0.146	0.112	0.134
3	0.139	0.028	0.083
4	0.110	0.021	0.064
5	0.092	0.025	0.041

The uncertainty of EMD values was estimated with the bootstrapping method (see section 4.4). For this 10 additional tests were done in order to get some statistics of EMD values, and each test was implemented on the 10% (149 stations) of data randomly selected from initial data set and increased in 10 times in order to fit with the original data size.

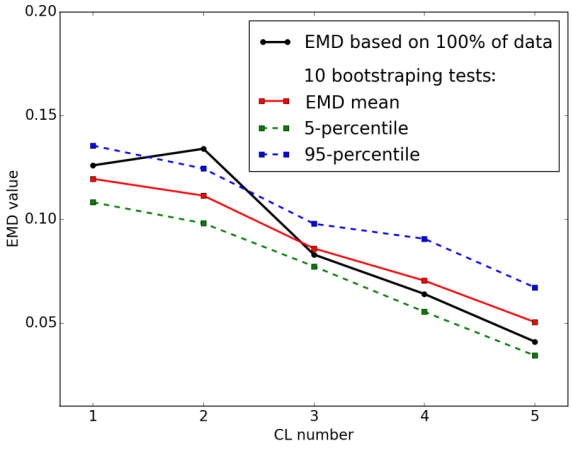

Figure 5.41. EMD values in clusters obtained for the full data set and for 10 bootstrapping tests, based on 10% of data for each test.

The average EMD value and the distributions of EMD 5-95 percentiles within 10 tests obtained for every cluster are plotted (Figure 5.41) in comparison to previously reported EMD values for the full data set (presented in Table 5.20, the last column). There is quite good agreement between the real EMD values and the EMD values, averaged over 10 bootstrapping tests, except for CL2 (Figure 5.41). For all other clusters the actual EMD is consistent with the test statistics and keep general tendency of EMD change within the range of the 5-95 percentiles. This result shows the stability of Airbase-MACC data differences in clusters, even for small samples consisting of random 149 stations out of 1492.

5.2.5.2 Second CA

Frequency distributions of the 3-hourly surface ozone values of Airbase and MACC for each cluster of the 2nd CA are presented in Figure 5.42. As anticipated from the previous discussion, clusters

with urban signatures CL1 and CL2 are expected to show a peak at low ozone concentrations, related to their higher pollution level. Indeed, the peaks of Airbase probabilities of zero ozone concentrations are pronounced for both clusters in comparison to the moderately polluted CL3, for example, where "zero" ozone has twice less probability and the ozone maximum appears in the range 25-30 nmol/mol. The shape of the relatively clean CL4 curve resembles a Gaussian distribution with maximum probability at ≈ 35 nmol/mol.

EMD calculated for comparison of observations to modeled frequency distributions (Table 5.21) show the strongest disagreement for CL1 (0.15), then follow CL2 and CL3 with quite similar values 0.106 and 0.091, respectively, and at the end is the smallest value of 0.051 for CL4.

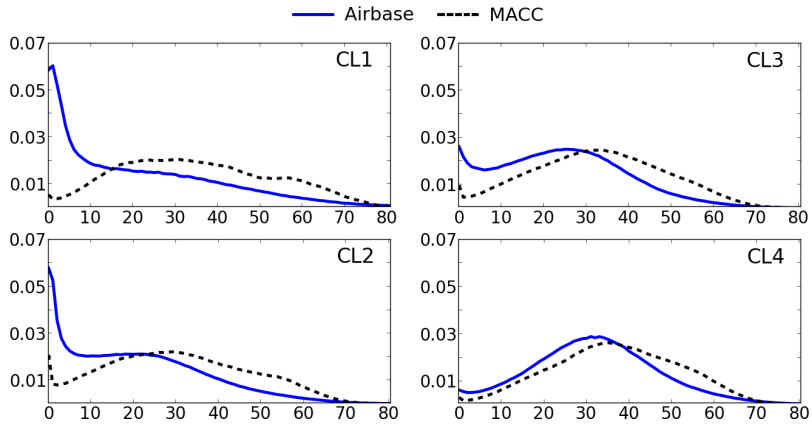

Figure 5.42. Normalized frequency distributions of 3-hourly ozone values in clusters (2007-2010), Airbase vs MACC. 2nd CA.

In section 5.2.2 we mentioned similarities between clusters of the 1st and 2nd CAs, and here we see analogous pictures of frequency distributions for CL1 (2nd CA) and CL2 (1st CA), for CL2 (2nd CA) and CL1 (1st CA), for CL3 and CL4 of both CAs, though the EMD values coincide only for CL4 of both CAs.

Table 5.21. EMD values for each cluster between Airbase and MACC data. 2nd CA.

cluster	EMD (obs-mod)
1	0.15
2	0.106
3	0.091
4	0.051

5.2.6 Analysis of annual, diurnal, and weekly variations

5.2.6.1 First CA

The mean seasonal amplitudes, i.e. the difference between the highest and lowest 4-year average monthly mean ozone concentrations (Figure 5.43) of the Airbase clusters are generally between 18 and 24 nmol/mol (25%-ile to 75%-ile), with the exception of CL2 (Po Valley stations), where seasonal amplitudes range from about 26 to 37 nmol/mol (25%-ile to 75%-ile). The MACC model data show a similar pattern among the clusters. However, the seasonal amplitude is often overestimated by 5-10 nmol/mol due to the overestimation of summer time ozone. The seasonal amplitude of CL2 stations is captured relatively well, although the mean values in CL2 exhibited the second highest bias (12 nmol/mol, Figure 5.35).

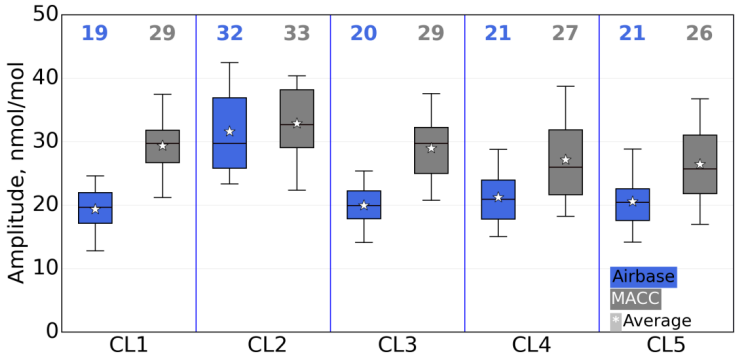

Figure 5.43. Percentiles (5-25-50-75-95) of ozone annual amplitudes in clusters, Airbase vs MACC. Upper values indicate the mean annual amplitude of each cluster. 1st CA.

The seasonal cycles of the 1st CA cluster centroids are displayed in Figure 5.44. In the observed data CL1 and CL3 run almost parallel and show a broad maximum extending from April to July for CL1 and a slight maximum in April for CL3. More prominent spring maxima are evident in CL4 and CL5, but CL5 also exhibits a second small peak in July. The only cluster with a single pronounced maximum in summer (July) is CL2.

As already mentioned in section 2.2.2 “Stratosphere-troposphere exchange” and 5.1.3 “Selected European stations (1998-2011)”, the spring maximum is typical for seasonal cycles of western European sites (Monks, 2000), and considered as Northern Hemispheric phenomenon. Indeed, a substantial subset of stations in CL3, CL4 and CL5 are situated along the western edge of the continent (see map, Figure 5.20). The decline of ozone mixing ratios from spring till autumn in CL3 and CL4 suggests that summer photochemical ozone formation plays only a minor role at these sites. On the other hand, the double peak of CL5 suggests a superposition of the “natural” spring maximum with the “anthropogenic” summertime photochemical ozone production. The stations in

CL5 are more elevated, therefore they can be influenced by ozone from the stratosphere-troposphere exchange, which is considered as a possible reason for the ozone spring maximum on high mountains (Elbern et al., 1997; Harris et al., 1998; Stohl et al., 2000; Monks, 2000; Zanis et al, 2003) (chapter "Theory", section 2.2.2 "Stratosphere-troposphere exchange").

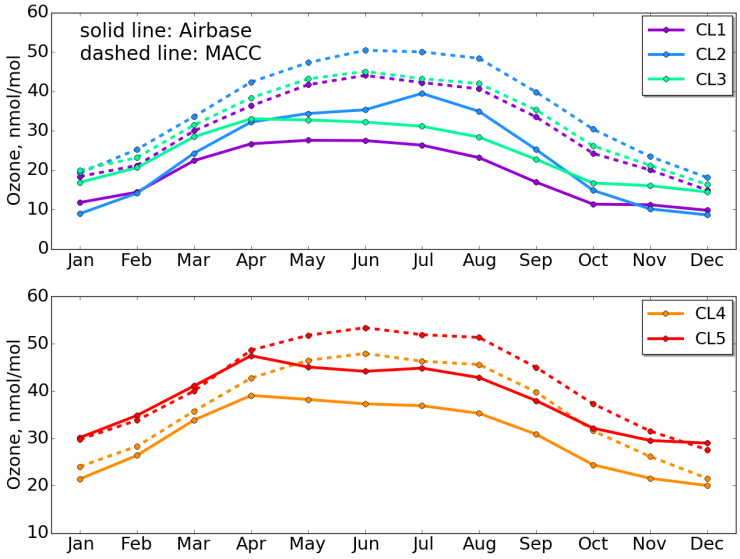

Figure 5.44. Seasonal cycles of cluster centroids, Airbase vs MACC. 1st CA.

In contrast to the seasonal cycles of the Airbase cluster centroids, the cluster mean seasonal cycles of the MACC data all show a summer maximum of similar shape with peak in June. This suggests that either the summertime chemical ozone formation is exaggerated in the model, or the largely transport-driven springtime maximum is underestimated. A potential influence from inconsistencies in the data assimilation (see Inness et al., 2013) is unlikely, but cannot be excluded.

The seasonal cycles in Figure 5.44 confirm the results from section 3.4 "Initial model-data comparison" (Figures 3.6 and 3.7) that the MACC model performs better during winter than during the summer. This is particularly evident for clusters 3, 4, and 5, whereas a significant bias persists throughout the year for CL1 and CL2. In the Validation Report of the MACC reanalysis (2013) a comparison with GAW surface ozone data shows that in most regions of the world ozone mixing ratios are generally underestimated during winter and overestimated during summer time. Inness et al. (2013) present an evaluation with EMEP data, which is also consistent with this analysis. EMEP stations are almost exclusively characterized as background sites and are partly contained in the Airbase database as well.

Diurnal amplitudes were calculated from averaged diurnal cycles of each station as an absolute difference between daily maximum and minimum, and then gathered into distributions for each

cluster. Box and whisker plots of ozone average diurnal amplitudes (Figure 5.45) show a clear signature that appears to be correlated with the ozone precursor concentrations as simulated by the MACC model (see Figure 5.36). The largest diurnal amplitudes (mean 27 nmol/mol) are obtained for CL2 (Po Valley), followed by CL1 (mean 18 nmol/mol), CL3 (mean 18 nmol/mol) and CL4 (mean 17 nmol/mol). CL5 (relatively clean elevated) stations exhibit the lowest diurnal amplitude (mean 9 nmol/mol). This is consistent with earlier findings by Flemming et al. (2005) and Chevalier et al. (2007), who show the smallest diurnal amplitudes for clean sites. The average diurnal amplitudes of the MACC model are generally consistent with the measurement data, except that the distributions are somewhat broader, and there is no big difference between the diurnal amplitudes in CL2 compared to CL1 and CL3. We note that the MACC model does not prescribe a diurnal cycle for ozone precursor emissions.

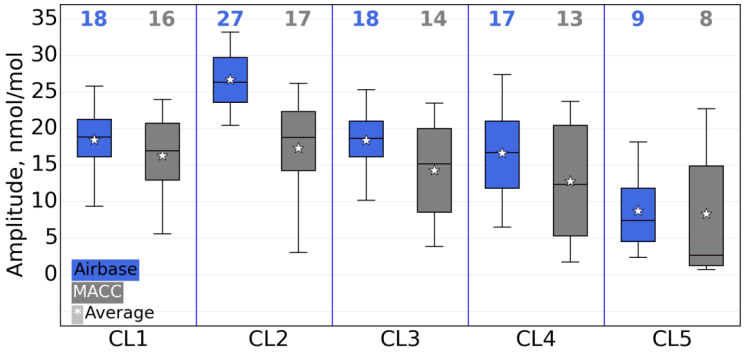

Figure 5.45. Percentiles (5-25-50-75-95) of ozone diurnal amplitudes in clusters, Airbase vs MACC. Upper values indicate the mean daily amplitude of each cluster. 1st CA.

As stated above, the percentile distributions of Airbase seasonal amplitudes and ozone means for individual clusters are quite narrow. This indicates that the clustering of stations was mainly determined by these parameters. At the same time, the diurnal amplitude distributions differ especially among clusters 1 and 3 versus 5, which likely helped the method to discriminate the stations against each other.

The diurnal cycles of the Airbase cluster centroids (Figure 5.46) show rather similar patterns with peak values between noon and 15:00 h for all clusters. As stated above, CL2 shows the most pronounced maximum, while CL5 exhibits the flattest curve. Ignoring the overall bias the model diurnal cycles are similar to the observations except that ozone mixing ratios show a lesser decline from 00:00 h to 06:00 h in all clusters except for CL5. This could indicate underestimation of ozone dry deposition, possibly in conjunction with errors in the calculation of mixing in the nocturnal boundary layer. Underestimation of the diurnal amplitude in CL2 (Figure 5.45) is largely due to the model failure of capturing low ozone concentrations around 6 am (Figure 5.46).

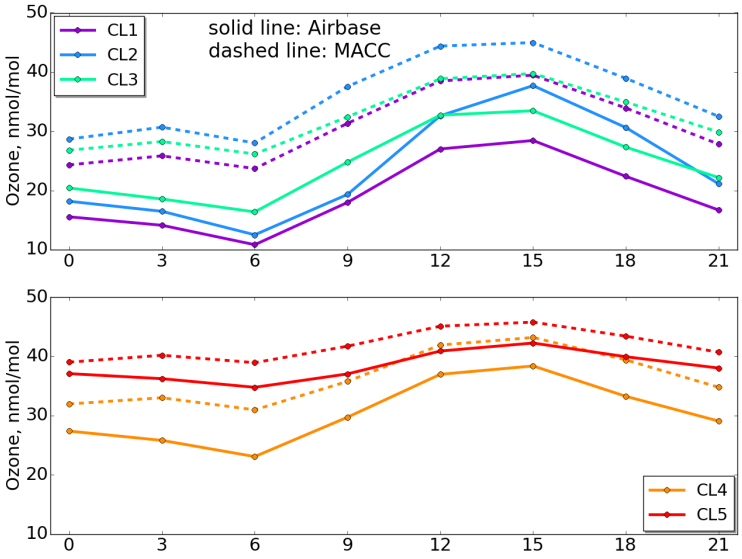

Figure 5.46. Diurnal cycles of cluster centroids, Airbase vs MACC. 1st CA.

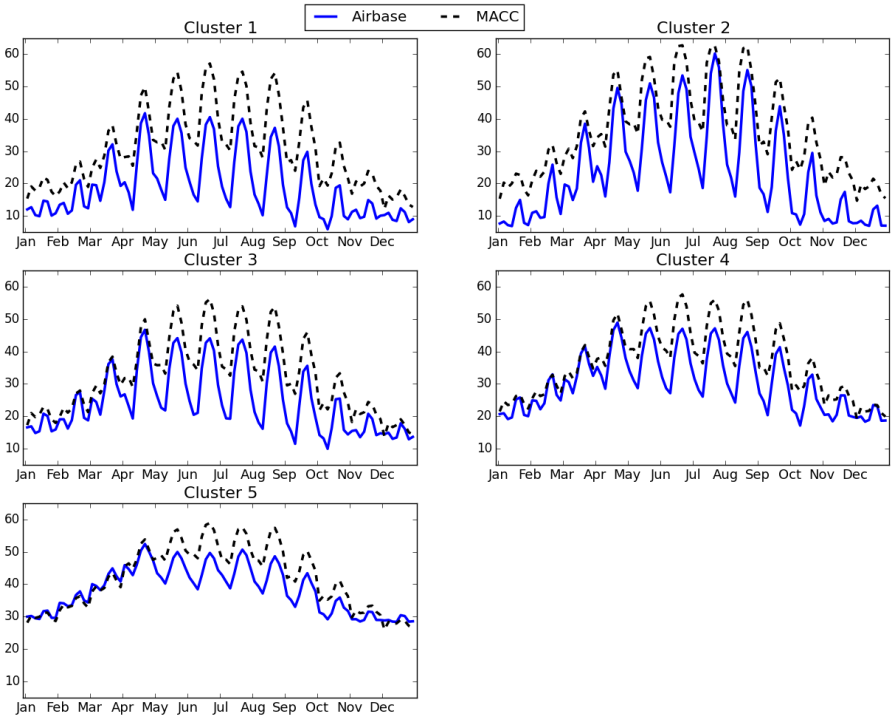

Figure 5.47. Seasonal-diurnal cycles of cluster centroids (in nmol/mol), Airbase vs MACC. 1st CA.

Seasonal-diurnal variations for all Airbase clusters combined on the single plot vs MACC model groups are depicted in Figure 5.47.

Weekly amplitudes are shown in Figure 5.48. These were not used as initial parameters in the CA, but interestingly the classification of Airbase data shows a clear tendency of the weekly amplitudes decreasing from CL1 to CL5, even though there is considerable overlap between the various frequency distributions. The weekly cycles of all cluster centroids show growth from Friday till Sunday, but no significant change during the week (Figure 5.49). This confirms our characterization of the clusters from more to less polluted, meaning that the less polluted sites are less influenced by local precursor emissions with distinct weekday cycles, notably traffic emissions (Beirle et al., 2003). As for the MACC model, the boundary conditions of its chemical equation system don't contain weekly variations of ozone precursor emissions, therefore simulated ozone has no significant weekly cycle.

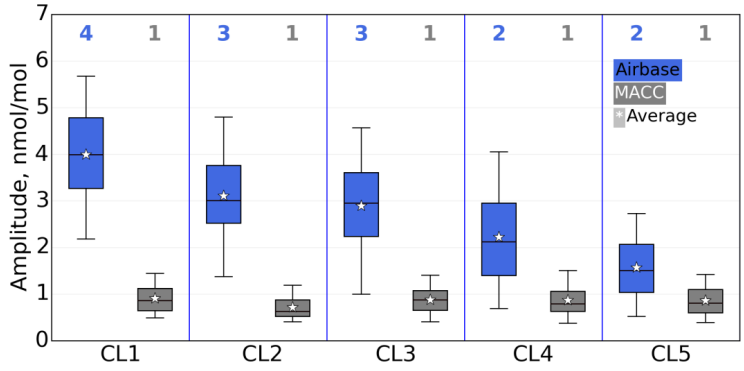

Figure 5.48. Percentiles (5-25-50-75-95) of ozone weekly amplitudes in clusters, Airbase vs MACC. Upper values indicate the mean weekly amplitude of each cluster. 1st CA.

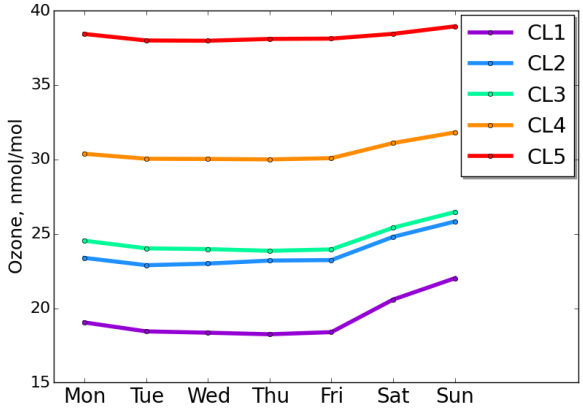

Figure 5.49. Weekly cycles of Airbase cluster centroids. 1st CA.

Schipa et al. (2009) and Pollack et al. (2012) concluded that for polluted areas the higher ozone values during the weekend result from the fact that reduced NO emissions and relatively small changes in VOC emissions facilitate ozone production due to an increased VOC/NOx ratio. The median of weekly amplitudes in urban CL1 is 4 nmol/mol, which is consistent with Murphy et al. (2007). The MACC model results exhibit much smaller weekly amplitudes (generally less than 1 nmol/mol) with no apparent difference among clusters. It would be interesting to see how much of the weekly cycle can be produced by a global model if weekly variations of ozone precursor emissions were included, but this is beyond the scope of this study.

The large seasonal and diurnal amplitudes in the Airbase data of CL2 are consistent with the relatively large emissions and active photochemistry in the Po Valley region (Bigi et al., 2012). While ozone precursor concentrations at stations in CL1 may be as large as those in CL2 (based on emission inventories and the MACC simulation results for CO and NOx, see Figure 5.36), the mean ozone concentrations at these stations are lower. As can be seen from the time series in Figure 5.25 and the frequency distributions in Figure 5.40, there are a lot more incidents with very low ozone concentrations at the stations in CL1, and these occur both in winter as well as in summer. In the Northern and Central part of Europe, where the majority of CL1 stations are located, the photochemistry is slow especially during winter, so that not much NO_2 is converted back to NO and ozone via photolysis. CL2 also exhibits ozone titration, but in summer to a lesser extent than for CL1 (Figure 5.25). For CL2 ozone destruction by NO and dry deposition still occurs during night time but in contrast to CL1 this is compensated by elevated ozone concentrations from photochemical production during daytime. In addition, the seasonal cycle is more pronounced for CL2 than for CL1 (Figure 5.44). This may be explained by the basin type of the Po Valley region and by its partly sub-tropical climate with plenty of available UV light, which is favorable for summer diurnal photochemical ozone production.

5.2.6.2 Second and third CA

We provide in this subsection results mainly from the 2nd CA, as the results of the 3rd CA have much resemblance with them and are mainly left for consideration of robustness check.

The mean seasonal amplitudes for clusters of the 2nd CA are presented in normalized units in Figure 5.50. MACC data was normalized in the same way as the Airbase data, and then grouped according to the clustering results. We notice narrowness of seasonal amplitudes distributions and the decrease of their average in order CL1 → CL2 → CL3 → CL4. MACC seasonal amplitudes follow the same dependence, but in a more "smoothed" way, and they have broader distributions. The means of modeled amplitudes slightly overestimate average observed amplitudes for CL3 and CL4, are nearly equal for CL2 and underestimate CL1.

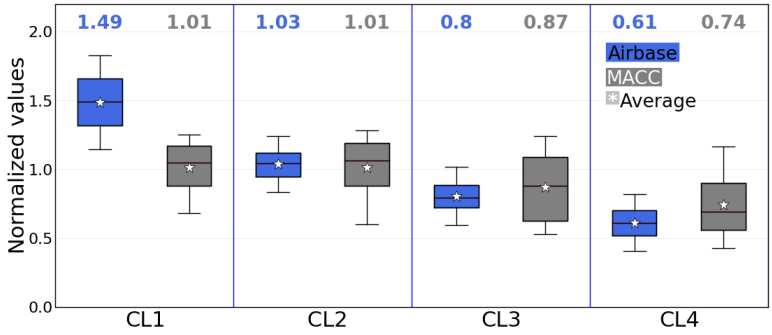

Figure 5.50. Percentiles (5-25-50-75-95) of ozone annual amplitudes in clusters, Airbase vs MACC. Upper values indicate the mean annual amplitude of each cluster. 2nd CA.

The seasonal cycles in normalized values of the cluster centroids from the 2nd CA are depicted in Figure 5.51. In contrast to the results from the 1st CA, the seasonal cycles of centroids show gradual change from the smoothest cycle of CL4 ("background rural") with only April maximum to the most prominent cycle of CL1 ("background urban") with strong July maximum. CL2 presents intermediate cycle with a broad maximum, and CL3, although it has a more pronounced amplitude than CL4, still preserves the same features with a dominant spring peak. MACC centroids all show similar seasonal cycles and broad maxima from spring till autumn. The model underestimates normalized seasonal cycles in the beginning of the calendar year (except for CL1) and spring time as well as overestimates in autumn for CL1 and 2 and also in summer for CL3 and 4.

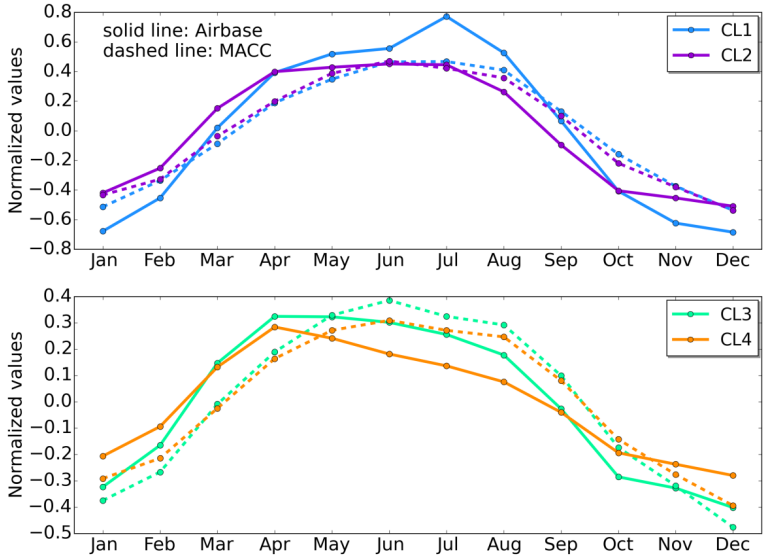

Figure 5.51. Seasonal cycles of cluster centroids, Airbase vs MACC. 2nd CA.

Box and whisker plots of average diurnal ozone amplitudes expressed in normalized values (Figure 5.52) are continuously decreasing in their mean from CL1 to CL4, likewise the distributions of seasonal amplitudes (Figure 5.50). For all clusters modeled ozone diurnal amplitudes distributions are broader and underestimating observed ones.

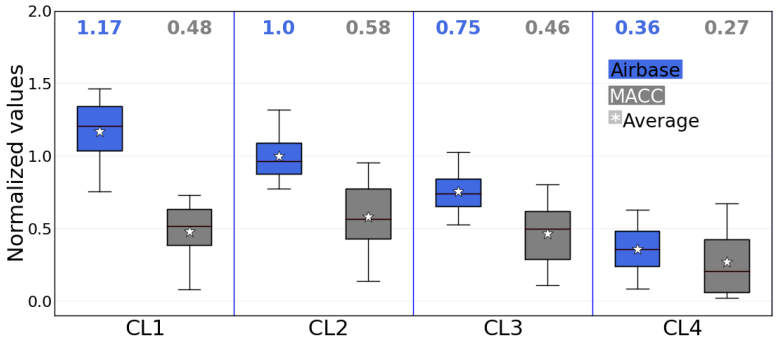

Figure 5.52. Percentiles (5-25-50-75-95) of ozone diurnal amplitudes in clusters, Airbase vs MACC. Upper values indicate the mean annual amplitude of each cluster. 2nd CA.

The diurnal cycles (Figure 5.53) give also similar dependence on cluster number as seasonal cycles: the smoothest for CL4 and most pronounced for CL1. As expected from the 1st CA, all clusters exhibit diurnal minima at 6 am and maxima between midday and 3 pm, except for CL1, which maximizes in the late afternoon - after 3 pm, similarly to CL2 of the 1st CA. Modeled diurnal minima and maxima are in accordance with the observations, except for CL1, where MACC shows daily maxima in between 12 and 3 pm like for other modeled groups.

With respect to seasonality the best model description is achieved in CL3, while the shape and amplitude of the diurnal cycle is well predicted at CL4.

The complete picture of seasonal-diurnal variations is presented in Figure 5.54, and illustrates overall differences between Airbase and MACC centroids, expressed in normalized units. The least well predicted centroid of CL1 has strong disagreements between model and observations. Centroid of CL4 shows a relatively good match of both with some underestimation in winter and spring and overestimation in summer.

Similar underestimation is evident also for CL3, and though in summer time there is a good fit of diurnal cycles in daytime, there is more ozone titration during the night, which is not captured by model.

Clustering based on the normalized set of properties gives as a result a clear division of stations relevant to variability, and amplitudes of seasonal and diurnal cycles (Figure 5.50, 5.52). Both these amplitudes as well as variability decrease uniformly and gradually from CL1 to CL4 in accordance with the level of pollution of these clusters.

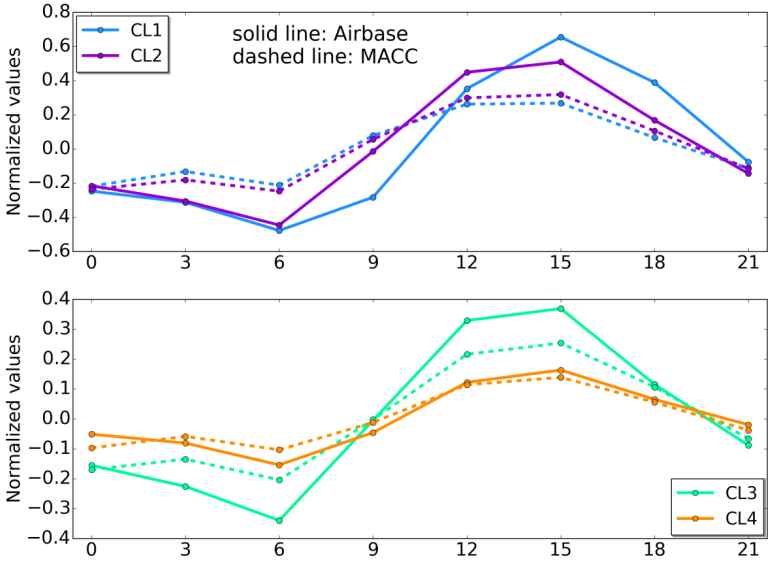

Figure 5.53. Diurnal cycles of cluster centroids, Airbase vs MACC. 2nd CA.

CA based on 20 normalized seasonal and diurnal cycles (3rd set of properties) is giving very similar pictures of seasonal and diurnal amplitudes distributions and cycles in clusters as the 2nd CA. Centroid of the 3rd CA is represented in different coordinates than in 2nd CA, but the sense of the analysis is similar and thus the comparison with the model yields the same conclusion.

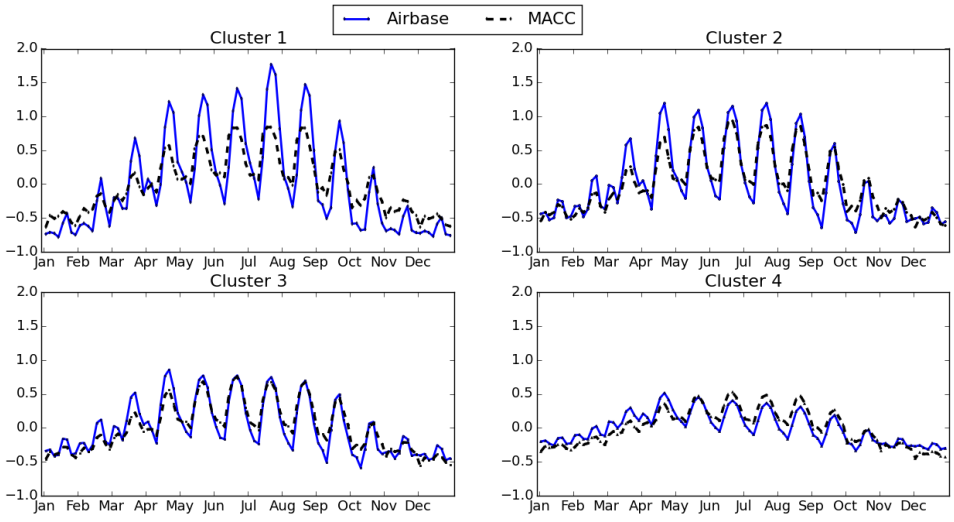

Figure 5.54. Airbase cluster centroids vs MACC group means. 2nd CA.

The shape of Airbase diurnal cycles is somehow better predicted by MACC than the seasonal cycles (Figure 5.55), while the seasonal amplitudes are better described than diurnal. Seasonal cycles of MACC group means are more symmetrical and "round"-shaped than Airbase centroids, spring maxima and summer peaks are not predicted. CL1 has most of discrepancies between model and observations. Airbase diurnal cycles have more pronounced daily minima and maxima, though for CL4 modeled and observed diurnal cycles are quite consistent (Figure 5. 55).

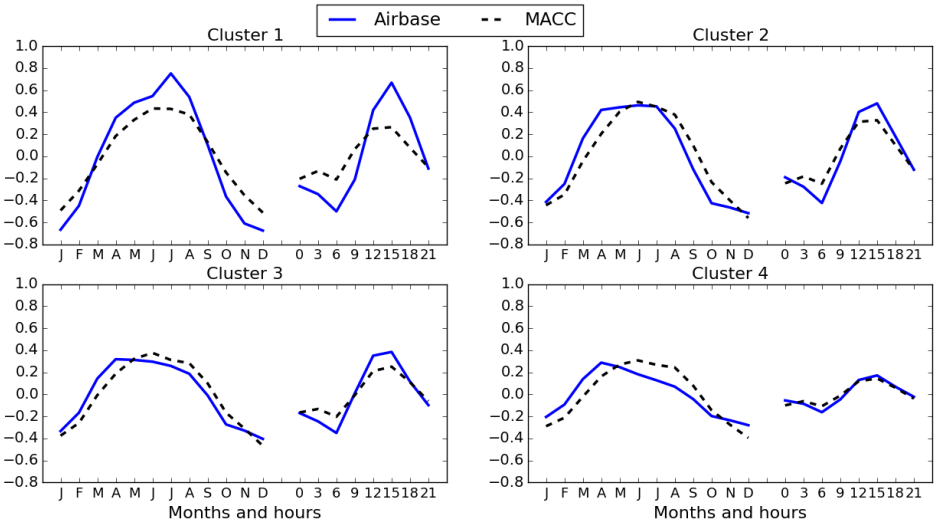

Figure 5.55. Airbase cluster centroids vs MACC group means. 3rd CA.

The weekly amplitudes are calculated from average weekly amplitudes for each station and collected to distributions for each cluster (Figure 5.56). The highest and the broadest distribution is obtained for CL2, indicting, as previously noted from the 1st CA results, the higher level of emissions for CL2 and the so called "weekend effect".

The weekly amplitudes distributions correspond to Airbase classification comparison made in section 5.2.2, established that CL2 has more stations than CL1 potentially having more emission sources. According to this classification, CL1 contains predominantly background urban stations, but CL2 – background urban and traffic urban stations with some industrial sites.

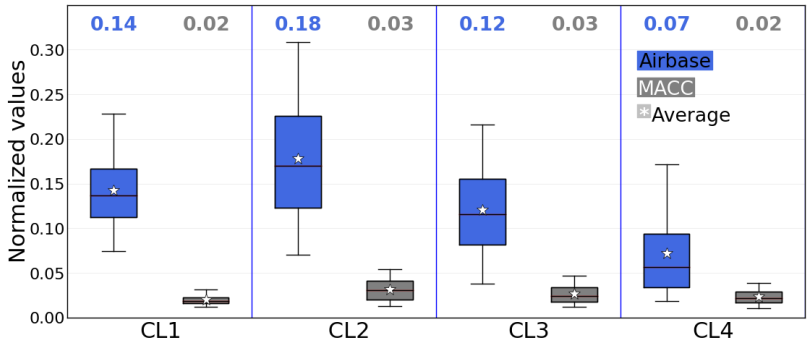

Figure 5.56. Percentiles (5-25-50-75-95) of ozone weekly amplitudes in clusters, Airbase vs MACC. Upper values indicate the mean weekly amplitude of each cluster. 2nd CA.

5.2.7 Cluster Analysis with 7 clusters

Section 5.1.3 concludes that there are different seasonal ozone patterns between Southern, Western and Central Europe, but the CA results do not reproduce this geographical distinction. Therefore we tested a CA with higher k in order to see whether it will lead to better regional separation of clusters.

As mentioned in section 4.2.1 "K-means", the appropriate number of clusters for CA is the maximum possible number at which the stability of the SSD value for arbitrary k-means run is still observed. Moreover at this number the SSD curve grows sharply towards lower numbers. On the "elbow" plot produced for the 2nd set of properties (Figure 4.4) after k = 4 the SSD curves are deviating from one another, thus showing poor reproducibility of CA results if k >= 5 is used. According to all rules, k = 4 had been chosen for the 2nd CA. Nevertheless the next best case is k = 7, as in this case the SSD don't show as much spread like for k = 5 and 6, and k = 7 should be large enough for sufficient description of various regions. At this number some SSD curves diverge, while many other runs come to good agreement (within the scale of the plot). Therefore we decided to find out the clustering behind and made CA for the 2nd set of properties taking k = 7. The results from this analysis are presented below.

The map of cluster distributions is shown in Figure 5.57. There are clusters, which remain geographically similar to the original CA, like CL1 (= CL1) in the Po Valley region or CL7 (former CL4) spread over Scandinavia, Great Britain, Spain, coastal areas and mountainous sites. Other clusters also retain some features of the 1st CA: CL2 extends from Slovenia to Germany (similar to CL1 in the 1st CA), CL4 here is similar to CL3 in the 1st CA, but here it is not including much of western stations. In this CA three new clusters appear: CL3, 5 and 6. The first two are small agglomerations with ≈ 150 stations each, while CL6 contains > 300 stations, located mainly in Western Europe. CL3 is distributed over the Mediterranean region and Spain, while CL5 in Central Europe, Italy and the Balkans.

Quantitatively CL1 is formed only from CL1 of the 2nd CA, and CL7 from CL4. Other clusters are combinations of the stations, which were present in two earlier clusters of the 2nd CA. The prior CL2 contributed to the new CL2, 3, 4 and 5, while CL3 constituted clusters CL3, 4, 5 and 6 of the new CA. CL4 mainly composed CL7, but also gives part of stations to CL6, though the majority of stations in CL6 are from previous CL3.

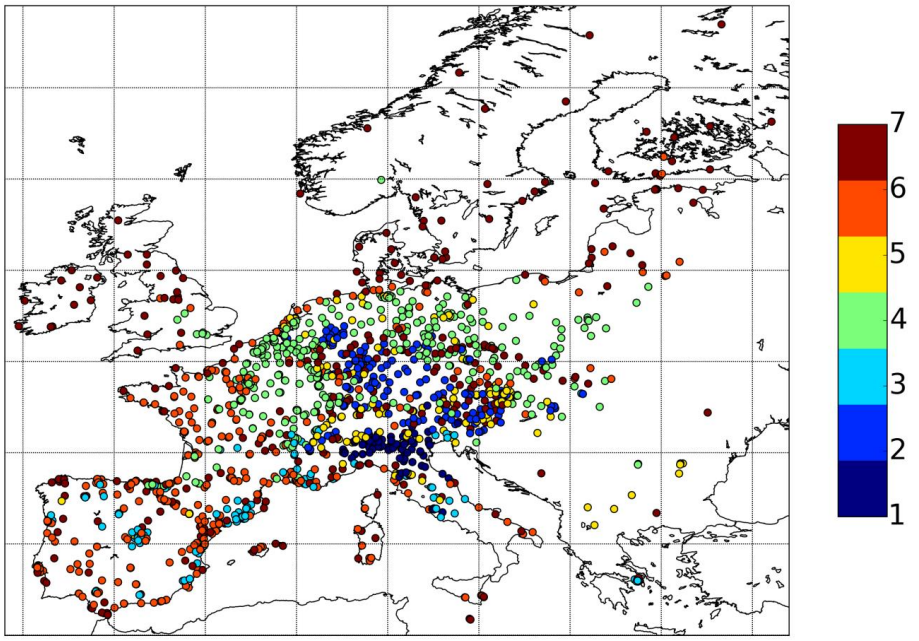

Figure 5.57. Map of 1492 Airbase stations clustered to 7 groups, 2nd set of properties.

Table 5.22 describes the cluster characteristics, based on the Airbase classification, geography and altitude range. The difference between CL2 and CL5 is not clear here. Both clusters CL2 and CL5 are presenting similar altitude range and Airbase classification, including nearly equal amounts of urban, suburban background and urban traffic stations. CL1 in comparison to them has very few traffic stations, but has the largest number of urban background stations (50%). CL3 is the only cluster, which contains more than 20% of stations of industrial type according to the Airbase classification.

The picture of the normalized frequency distributions for each cluster in comparison to those of MACC reveals main differences (see Figure 5.58). The high peak of low ozone concentrations is present in all clusters, except for CL6 and CL7, with decreasing frequency from CL1 to CL5. The MACC model is not able to fully describe low ozone, the model zero-peak is either absent or not completely pronounced. In all clusters MACC overestimates observations and in some cases shows a second maximum.

Table 5.22. Statistics of 7 clusters, obtained from the CA based on the 2nd set of properties, and their description, based on the Airbase classification, geographical location and altitude range of clusters.

cluster	cluster description	number of stations
1	urban/suburban, Po Valley	79
2	urban/suburban, traffic	171
3	urban/suburban, industrial, traffic	131
4	urban/suburban, moderately polluted	328
5	urban/suburban, traffic	159
6	background, moderately polluted	321
7	rural background, middle-elevated, remote	303

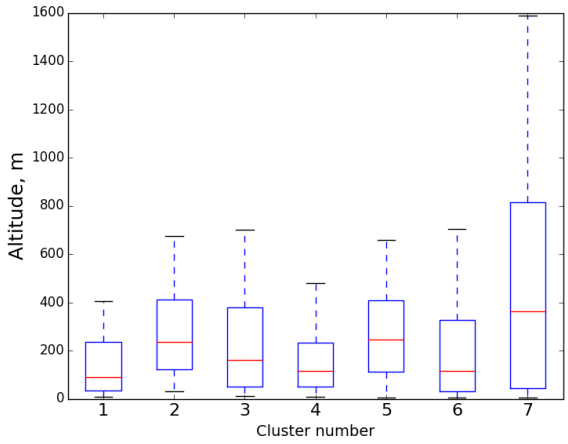

Figure 5.58. The 5-25-50-75-95 percentile distributions of station altitudes in 7 clusters.

Both CL4 (Central Europe) and CL6 (Western Europe) are moderately polluted according to the Airbase classification, but CL4 includes more urban stations than CL6 (Table 5.22) and thus exhibits higher ozone titration than CL6. The same situation is for CL2 and CL5. CL2 shows the highest amount of zero ozone in comparison to other clusters (Figure 5.59).

Though there are many clusters with high pollution levels, the seasonal cycles of obtained cluster centroids in normalized values (Figure 5.60) show specific behavior for every cluster. For clusters, which have common characteristics with previously obtained clusters in other CAs, the seasonality is quite expectable (CL1, CL2, CL4, CL7), but for new clusters like CL3, CL5 and CL6 some other features appear. For clusters with much of low ozone concentrations (CL1 and CL2) the annual cycle has the largest amplitude.

CL3 is concentrated mostly in the Southern and Western regions and exhibits a pronounced late summer maximum. Similar picture of cycles we found out in section 5.1.3 “Selected European

stations (1998-2011)" of chapter "Trend analysis" for the 3 stations, located in the South and West of Europe (Krvavec, Monte-Cimone and Campisabalos, see Figure 5.19,b). They have also shown July-August maxima as well as visible April maxima for more western Campisabalos.

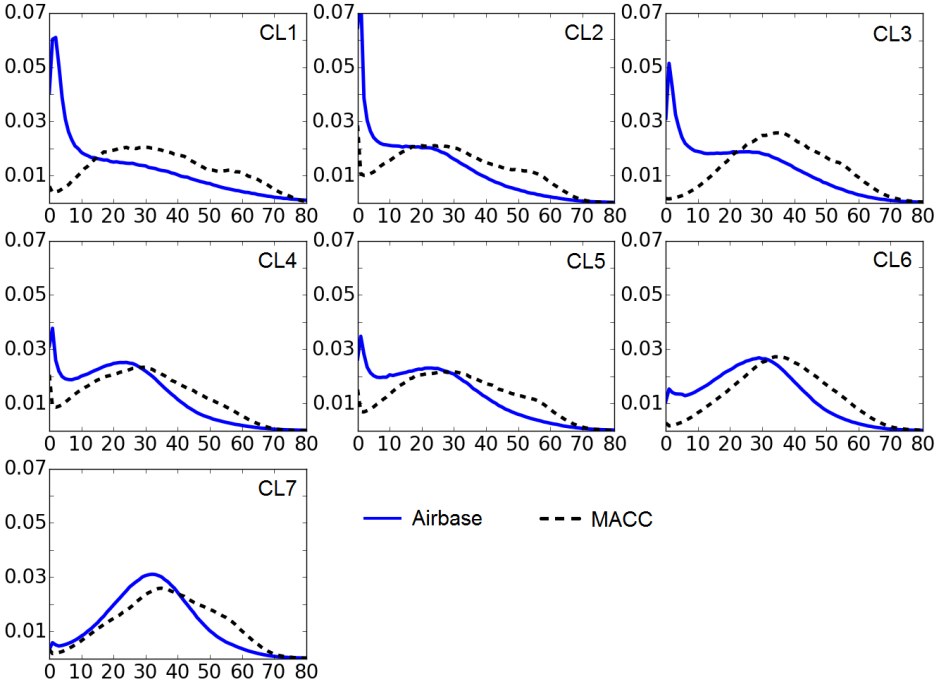

Figure 5.59. Normalized frequency distributions of 3-hourly ozone values in clusters (2007-2010), Airbase vs MACC. 7 clusters.

CL5 is mainly located in Central Europe like CL2 or CL4, but in contrast to them, it has a July peak (Figure 5.60). As discussed before, CL2 and CL5 have nearly equal altitude range, and according to Airbase classification they show similar amount of urban background and urban traffic stations (Table 5.22). Figure 5.59 shows lower ozone for CL2 than for CL5, but only here the main difference becomes evident. Western stations mostly belong to CL6 and CL7, which show pronounced spring maximum on the annual cycles (Figure 5.60). Similar feature was already observed for western stations Iraty and Puy du Dome (section 5.1.3 "Selected European stations (1998-2011)", see Figure 5.19, c).

Diurnal cycles (Figure 5.61) differ mostly only in the amplitude between daily minima at 6 am and daily maxima at 3 pm. The amplitude is decreasing from CL1 to CL7 (Figure 5.63), though for CL3 it is slightly larger than for CL2.

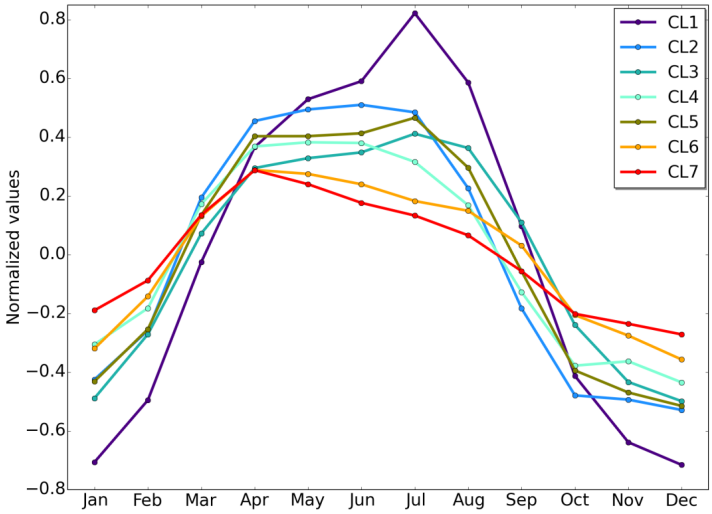

Figure 5.60. Seasonal cycles of cluster centroids, Airbase. 7 clusters.

Distributions of annual and diurnal amplitudes of Airbase clusters in comparison to MACC are shown in Figures 5.62 and 5.63. Like in the previous CA with 4 clusters, annual amplitudes are better predicted by MACC than diurnal, and have relatively good match between the model and observations with exception for CL1 and CL3. For them MACC underestimates the annual amplitudes, but also as shown in Figure 5.59, it is not predicting their zero-ozone.

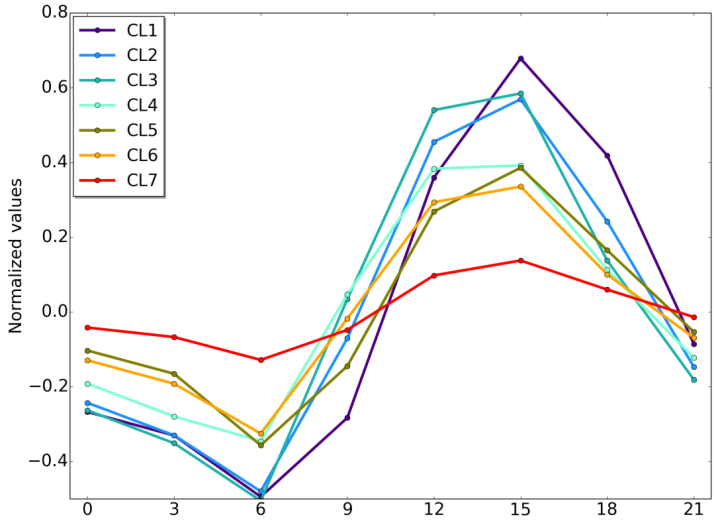

Figure 5.61. Diurnal cycles of cluster centroids, Airbase. 7 clusters.

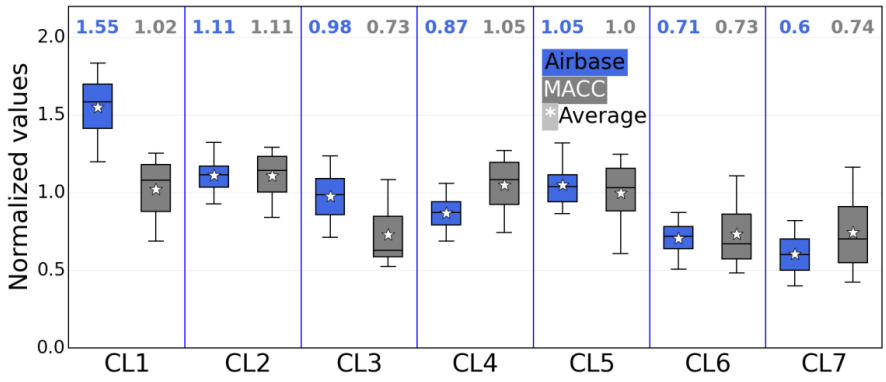

Figure 5.62. Percentiles (5-25-50-75-95) of ozone annual amplitudes in clusters, Airbase vs MACC. Upper values indicate the mean annual amplitude of each cluster. 7 clusters.

Using 7 clusters for the CA based on the 2nd set of properties gives as a result more various agglomerations than the CA with 4 clusters, though the analysis itself is less reproducible. Among the 100 k-means runs with k = 7 only 12 would give similar cluster allocations (>= 95% of similarity) and 23 – at least 85% of agreement (the SSD curve is not shown). While for the CA with 4 clusters all 100 runs produce results at least on 95% similar to one with the lowest SSD (Figure 5.70).

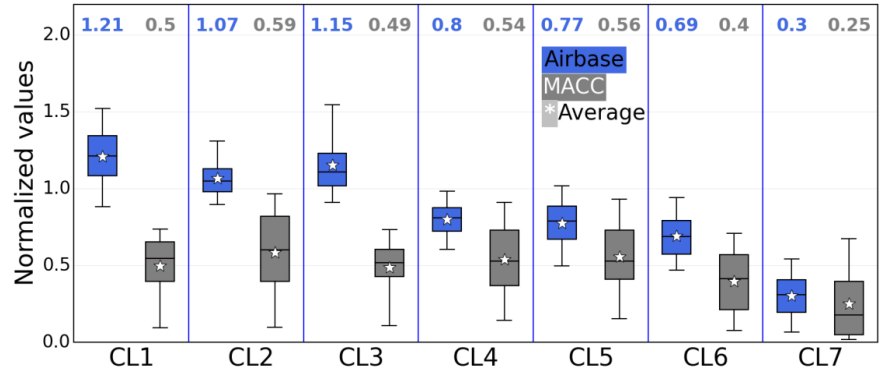

Figure 5.63. Percentiles (5-25-50-75-95) of ozone diurnal amplitudes in clusters, Airbase vs MACC. Upper values indicate the mean diurnal amplitude of each cluster. 7 clusters.

5.2.8 Quality of cluster separation

5.2.8.1 First CA

In this subsection we check the quality or goodness of clustering, i.e. how well clusters are separated from each other. In the discussion below we present Euclidean distances, calculated between stations and centroids, and we will call them internal distances, if they are distances of the stations to

their own centroid, and external distances, if we mean distances of the stations to centroids of other clusters.

It is not possible to show stations distribution in 96-dimensional space, but for illustration we selected 2 distinctive properties out of 96 (1st CA, i.e. absolute ozone seasonal-diurnal variations): January at 0h vs July at 15h (Figure 5.64). Within the limits of this image we note well distinguishable separation of CL5, but much overlap between clusters CL1, 2, 3 and 4.

The distribution of internal distances for each cluster in dependence on the normalized number of stations (i.e. function of 0÷1 values) shows that density of agglomerations is the highest for CL3 and CL1 and the lowest for CL5, while CL2 and CL4 have intermediate density (not shown). This is at some extent also derivable from Figure 5.64.

The relative distances of stations of each cluster to the next nearest centroids were calculated and combined into distributions (Figure 5.65). Under "relative" here is understood the ratio of absolute distances of a station to own centroid in comparison to the next nearest centroid.

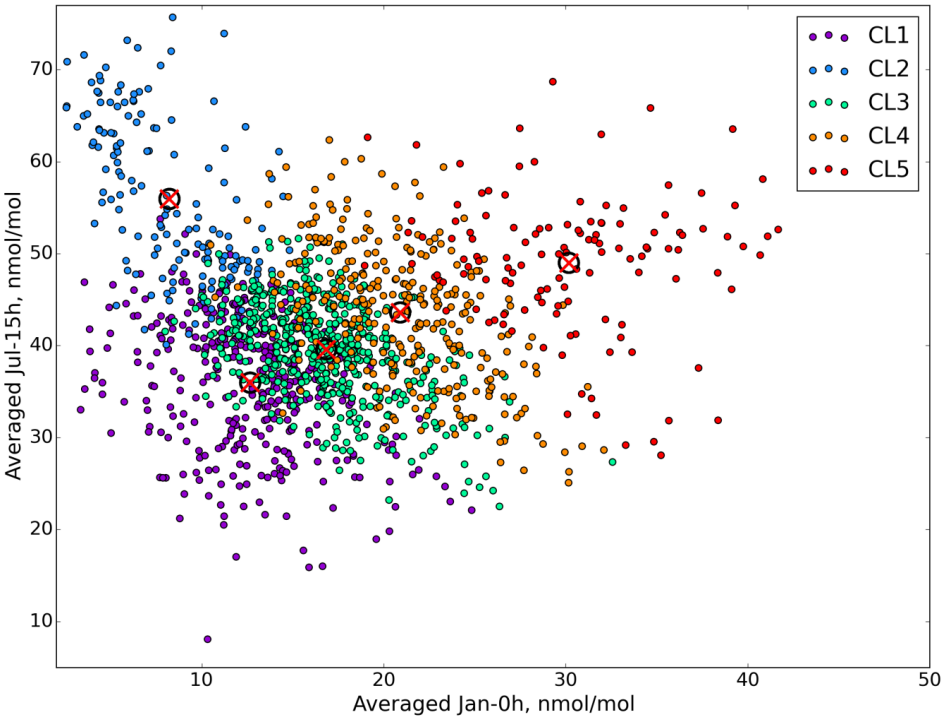

Figure 5.64. Stations distribution in the space of 2 properties out of 96: January at 0h vs July at 15h. Centroids of each cluster are marked as black circles with a red cross. 1st CA.

For example, for CL1 there are two distributions, named as cent2 and cent3, which means that for any station of cluster 1 the only second-nearest centroids are either centroids of CL2 or CL3, while none of the stations in CL1 have centroids of CL4 or CL5 as the second-nearest.

The lowest percentiles of all distributions are close to 1.0, which means that next centroids for some stations are not much farther than own centroids (Figure 5.65). This is also expected from Figure 5.64, as there is no clear distinguishable border between clusters. Medians of many distributions are less or around 1.5. For all clusters 95-percentiles of distributions are normally not higher than 3.25. The only neighboring centroid of all stations of CL5 is CL4. In this case the median of the relative distances distribution reaches ≈ 2.0, while 95-percentile is more than 3.0, which indicates a good separation of CL5 from the other clusters. The less separated clusters are CL2, CL3 and CL4, as they are surrounded by 3 nearest centroids, which for many stations are 1.5 times or less remote than the own centroid.

Average median over all distributions is ≈ 1.6 per cluster, i.e. the next nearest centroid for stations of any cluster is on average 1.6 times more distant than the own centroid.

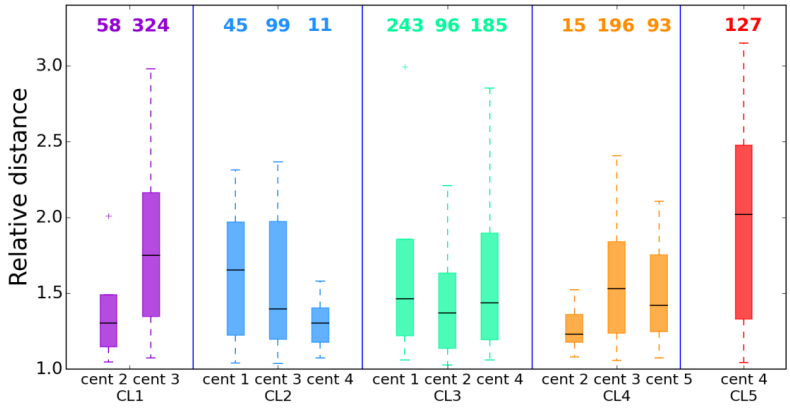

Figure 5.65. Distributions of the relative distances of each cluster to the next nearest centroids with amount of stations (written at the top of the graph), belonging to each distribution. Distributions are given in 5-25-50-75-95 percentile range. 1st CA.

5.2.8.2 Second and third CAs

Analogous to Figure 5.64 we got the picture of stations distribution in 2 dimensional space (out of 96 normalized ozone seasonal-diurnal variations) for the 2nd CA (see Figure 5.66). In this case we note more isolated position of CL1, while other clusters quite strong overlay one onto another.

Similar plot, but for the 3rd CA is shown in Figure 5.67, where 2 properties - normalized means of January and July - out of 20 were taken into consideration. Here we see even stronger overlap between CL2, 3 and 4, while CL1 is still well separated, but more than in the 2nd CA embedded into CL2.

The computation of internal distances revealed comparable densities in clusters CL2, 3 and 4 for the 2nd as well as for the 3rd CA, but thinner distribution of stations in CL1.

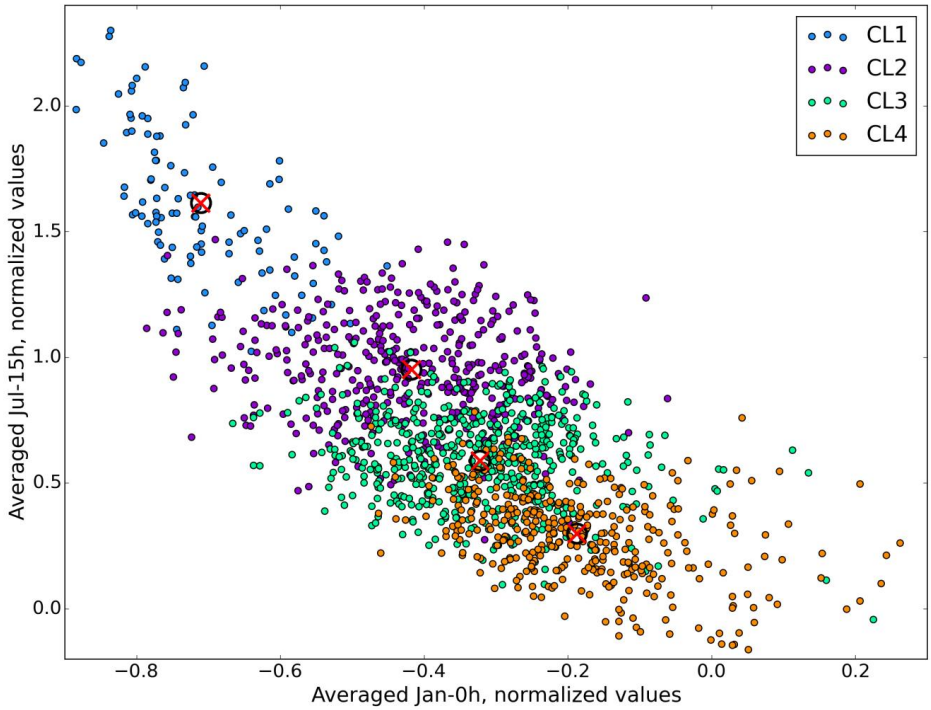

Figure 5.66. Stations distribution in the space of 2 properties out of 96: January at 0h vs July at 15h. Centroids of each cluster are marked as black circles with a red cross. 2nd CA.

Distributions of the relative distances of each cluster to the next nearest centroids are very similar for the 2nd and 3rd CAs. We provide only one picture of the 2nd CA (Figure 5.68). Generally clusters of 2nd and 3rd CAs have no more than 2 next nearest centroids.

Better separation is reached for two opponent clusters CL1 and CL4, which show medians of relative distances at ≈ 1.75. Next centroids for stations of CL2 and CL3 are equally distant centroids 1 and 3 and centroids 2 and 4 respectively. These are less than 1.5 times remote from stations than their own centroids.

Average median over all distributions is ≈ 1.5 per cluster for the 2nd CA and ≈ 1.6 for the 3rd CA, which indicates similar relative remoteness of the next centroids from stations in both CAs. But according to Figures 5.66 and 5.67, in the plotted coordinates (2 properties) the separation is visibly better in the 2nd CA rather than in the 3rd, as in the last case there is stronger overlap between clusters.

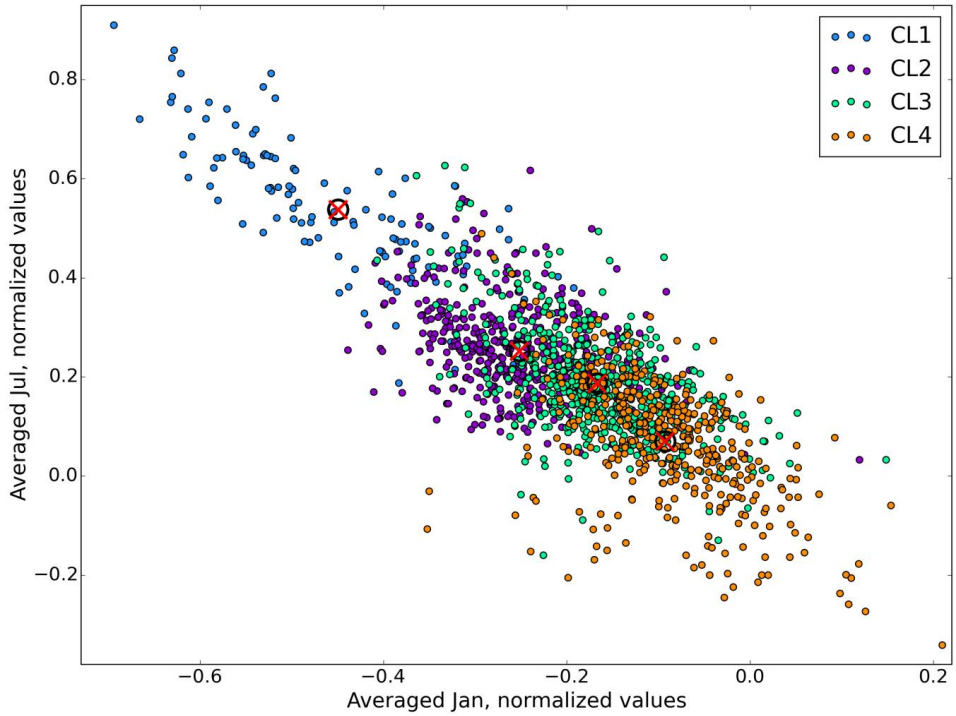

Figure 5.67. Stations distribution in the space of 2 properties out of 20: January vs July. Centroids of each cluster are marked as black circles with a red cross. 3rd CA.

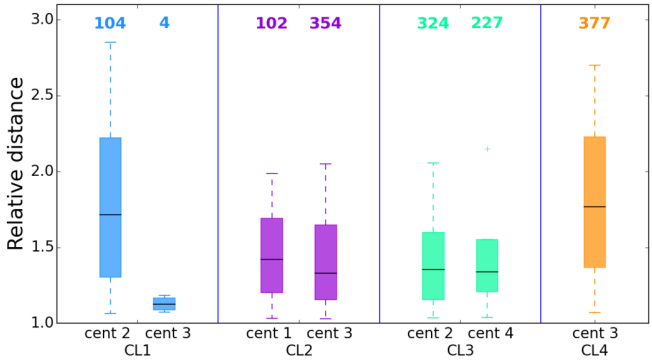

Figure 5.68. Distributions of the relative distances of each cluster to the next nearest centroids with amount of stations (written at the top of the graph), belonging to each distribution. Distributions are given in 5-25-50-75-95 percentile range. 2nd CA.

5.2.9 Robustness of the cluster analyses

5.2.9.1 First CA

As described in section 5.2 “Cluster analysis”, repeated k-means runs do not necessarily lead to the same allocation of stations to clusters. When applying random generation of k centroids, independent k-means runs will produce slightly different SSD values and therefore distinguishable CA results. Thus it is important to test the robustness of the CA by analyzing the results from repeated invocations of the method. Another aspect of robustness concerns the reproducibility of results when random subsets of stations or data of any given year are excluded from the analysis. These aspects are analyzed in this section.

As mentioned in section 4.2.1 “K-means”, we made 100 independent k-means runs for each CA and from these runs the one was chosen which has shown the smallest SSD. The results described in chapter “Results and discussion” were derived from these 3 runs (for the 1st, 2nd and 3rd CAs). Minimum SSD runs are obtained with full data sets and we will name further such runs as reference runs. In this section all other k-means runs are compared to the reference runs for the consideration of the robustness statistics of cluster analyses.

The plot of the SSD for each of 100 runs (Figure 5.69) reveals at least three “stable states” with relatively small SSD values, moderate and higher outliers.

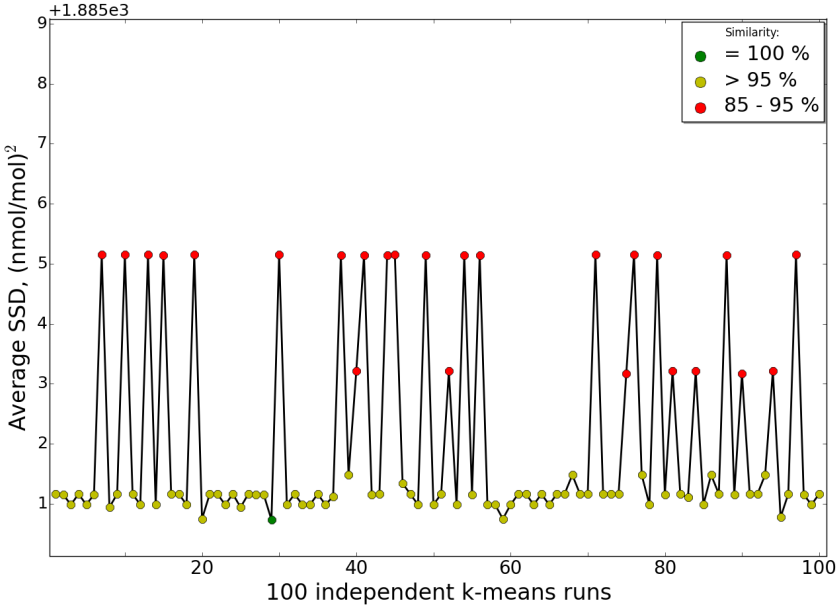

Figure 5.69. Averaged SSD for 100 independent k-means runs with cluster number k = 5 for all runs. 1st set of properties. Percentage ranges in legend are indicating similarity of corresponding k-means runs with the 1st CA results, presented in this work (green value – reference run).

The majority of runs belong to the smallest "stable state" (75 runs out of 100). These k-means runs with full data set generally yield a very similar classification of stations (more than 95% of similarity to reported results), whereas the runs with larger SSD lead to some changes in the attribution of stations to the five clusters.

Besides the 100 k-means runs with all 1492 stations we performed another 100·100 k-means runs with data arrays reduced to 90, 80, 70, 60 and 50% of the initial data set. They were reduced by randomly excluding the respective number of stations for every run. For statistics each of the 100 different variations of reduced data sets was subjected to 100 k-means runs. This was done in order to get the best k-means run corresponding to minimum SSD from 100 runs of every reduced data set variation, and then compare these 100 chosen best runs of 100 variations of reduced data set with each other.

The consistency of CA results can be obtained from contingency tables, where off-diagonal elements reveal the number of stations that were allocated to a different cluster in the new run. An example for such a contingency table is given in Table 5.23. In this case 1343 stations (90% of 1492) were randomly chosen. 1324 (i.e. ≈ 99% of 1343) of these stations lie on the main diagonal, which means that they were attributed to the same cluster as in the reference run with 99% similarity.

Table 5.23. Example of the contingency table with stations distribution in clusters: reference run (rows) vs k-means run with 90% of data set (columns).

cluster	CL1	CL2	CL3	CL4	CL5
CL1	**327**	3	10	0	0
CL2	0	**191**	0	0	0
CL3	0	0	**450**	5	0
CL4	0	0	0	**277**	1
CL5	0	0	0	0	**79**

Table 5.24 summarizes the results of all robustness tests by grouping the contingency results into three categories: better than 95% agreement, 85-95% agreement, and less than 85% agreement of cluster allocations (in this case there were no cases with less than 85% agreement for k-means runs of the 1st set of properties). Each row in Table 5.24 represents the results for one particular dataset size (full: 100%, reduced: 90, 80, 70, 60, 50%).

As the first row in Table 5.24 shows, there were 75 out of 100 runs with the full dataset which sorted at least 95% of the stations into the same clusters as the reference run. It is interesting to see that the remaining cases (i.e. 25 runs with 85-95% of "correct" classification) are associated with larger SSD values (Figure 5.69). This highlights the necessity to perform repeated k-means analyses in order to obtain meaningful results. Exemplary checks of how the stations are re-distributed when the results differ indicate that we usually find CL3 stations from the reference run in CL1 and CL2,

while some CL4 stations are moved to CL3. This indicates that the distinctions between these clusters may be less obvious if we base our analysis on mean concentrations as we did in this study.

Table 5.24. Statistics regarding the robustness of the 1st CA analysis (see text).

data		number of k-means runs (out of 100) or probability with % of stations clustered as reference run		
amount of data array,%	number of stations (96 dimension)	> 95% stations (cat.1)	85 - 95% stations (cat.2)	< 85% stations (cat.3)
100	1492	75	25	0
90	1343	100	0	0
80	1194	99	1	0
70	1044	97	3	0
60	895	99	1	0
50	746	92	8	0

To repeat, Table 5.24 includes the resulting minimization amoung 100 runs of 100 variations of reduced data sets. This reflects in generally better results for reduced data sets in comparison to the full data set. Nevertheless, even when the data reduced to the half-size, similarity with the reference run remains high (92 out of 100 runs with at least 95% identical cluster allocations), pointing to the robustness of clustering.

5.2.9.2 Second and third CAs

Similar analyses on robustness of CA were done for the 2nd and 3rd set of properties. Previously in chapter "Results and discussion" we more often considered the 2nd CA mentioning that the 3rd CA produces similar results. In this section we aim to find the differences between them and to identify the most optimal set of normalized properties suitable for clustering of ozone pollution regimes.

Similar to the robustness tests made with the 1st set of 96 absolute properties, we repeated the same procedure for 2nd and 3rd sets of properties. SSD curves of 100 series of k-means runs for both of them are presented in Figures 5.70 and 5.71, respectively. Results of the additional k-means runs with data arrays reduced to 90, 80, 70, 60 and 50% and compared with runs, which have shown minimum SSD, are given in Tables 5.25 and 5.26.

From the first look at Figure 5.70 we notice that the SSD curve of 100 k-means runs based on 2nd set of properties is very "jumpy" and has no "stable states" like it was in previous section for the 1st set of properties. But the scale of SSD values is also very narrow here, and all the points correspond to more than 95% similarity with the reference run for the 2nd CA. Table 5.25 reflects this, and also provides the information about the k-means runs with reduced data sets. In reductions down to 80% of data array there are always not less than 95% of stations of this set clustered similar to the

reference run. With further reduction similarity slightly decreases, but also as in case of the 1st set of properties, here 92 out of 100 runs show 95% of similarity when half of data array is eliminated.

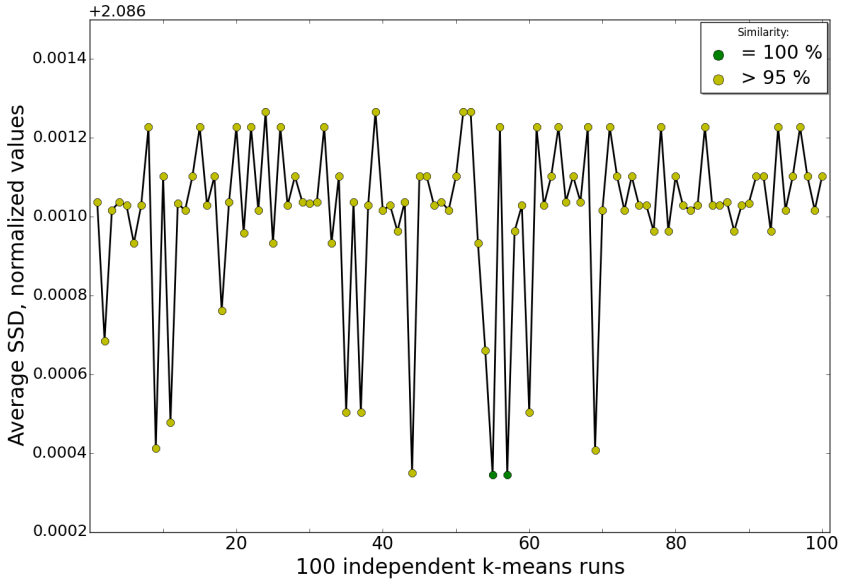

Figure 5.70. Averaged SSD for 100 independent k-means runs with cluster number k = 4 for all runs. 2nd set of properties. Percentage ranges in legend are indicating similarity of corresponding k-means runs with the 2nd CA results, presented in this work (green value – reference run).

Table 5.25. Statistics regarding the robustness of the 2nd CA analysis (see text).

data		number of k-means runs (out of 100) or probability with % of stations clustered as reference run		
amount of data array,%	number of stations (96 dimension)	> 95% stations (cat.1)	85 - 95% stations (cat.2)	< 85% stations (cat.3)
100	1492	100	0	0
90	1343	100	0	0
80	1194	100	0	0
70	1044	99	1	0
60	895	99	1	0
50	746	92	8	0

For the 3rd CA the 100 k-means runs SSD curve is less stable than for the 2nd CA (Figure 5.71). There are 78 runs with more than 95% similar to reference run stations allocations, and even one run with only ≈ 70% of agreement. Reduction of data set produces worse results in comparison to the 1st and 2nd sets of properties (Table 5.26).

Table 5.26. Statistics regarding the robustness of the 3rd CA analysis (see text).

data		number of k-means runs (out of 100) or probability with % of stations clustered as reference run		
amount of data array,%	number of stations (20 dimension)	> 95% stations (cat.1)	85 - 95% stations (cat.2)	< 85% stations (cat.3)
100	1492	78	21	1
90	1343	99	1	0
80	1194	95	5	0
70	1044	99	1	0
60	895	93	7	0
50	746	88	12	0

Here we get never less than 88% of probability to achieve more than 95% of similarity with the reference run, in contrast to the 1st and 2nd set of properties (never less than 92% of probability). Therefore 20 normalized properties data set stands out as less robust to obtain similar and stable results than 96 normalized set of properties.

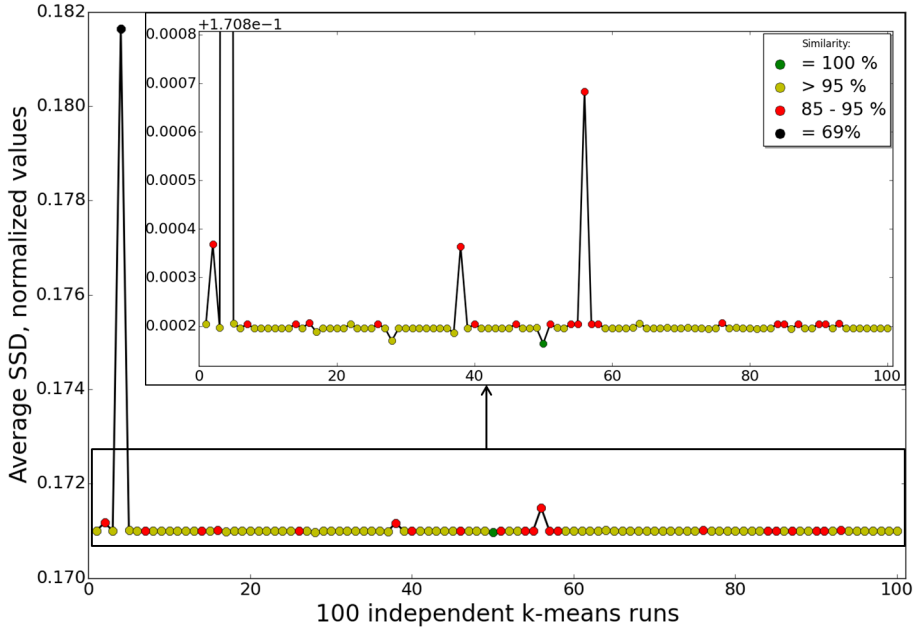

Figure 5.71. Averaged SSD for 100 independent k-means runs with cluster number k = 4 for all runs. 3rd set of properties. Percentage ranges in legend are indicating similarity of corresponding k-means runs with the 3rd CA results, presented in this work (green value – reference run).

5.2.9.3 Robustness of the CAs, excluding yearly data from data sets

In this part of analysis we have implemented CAs based on the same set of properties (1st -96 absolute seasonal-diurnal variations, 2nd - 96 normalized seasonal-diurnal variations, 3rd – 20 normalized seasonal and diurnal cycles) and the same set of stations, but the time series used for properties computation were reduced. Each set of properties was re-calculated 4 times excluding data for complete 2007, 2008, 2009 and 2010 years respectively, i.e. time series of 3 years-long periods were extracted. We have repeated 100 k-means runs with each such shortened set of properties, i.e. $4 \cdot 100$ times for every type of CA: 1st, 2nd and 3rd.

Afterwards single runs with minimum SSD were chosen out of every 100 k-means series, and compared to reference runs, based on the full period of time (2007-2010). Percentages of the stations were computed from the diagonals of contingency tables for all comparisons and are given in Table 5.27. In the last column there is the average similarity of 4 runs with missing years.

CAs based on 1st and 2nd sets of properties give ≈ 95% average similarities with their reference runs, while there are only ≈ 91% for the 3rd set of properties, which is provided by low (≈ 79%) agreement when data for 2009 year are excluded. Again the 3rd CA is less stable than the 2nd CA, which always produces more than 93% of the same allocation of stations to clusters.

The time series of individual stations show that the data from 2009 are often presenting the pronounced April maximum and sometimes secondary annual maximum in August-September, while June-July exhibit minima. This is observable more for Central European stations rather than for Southern or South-Western locations. Most probably this effect is influencing the CA, based on 20-properites (which includes complete averaged annual cycle) stronger than the CA based on 96-properties set.

Table 5.27. Similarities (percentages of stations) between reference CA runs and runs based on data sets with excluded years (see text).

set of properties	missing year				
	-2007	-2008	-2009	-2010	average
1st	94.8	95.1	95.0	94.9	95.0
2nd	93.0	96.3	96.2	94.0	94.9
3rd	94.5	95.4	79.2	94.5	90.9

For all mentioned above k-means runs we computed also relative distances of each obtained cluster to the next nearest centroids, like it was done for reference CA runs (see previous subsection). Distances were combined into distributions and the sum of their medians divided by number of clusters was calculated (Table 5.28). Before we already described the values of average medians for each of CAs (see the last column of Table 5.28 for comparison). According to obtained indicators,

we consider that cluster separation is comparable in all analyses, because all values are of similar magnitudes.

Table 5.28. Average sums of medians, calculated from distributions of the relative distances of each cluster to the next nearest centroids (see text).

set of properties	runs with missing year					reference run
	-2007	-2008	-2009	-2010	average	2007-2010
1st	1.90	1.89	1.64	1.56	1.75	1.60
2nd	1.54	1.52	1.54	1.51	1.53	1.54
3rd	1.58	1.57	1.58	1.58	1.58	1.58

To conclude, the 1st set of properties is giving quite stable k-means runs with never less than 85% of similarity, and 92% of probability to reproduce results presented in this work in better than 95% identity. Reducing the time series to 3 years yields as high as ≈ 95% similarity in the allocation of stations to clusters.

As for normalized properties, our preference would be in favor of the 2nd set rather than 3rd. This is based on the finding that 96 properties show much higher reproducibility of results for full as well as for reduced data sets than 20 properties. Secondly, when excluding one arbitrary year from the data, CAs based on 96 properties results in higher similarity (≈ 95%) to the reference CA run than 20 properties based CAs (≈ 91%).

CHAPTER 6

6 Summary and outlook

Summary

The high density of European surface ozone monitoring sites offers good opportunities for investigation of the regional ozone representativeness. In the literature the term representativeness is related to a single monitoring station or to a network of stations. In the first case a station is considered representative for some area, if this area shows ozone characteristics similar to this station. A station network aims to be representative for a territory, covered by this network (Spangl et al., UBA report, 2007). Ozone time series contain several features (parameters), which can be taken for analysis of the representativeness.

This definition opens several questions, which we tried to answer in the present work. What kind of ozone parameters would divide Europe into representative regions? How to identify the representative regions? Would each representative set of stations characterize some particular contiguous geographical area, or, conversely, can one territory be described by several ozone patterns regarding the chosen parameter? How large can the ozone representative areas in Europe be? How many stations would one need in order to obtain a "representative picture" of surface ozone concentrations in Europe? How similar can concentrations at neighboring stations be? Besides we were also interested to find out how the observed long-term trends in surface ozone concentrations are consistent across stations that share similar behaviour in recent years.

A second motivation of the present work is related to the evaluation of global chemistry-climate models. Very often for that purpose the simulated output mean is compared to individual ozone observations or arbitrarily aggregated sets of observations, which can provide general information about the model biases for area, captured by sites, but does not help in the interpretation of these biases.

As starting point we analyzed ozone trends and seasonal behaviour of ozone concentrations at selected individual stations in different regions of Europe. These included three Alpine stations (Jungfraujoch, Sonnblick and Zugspitze) and several other stations (15 in total) as well as some stations from the German network of the regional air quality data (UBA).

The trend analysis for three Alpine stations is consistent with previously reported results, though in our case the analysis was extended to a longer time period (1990-2011). The Alpine stations show consistent positive winter trends, and insignificant or negative summer trends. Summer ozone decline during the period 1990-2011 is also apparent in the data from the network of rural background stations over Germany, while more polluted sites have insignificant summer ozone

trends. Similarly to the Alpine stations winter ozone trends are positive for all types of stations in Germany from 1990 to 2011. For the period 1998-2011 annual ozone trends are negative for the Alpine region stations as well as for several other European stations. This is mostly driven by summertime ozone. This analysis shows that ozone trends are quite consistent within Europe, and one cannot identify individual regions in Europe where the trends would differ.

Data from the 15 individual stations selected from all over Europe together with the three Alpine stations during 1998-2011 revealed at least 3 different seasonal ozone concentration patterns which are rather consistent among stations in Central, Southern and Western Europe, respectively. The data from the Alpine stations exhibit features similar to the stations from the Central European group rather than other groups. The differences observed in the annual cycles obtained for 3 European regions led to a more thorough analysis of the ozone representativeness. At the next step the ozone parameters for investigation of the representativeness are extended to seasonal-diurnal variations, which appear as the main components of ozone time series and therefore allow to describe the ozone behavior more comprehensively.

The regional representativeness of European ozone measurements is investigated through a cluster analysis (CA) of ozone air quality data from 1492 European surface monitoring stations of all types (Airbase database). K-means clustering was implemented for 3 sets of properties: (i) seasonal-diurnal variations in absolute mixing ratio units [96 properties], (ii) normalized seasonal-diurnal variations [96 properties], and (iii) averaged and normalized seasonal and diurnal variations [20 properties]. Each CA identified different ozone pollution regimes, and each of them was compared with the output of the multi-year global reanalysis produced within the Monitoring of Atmospheric Composition and Climate (MACC) project. Comparing the model output to cluster results allows to see whether the model is able to capture specifics of each group and describe various ozone pollution regimes.

Regarding the evaluation of the MACC model with respect to average ozone concentrations we obtained results which are generally consistent with Inness et al. (2013) for Northern and Southern Europe (i.e. positive biases in summer and negative in winter for Northern Europe and year-round positive biases for Southern Europe). In contrast to the previous study, however, Central European observations are not underestimated everywhere in wintertime, but there are regions where the model overestimates ozone in winter, namely in the Alpine region, Benelux area, parts of France and Germany (≈ + 8-10 nmol/mol). Summertime biases in Central Europe are somewhat larger than reported by Inness et al. (2013) (+ 8-32 nmol/mol).

The classification of stations in our CA is to some extent related to the Airbase description of area types, which divides station types into background, industrial and traffic and station area types into urban, suburban and rural. The consistency between this Airbase characterization and our classification is mainly reflecting the pollution levels in the individual clusters.

In the first cluster analysis (1st CA) based on absolute seasonal-diurnal variations stable results are obtained with a classification into 5 clusters (CL1 – CL5). The first 3 clusters represent more polluted regimes, while the other two exhibit characteristics of more rural and clean sites. This interpretation is supported by simulated data for CO and NOx from the MACC reanalysis. CL1 – CL3 contain roughly 70% of all considered stations. CL3 is geographically distributed all over Europe, while CL1 stations are mostly located in Central Europe and CL2 stations are concentrated in the North of Italy (Po Valley region). The frequency distributions of hourly ozone values for those clusters show significant amount of very low ozone concentrations especially for CL1 and CL2, which is consistent with ozone destruction due to titration with freshly emitted NO and thus indicative of urban or suburban pollution signatures. Stations in CL4 and CL5 are generally located further away from large cities or industrial agglomerations. The ozone time series from these stations exhibit a seasonal cycle which is typical for less polluted conditions with less variability and fewer titration events than at stations in CL1 – CL3.

The 2nd and 3rd CAs yield similar station classifications with respect to each other (≈ 88% of stations end up in the same groups). Both CAs indicate 4 as the optimum number of clusters. Two of them, CL1 and CL2, exhibit more polluted signatures, CL3 indicates moderately polluted conditions, and CL4 consists mainly of relatively clean stations, according to the Airbase classification scheme and simulated CO and NOx data from the MACC reanalysis. Frequency distributions of the 2nd and 3rd CAs show a peak of higher frequencies at low ozone concentrations and no clear maxima for CL1 and CL2; CL4 resembles a Gaussian curve, and CL3 has an intermediate shape indicating the influence of intensive photochemistry as well as ozone titration processes.

The geographical distribution of clusters is different than in the 1st CA, but contains similar features. For example, the position of “Po Valley” stations (CL1 in the 2nd and 3rd CA) geographically looks similar to CL2 of the 1st CA, but is smaller and more concentrated. CL4 of the 2nd CA, which shows characteristics of “elevated” sites, represents a mix of clusters of the 1st CA: it captures the complete “elevated” cluster CL5, plus ≈ 160 stations from CL4 and some from CL3. CL3 (“moderately polluted”) is the largest cluster in both the 2nd and 3rd CA; it contains ≈ 550 stations of which ≈ 320 are shared with CL3 of the 1st CA. Clusters CL1, 2 and 3 are of low-altitudes, while “middle-elevated” CL4 includes low-level stations as well as elevated ones.

In the 1st CA clusters are distinguished first of all by the mean ozone concentrations, and as a consequence, station altitudes play a major role. In contrast, using the same set of properties with normalized values (2nd and 3rd CAs) the seasonal and diurnal amplitudes dominate the clustering. Indeed, distributions of ozone mean concentrations are narrow in clusters of the 1st CA, and their averages increase from CL1 to CL5, while for the 2nd CA these distributions are almost twice as broad and there is no clear tendency from cluster to cluster. Conversely, distributions of amplitudes of seasonal and diurnal cycles of the 1st CA show no distinction across the clusters, while they are relatively narrow and decrease from CL1 to CL4 in the 2nd CA.

The ozone variability (expressed as difference between 95- and 5-percentiles) was not included as an input parameter for any of the CAs. As an outcome there are no substantial differences of variability between clusters of the 1st CA. In contrast, for the CAs based on the normalized properties the variability reduces from CL1 to CL4. This implies that the short-term variability of ozone concentrations at European stations is generally correlated with the seasonal and diurnal amplitudes at these sites.

Differences in the seasonal cycles among the clusters of the 1st CA reflect typical patterns of the ozone behavior in traffic, urban, suburban, rural and elevated regions. CL5 presents a combination of spring and summer maxima, while CL4 has only a spring maximum and CL3 reveals a slight maximum in April. The "dirtier" CL1 has a broad summer peak, while CL2 ("Po Valley") has the pronounced July maximum as well as the largest annual amplitude among all clusters.

When we compare simulated ozone concentrations from the MACC reanalysis to the measurements in each cluster of the 1st CA, we find that the reanalysis generally overestimates ozone by 10 nmol/mol at the more polluted sites, but it is able to reproduce average ozone concentrations in clusters with more remote characteristics. The best match is seen for CL5, the cluster which contains primarily remote mountainous stations.

The MACC reanalysis generally shows better agreement in winter than in summer for clusters of the 1st CA. Concentrations are especially well reproduced for clusters CL4 – CL5 in winter with a bias less than 5 nmol/mol on average. Depending on the month and cluster, the summer biases vary from ≈ 5 to ≈ 15 nmol/mol. The model overestimates annual amplitudes by 5-10 nmol/mol except for CL2 (< 5 nmol/mol) and also doesn't capture spring maxima or summer peaks in July: all MACC annual cycles show a broad summer peak with a slight maximum in June.

Diurnal variations are predicted more skilfully than seasonality by the MACC reanalysis: the cluster diurnal maxima are between noon and 3 pm. Diurnal amplitudes are always underestimated by MACC. The strongest underestimation occurs in CL2 (≈ 10 nmol/mol).

The seasonal cycles of the 2nd and 3rd CAs show a gradual change from the smoothest cycle of CL4 with a maximum in April to the most pronounced cycle of CL1 with a strong July maximum. CL2 presents intermediate conditions with a broad maximum, and CL3, although it has a more pronounced amplitude than CL4, still preserves the same features with a dominant spring peak. Diurnal cycles exhibit similar tendencies with a more pronounced cycle in CL1 and a flat one in CL4.

In normalized representation the MACC reanalysis also shows almost bell-shaped symmetrical seasonal cycles for all clusters of the 2nd and 3rd CAs with amplitudes barely distinguishable from each other. These amplitudes are also similar to the observed ones, with only pronounced underestimation for CL1 and slight overestimation for CL4. The modelled normalized cycles don't capture the strong rise of the observed cycles in the beginning of the calendar year (except for CL1)

and spring time, as well as they are more pronounced in August-October for CL2-CL4 than observed ones. Features like spring maxima (CL3, CL4) and July peak (CL1) are not reproduced.

Normalized diurnal cycles of the MACC groups also don't show clearly distinguishable patterns, but they preserve the features of Airbase clusters of the 2nd and 3rd CAs: diurnal minima at 6 am and maxima between noon and 3 pm. But in contrast to annual amplitudes, diurnal ones are underestimated by the MACC reanalysis for all Airbase clusters, in more extent for CL1 and the least for CL4.

The choice of the number of clusters in each CA was based on the consistency of the sum of square distances (SSD) in multiple k-means runs. According to obtained SSD-statistics, 5, 4 and 4 clusters were found appropriate for the 1st, 2nd and 3rd CA respectively, i.e. these numbers are enough to distinguish main ozone pollution regimes for the comparison with the model. However, with only 4 clusters it is scarcely possible to identify meaningful geographical regions of representative surface ozone concentration patterns. Therefore, additional analyses were performed with 7 clusters and based on normalized properties (similar to the 2nd CA). These 7 clusters weren't compared with the MACC model output, but were obtained to look at diversity of seasonal-diurnal variations in clusters.

Among all clusters there are some which keep the features from the previous 2nd CA (based on the same normalized properties set but with k = 4). For example CL1 in the Po Valley region, which is formed only from the same CL1 of the 2nd CA, or CL7 which is formed only from the previous CL4. Other clusters are combinations of the stations from two of the previous clusters. There are 3 new clusters. In particular, the new CL6 contains > 300 stations which are located mainly in Western Europe. This is a new geographical constraint which wasn't observed in the other CAs.

Though among these 7 there are many clusters with high pollution levels, the seasonality is specific for each of them. For clusters, which have common characteristics with the 2nd or 3rd CA (CL1, CL2, CL4, CL7), the seasonal behavior is quite similar, but for the new clusters some new features arise. CL3 exhibits a late summer maximum. CL5 is mainly located in Central Europe like CL2 or CL4, but in contrast to them, it shows a July peak. CL6 located mainly in Western Europe has a pronounced spring maximum, similarly to what was observed for the western stations Iraty and Puy du Dome in the analysis of individual European stations. It thus appears that 7 clusters indeed allow for some regional distinction among the European stations in addition to their characterization by pollution influence.

The quality of cluster separation was investigated through computing the distances of stations to the next nearest centroids. The clusters of the 1st CA exhibit relatively good division. Among all, CL5 is the best isolated, and is proximate only to the centroid of CL4, while the less separated clusters are CL2, CL3 and CL4.

Clusters of the 2nd and 3rd CAs have never more than 2 next nearest centroids. The "extreme" clusters CL1 and CL4 are better separated than CL2 and CL3. In general, the separation is slightly worse than for the 1st CA.

The technique of k-means clustering does not produce unequivocal results due to the random initialization of cluster centers. Hence, it was essential to test the robustness of results based on repeated analyses with the full and reduced data sets. For the 1st CA the results are reproducible on more than 95% for 75 k-means runs out of 100, which exhibit the lowest SSD. When half of all stations being randomly removed from the data set and minimum SSD runs are chosen from repeated runs based on reduced data, the allocation of stations to clusters gives better than 95% similarity for 92 out of 100 cases. In the rest of k-means runs there is never less than 85% agreement also for reduced data sets.

Generally the 2nd CA appeared as more robust in comparison to the 3rd CA. Repetitions with the full data set show more than 95% similarity in all 100 runs of the 2nd CA and in 78 cases out of 100 of the 3rd CA. Thus the CAs based on normalized sets of properties show even more stability than the 1st CA for runs with the full data set. However, they are slightly less robust when the data are thinned.

These results strongly suggest that k-means clustering presents a suitable analysis of ozone mixing ratio data if multiple runs are performed and results are selected based on the minimum SSD.

Excluding individual years from the time series and repeating CAs again based on 3 years data sets, results in more than 90% similarity with the analogous CA based on the full data set. Namely, for both 1st and 2nd CAs agreement is ≈ 95%. For the 3rd CA the similarity is lower and is ≈ 90% on average, therefore it is not as stable as the 2nd CA. To get an objective and stable classification based on the normalized seasonal-diurnal variability our preference would be in favor of the 2nd set of properties (96 variations) rather than 3rd (20 variations).

The chosen parameters for the investigation of ozone representativeness, namely absolute as well as normalized seasonal-diurnal variations, are providing several possibilities to distinguish representative groups of ozone over Europe. Relying on the most stable conditions, there are 5 and 4 clusters respectively, which adequately describe the seasonal-diurnal ozone European patterns in case of absolute and normalized properties. Even if the number of clusters is extended to 7, most clusters are spread across the entire European domain. This implies that differences in the local setting of stations (altitude, anthropogenic emissions) are more important than the geographic location for characterizing the seasonal-diurnal ozone cycles. As clusters strongly overlap, the representativeness of different ozone air quality regimes is not related to the territory covered by the stations set of any cluster.

The robustness and clarity of the cluster analysis might be further improved by adding observations of other compounds (ozone precursor concentrations) and/or meteorological variables.

Unfortunately, such data are not available for all Airbase measurement sites. Our results can be easily updated for future time series of existing stations as well as in case of new stations. The first is possible without loosing the allocation to current cluster, as the robustness tests have shown. It could be also interesting to repeat the cluster analysis for a time period longer than 2007-2010, but this will reduce the number of stations with available data.

Comparison of the observations and model without clustering detects significant biases, which can be partly explained by local pollution influences which are not captured by coarse-resolution models. Our CA approach yields useful information for the evaluation of numerical models, as it allows for a pre-selection of stations and use clusters as means to stratify the comparison with the respective model output. This shows not just how MACC biases change depending on the ozone pollution regime, but also how the model is able to capture features of each regime type.

In winter MACC simulates low ozone concentrations inside of the continent, which are increasing towards the coast line. In summer time there is a North - South gradient with the highest ozone concentrations in the Mediterranean region. Our cluster analyses revealed different ozone pollution regimes, which are not divided regionally, but rather explained by local factors. Summer gradual change is visible in observations too, but much weaker than MACC suggests. Comparison of the model with observations for individual clusters reveals first of all different overestimation biases, and secondly differences mainly in seasonal behavior rather than diurnal.

These biases are mostly driven by summertime ozone rather than wintertime, where ozone is generally well predicted. Such biases decrease from more polluted clusters to cleaner ones, as well as cycles are described better for clusters with relatively clean signatures. The best MACC fit is observed for CL5 of the 1st CA as well as for CL4 of the 2nd and 3rd CAs and is explained by the fact that their stations are influenced more by regional rather than local factors. The CAs based on the normalized properties help to compare the shapes and amplitudes of seasonal and diurnal cycles regardless of the ozone mean concentrations. In this case the model also performs better for the description of diurnal cycles rather than seasonal. Though diurnal amplitudes in normalized representation are normally underestimated, MACC is able to catch observed diurnal minima at 6 am and maxima between noon and 3pm. In case of seasonality while the annual amplitudes are generally well described, the model cannot distinguish different seasonal patterns, like spring maximum or July peak, but always presents broad symmetrical bell-shaped summer maxima.

This thesis has shown the usefulness of the k-means clustering as an objective classification method for surface ozone measurement stations. It investigated various aspects of representativeness of surface ozone measurements in Europe with the objective to improve the methods applied in the evaluation of global and regional chemistry climate models. It would be beneficial if similar analyses could also be performed for other world regions. Unfortunately, most regions still lack an

appropriate measurement network, and where such data do exist, they are sometimes difficult to obtain, poorly documented or of questionable quality.

Outlook

If the results we obtained for Europe are applicable also to other world regions, one can make the claim that stations which are located in relatively clean environments generally measure ozone concentrations which are representative of larger regions (several 100 km at least). However, one has to account for station altitude as an important factor that determines the absolute concentration values and to some extent their seasonal-diurnal variations. The frequency distributions of ozone concentrations may provide useful information about the local pollution influence at individual measurement sites. However, the frequency distributions of "clean" sites in Europe may differ from those of "clean" sites elsewhere. Performing a cluster analysis of a global surface ozone dataset, such as that of the World Meteorological Organization Global Atmosphere Watch (WMO GAW) program would thus require careful planning and some testing because we cannot expect the same station classification as in the regional analysis for Europe presented here.

References

Airbase database: http://acm.eionet.europa.eu/databases/airbase/.

European Monitoring and Evaluation Program database (EMEP): http://www.emep.int/.

Federal Environment Agency Umwelt Bundesamt (UBA): http://www.umweltbundesamt.de/ and http://www.env-it.de/umweltbundesamt/luftdaten.

World Meteorological Organization Global Atmosphere Watch program (WMO GAW): www.wmo.int/pages/prog/arep/gaw/gaw_home_en.html.

Monitoring Atmospheric Composition and Climate project (MACC): http://www.copernicus-atmosphere.eu/.

MOZAIC aircraft data: http://mozaic.aero.obs-mip.fr/.

Pollution Atmosphérique à Echelle Synoptique (PAES): http://paes.aero.obs-mip.fr/.

Scientific Python library: http://scipy.org/.

Clustering library for Python: https://pypi.python.org/pypi/Pycluster.

UNECE Convention on Long-range Transboundary Air Pollution (LRTAP), 1979: http://www.unece.org/env/lrtap/lrtap_h1.html.

UNECE eight protocols, 1984-1999: http://www.unece.org/env/lrtap/status/lrtap_s.html.

World Data Centre for Greenhouse Gases (WDCGG): http://ds.data.jma.go.jp/gmd/wdcgg/.

Federal Environment Agency, Unit II 4.2 “Air Quality Assessment”: Air quality 2012, Preliminary Analysis, German Federal Environment Agency (UBA), Germany, Dessau-Roßlau, 2013.

Agudelo, O.M., Barrero, O., Peter, V., and De Moor, B.: Assimilation of Ozone Measurements in the Air Quality Model AURORA by Using the Ensemble Kalman Filter, In Decision and Control and European Control Conference (CDC-ECC), 2011 50th IEEE Conference on, 4430–35, IEEE, 2011.

Baray, J.L., Ancellet, G., Taupin, F.G., Bessafi, M., Baldy, S., and Keckhut, P.: Subtropical Tropopause Break as a Possible Stratospheric Source of Ozone in the Tropical Troposphere, J. Atmos. Sol. Terr. Phys., 60, 1, 27–36, 1998.

Beaver, S. and Palazoglu, A.: Cluster Analysis of Hourly Wind Measurements to Reveal Synoptic Regimes Affecting Air Quality, J. Appl. Meteor. Climatol., 45, 1710–1726, 2006.

Beirle, S., Platt, U., Wenig, M., and Wagner, T.: Weekly cycle of NO_2 by GOME measurements: a signature of anthropogenic sources, Atmos. Chem. Phys., 3, 2225–2232, 2003.

Benedictow, A., Blechschmidt, A.M., Bouarar, I., Cuevas, E., Clark, H., Flentje, H., Gaudel, A., Griesfeller, J., Huijnen, V., Huneeus, N., Jones, L., Kapsomenakis, J., Kinne, S., Lefever, K., Razinger, M., Richter, A., Schulz, M., Thomas, W., Thouret, V., Vrekoussis, M., Wagner, A., and Zerefos, C.: Validation Report of the MACC reanalysis of global atmospheric composition: Period 2003-2012, MACC-II Deliverable D_83.5, 2013.

Bigi, A., Ghermandi, G., and Harrison, R.M.: Analysis of the air pollution climate at a background site in the Po valley, J. Environ. Monit., 14, 552–563, 2012.

Bojkov, R.D.: Surface Ozone During the 2nd-Half of the 19th-Century, J. Clim. Appl. Meteorol., 25, 3, 343–352, 1986.

Camargo, S.J., Robertson, A.W., Gaffney, S.J., Smyth, P., and Ghil, M.: Cluster Analysis of Typhoon Tracks. Part II: Large-Scale Circulation and ENSO, J. Climate, 20, 3654–3676, 2007.

Chameides, W.L., Fehsenfeld, F., Rodgers, M.O., Cardelino, C., Martinez, J., Parrish, D., Lonneman, W., et al.: Ozone Precursor Relationships in the Ambient Atmosphere, J. Geophys. Res. Atmos., 97, D5, 6037–6055, 1992.

Chevalier, A., Gheusi, F., Delmas, R., Ordóñez, C., Sarrat, C., Zbinden, R., Thouret, V., Athier, G., and Cousin, J.-M.: Influence of altitude on ozone levels and variability in the lower troposphere: a ground-based study for western Europe over the period 2001–2004, Atmos. Chem. Phys., 7, 4311–4326, 2007.

Christiansen, B.: Atmospheric Circulation Regimes: Can Cluster Analysis Provide the Number?, J. Climate, 20, 2229–2250, 2007.

Coman, A., Foret, G., Beekmann, M., Eremenko, M., Dufour, G., Gaubert, B., Ung, A., Schmechtig, C., Flaud, J.-M., and Bergametti, G.: Assimilation of IASI Partial Tropospheric Columns with an Ensemble Kalman Filter over Europe, Atmos. Chem. Phys., 12, 5, 2513–32, 2012.

Committee on Tropospheric Ozone and National Research Council: Rethinking the Ozone Problem in Urban and Regional Air Pollution, National Academy Press, Washington, D.C., 1991.

Crutzen, P.J.: Chemistry of Important Minor Constituents in Atmosphere, Trans. Am. Geophys. Union, 54, 3, 128–128, 1973.

Crutzen, P.J.: The Role of NO and NO_2 in the Chemistry of the Troposphere and Stratosphere, Annu. Rev. Earth. Planet. Sci., 7, 443–472, 1979.

Crutzen, P.J., and Zimmermann, P.H.: The Changing Photochemistry of the Troposphere, Tellus Series a-Dynamic Meteorology and Oceanography, 43, 4, 136–151, 1991.

Cui, J., Deolal, S.P., Sprenger, M., Henne, S., Staehelin, J., Steinbacher, M., and Nédélec, P.: Free Tropospheric Ozone Changes over Europe as Observed at Jungfraujoch (1990–2008): An Analysis Based on Backward Trajectories, J. Geophys. Res., 116, D10, 2011.

Danielsen, E.F.: Stratospheric-tropospheric exchange based on radioactivity, ozone and potential vorticity, J. Atmos. Sci., 25, 502– 518, 1968.

Decision 97/101/EC: Council Decision of 27 January 1997 establishing a reciprocal exchange of information and data from networks and individual stations measuring ambient air pollution within the Member States, Official Journal of the European Union, 35, 14–22, 1997.

Decision 2001/752/EC: Commission Decision of 17 October 2001 amending the Annexes to Council Decision 97/101/EC establishing a reciprocal exchange of information and data from networks and individual stations measuring ambient air pollution within the Member States, Official Journal of the European Communities, 282, 69–76, 2001.

Decision 2011/850/EU: Commission Implementing Decision of 12 December 2011 laying down rules for Directives 2004/107/EC and 2008/50/EC of the European Parliament and of the Council as regards the reciprocal exchange of information and reporting on ambient air quality, Official Journal of the European Union, 335, 86–106, 2011.

Dentener, F.J., and Crutzen, P.J: Reaction of N_2O_5 on Tropospheric Aerosols - Impact on the Global Distributions of NOx, O_3, and OH, J. Geophys. Res. Atmos., 98, D4, 7149–7163, 1993.

Derwent, R.G., Manning, A.J., Simmonds, P.G., Spain, T.G., and O'Doherty, S.: Analysis and Interpretation of 25 Years of Ozone Observations at the Mace Head Atmospheric Research Station on the Atlantic Ocean Coast of Ireland from 1987 to 2012, Atmos. Environ., 80, 361–68, 2013.

Directive 2004/107/EC: Directive of the European Parliament and of the Council of 15 December 2004 relating to arsenic, cadmium, mercury, nickel and polycyclic aromatic hydrocarbons in ambient air, Official Journal of the European Union, L 23, 3–16, 2005.

Directive 2008/50/EC: Directive of the European Parliament and of the Council of 21 May 2008 on ambient air quality and cleaner air for Europe, Official Journal of the European Union, L 152, 1–44, 2008.

Dibb, J.E., Meeker, L.D., Finkel, R.C., Southon J.R., Caffee, M.W., and Barrie, L.A.: Estimation of the stratospheric input to the Arctic troposphere: 7Be and 10Be in aerosols at Alert, Canada, J. Geophys. Res., 99, 12855–12864, 1994.

Dorling, S.R. and Davies, T.D.: Extending cluster analysis—synoptic meteorology links to characterise chemical climates at six northwest European monitoring stations, Atmos. Environ., 29, 145–167, 1995.

Efron, B., and Tibshirani, R.J.: An Introduction to the Bootstrap. Chapman & Hall. CRC Press, 1994.

Elbern, H., Kowol, J., Sladkovic, R., and Ebel, A.: Deep Stratospheric Intrusions: A Statistical Assessment with Model Guided Analyses, Atmos. Environ., 31, 19, 3207–3226, 1997.

Flemming, J., Stern, R., and Yamartino, R.J.: A new air quality regime classification scheme for O_3, NO_2, SO_2 and PM_{10} observations sites, Atmos. Environ., 39, 6121–6129, 2005.

Flemming, J., Inness, A., Flentje, H., Huijnen, V., Moinat, P., Schultz, M.G., and Stein, O.: Coupling global chemistry transport models to ECMWF's integrated forecast system, Geosci. Model Dev., 2, 253–265, 2009.

Finlayson-Pitts, B.J., and Pitts, J.N.: Atmospheric Chemistry: Fundamentals and Experimental Techniques, John Wiley& Sons, USA, 1986.

Fiore, A.M., Dentener, F.J., Wild, O., Cuvelier, C., Schultz, M.G., Hess, P., Textor, C., et al.: Multimodel Estimates of Intercontinental Source-Receptor Relationships for Ozone Pollution, J. Geophys. Res., 114, D4, 2009.

Galbally, I.E., and Roy, C.R.: Destruction of ozone at the Earth's surface, Q. J. R. Meteorol. Soc., 106, 449, 599-620, 1980.

Galbally, I.E., Bentley, S.T. and Meyer, C.P.: Mid–latitude marine boundary-layer ozone destruction at visible sunrise observed at Cape Grim, Tasmania, 41°S, Geophys. Res. Lett., 27, 23, 3841-3844, 2000.

Galbally, I.E. and Schultz, M.G.: GAW Report No. 209, Guidelines for Continuous Measurements of Ozone in the Troposphere, World Meteorological Organization, Geneva, Switzerland, 2013.

Gilge, S., Plass-Duelmer, C., Fricke, W., Kaiser, A., Ries, L., Buchmann, B., and Steinbacher M.: Ozone, Carbon Monoxide and Nitrogen Oxides Time Series at Four Alpine GAW Mountain Stations in Central Europe, Atmos. Chem. Phys., 10, 24, 12295–12316, 2010.

Gosset, W.S.: The probable error of a mean, Biometrika, 6, 1, 1–25, 1908.

Graustein, W., and Turekian, K.K.: 7Be and 210Pb indicate an upper troposphere source for elevated ozone in the summertime subtropical free troposphere of the eastern North Atlantic, Geophys. Res. Lett., 23, 539–542, 1996.

Guerreiro, C., de Leeuw, F., Foltescu, V., Schilling, J., van Aardenne, J., Adams, M.: Air quality in Europe – 2012 report, EEA Technical report No 4/2012, European Environment Agency, Copenhagen, 2012.

Haagen-Smit, A.J.: Chemistry and Physiology of Los Angeles Smog, Industrial &Engineering Chemistry, 44, 6, 1342–1346, 1952.

Harris, J.M., Oltmans, S.J., Dlugokencky, E.J., Novelli, P.C., Johnson, B.J., and Mefford, T.: An Investigation into the Source of the Springtime Tropospheric Ozone Maximum at Mauna Loa Observatory, Geophys. Res. Lett., 25, 11, 1895–1898, 1998.

Hauglustaine, D.A., Granier, C., Brasseur, G.P. and Mégie, G.: The importance of atmospheric chemistry in the calculation of radiative forcing on the climate system, J. Geophys. Res., 99, 1173-1186, 1994.

Helmig, D., Ganzeveld, L., Butler, T. and Oltmans, S.J.: The role of ozone atmosphere-snow gas exchange on polar, boundary-layer tropospheric ozone – a review and sensitivity analysis, Atmos. Chem. Phys., 7, 15-30, 2007.

Helmig, D., Lang, E.K., Bariteau, L., Boylan, P., Fairall, C.W., Ganzeveld, L., Hare, J.E., Hueber, J., and Pallandt, M.: Atmosphere-ocean ozone fluxes during the TexAQS 2006, STRATUS 2006, GOMECC 2007, GasEx 2008, and AMMA 2008 cruises, J. Geophys. Res., 117, D04305, 2012.

Henne, S., Brunner, D., Folini, D., Solberg, S., Klausen, J., and Buchmann, B.: Assessment of parameters describing representativeness of air quality in-situ measurement sites, Atmos. Chem. Phys., 10, 3561–3581, 2010.

Hollingsworth, A., Engelen, R.J., Textor, C., Benedetti, A., Boucher, O., Chevallier, F., Dethof, A., Elbern, H., Eskes, H., Flemming, J., Granier, C., Kaiser, J.W., Morcrette, J-J., Rayner, P., Peuch, V.-H., Rouil, L., Schultz, M.G., Simmons, A.J.: Toward a monitoring and forecasting system for atmospheric composition: The GEMS project, Bull. Amer. Meteor. Soc., 89, 1147–1164, 2008.

Holton, J.R., Haynes, P.H., Mcintyre, M.E., Douglass, A.R., Rood, R.B., and Pfiste, L.: Stratosphere-Troposphere Exchange, Rev. Geophys., 33, 4, 403–439, 1995.

Hsu, J., Prather, M.J., and Wild, O.: Diagnosing the Stratosphere-to-Troposphere Flux of Ozone in a Chemistry Transport Model, J. Geophys. Res. Atmos., 110, D19305, 2005.

Inness, A., Baier, F., Benedetti, A., Bouarar, I., Chabrillat, S., Clark, H., Clerbaux, C., Coheur, P., Engelen, R.J., Errera, Q., Flemming, J., George, M., Granier, C., Hadji-Lazaro, J., Huijnen, V., Hurtmans, D., Jones, L., Kaiser, J.W., Kapsomenakis, J., Lefever, K., Leitão, J., Razinger, M., Richter, A., Schultz, M.G., Simmons, A.J., Suttie, M., Stein, O., Thépaut, J.-N., Thouret, V., Vrekoussis, M., Zerefos, C., and the MACC team: The MACC reanalysis: an 8-yr data set of atmospheric composition, Atmos. Chem. Phys., 13, 4073–4109, 2013.

Jeffries, H.E., and Crouse, R.: Scientific and technical issues related to the application of incremental reactivity, Department of Environmental Sciences and Engineering, University of North Carolina, Chapel Hill, NC, 1990.

Jin, L., Harley, R.A., and Brown, N.J.: Ozone pollution regimes modeled for a summer season in California's San Joaquin Valley: A cluster analysis, Atmos. Environ., 45, 4707–4718, 2011.

Joly, M. and Peuch, V.-H.: Objective classification of air quality monitoring sites over Europe, Atmos. Environ., 47, 111–123, 2012.

JCGM (Joint Committee for Guides in Metrology): Evaluation of measurement data – Guide to the expression of uncertainty in measurement (GUM), GUM 1995 with minor corrections, JCGM, 2008.

Kenney, J.F. and Keeping, E.S.: Linear Regression and Correlation, Ch. 15 in Mathematics of Statistics, Pt. 1, 3rd ed. Princeton, NJ: Van Nostrand, 252-285, 1962.

Kim, Ki-H., Jahan, S.A. and Kabir, E.: A Review on Human Health Perspective of Air Pollution with Respect to Allergies and Asthma, Environ. Int., 59, 41–52, 2013.

Klemp, D., Mihelcic, D., and Mittermaier, B.: Messung und Bewertung von Verkehrsemis-sionen, Schriften des Forschungszentrums Jülich, Reihe Energie und Umwelt, 21, Forschungszentrum Jülich, Jülich, 2012 (in German).

Koch, D., and Rind, D.: Beryllium10/beryllium7 as a tracer of stratospheric transport, J. Geophys. Res., 103, 3907–3917, 1998.

Lamarque, J.-F., Bond, T.C., Eyring, V., Granier, C., Heil, A., Klimont, Z., Lee, D., et al.: Historical (1850–2000) Gridded Anthropogenic and Biomass Burning Emissions of Reactive Gases and Aerosols: Methodology and Application, Atmos. Chem. Phys. 10, 15, 7017–7039, 2010.

Langford, A.O.: Stratosphere-Troposphere Exchange at the Subtropical Jet: Contribution to the Tropospheric Ozone Budget at Midlatitudes, Geophys. Res. Lett., 26, 16, 2449–2452, 1999.

Lee, S. and Feldstein, S.B.: Detecting Ozone- and Greenhouse Gas–Driven Wind Trends with Observational Data, Science, 339, 563–567, 2013.

Leighton, P. A.: Photochemistry of Air Pollution, Academic Press, New York, 1961.

Levy, H.: Normal Atmosphere - Large Radical and Formaldehyde Concentrations Predicted, Science, 173, 3992, 141–143, 1971.

Levy, H., Mahlman, J., Moxim, W.J., Liu, S.: Tropospheric ozone: the role of transport, J. Geophys. Res., 90, 3753-3772, 1985.

Logan, J.A.: Tropospheric Chemistry: a Global Perspective, J. Geophys. Res., 86, 7210-7254, 1981.

Logan, J.A.: An analysis of ozonesonde data for the troposphere: Recommendations for testing 3-D models, and development of a gridded climatology for tropospheric ozone, J. Geophys. Res., 104, 16115 –16149, 1999.

Logan, J.A., Staehelin, J., Megretskaia, I.A., Cammas, J.-P., Thouret, V., Claude, H., De Backer, H., et al.: Changes in Ozone over Europe: Analysis of Ozone Measurements from Sondes, Regular Aircraft (MOZAIC) and Alpine Surface Sites, J. Geophys. Res. Atmos., 117, D09301, 2012.

Van Loon, M., Vautard, R., Schaap, M., Bergström, R., Bessagnet, B., Brandt, J., Builtjes, P. J.H., et al.: Evaluation of Long-Term Ozone Simulations from Seven Regional Air Quality Models and Their Ensemble, Atmos. Environ., 41, 10, 2083–97, 2007.

Marenco, A., Gouget, H., Nédélec, P., and Pagés, J.-P.: Evidence of a long-term increase in tropospheric ozone from Pic du Midi data series: Consequences: Positive radiative forcing, J. Geophys. Res., 99, 16617–16632, 1994.

Marzban, C. and Sandgathe, S.: Cluster Analysis for Verification of Precipitation Fields, Wea. Forecasting, 21, 824–838, 2006.

Matsumi, Y. and Kawasaki, M.: Photolysis of Atmospheric Ozone in the Ultraviolet Region, Chem. Rev., 103 (12), 4767–4782, 2003.

Megie, G., Bonte, J., Carlier, P., Chavaudra, J., Dizengremel, P., Feugier, A., Granier, C., et al.: Ozone and Oxidizing Properties of the Troposphere, Revue de l'Institut Francais du Petrole, 49, 1, 83–104, 1994.

Midgley, P. and Reuther, M.: Towards cleaner air for Europe - Science, Tools and Applications, Part 1: Results from the EUROTRAC-2 Synthesis and Integration Project, Margraf Publishers, Weikersheim, Germany, 2003.

Mailler, S., Khvorostyanov, D., and Menut, L.: Impact of the Vertical Emission Profiles on Background Gas-Phase Pollution Simulated from the EMEP Emissions over Europe, Atmos. Chem. Phys., 13, 12, 5987–98, 2013.

Mol, W., Hooydonk, P., and de Leeuw, F.: European exchange of monitoring information and state of the air quality in 2006, Tech. rep., ETC/ACC, 2008.

Monks, P.S.: A review of the observations and origins of the spring ozone maximum, Atmos. Environ., 34, 3545–3561, 2000.

Murphy, J.G., Day, D.A., Cleary, P.A., Wooldridge, P.J., Millet, D.B., Goldstein, A.H., and Cohen, R.C.: The weekend effect within and downwind of Sacramento – Part 1: Observations of ozone, nitrogen oxides, and VOC reactivity, Atmos. Chem. Phys., 7, 5327–5339, 2007.

Nopmongcol, U., Koo, B., Tai E., Jung, J., Piyachaturawat, P., Emery, C., Yarwood, G., Pirovano, G., Mitsakou, C., and Kallos, G.: Modeling Europe with CAMx for the Air Quality Model Evaluation International Initiative (AQMEII), Atmos. Environ., 53, 177–85, 2012.

Oltmans, S.J., Lefohn, A.S., Harris, J.M., Galbally, I., Scheel, H.E., Bodeker, G., Brunke, E., et al.: Long-Term Changes in Tropospheric Ozone, Atmos. Environ., 40, 17, 3156–3173, 2006.

Parrish, D.D., Lamarque, J.-F., Naik, V., Horowitz, L., Shindell, D.T., Staehelin, J., Derwent, R., Cooper, O.R., Tanimoto, H., Volz-Thomas, A., Gilge, S., Scheel, H.-E., Steinbacher, M., Fröhlich, M.: Long-term changes in lower tropospheric baseline ozone concentrations: Comparing chemistry-climate models and observations at northern mid latitudes, J. Geophys. Res., 119, 9, 5719–5736, 2014.

Pires, J.C.M., Sousa, S.I.V., Pereira, M.C., Alvim-Ferraz, M.C.M., and Martins, F.G.: Management of air quality monitoring using principal component and cluster analysis – Part II: CO, NO_2 and O_3, Atmos. Environ., 42, 1261–1274, 2008.

Pollack, I. B., Ryerson, T.B., Trainer, M., Parrish, D.D., Andrews, A.E., Atlas, E.L., Blake, D.R., Brown, S.S., Commane, R., Daube, B.C., de Gouw, J.A., Dubé, W.P., Flynn, J., Frost, G.J., Gilman, J.B., Grossberg, N., Holloway, J.S., Kofler, J., Kort, E.A., Kuster, W.C., Lang, P.M., Lefer, B., Lueb, R.A., Neuman, J.A., Nowak, J.B., Novelli, P.C., Peischl, J., Perring, A. E., Roberts, J.M., Santoni, G., Schwarz, J P., Spackman, J.R., Wagner, N.L., Warneke, C., Washenfelder, R.A., Wofsy, S.C., and Xiang, B.: Airborne and ground-based observations of a weekend effect in ozone, precursors, and oxidation products in the California South Coast Air Basin, J. Geophys. Res., 117, D00V05, 2012.

Rabin, J., Delon, J., and Gousseau, Y.: Circular earth mover's distance for the comparison of local features, 19th International Conference on Pattern Recognition, IEEE, 3576–3579, 2008.

Richter, C.A.: Ozone Production in the Atmosphere Simulation Chamber SAPHIR, PhD thesis, Forschungszentrum Jülich, Zentralbibliothek, 2008.

Roelofs, G.J., Scheeren, H.A., Heland, J., Ziereis, H., and Lelieveld, J.: A Model Study of Ozone in the Eastern Mediterranean Free Troposphere during MINOS (August 2001), Atmos. Chem. Phys., 3, 1199–1210, 2003.

Rubner, Y., Tomasi, C., and Guibas, L.J.: A metric for distributions with applications to image databases, Sixth International Conference on Computer Vision, IEEE, 59–66, 1998.

Rubin, M.B.: The history of ozone. The Schoenbein period, 1839-1868, Bull. Hist. Chem., 26, 1, 40-56, 2001.

Schipa, I., Tanzarella, A., and Mangia, C.: Differences between weekend and weekday ozone levels over rural and urban sites in Southern Italy, Environ. Monit. Assess., 156, 509–523, 2009.

Schindlbacher, S., Tista, M., Gager, M., Haider, S., Moosmann, L. and Kampel, E.: European Union emission inventory report 1990–2011 under the UNECE Convention on Longrange Transboundary Air Pollution (LRTAP), EEA Technical report No 10/2013, European Environment Agency, Copenhagen, 2013.

Schultz, M.G., Backman, L., Balkanski, Y., Bjoerndalsaeter, S., Brand, R., Burrows, J.P., Dalsoeren, S., de Vasconcelos, M., Grodtmann, B., Hauglustaine, D.A., Heil, A., Hoelzemann, J.J., Isaksen, I.S. A., Kaurola, J., Knorr, W., Ladstaetter-Weißenmayer, A., Mota, B., Oom, D., Pacyna, J., Panasiuk, D., Pereira, J.M.C., Pulles, T., Pyle, J., Rast, S., Richter, A., Savage, N., Schnadt, C., Schulz, M., Spessa, A., Staehelin, J., Sundet, J.K., Szopa, S., Thonicke, K., van het Bolscher, M., van Noije, T., van Velthoven, P., Vik, A.F., and Wittrock, F.: REanalysis of the TROpospheric chemical composition over the past 40 years (RETRO) – A long-term global modeling study of tropospheric chemistry, Final Report, Report no. 48/2007 in the series “Reports on Earth System Science”, Max Planck Institute for Meteorology, Hamburg, Germany, 2007.

Scheel, H.E., Areskoug, H., Geiss, H., Gomiscel, B., Granby, K., Haszpra, L., Klasinc, L., Kley, D., Laurila, T., Lindskog, T., Roemer, M., Schmitt, R., Simmonds, P., Solberg, S., and Toupance, G.: On the spatial distribution and seasonal variation of lower-troposphere ozone over Europe, J. Atmos. Chem., 28, 11-28, 1997.

Seinfeld, J.H. and Pandis, S.N.: Atmospheric Chemistry and Physics: From Air Pollution to Climate Change, 2nd edition, J. Wiley, New York, 2006.

Solazzo, E., Bianconi, R., Vautard, R., Appel, K. W., Moran, M.D., Hogrefe, C., Bessagnet, B., et al.: Model Evaluation and Ensemble Modelling of Surface-Level Ozone in Europe and North America in the Context of AQMEII, Atmos. Environ., 53, 60–74, 2012.

Solberg, S., Jonson, J.E., Horalek, J., Larssen, S., de Leeuw, F.: Assessment of ground-level ozone in EEA member countries, with a focus on long-term trends, EEA Technical report No 7/2009, European Environment Agency, Copenhagen, 2009.

Solomon, S., Qin, D., Manning, M., Chen, Z., Marquis, M., Averyt, K.B., Tignor, M. and Miller, H.L.: IPCC, 2007: “Climate Change 2007: The Physical Science Basis.” Contribution of Working Group I to the Fourth Assessment Report of the Intergovernmental Panel on Climate Change, Cambridge University Press, United Kingdom and New York, 2007.

Spang, W., Schneider, J., Moosmann, L., and Nagl, C.: FINAL REPORT: Representativeness and classification of air quality monitoring stations, Umweltbundesamt, REPORT REP-0121, Vienna, 2007.

Staehelin, J., Thudium, J., Buehler, R., Volz-Thomas, A., and Graber, W.: Trends in Surface Ozone Concentrations at Arosa (Switzerland), Atmos. Environ., 28, 1, 75–87, 1994.

Stein, O., Flemming, J., Inness, A., Kaiser, J.W., and Schultz, M.G.: Global reactive gases forecasts and reanalysis in the MACC project, J. Integr. Environ. Sci., 9, 57–70, 2012.

Stevenson, D.S., Dentener, F.J., Schultz, M.G., Ellingsen, K., van Noije, T.P.C., Wild, O., Zeng, G., Amann, M., Atherton, C.S., Bell, N., Bergmann, D.J., Bey, I., Butler, T., Cofala, J., Collins, W.J., Derwent, R.G., Doherty, R.M., Drevet, J., Eskes, H.J., Fiore, A.M., Gauss, M., Hauglustaine, D.A., Horowitz, L.W., Isaksen, I.S.A., Krol, M.C., Lamarque, J.-F., Lawrence, M.G., Montanaro, V., Müller, J.-F., Pitari, G., Prather., M.J., Pyle., J.A., Rast., S., Rodriguez, J.M., Sanderson, M.G., Savage, N.H., Shindell, D.T., Strahan, S.E., Sudo, K. and Szopa, S.: Multimodel ensemble simulations of present-day and near-future tropospheric ozone, J. Geophys. Res., 111, D8, D08301, 2006.

Stohl, A., Spichtinger-Rakowsky, N., Bonasoni, P., Feldmann, H., Memmesheimer, M., Scheel, H.E., Trickl, T., Hubener, S., Ringer, W., and Mandl, M.: The Influence of Stratospheric Intrusions on Alpine Ozone Concentrations, Atmos. Environ., 34, 9, 1323–1354, 2000.

Stocker, T.F., Qin, D., Plattner, G.-K., Tignor, M.B., Allen, S.K., Boschung, J., Nauels, A., Xia, Y., Bex, V., and Midgley, P.M.: IPCC, 2013: "Climate Change 2013: The Physical Science Basis." Intergovernmental Panel on Climate Change, Contribution of Working Group I to the Fifth Assessment Report (AR5) of the Intergovernmental Panel on Climate Change, Cambridge University Press, United Kingdom and New York, 2013.

Stull, R.B.: An Introduction to Boundary Layer Meteorology, Kluwer Academic Publishers, Dordrecht, Netherlands, 1988.

Tarasova, O.A., Brenninkmeijer, C.A.M., Jöckel P., Zvyagintsev, A.M., and Kuznetsov, G.I.: A climatology of surface ozone in the extra tropics: cluster analysis of observations and model results, Atmos. Chem. Phys., 7, 6099–6117, 2007.

Tarasova, O.A., Senik, I.A., Sosonkin, M.G., Cui, J., Staehelin, J., and Prévôt, A.S.H.: Surface Ozone at the Caucasian Site Kislovodsk High Mountain Station and the Swiss Alpine Site Jungfraujoch: Data Analysis and Trends (1990–2006), Atmos. Chem. Phys. 9, 12, 4157–4175, 2009.

Thunis, P., Pernigotti, D., and Gerboles, M.: Model Quality Objectives Based on Measurement Uncertainty. Part I: Ozone, Atmos. Environ., 79, 861–68, 2013.

Tilmes, S., Lamarque, J.-F., Emmons, L.K., Conley, A., Schultz, M.G., Saunois, M., Thouret, V., Thompson, A.M., Oltmans, S.J., Johnson, B., and Tarasick, D.: Technical Note: Ozonesonde climatology between 1995 and 2011: description, evaluation and applications, Atmos. Chem. Phys., 12, 7475–7497, 2012.

Tryon, R.C.: Cluster Analysis. Edwards Brothers, Ann Arbor, Michigan, 1939.

Uekötter, F.: Von der Rauchplage zur ökologischen Revolution. Eine Geschichte der Luftverschmutzung in Deutschland und den USA 1880-1970 (Veröffentlichungen des Instituts für soziale Bewegungen, Schriftenreihe A: Darstellungen; Bd. 26), Essen: Klartext 2003, 637 S., ISBN 3-89861-195-7.

Van Velthoven, P.F.J., and Kelder, H.: Estimates of Stratosphere-Troposphere Exchange: Sensitivity to Model Formulation and Horizontal Resolution, J. Geophys. Res. Atmos., 101, D1, 1429–1434, 1996.

Viallon, J., Moussay, P., Norris, J.E., Guenther, F.R., and Wielgosz, R.I.: A study of systematic biases and measurement uncertainties in ozone mole fraction measurements with the NIST Standard Reference Photometer, Metrologia, 43, 441-450, 2006a.

Volz, A. and Kley, D.: Evaluation of the Montsouris series of ozone measurements made in nineteenth century, Nature, 332, 240–242, 1988.

World Meteorological Organization: Guide to Meteorological Instruments and Methods of Observation, WMO-No.8, World Meteorological Organization, Geneva, Switzerland, 2008.

Zanis, P., Trickl, T., Stohl, A., Wernli, H., Cooper, O., Zerefos, C., Gaeggeler, H., Schnabel, C., Tobler, L., Kubik, P.W., Priller, A., Scheel, H.E., Kanter, H.J., Cristofanelli, P., Forster, C., James, P., Gerasopoulos, E., Delcloo, A., Papayannis, A., and Claude, H.: Forecast, observation and modelling of a deep stratospheric intrusion event over Europe, Atmos. Chem. Phys., 3, 763–777, 2003a.

Zanis, P., Gerasopoulos, E., Priller, A., Schnabel, C., Stohl, A., Zerefos, C., Gaeggeler, H.W., Tobler, L., Kubik, P.W., Kanter, H.J., Scheel, H.E., Luterbacher, J., and Berger, M.: An Estimate of the Impact of Stratosphere-to-Troposphere Transport (STT) on the Lower Free Tropospheric Ozone over the Alps Using 10 Be and 7 Be Measurements, J. Geophys. Res., 108, D12, 2003b.

Zhang, Y., Klein, S., Mace, G.G., and Boyle, J.: Cluster analysis of tropical clouds using CloudSat data, Geophys. Res. Lett., 34, L12813, 2007.

Appendix A

Pycluster - the C clustering library used in Python (https://pypi.python.org/pypi/Pycluster). It provides the function "kcluster", which classifies a set of observations into k clusters using the k-means algorithm.

clusterid, error, nfound = kcluster (data, nclusters=k, mask=None, weight=None, transpose=0, npass=1, method='a', dist='e', initialid=None)

Arguments:

• *data*:
  - array containing the data. Each vector (station) is stored row-wise and properties of each vector - column-wise;
• *nclusters*:
  - the number of clusters k;
• *mask*:
  - array of integers showing which data are missing. Here *mask=None* (no missing data);
• *weight*:
  - contains the weights to be used when calculating distances. Here *weight=None* (equal weights are assumed);
• *transpose*:
  - determines if rows or columns are being clustered. Here *transpose=0* (stations (rows) are being clustered);
• *npass*:
  - the number of times the k -means clustering algorithm is performed, each time with a different (random) initial condition. Here *npass = 1*;
• *method*:
  - describes how the center of a cluster is found. Here *method='a'*: arithmetic mean;
• *dist*:
  - defines the distance function to be used: Here *dist='e'*: Euclidean distance;
• *initialid*:
  - specifies the initial clustering to be used for the algorithm. If initialid is not None, it should be equal to a 1D array containing the cluster number (between 0 and nclusters-1) for each item (station). Here *initialid=None*, i.e. a different random initial clustering is used for each of the npass runs of the algorithm.

Return values:

This function returns a tuple (*clusterid, error, nfound*).

• *clusterid*:
  - an array containing the number of the cluster to which each item was assigned;
• *error*:
  - the within-cluster sum of distances for the optimal clustering solution;
• *nfound*:
  - the number of times the optimal solution was found.

Appendix B

In section 4.1.3 there are formulas given for calculation of trend statistics. In Python this was implemented with the help of Scipy - scientific Python library (http://scipy.org/).

Python code	Comments
from scipy import polyval, polyfit, stats, sqrt, mean	importing the necessary functions from the library
(a,b) = polyfit(x,y,1) f = polyval([a,b],x)	x – time y – ozone mixing ratio
n = len(x)	a – slope value of a trend b – intercept
df = n-2	f – linear fit function n – length of x
mean = mean(x)	df – degrees of freedom
Sa = sqrt(sum((f-y)**2)/sum((x-mean)**2)/(n-2))	Sa – standard error of a slope (see formula 4.8)
alpha = 0.9 pstar = (1+alpha)/2	alpha – confidence level pstar – 0.95-quantile of t-distribution
vstar = stats.t.ppf(pstar,df)	vstar – t-value from t-distribution, corresponding to 0.95-quantile
Ea=vstar*Sa	Ea – error of a slope
	_____
	# The resulting confidence interval of a slope = a ± Ea.

Appendix C

List of the 33 stations that were removed after visual inspection of their time series.

	station ID	station name	station type	station area type	lon.	lat.	alt., m
1	AT60170	Graz Süd Tiergartenweg	background	urban	15.43	47.04	345
2	BG0051A	Evmolpia-AMS	background	urban	24.78	42.15	166
3	BG0012A	Yan Palah-Varna	traffic	urban	27.90	43.23	60
4	CZ0EPAO	Pardubice-Rosice	background	suburban	15.74	50.04	217
5	CZ0PPLB	Plzen-Bory	background	urban	13.38	49.73	346
6	CZ0PPLA	Plzen-Slovany	traffic	urban	13.40	49.73	340
7	ES1137A	ARENAL	traffic	urban	-8.74	42.22	53
8	ES1270A	HERMANOS FELGUEROSO	traffic	urban	-5.66	43.54	10
9	ES1346A	MIRANDA DE EBRO 2	industrial	urban	-2.94	42.69	471
10	ES1464A	MOLLABAO	traffic	urban	-8.66	42.42	15
11	ES1569A	LORCA	industrial	suburban	-1.70	37.69	340
12	ES1617A	ALZIRA	background	suburban	-0.46	39.15	60
13	ES1624A	ELX-AGROALIMENTARI	background	suburban	-0.68	38.24	44
14	FR24023	CONTES 2	industrial	suburban	7.33	43.79	186
15	FR20037	TERNAY	background	suburban	4.80	45.60	235
16	GR0032A	PATISION	traffic	urban	23.73	38.00	105
17	GR0008A	PATRA-1	traffic	urban	21.74	38.25	16
18	IT0524A	CASSANO VIA DI VONA 301508	background	urban	9.52	45.54	133
19	IT1309A	CENS10 2009017	traffic	urban	9.50	40.93	15
20	IT0775A	COLICO 301301	background	suburban	9.38	46.14	228
21	IT0995A	CORMANO 301513	traffic	urban	9.17	45.54	146
22	IT0854A	CORSO FIRENZE - GENOVA 701009	background	urban	8.93	44.42	105
23	IT1683A	MANDURIA 1607387	traffic	urban	17.63	40.39	20
24	IT1178A	PASSO DEI GIOVI 701013	background	rural	8.94	44.56	80
25	IT0612A	SAN CUSMANO 1908909	background	suburban	15.15	37.21	30
26	IT1578A	VIA SCARPELLINI 1104105	background	suburban	12.92	43.89	20
27	IT1745A	Santo Chiodo 1005405	Industrial	suburban	12.71	42.74	282
28	IT0953A	VILLA ADA 1205820	background	urban	12.51	41.93	50
29	LV0RKE2	Riga Kengarags-2	background	urban	24.16	56.94	7
30	LV0RVL7	Riga-Valdemara street	traffic	urban	24.12	56.96	6
31	PT02004	Estarreja/Teixugueira	industrial	suburban	-8.58	40.68	20
32	RS0007A	Omladinskih brigada	background	urban	20.40	44.81	90
33	SK0016A	Podhradova	background	suburban	21.25	48.76	248

Appendix D

The final list of 1492 stations used in the CA. Indicated number of data points, removed with the automatic data quality filter: “N mis.” – number of missing data points; “N flag.” – number of all data points below zero, above threshold, near missing value, or outliers; “N valid” – total number of valid data points. Last two columns – number of cluster each station belongs to.

	station ID	station name	lon.	lat.	alt., m	N mis.	N flag.	N valid	CL, 1CA	CL, 2CA
1	AT30101	Amstetten	14.88	48.12	270	1764	156	33144	1	2
2	AT31102	Annaberg - Joachimsberg	15.32	47.86	891	2132	133	32799	5	4
3	AT60190	Arnfels - Remschnigg	15.37	46.65	785	2018	100	32946	5	4
4	AT2M121	Arnoldstein Gailitz Waldsiedlungsweg	13.71	46.56	574	1618	100	33346	2	2
5	AT4S125	Bad Ischl	13.63	47.72	460	3580	150	31334	3	2
6	AT30201	Bad Vöslau - Gainfarn	16.21	47.96	286	2407	137	32520	4	3
7	AT2VK26	Bleiburg Koschatstrasse	14.8	46.59	480	1711	107	33246	1	2
8	AT82708	Bludenz Herrengasse	9.83	47.16	580	1775	56	33233	2	2
9	AT60151	Bockberg	15.5	46.87	449	1776	137	33151	4	3
10	AT4S156	Braunau Zentrum	13.04	48.26	350	3494	217	31353	1	2
11	AT60195	Deutschlandsberg Rathausgasse	15.21	46.81	368	1800	144	33120	2	2
12	AT31701	Dunkelsteinerwald	15.55	48.37	305	1905	171	32988	3	3
13	AT60196	Grebenzen	14.33	47.04	1648	3036	201	31827	5	4
14	AT10001	Eisenstadt - Laschoberstraße	16.53	47.84	160	1921	145	32998	3	3
15	AT4S165	Enns Kristein A1	14.45	48.21	282	3346	267	31451	1	2
16	AT0ENK1	Enzenkirchen im Sauwald	13.67	48.39	525	2110	114	32840	4	3
17	AT30202	Forsthof am Schöpfl	15.92	48.11	581	2457	122	32485	4	4
18	AT60198	Fürstenfeld	16.08	47.05	276	1752	149	33163	2	2
19	AT2VL52	Gerlitzen Steinturm	13.9	46.68	1895	1677	147	33240	5	4
20	AT60138	Graz Nord	15.41	47.1	348	2066	199	32799	2	1
21	AT60018	Graz Schlossberg	15.44	47.08	450	1957	146	32961	2	1
22	AT60157	Grundlsee	13.8	47.62	980	2011	98	32955	5	4
23	AT4S108	Grünbach bei Freistadt	14.57	48.53	918	4008	265	30791	5	4
24	AT30401	Gänserndorf	16.73	48.33	161	1756	163	33145	4	3
25	AT30301	Hainburg	16.96	48.14	165	1832	151	33081	4	3
26	AT52100	Hallein Winterstall	13.11	47.67	650	1781	142	33141	4	4
27	AT53055	Haunsberg	13.02	47.97	730	1819	94	33151	5	4
28	AT30502	Heidenreichstein Thaures	15.05	48.88	560	2144	105	32815	4	3
29	AT30603	Himberg	16.43	48.09	172	1825	125	33114	3	2
30	AT60137	Hochgössnitz	15.02	47.06	900	2098	198	32768	5	4
31	AT60189	Hochwurzen	13.63	47.36	1850	1782	144	33138	5	4
32	AT72705	Höfen Lärchbichl	10.68	47.47	880	1354	55	33655	4	4
33	AT0ILL1	Illmitz	16.77	47.77	117	2208	185	32671	4	3
34	AT72123	Innsbruck Nordkette	11.38	47.31	1910	1369	66	33629	5	4
35	AT72106	Innsbruck Reichenau	11.42	47.27	570	1416	97	33551	1	1
36	AT72113	Innsbruck Sadrach	11.37	47.27	670	1800	58	33206	3	2

	station ID	station name	lon.	lat.	alt., m	N mis.	N flag.	N valid	CL, 1CA	CL, 2CA
37	AT30801	Irnfritz	15.5	48.72	556	1700	143	33221	4	4
38	AT60118	Judenburg	14.68	47.18	715	1878	126	33060	1	2
39	AT72218	Karwendel West	11.23	47.34	1730	1404	87	33573	5	4
40	AT10003	Kittsee	17.07	48.11	138	2012	160	32892	3	2
41	AT2KA11	Klagenfurt Koschatstrasse	14.3	46.63	440	1790	161	33113	1	1
42	AT2KA41	Klagenfurt Kreuzbergl	14.29	46.63	550	1798	126	33140	2	1
43	AT2F202	Klein St. Paul - Pemberg	14.53	46.84	810	1676	147	33241	3	2
44	AT30601	Klosterneuburg Wiesentgasse	16.3	48.3	200	2127	142	32795	3	3
45	AT60185	Klöch bei Bad Radkersburg	15.96	46.75	300	1729	193	33142	5	4
46	AT30103	Kollmitzberg	14.87	48.18	465	2327	167	32570	4	3
47	AT72538	Kramsach Angerberg	11.91	47.46	600	1397	34	33633	1	1
48	AT32501	Krems	15.62	48.41	190	2697	174	32193	3	2
49	AT72547	Kufstein Festung	12.17	47.58	550	1576	65	33423	1	1
50	AT4S418	Lenzing	13.6	47.97	510	3105	160	31799	3	3
51	AT60143	Leoben Zentrum	15.09	47.38	540	2376	114	32574	1	2
52	AT72908	Lienz Sportzentrum	12.77	46.83	670	3462	75	31527	2	2
53	AT60182	Liezen	14.24	47.57	665	2106	102	32856	1	2
54	AT4S416	Linz Neue Welt	14.31	48.27	265	2817	191	32056	1	2
55	AT80706	Lustenau Wiesenrain	9.65	47.41	410	1694	78	33292	2	2
56	AT60156	Masenberg	15.88	47.35	1137	2646	238	32180	5	4
57	AT31301	Mistelbach	16.58	48.58	250	1691	158	33215	4	3
58	AT31401	Mödling	16.3	48.09	210	2020	118	32926	3	3
59	AT60194	Mürzzuschlag Roseggerpark	15.67	47.6	679	1936	96	33032	1	2
60	AT2SP20	Oberdrauburg Bundesstraße	12.97	46.75	612	1620	56	33388	1	2
61	AT10002	Oberschützen	16.19	47.3	330	2709	153	32202	3	2
62	AT2SP10	Obervellach Schulzentrum	13.2	46.94	686	1770	153	33141	3	2
63	AT31502	Payerbach	15.85	47.67	890	1997	135	32932	5	4
64	AT0PIL1	Pillersdorf bei Retz	15.94	48.72	315	2008	230	32826	4	3
65	AT30065	Purkersdorf	16.18	48.21	248	1959	130	32975	1	2
66	AT31204	Pöchlarn	15.21	48.21	216	1827	118	33119	2	2
67	AT60150	Rennfeld	15.36	47.41	1620	2248	199	32617	5	4
68	AT51200	Salzburg Lehen Martinstraße	13.03	47.82	455	2499	170	32395	1	2
69	AT51066	Salzburg Mirabellplatz	13.05	47.81	430	2020	137	32907	1	2
70	AT32701	Schwechat Sportplatz	16.47	48.15	155	1699	146	33219	3	2
71	AT4S420	Schöneben	13.95	48.71	920	2405	153	32506	4	4
72	AT2SP18	Spittal a.d.Drau Oktoberstrasse	13.5	46.8	560	2076	114	32874	1	1
73	AT2WO35	St. Georgen im Lavanttal - Herzogberg	14.89	46.71	540	1719	90	33255	2	2
74	AT54057	St. Johann im Pongau	13.21	47.35	620	1983	97	32984	1	1
75	AT52055	St. Koloman Kleinhorn	13.23	47.65	1005	2492	143	32429	5	4
76	AT32301	St. Pölten - Eybnerstraße	15.63	48.21	270	1863	172	33029	2	2
77	AT30104	St. Valentin A1	14.55	48.18	295	1822	158	33084	1	2
78	AT4S409	Steyr	14.44	48.05	307	3926	145	30993	1	2
79	AT30302	Stixneusiedl	16.68	48.05	210	2318	157	32589	4	3

	station ID	station name	lon.	lat.	alt., m	N mis.	N flag.	N valid	CL, 1CA	CL, 2CA
80	AT30902	Stockerau West	16.21	48.39	186	1632	194	33238	1	2
81	AT31904	Streithofen im Tullnerfeld	15.94	48.28	220	2111	136	32817	3	3
82	AT80503	Sulzberg im Bregenzerwald	9.93	47.53	1020	2150	102	32812	5	4
83	AT55032	Tamsweg - Untere Postgasse	13.81	47.13	1025	2360	131	32573	3	2
84	AT31501	Ternitz	16.04	47.72	380	1652	90	33322	4	3
85	AT4S404	Traun	14.24	48.23	274	2956	140	31968	1	2
86	AT2VI12	Villach Tirolerbruecke	13.84	46.61	490	1633	170	33261	1	1
87	AT60107	Voitsberg Mühlgasse	15.15	47.04	390	2021	150	32893	1	1
88	AT0VOR1	Vorhegg bei Kötschach-Mauthen	12.97	46.68	1020	3232	129	31703	5	4
89	AT82801	Wald am Arlberg	10.05	47.13	940	2105	53	32906	1	2
90	AT60181	Weiz	15.63	47.22	468	1649	135	33280	2	2
91	AT9JAEG	Wien Hermannskogel	16.3	48.27	520	1696	146	33222	4	4
92	AT900ZA	Wien Hohe Warte - Zentralanstalt für Meteorologie und Geodynamik	16.36	48.25	207	1798	161	33105	3	2
93	AT90LAA	Wien Laaer Berg	16.39	48.16	250	1767	192	33105	3	3
94	AT90LOB	Wien Lobau - Grundwasserwerk	16.53	48.16	150	1783	190	33091	3	2
95	AT9STEF	Wien Stephansplatz	16.37	48.21	173	2747	158	32159	2	2
96	AT32401	Wiener Neustadt - Neuklosterwiese	16.26	47.81	265	1802	130	33132	3	2
97	AT32101	Wiesmath	16.29	47.61	738	1823	133	33108	5	4
98	AT2WO15	Wolfsberg Hauptschule	14.84	46.84	440	1643	126	33295	1	1
99	AT30403	Wolkersdorf	16.52	48.39	190	1717	187	33160	4	3
100	AT55018	Zederhaus A10	13.51	47.15	1205	2233	129	32702	1	2
101	AT56071	Zell am See Krankenhaus	12.81	47.34	770	3014	122	31928	3	3
102	AT30701	Ziersdorf	15.94	48.53	230	1785	174	33105	3	2
103	AT72807	Zillertaler Alpen	11.87	47.14	1970	2787	133	32144	5	4
104	AT0ZOE2	Zöbelboden - Reichraminger Hintergebirge	14.44	47.84	899	2761	182	32121	5	4
105	BA0029A	SARAJEVO-BJ-AUTOMAT	18.42	43.87	630	3601	15	31448	3	4
106	BETB006	41B006 - PARL.EUROPE	4.37	50.84	80	1455	47	33562	1	2
107	BETB011	41B011 - BERCHEM S.A	4.29	50.86	30	1245	45	33774	1	2
108	BETN043	41N043 - HAREN	4.38	50.88	15	1442	69	33553	1	2
109	BETR001	41R001 - MOLENBEEK	4.33	50.85	15	1063	44	33957	1	2
110	BETR012	41R012 - UCCLE	4.36	50.8	100	1034	41	33989	3	3
111	BETWOL1	41WOL1 - WOL.ST.L.	4.43	50.86	77	2142	66	32856	1	2
112	BETN016	42N016 - DESSEL	5.16	51.23	30	3761	77	31226	1	2
113	BETN035	42N035 - AARSCHOT	4.84	50.98	55	3434	84	31546	1	2
114	BETN040	42N040 - ST.P.LEEUWG	4.23	50.77	20	3766	124	31174	1	3
115	BETN054	42N054 - WALSHOUTEM	5.1	50.71	135	3839	77	31148	1	3
116	BETR801	42R801 - BORGERHOUT	4.43	51.21	6	3256	131	31677	1	2
117	BETR811	42R811 - SCHOTEN	4.49	51.25	8	4295	88	30681	1	2
118	BETR831	42R831 - BERENDRECHT	4.34	51.35	3	4014	95	30955	1	2
119	BETR841	42R841 - MECHELEN	4.47	51	8	4511	130	30423	1	2

	station ID	station name	lon.	lat.	alt., m	N mis.	N flag.	N valid	CL, 1CA	CL, 2CA
120	BETN063	43N063 - CORROY L.G.	4.67	50.66	145	2726	71	32267	3	3
121	BETN066	43N066 - EUPEN	6	50.63	295	2778	170	32116	3	3
122	BETN070	43N070 - MONS	3.94	50.47	30	1788	68	33208	1	2
123	BETN073	43N073 - VEZIN	4.99	50.5	160	2056	68	32940	3	3
124	BETN085	43N085 - VIELSALM	6	50.3	490	3219	85	31760	3	3
125	BETN093	43N093 - SINSIN	5.24	50.27	265	2669	96	32299	3	3
126	BETN100	43N100 - DOURBES	4.59	50.1	225	2336	77	32651	3	3
127	BETN113	43N113 - SAINT-ODE	5.59	50.03	510	2443	87	32534	4	4
128	BETN121	43N121 - OFFAGNE	5.2	49.88	430	2085	78	32901	3	4
129	BETN132	43N132 - HABAY-LA-N.	5.63	49.72	375	2833	107	32124	3	3
130	BETR201	43R201 - LIEGE	5.58	50.63	65	2467	98	32499	1	2
131	BETR222	43R222 - SERAING	5.57	50.61	65	4633	67	30364	1	2
132	BETR240	43R240 - ENGIS	5.4	50.58	135	2874	64	32126	1	2
133	BETM705	44M705 - ROESELARE	3.15	50.95	19	3294	84	31686	1	3
134	BETN012	44N012 - MOERKERKE	3.36	51.25	3	3894	61	31109	1	3
135	BETN029	44N029 - HOUTEM	2.58	51.02	2	3070	68	31926	3	3
136	BETN051	44N051 - IDEGEM	3.93	50.8	15	3218	136	31710	1	2
137	BETN052	44N052 - ZWEVEGEM	3.32	50.81	27	3069	94	31901	1	2
138	BETR701	44R701 - GENT	3.73	51.06	5	2960	160	31944	1	2
139	BETR710	44R710 - DESTELBERGE	3.78	51.06	6	3777	193	31094	1	2
140	BETR740	44R740 - ST.KRUIS-WI	3.81	51.15	5	3796	84	31184	1	2
141	BETR502	45R502 - LODELINSART	4.46	50.43	135	2105	55	32904	1	2
142	BG0045A	AMS Vazragdane-Ruse	25.98	43.86	50	1922	78	33064	3	3
143	BG0052A	Drujba -Sofia	23.38	42.67	540	1856	92	33116	1	2
144	BG0053R	Rojen peak	24.74	41.7	1750	2751	142	32099	5	4
145	CH0045A	Anières-Débarcadère	6.22	46.28	375	18	1	35045	3	3
146	CH0051A	Avully-Passeiry	6.01	46.16	427	96	19	34949	3	2
147	CH0008A	Basel-Binningen	7.58	47.54	317	209	34	34821	2	2
148	CH0017A	Basel-St-Johann	7.58	47.57	260	91	0	34973	1	2
149	CH0031A	Bern-Bollwerk	7.44	46.95	536	190	109	34765	1	2
150	CH0020A	Bern-Brunngasshalde	7.45	46.95	533	194	4	34866	1	2
151	CH0004R	Chaumont	6.98	47.05	1137	275	23	34766	5	4
152	CH0005A	Dübendorf-EMPA	8.61	47.4	433	118	32	34914	2	2
153	CH0022A	Ebikon-Sedel	8.3	47.07	484	769	28	34267	2	2
154	CH0049A	Genève-Ste-Clotilde	6.13	46.2	374	150	4	34910	1	2
155	CH0048A	Genève-Wilson	6.15	46.22	376	48	2	35014	1	3
156	CH0041A	Ittigen	7.48	46.98	550	235	48	34781	3	2
157	CH0028A	Lausanne-César-Roux	6.64	46.52	526	135	28	34901	1	3
158	CH0043A	Lugano-Pregassona	8.97	46.03	305	215	5	34844	2	1
159	CH0011A	Lugano-Universita	8.96	46.01	281	165	13	34886	2	1
160	CH0040A	Luzern-Museggstrasse	8.31	47.06	460	702	39	34323	1	1
161	CH0016A	Lägeren	8.36	47.48	689	254	3	34807	4	4
162	CH0033A	Magadino-Cadenazzo	8.93	46.16	204	180	128	34756	2	1
163	CH0050A	Meyrin-Vaudagne	6.07	46.23	439	311	25	34728	1	2

	station ID	station name	lon.	lat.	alt., m	N mis.	N flag.	N valid	CL, 1CA	CL, 2CA
164	CH0002R	Payerne	6.94	46.81	489	468	8	34588	3	3
165	CH0005R	Rigi-Seebodenalp	8.46	47.07	1031	269	22	34773	5	4
166	CH0024A	Saxon	7.15	46.14	460	113	2	34949	2	2
167	CH0042A	St-Gallen-Rorschacherstrasse	9.39	47.43	660	66	128	34870	3	2
168	CH0019A	St-Gallen-Stuelegg	9.39	47.41	920	245	5	34814	5	4
169	CH0046A	Thônex-Foron	6.21	46.2	422	412	52	34600	1	2
170	CH0003R	Tänikon	8.9	47.48	539	157	6	34901	3	3
171	CH0014A	Winterthur-Obertor	8.73	47.5	448	374	8	34682	1	2
172	CH0010A	Zürich-Kaserne	8.53	47.38	410	223	16	34825	2	2
173	CH0013A	Zürich-Stampfenbachstrasse	8.54	47.39	445	526	21	34517	1	2
174	CZ0TBKR	Bily Kriz	18.54	49.5	890	360	5	34699	5	4
175	CZ0BBNY	Brno-Turany	16.7	49.15	241	405	4	34655	3	2
176	CZ0TCER	Cervena	17.54	49.78	749	811	7	34246	5	4
177	CZ0CCBD	Ceske Budejovice	14.47	48.98	383	539	3	34522	3	2
178	CZ0CCHU	Churanov	13.61	49.07	1118	131	3	34930	5	4
179	CZ0CHVO	Hojna Voda	14.72	48.72	818	737	4	34323	5	4
180	CZ0HHKO	Hr.Kral.-observator	15.84	50.18	276	1476	7	33581	3	3
181	CZ0HHKB	Hradec Kralove-Brnen	15.85	50.2	232	450	6	34608	3	2
182	CZ0MJES	Jesenik	17.19	50.24	625	1106	5	33953	5	4
183	CZ0JJIH	Jihlava	15.61	49.4	502	533	5	34526	3	3
184	CZ0TKAR	Karvina	18.55	49.86	238	247	6	34811	3	2
185	CZ0SKLM	Kladno-stred mesta	14.1	50.14	303	691	4	34369	3	3
186	CZ0CKOC	Kocelovice	13.84	49.47	519	524	4	34536	4	3
187	CZ0JKOS	Kosetice	15.08	49.57	535	813	10	34241	4	4
188	CZ0JKMY	Kostelni Myslova	15.44	49.16	569	300	17	34747	4	4
189	CZ0HKRY	Krkonose-Rychory	15.85	50.66	1001	1167	7	33890	5	4
190	CZ0BKUC	Kucharovice	16.09	48.88	334	239	13	34812	4	3
191	CZ0LLIM	Liberec-mesto	15.06	50.76	350	288	5	34771	3	3
192	CZ0ULTT	Litomerice	14.12	50.54	190	466	5	34593	3	2
193	CZ0ULOM	Lom	13.67	50.59	265	112	4	34948	3	2
194	CZ0BMIS	Mikulov-Sedlec	16.73	48.79	245	499	6	34559	4	3
195	CZ0SMBO	Mlada Boleslav	14.91	50.43	398	587	0	34477	3	3
196	CZ0UMOM	Most	13.65	50.51	221	225	6	34833	3	2
197	CZ0SONR	Ondrejov	14.78	49.92	514	624	7	34433	4	4
198	CZ0TOFF	Ostrava-Fifejdy	18.27	49.84	220	257	3	34804	3	2
199	CZ0EPAU	Pardubice Dukla	15.76	50.02	239	845	19	34200	3	3
200	CZ0ALIB	Pha4-Libus	14.45	50.01	301	2151	119	32794	3	2
201	CZ0ASMI	Pha5-Smichov	14.4	50.09	216	2571	108	32385	1	2
202	CZ0ASTO	Pha5-Stodulky	14.33	50.05	309	675	2	34387	3	2
203	CZ0ASUC	Pha6-Suchdol	14.38	50.13	277	875	5	34184	3	2
204	CZ0AVEL	Pha6-Veleslavin	14.35	50.1	286	1862	90	33112	1	2
205	CZ0AKOB	Pha8-Kobylisy	14.47	50.12	269	1696	71	33297	3	2
206	CZ0AVYN	Pha9-Vysocany	14.5	50.11	219	1691	116	33257	1	2
207	CZ0PPLV	Plzen-Doubravka	13.43	49.77	348	451	10	34603	3	2

	station ID	station name	lon.	lat.	alt., m	N mis.	N flag.	N valid	CL, 1CA	CL, 2CA
208	CZ0PPLL	Plzen-Lochotin	13.37	49.77	360	1245	8	33811	3	2
209	CZ0KPRB	Prebuz	12.62	50.37	904	388	17	34659	4	4
210	CZ0MPRR	Prerov	17.46	49.45	210	213	5	34846	3	2
211	CZ0PPRM	Primda	12.68	49.67	740	2073	6	32985	4	4
212	CZ0MPST	Prostejov	17.11	49.47	218	196	9	34859	3	2
213	CZ0URVH	Rudolice v Horach	13.42	50.58	840	199	6	34859	4	4
214	CZ0HSER	Serlich	16.38	50.32	1011	656	13	34395	4	4
215	CZ0USNZ	Sneznik	14.09	50.79	590	266	3	34795	4	4
216	CZ0KSOM	Sokolov	12.67	50.18	476	93	3	34968	3	3
217	CZ0LSOU	Sous	15.32	50.79	771	494	31	34539	4	4
218	CZ0ZSNV	Stitna n.Vlari	18.01	49.05	600	135	15	34914	5	4
219	CZ0TSTD	Studenka	18.09	49.72	231	81	5	34978	3	3
220	CZ0ESVR	Svratouch	16.04	49.74	735	457	6	34601	4	4
221	CZ0CTAB	Tabor	14.68	49.41	400	2222	42	32800	3	2
222	CZ0TTRO	Trinec-Kosmos	18.68	49.67	320	166	6	34892	3	3
223	CZ0UTUS	Tusimice	13.33	50.38	322	167	7	34890	3	3
224	CZ0UULK	Usti n.L.-Kockov	14.04	50.68	367	302	13	34749	3	3
225	CZ0UULM	Usti n.L.-mesto	14.04	50.66	147	267	11	34786	1	2
226	CZ0UVAL	Valdek	14.52	50.97	438	775	13	34276	4	4
227	CZ0ZZLN	Zlin	17.67	49.23	258	174	0	34890	3	3
228	DENW094	Aachen-Burtscheid	6.09	50.75	205	3799	154	31111	3	3
229	DEBW029	Aalen	10.1	48.85	420	1927	86	33051	3	2
230	DENI052	Allertal	9.62	52.83	50	1452	79	33533	3	2
231	DETH011	Altenburg Theaterplatz	12.44	50.99	185	1301	109	33654	3	2
232	DESH001	Altendeich	9.59	53.67	8	142	5	34917	3	3
233	DENI063	Altes Land	9.69	53.52	3	1495	72	33497	3	3
234	DEBY109	Andechs/Rothenfeld	11.22	47.97	700	962	5	34097	4	3
235	DESN001	Annaberg-Buchholz	13	50.57	545	409	9	34646	3	3
236	DEBY001	Ansbach/Residenzstraße	10.57	49.3	400	597	5	34462	1	2
237	DEBY002	Arzberg/Egerstraße	12.19	50.06	480	240	4	34820	1	2
238	DEBY005	Aschaffenburg/Bussardweg	9.12	49.99	134	193	3	34868	1	2
239	DEBY099	Augsburg/LfU	10.9	48.33	495	68	3	34993	3	2
240	DEBE051	B Buch	13.49	52.64	60	1823	91	33150	3	2
241	DEBE056	B Friedrichshagen	13.65	52.45	35	2254	61	32749	3	3
242	DEBE062	B Frohnau Funkturm	13.3	52.65	50	1858	80	33126	3	2
243	DEBE032	B Grunewald	13.23	52.47	50	1202	34	33828	1	2
244	DEBE027	B Marienfelde-Schichauweg	13.37	52.4	45	2096	74	32894	3	2
245	DEBE034	B Neukölln-Nansenstraße	13.43	52.49	35	2193	97	32774	1	2
246	DEBE010	B Wedding-Amrumer Str.	13.35	52.54	35	1891	90	33083	1	2
247	DEHE046	Bad Arolsen	8.93	51.43	343	277	31	34756	4	4
248	DERP022	Bad Kreuznach-Bosenheimer Straße	7.87	49.84	108	1866	78	33120	1	2
249	DEBY079	Bad Reichenhall/Nonn	12.86	47.72	465	1555	3	33506	3	3
250	DESH016	Barsbüttel	10.21	53.57	42	326	2	34736	3	3

	station ID	station name	lon.	lat.	alt., m	N mis.	N flag.	N valid	CL, 1CA	CL, 2CA
251	DESN004	Bautzen	14.44	51.18	203	376	8	34680	3	3
252	DEHE032	Bebra	9.8	50.97	204	382	25	34657	1	2
253	DEBW042	Bernhausen	9.23	48.68	370	2074	123	32867	1	2
254	DESL002	Bexbach Schule	7.26	49.36	273	373	42	34649	3	2
255	DEBW046	Biberach	9.8	48.09	560	2003	75	32986	3	2
256	DENW067	Bielefeld-Ost	8.55	52.02	102	2458	194	32412	1	2
257	DESL019	Biringen	6.55	49.42	339	504	23	34537	4	4
258	DEST015	Bitterfeld/Wolfen	12.3	51.65	90	438	11	34615	3	2
259	DENW081	Borken-Gemen	6.87	51.86	45	2314	455	32295	1	2
260	DESH008	Bornhöved	10.24	54.09	45	288	4	34772	4	4
261	DENW021	Bottrop-Welheim	6.98	51.53	40	2664	887	31513	1	2
262	DEBB055	Brandenburg a.d. Havel	12.55	52.42	33	1597	74	33393	3	3
263	DENI011	Braunschweig	10.47	52.23	98	1506	65	33493	3	3
264	DEHB001	Bremen-Mitte	8.81	53.09	10	4458	120	30486	1	2
265	DEHB004	Bremen-Nord	8.63	53.18	20	1959	103	33002	3	3
266	DEHB002	Bremen-Ost	8.92	53.06	7	2433	96	32535	1	2
267	DEHB005	Bremerhaven	8.57	53.56	3	3286	143	31635	3	3
268	DEST039	Brocken	10.62	51.8	1142	241	20	34803	5	4
269	DESH011	Brunsbüttel	9.22	53.91	0	76	10	34978	3	3
270	DEST002	Burg	11.86	52.27	40	394	12	34658	3	3
271	DESN049	Carlsfeld	12.61	50.43	896	517	4	34543	5	4
272	DESN011	Chemnitz-Mitte	12.92	50.83	300	501	10	34553	3	2
273	DESN076	Collmberg	13.01	51.3	313	846	16	34202	4	4
274	DEBB064	Cottbus	14.33	51.75	75	1221	41	33802	3	3
275	DEHE001	Darmstadt	8.66	49.87	158	311	39	34714	1	2
276	DEST030	Dessau	12.25	51.84	60	342	19	34703	3	2
277	DESL003	Dillingen City	6.73	49.36	185	491	24	34549	3	2
278	DENW008	Dortmund-Eving	7.46	51.54	75	2510	447	32107	1	2
279	DETH026	Dreißigacker	10.38	50.56	450	1359	96	33609	4	3
280	DESN061	Dresden-Nord	13.74	51.06	112	523	11	34530	1	2
281	DENW034	Duisburg-Walsum	6.75	51.52	28	3310	777	30977	1	2
282	DENW071	Düsseldorf-Lörick	6.73	51.25	32	2254	288	32522	1	2
283	DEBW004	Eggenstein	8.4	49.08	110	1703	83	33278	1	2
284	DENI028	Eichsfeld	10.24	51.51	185	1424	72	33568	3	3
285	DETH013	Eisenach Wernebrg.Str	10.32	50.98	210	1373	117	33574	3	2
286	DEBB032	Eisenhüttenstadt	14.64	52.15	40	1231	76	33757	3	3
287	DENI059	Elbmündung	8.8	53.83	3	1478	117	33469	3	4
288	DEBB007	Elsterwerda	13.53	51.46	89	1221	96	33027	3	2
289	DENI043	Emsland	7.32	52.5	30	1423	80	33561	3	3
290	DETH020	Erfurt Krämpferstr.	11.04	50.98	195	1365	122	33577	1	3
291	DEBY113	Erlangen/Kraepelinstraße	10.96	49.61	284	25	0	35039	1	2
292	DESH013	Fehmarn	11.22	54.41	2	528	1	34535	4	4
293	DESN053	Fichtelberg	12.95	50.43	1214	492	7	34565	5	4
294	DEBB042	Frankfurt (Oder)	14.53	52.34	45	1306	70	33688	3	3

	station ID	station name	lon.	lat.	alt., m	N mis.	N flag.	N valid	CL, 1CA	CL, 2CA
295	DEHE005	Frankfurt-Höchst	8.54	50.1	104	327	51	34686	1	2
296	DEHE008	Frankfurt-Ost	8.75	50.13	100	596	34	34434	1	2
297	DEBW084	Freiburg-Mitte	7.83	48	240	1827	92	33145	3	2
298	DEBW037	Freudenstadt	8.41	48.47	750	1686	45	33333	4	4
299	DEBW038	Friedrichshafen	9.49	47.66	402	1890	129	33045	1	2
300	DEHE058	Fulda-Mitte	9.68	50.55	272	136	13	34915	1	2
301	DEHE028	Fürth/Odenwald	8.82	49.65	484	545	20	34499	4	4
302	DEBY081	Garmisch-Partenkirchen/ Kreuzeckbahnstraße	11.06	47.48	735	1424	21	33619	3	3
303	DETH009	Gera Friedericistr.	12.07	50.88	190	1454	146	33464	1	2
304	DESH017	Glücksburg	9.57	54.84	34	2321	3	32740	4	4
305	DEHE023	Grebenau	9.46	50.76	373	523	33	34508	3	3
306	DETH036	Greiz Mollbergstr.	12.21	50.66	265	1348	144	33572	1	2
307	DETH040	Großer Eisenberg	10.79	50.62	907	1330	96	33638	5	4
308	DEBW112	Gärtringen	8.9	48.65	463	1992	108	32964	3	2
309	DEMV017	Göhlen	11.36	53.3	25	1488	93	33483	3	3
310	DENI042	Göttingen	9.95	51.55	165	1417	52	33595	3	2
311	DEMV004	Gülzow	12.06	53.82	17	1518	99	33447	3	3
312	DEMV019	Güstrow	12.18	53.78	17	1398	101	33565	3	3
313	DEST044	Halberstadt	11.06	51.9	110	612	10	34442	3	3
314	DEST050	Halle/Nord	11.98	51.5	120	667	10	34387	3	2
315	DEHH049	Hamburg Blankenese-Baursberg	9.79	53.57	75	2957	138	31969	3	3
316	DEHH047	Hamburg Bramfeld	10.11	53.63	31	3139	204	31721	3	3
317	DEHH033	Hamburg Flughafen Nord	10	53.64	13	3194	169	31701	1	3
318	DEHH050	Hamburg Neugraben	9.86	53.48	3	2852	153	32059	3	3
319	DEHH008	Hamburg Sternschanze	9.97	53.56	15	2952	142	31970	1	2
320	DEHH021	Hamburg Tatenberg	10.08	53.49	2	3111	161	31792	1	3
321	DEHE011	Hanau	8.92	50.13	106	368	35	34661	1	2
322	DENI054	Hannover	9.71	52.36	80	1666	91	33307	3	3
323	DEBB053	Hasenholz	14.02	52.56	88	1248	75	33741	3	3
324	DEBW009	Heidelberg	8.68	49.42	110	1748	89	33227	1	2
325	DEBW015	Heilbronn	9.22	49.17	152	1839	108	33117	1	2
326	DEBY020	Hof/Berliner Platz	11.9	50.32	518	761	9	34294	3	2
327	DETH061	Hummelshain	11.66	50.79	357	1419	66	33579	3	3
328	DERP014	Hunsrück-Leisel	7.19	49.74	650	1808	97	33159	4	4
329	DENW058	Hürth	6.87	50.88	90	2468	243	32353	1	2
330	DESH015	Itzehoe	9.53	53.92	40	192	11	34861	3	3
331	DENI031	Jadebusen	8.09	53.6	2	1482	100	33482	3	3
332	DETH041	Jena Dammstr.	11.6	50.93	140	1852	103	33109	1	2
333	DERP019	Kaiserslautern-Rathausplatz	7.77	49.45	232	1711	155	33198	1	2
334	DEBW001	Karlsruhe-Mitte	8.42	49.01	115	1887	123	33054	1	2
335	DEBW081	Karlsruhe-Nordwest	8.36	49.03	113	2002	104	32958	2	2
336	DEBW022	Kehl-Hafen	7.8	48.58	135	1828	96	33140	1	2
337	DEHE060	Kellerwald	9.03	51.15	483	882	28	34154	4	4

	station ID	station name	lon.	lat.	alt., m	N mis.	N flag.	N valid	CL, 1CA	CL, 2CA
338	DEBY031	Kempten (Allgäu)/Westendstraße	10.31	47.73	678	371	3	34690	3	2
339	DEHE052	Kleiner Feldberg	8.45	50.22	811	378	11	34675	5	4
340	DEBY004	Kleinwallstadt/Hofstetter Straße	9.17	49.87	124	551	3	34510	1	2
341	DERP024	Koblenz-Friedrich-Ebert-Ring	7.6	50.36	68	1722	186	33156	1	2
342	DEBW052	Konstanz	9.17	47.66	400	1720	74	33270	3	2
343	DENW042	Krefeld-Linn	6.64	51.34	32	1989	178	32897	1	2
344	DEBY032	Kulmbach/Konrad-Adenauer-Straße	11.44	50.1	303	189	5	34870	1	2
345	DENW053	Köln-Chorweiler	6.88	51.02	45	2407	210	32447	1	2
346	DENW059	Köln-Rodenkirchen	6.99	50.89	45	2854	1341	30869	1	2
347	DESN082	Leipzig-Thekla	12.43	51.38	110	370	6	34688	1	2
348	DESN059	Leipzig-West	12.3	51.32	115	306	9	34749	3	2
349	DERP040	Trier-Universität	6.67	49.75	256	1546	49	33469	3	3
350	DEST090	Leuna	12.03	51.32	100	1030	10	34024	3	2
351	DENW079	Leverkusen-Manfort	7.01	51.03	50	2244	596	32224	1	2
352	DEHE044	Limburg	8.06	50.38	128	293	46	34725	1	2
353	DEHE042	Linden/Leihgestern	8.68	50.53	172	292	42	34730	1	2
354	DEBW024	Ludwigsburg	9.17	48.9	300	1948	78	33038	1	2
355	DERP001	Ludwigshafen-Oppau	8.4	49.52	91	1546	87	33431	1	2
356	DEMV012	Löcknitz	14.26	53.52	17	1965	123	32976	3	3
357	DESH023	Lübeck-St. Jürgen	10.7	53.84	12	108	1	34955	3	3
358	DENI062	Lüneburger Heide	10.46	53.25	13	1429	100	33535	3	3
359	DENW006	Lünen-Niederaden	7.57	51.59	58	2164	209	32691	1	2
360	DEBB065	Lütte (Belzig)	12.56	52.19	114	1497	121	33446	3	3
361	DEST076	Magdeburg/Damaschke-platz	11.62	52.13	50	661	17	34386	1	2
362	DEST077	Magdeburg/West	11.61	52.13	50	1102	25	33937	3	2
363	DERP007	Mainz-Mombach	8.22	50.02	120	1558	124	33382	1	2
364	DEBW006	Mannheim-Mitte	8.48	49.48	95	1776	98	33190	1	2
365	DEBW005	Mannheim-Nord	8.47	49.54	95	1941	134	32989	1	2
366	DEBW007	Mannheim-Süd	8.53	49.43	95	2083	149	32832	1	2
367	DEHE030	Marburg	8.77	50.8	182	154	25	34885	1	2
368	DENW015	Marl-Sickingmühle	7.12	51.7	42	2077	224	32763	1	2
369	DEBY013	Mehring/Sportplatz	12.78	48.18	415	1219	3	33842	1	2
370	DEHE045	Michelstadt	9	49.67	209	584	48	34432	1	2
371	DENW096	Mönchengladbach-Rheydt	6.43	51.15	78	1954	342	32768	1	2
372	DENW038	Mülheim-Styrum	6.87	51.45	37	2342	885	31837	1	2
373	DEBY089	München/Johannes-kirchen	11.65	48.17	513	31	3	35030	1	2
374	DEBY039	München/Lothstraße	11.55	48.15	521	14	0	35050	1	2
375	DEBY037	München/Stachus	11.56	48.14	521	222	0	34842	1	2
376	DENW095	Münster-Geist	7.61	51.94	63	2060	217	32787	1	2
377	DEBY047	Naila/Selbitzer Berg	11.72	50.32	534	147	2	34915	3	3
378	DEBB067	Nauen	12.89	52.61	31	1221	102	33741	3	3
379	DENW065	Netphen Rothaargebirge	8.19	50.93	635	2209	68	32787	4	4
380	DEBY052	Neu-Ulm/Gabelsbergerstraße	10.01	48.4	470	784	8	34272	1	2

	station ID	station name	lon.	lat.	alt., m	N mis.	N flag.	N valid	CL, 1CA	CL, 2CA
381	DEMV003	Neubrandenburg	13.27	53.56	15	1445	138	33481	1	3
382	DEBW073	Neuenburg	7.57	47.82	227	2067	76	32921	3	2
383	DEUB030	Neuglobsow	13.03	53.14	65	1921	214	32929	3	3
384	DETH027	Neuhaus	11.13	50.5	840	1478	89	33497	4	4
385	DEBB048	Neuruppin	12.81	52.93	43	1257	103	33704	3	3
386	DEBY049	Neustadt a.d. Donau/Eining	11.78	48.85	359	299	7	34758	3	2
387	DERP027	Neustadt-Strohmarkt	8.14	49.35	138	1609	112	33343	1	2
388	DERP021	Neuwied-Hafenstraße	7.48	50.42	65	1889	116	33059	1	2
389	DENW074	Niederzier	6.47	50.88	105	1962	126	32976	1	3
390	DESN079	Niesky	14.75	51.29	148	459	7	34598	3	3
391	DETH018	Nordhausen	10.79	51.5	185	1301	118	33645	1	2
392	DEBY053	Nürnberg/Bahnhof	11.09	49.45	307	20	1	35043	1	2
393	DEBW103	Odenwald	8.75	49.46	520	1768	76	33220	4	4
394	DEBW111	Offenburg	7.94	48.48	150	1875	87	33102	1	2
395	DENI016	Oker/Harlingerode	10.48	51.9	220	1471	61	33532	3	3
396	DENI038	Osnabrück	8.05	52.26	95	1591	111	33362	1	3
397	DENI058	Ostfries. Inseln	7.21	53.72	1	1445	110	33509	4	4
398	DENI029	Ostfriesland	7.21	53.36	1	1509	48	33507	3	3
399	DEBY118	Passau/Stelzhamerstraße	13.42	48.57	300	329	0	34735	1	2
400	DEBW110	Pfullendorf	9.24	47.93	623	1886	87	33091	3	2
401	DERP017	Pfälzerwald-Hortenkopf	7.83	49.27	606	1814	87	33163	4	4
402	DERP034	Pirmasens-Lemberger Straße	7.61	49.19	370	1555	153	33356	3	3
403	DESN081	Plauen-DWD	12.13	50.48	385	1307	8	33749	3	3
404	DEBW026	Plochingen	9.41	48.71	250	2189	176	32699	1	2
405	DETH042	Possen	10.87	51.33	420	1316	75	33673	4	4
406	DEBB021	Potsdam-Zentrum	13.06	52.4	31	1316	85	33663	3	3
407	DESN051	Radebeul-Wahnsdorf	13.68	51.12	246	594	16	34454	3	3
408	DENW078	Ratingen-Tiefenbroich	6.82	51.3	41	2103	252	32709	1	2
409	DEHE018	Raunheim	8.45	50.01	90	233	44	34787	1	2
410	DEBY062	Regen/Bodenmaiser Straße	13.13	48.97	545	141	5	34918	1	2
411	DEBY063	Regensburg/Rathaus	12.1	49.02	335	162	5	34897	1	2
412	DEBW027	Reutlingen	9.21	48.49	385	2140	146	32778	3	2
413	DEHE043	Riedstadt	8.52	49.83	87	298	26	34740	2	2
414	DEMV007	Rostock-Stuthof	12.17	54.16	5	1293	123	33648	3	3
415	DEMV021	Rostock-Warnemünde	12.08	54.17	2	1758	88	33218	3	4
416	DETH005	Saalfeld	11.37	50.65	210	1594	135	33335	1	2
417	DESL011	Saarbrücken-Eschberg	7.04	49.24	315	573	24	34467	3	3
418	DEST069	Salzwedel	11.17	52.86	23	612	13	34439	3	3
419	DEUB004	Schauinsland	7.91	47.91	1205	1537	134	33393	5	4
420	DESN080	Schkeuditz	12.23	51.4	122	556	4	34504	3	2
421	DESH006	Schleswig	9.55	54.53	42	28	0	35036	4	4
422	DEUB029	Schmücke	10.77	50.65	937	2328	149	32587	5	4
423	DESN074	Schwartenberg	13.47	50.66	785	644	7	34413	4	4
424	DEBW031	Schwarzwald Süd	7.76	47.81	920	1825	71	33168	5	4

	station ID	station name	lon.	lat.	alt., m	N mis.	N flag.	N valid	CL, 1CA	CL, 2CA
425	DEBB029	Schwedt (Oder)	14.29	53.06	10	1417	132	33515	3	3
426	DEBY068	Schweinfurt/Obertor	10.23	50.05	231	72	2	34990	1	2
427	DENW179	Schwerte	7.58	51.45	157	2093	248	32723	1	2
428	DEBW056	Schwäbisch Hall	9.73	49.11	300	1816	105	33143	1	2
429	DEBW087	Schwäbische Alb	9.21	48.35	799	1706	64	33294	4	4
430	DENW064	Simmerath Eifel	6.28	50.65	572	2396	119	32549	4	4
431	DENW068	Soest-Ost	8.15	51.57	110	2085	136	32843	3	3
432	DENW080	Solingen-Wald	7.05	51.18	207	1659	81	33324	1	3
433	DEHE026	Spessart	9.4	50.16	502	488	40	34536	4	4
434	DERP018	Speyer-St.-Guido-Stifts-Platz	8.44	49.32	110	1590	97	33377	1	2
435	DEBB066	Spreewald	14.06	51.9	52	1284	33	33747	3	3
436	DESH014	St.-Peter-Ording	8.6	54.33	2	283	1	34780	4	4
437	DEBW013	Stuttgart Bad Cannstatt	9.23	48.81	235	2001	121	32942	1	2
438	DEBW011	Stuttgart-Zuffenhausen	9.17	48.83	260	2100	123	32841	1	2
439	DESL018	Sulzbach	7.06	49.3	236	340	41	34683	1	2
440	DENI053	Südoldenburg	7.94	53	40	1797	70	33197	3	3
441	DEBW059	Tauberbischofsheim	9.66	49.63	177	1991	70	33003	1	2
442	DEBY072	Tiefenbach/Alten-schneeberg	12.55	49.44	755	672	9	34383	4	4
443	DEBY088	Trostberg/Schwimmbad-straße	12.54	48.02	488	47	2	35015	1	2
444	DEBW107	Tübingen	9.05	48.51	320	1783	87	33194	1	2
445	DEBW019	Ulm	9.98	48.4	480	2065	102	32897	1	2
446	DEST098	Unterharz / Friedrichsbrunn	11.04	51.66	410	581	15	34468	3	3
447	DEBW039	Villingen-Schwenningen	8.46	48.05	705	1835	82	33147	3	2
448	DESL017	Völklingen-City Stadionstr.	6.87	49.25	189	508	27	34529	1	2
449	DEBW034	Waiblingen	9.3	48.83	275	2057	88	32919	1	2
450	DEUB005	Waldhof	10.76	52.8	74	1807	129	33128	3	3
451	DEBW040	Waldshut	8.22	47.62	340	1976	52	33036	1	2
452	DEHE051	Wasserkuppe	9.94	50.5	931	313	11	34740	5	4
453	DEBY075	Weiden i.d.OPf./Nikolaistraße	12.16	49.68	400	396	21	34647	1	2
454	DEBW023	Weil am Rhein	7.63	47.59	275	1766	69	33229	3	2
455	DENI060	Wendland	11.17	52.96	50	1525	87	33452	3	3
456	DEST011	Wernigerode/Bahnhof	10.79	51.84	230	467	12	34585	3	3
457	DENW030	Wesel-Feldmark	6.63	51.67	25	2642	608	31814	1	2
458	DENI041	Weserbergland	9.07	52.18	58	1581	59	33424	3	3
459	DERP015	Westeifel Wascheid	6.38	50.27	680	1988	100	32976	4	4
460	DEUB001	Westerland	8.31	54.92	12	1858	172	33034	4	4
461	DERP016	Westerwald-Herdorf	7.97	50.77	480	1585	115	33364	4	4
462	DERP028	Westerwald-Neuhäusel	7.73	50.42	540	2375	89	32600	4	4
463	DERP013	Westpfalz-Waldmohr	7.29	49.42	455	1835	101	33128	4	4
464	DEHE020	Wetzlar	8.5	50.57	152	461	51	34552	1	2
465	DEHE022	Wiesbaden-Süd	8.24	50.05	121	492	47	34525	1	2
466	DEBW010	Wiesloch	8.7	49.3	160	1849	50	33165	2	2
467	DEST066	Wittenberg/Bahnstrasse	12.66	51.87	80	1104	16	33944	3	2
468	DEBB063	Wittenberge	11.74	53	22	1288	92	33684	4	3

	station ID	station name	lon.	lat.	alt., m	N mis.	N flag.	N valid	CL, 1CA	CL, 2CA
469	DEHE024	Witzenhausen/Wald	9.77	51.29	610	661	19	34384	4	4
470	DENI020	Wolfsburg	10.82	52.44	60	1464	79	33521	3	3
471	DERP023	Worms-Hagenstraße	8.36	49.63	90	2365	105	32594	1	2
472	DENW114	Wuppertal-Langerfeld	7.23	51.28	186	1890	261	32913	1	2
473	DENI051	Wurmberg	10.61	51.76	930	1494	39	33531	5	4
474	DERP025	Wörth-Marktplatz	8.25	49.05	104	1963	95	33006	3	2
475	DEBY077	Würzburg/Kopfklinik	9.96	49.8	226	58	5	35001	1	2
476	DEST089	Zartau/Waldstation	11.17	52.59	95	577	19	34468	3	3
477	DEST028	Zeitz	12.14	51.05	160	246	13	34805	3	2
478	DETH060	Zella-Mehlis	10.67	50.65	490	1313	166	33585	3	2
479	DEUB028	Zingst	12.72	54.44	1	1694	207	33163	4	4
480	DESN052	Zinnwald	13.75	50.73	877	425	6	34633	5	4
481	DESN045	Zittau-Ost	14.82	50.89	230	322	11	34731	3	3
482	DK0053A	Aalborg/8158	9.93	57.05	30	2105	224	32735	3	4
483	DK0034A	Copenhagen/1103	12.57	55.67	5	4090	158	30720	1	4
484	DK0030A	Copenhagen/1257	12.55	55.7	5	2480	297	32287	1	4
485	DK0045A	Copenhagen/1259	12.56	55.7	25	2814	177	32073	3	4
486	DK0054A	Keldsnor/9054	10.74	54.75	3	3033	247	31784	4	4
487	DK0046A	Odense/9159	10.39	55.4	25	3159	232	31673	3	4
488	DK0031R	Ulborg	8.43	56.28	37	4513	158	30393	4	4
489	DK0052A	Århus/6159	10.2	56.15	20	2989	414	31661	3	4
490	EE0019A	Kohtla-Järve	27.28	59.41	60	1225	5	33834	3	4
491	EE0009R	Lahemaa	25.93	59.49	32	451	6	34607	3	4
492	EE0020A	Liivalaia	24.76	59.43	5	195	18	34851	1	4
493	EE0015A	Rahu	24.7	59.46	9	1489	8	33567	3	4
494	EE0016A	Saarejärve	26.76	58.7	50	479	2	34583	3	4
495	EE0011R	Vilsandi	21.85	58.38	6	579	6	34479	4	4
496	EE0018A	Õismäe	24.65	59.41	6	625	16	34423	4	4
497	ES0007R	VÍZNAR	-3.53	37.24	1230	1123	67	33874	5	4
498	ES0008R	NIEMBRO	-4.85	43.44	134	425	33	34606	5	4
499	ES0009R	CAMPISABALOS	-3.14	41.27	1360	1186	54	33824	5	4
500	ES0010R	CABO DE CREUS	3.32	42.32	23	974	37	34053	5	4
501	ES0011R	BARCARROTA	-6.92	38.47	393	827	31	34206	4	3
502	ES0012R	ZARRA	-1.1	39.08	885	1164	22	33878	5	4
503	ES0013R	PEÑAUSENDE	-5.9	41.24	985	481	34	34549	5	4
504	ES0014R	ELS TORMS	0.73	41.39	470	674	42	34348	5	4
505	ES0016R	O SAVIÑAO	-7.7	42.63	506	856	25	34183	4	4
506	ES0094A	FRAGA REDONDA (F-2)	-7.99	43.41	480	1367	26	33671	4	4
507	ES0118A	ESCUELAS AGUIRRE	-3.68	40.42	672	725	20	34319	1	2
508	ES0124A	ARTURO SORIA	-3.64	40.44	698	108	9	34947	2	2
509	ES0126A	FAROLILLO	-3.73	40.39	625	123	10	34931	2	2
510	ES0201A	MAGDALENA (B-1)	-7.85	43.45	363	693	10	34361	4	4
511	ES0316A	MONAGREGA	-0.29	40.95	570	1465	5	33594	5	4
512	ES0324A	ESTANCA	-0.18	41.05	395	2096	3	32965	4	3

	station ID	station name	lon.	lat.	alt., m	N mis.	N flag.	N valid	CL, 1CA	CL, 2CA
513	ES0365A	VILLALBA DE GUARDO	-4.83	42.7	1050	1471	14	33579	4	3
514	ES0373A	CONGOSTO	-6.52	42.63	720	885	27	34152	4	4
515	ES0377A	CORTIGUERA	-6.64	42.61	560	585	22	34457	4	4
516	ES0584A	I6-MONTCADA I REIXAC	2.19	41.48	35	1984	15	33065	1	2
517	ES0587A	MUSKIZ	-3.11	43.32	30	993	53	34018	4	4
518	ES0588A	ABANTO	-3.07	43.32	136	1211	112	33741	3	3
519	ES0625A	CAMPOHERMOSO	-2.13	36.94	152	3369	9	31686	4	3
520	ES0651A	ALUMBRES	-0.91	37.6	60	1578	13	33473	4	3
521	ES0692A	I3-L'HOSPITALET DE LLOBREGAT	2.12	41.37	20	925	12	34127	1	2
522	ES0694A	I8-SANT VICENÇ DELS HORTS	2.01	41.39	22	532	22	34510	1	2
523	ES0805A	BASAURI	-2.88	43.24	125	2257	133	32674	1	3
524	ES0813A	LA CEROLLERA	-0.06	40.84	830	431	8	34625	5	4
525	ES0822A	LA ORDEN	-6.94	37.28	66	3929	23	31112	4	3
526	ES0824A	MERIÑAN	-5.7	43.31	220	614	7	34443	1	3
527	ES0825A	LA FELGUERA	-5.69	43.31	216	1819	9	33236	1	2
528	ES0879A	LLARANES	-5.88	43.55	15	521	28	34515	1	3
529	ES0880A	LLANOPONTE	-5.94	43.54	10	582	7	34475	1	3
530	ES0890A	TORNEO	-6	37.4	17	1735	30	33299	3	3
531	ES0893A	GUADARRANQUE	-5.41	36.18	2	2928	63	32049	4	4
532	ES0905A	GETXO	-3.01	43.35	64	1202	56	33806	1	3
533	ES0971A	IC-SANT ANDREU DE LA BARCA	1.98	41.45	39	1222	27	33815	1	2
534	ES1018A	E1-TERRASSA	2.01	41.56	277	596	26	34442	1	3
535	ES1033A	SASTAGO	-0.36	41.32	140	3146	23	31895	4	3
536	ES1038A	ZAPATÓN	-4.05	43.35	20	762	24	34278	3	3
537	ES1044A	EL PICARRAL	-0.87	41.67	195	427	5	34608	1	3
538	ES1072A	LA LANEA	-5.35	36.16	1	1717	46	33301	4	4
539	ES1076A	CORTIJILLOS	-5.43	36.19	26	1403	35	33626	4	4
540	ES1090A	JAIME FERRÁN	-0.86	41.67	196	890	17	34157	1	2
541	ES1095A	POZOS	4.25	39.89	55	4619	17	30428	4	4
542	ES1096A	GOMEZ FRANQUEIRA	-7.88	42.35	132	4937	55	30072	1	3
543	ES1117A	A4-VILA-SECA	1.07	41.11	60	1467	29	33568	3	3
544	ES1125A	A8-MANRESA	1.83	41.73	238	1304	14	33746	1	2
545	ES1126A	A9-MARTORELL	1.92	41.48	56	1142	20	33902	1	2
546	ES1135A	AA-IGUALADA	1.63	41.58	284	2323	14	32727	2	2
547	ES1138A	CORLAB 1	-8.42	43.37	35	2941	88	32035	1	4
548	ES1148A	I4-SANT ADRIÀ DE BESÒS	2.22	41.43	9	2196	31	32837	1	2
549	ES1169A	CARTEYA (S9)	-5.39	36.21	51	981	49	34034	4	4
550	ES1173A	VILANOVA (G-2)	-8.03	43.55	290	653	44	34367	4	4
551	ES1185A	SAGUNT PORT	-0.23	39.67	10	1012	8	34044	3	3
552	ES1193A	CASA DE CAMPO	-3.75	40.42	645	1091	47	33926	2	2
553	ES1201A	AL-AGULLANA	2.84	42.39	217	1221	17	33826	5	4
554	ES1208A	AF-REUS	1.12	41.15	110	1596	35	33433	4	3
555	ES1215A	AP-AMPOSTA	0.58	40.71	8	2097	22	32945	4	3

	station ID	station name	lon.	lat.	alt., m	N mis.	N flag.	N valid	CL, 1CA	CL, 2CA
556	ES1217A	AM-JUNEDA	0.81	41.55	264	2126	11	32927	4	3
557	ES1222A	AR-SANTA MARIA DE PALAUTORDERA	2.44	41.69	208	578	16	34470	3	2
558	ES1225A	AB-LLEIDA	0.61	41.63	220	1453	16	33595	2	2
559	ES1231A	AT-SANT CUGAT DEL VALLES	2.09	41.48	124	2128	39	32897	1	2
560	ES1244A	MAZARREDO	-2.92	43.27	33	729	24	34311	1	3
561	ES1248A	AO-SORT	1.13	42.41	692	2587	12	32465	4	3
562	ES1262A	AD-SABADELL (GRAN VIA)	2.1	41.56	190	1396	32	33636	1	2
563	ES1268A	PLAZA DE TOROS	-5.86	43.36	276	379	2	34683	1	3
564	ES1269A	PALACIO DE DEPORTES	-5.83	43.37	206	824	9	34231	1	3
565	ES1271A	ARGENTINA	-5.7	43.54	11	707	13	34344	1	3
566	ES1272A	CONSTITUCIÓN	-5.71	43.53	12	378	8	34654	1	3
567	ES1275A	AC-SANT CELONI	2.5	41.69	143	1268	21	33775	1	2
568	ES1277A	INSTITUTO Nº 3	-4.11	38.68	675	1007	64	33993	3	3
569	ES1278A	CALLE ANCHA	-4.11	38.69	705	975	49	34040	3	3
570	ES1279A	CAMPO DE FÚTBOL	-4.09	38.68	685	1498	102	33464	4	3
571	ES1285A	LOUSEIRAS (B-2)	-7.74	43.54	540	1089	11	33964	5	4
572	ES1297A	LA ROBLA	-5.62	42.8	945	3785	22	31257	3	3
573	ES1310A	AK-PARDINES	2.22	42.31	1226	800	17	34247	5	4
574	ES1311A	AV-BEGUR	3.21	41.96	200	1287	11	33766	5	4
575	ES1339A	AW-VILANOVA I LA GELTRÚ	1.72	41.22	22	1343	47	33674	3	3
576	ES1347A	AX-SANTA PAU	2.51	42.15	496	1131	31	33902	3	3
577	ES1348A	AZ-BELLVER DE CERDANYA	1.78	42.37	1060	1210	11	33843	4	3
578	ES1349A	LLODIO	-2.96	43.14	122	1792	46	33226	1	3
579	ES1350A	ARETA	-2.94	43.15	114	1990	57	33017	1	3
580	ES1351A	ARRIGORRIAGA	-2.98	43.21	53	1754	68	33242	1	2
581	ES1353A	SAMA I	-5.68	43.3	212	3240	12	31812	1	3
582	ES1359A	MOURENCE (C-9)	-7.69	43.31	465	667	3	34394	4	4
583	ES1363A	LUGONES	-5.81	43.4	163	1559	18	33487	1	3
584	ES1365A	BARRIO 630	-4.11	38.7	685	703	41	34320	4	3
585	ES1370A	MOTRIL	-3.52	36.75	50	2176	11	32877	4	3
586	ES1378A	TRUBIA	-5.99	43.34	250	292	1	34771	3	3
587	ES1379A	AY-GANDESA	0.44	41.06	363	991	18	34055	5	4
588	ES1386A	CASTELLÓ-PENYETA	-0.06	40.01	106	1942	13	33109	5	4
589	ES1387A	ONDA	-0.23	39.96	163	1705	19	33340	4	3
590	ES1393A	MEDITERRÁNEO	-2.46	36.85	51	1840	28	33196	4	4
591	ES1397A	E8-MANLLEU	2.29	42	460	2527	25	32512	2	2
592	ES1400A	BUJARALOZ	-0.15	41.51	327	2166	24	32874	4	3
593	ES1405A	VALLIBONA	0.01	40.58	1235	1374	4	33614	5	4
594	ES1417A	HUESCA	-0.4	42.14	488	2784	11	32269	4	3
595	ES1418A	ALAGÓN	-1.14	41.76	235	1488	17	33559	3	3
596	ES1420A	MONZÓN	0.2	41.92	279	1348	15	33701	4	3
597	ES1422A	PLAZA DEL CARMEN	-3.7	40.42	657	647	21	34396	1	2
598	ES1423A	LA ALJORRA	-1.06	37.69	80	1479	65	33520	4	3
599	ES1424A	PLAZA DE LA GUITARRA	-5.93	43.56	20	294	4	34766	3	3
600	ES1428A	CASTELLÓ-ERMITA	-0.04	39.96	44	3643	50	31371	1	2
601	ES1432A	CANGAS DE NARCEA	-6.55	43.18	330	670	15	34379	3	3

	station ID	station name	lon.	lat.	alt., m	N mis.	N flag.	N valid	CL, 1CA	CL, 2CA
602	ES1433A	BLIMEA	-5.6	43.28	267	404	6	34654	1	3
603	ES1435A	VILAFRANCA	-0.25	40.42	1125	2349	24	32691	5	4
604	ES1441A	MORELLA	-0.09	40.64	1150	1892	15	33157	5	4
605	ES1442A	ARRASATE	-2.49	43.06	218	1613	93	33358	1	2
606	ES1443A	BURGOS 4	-3.64	42.34	929	3035	31	31998	3	3
607	ES1449A	SALAMANCA 4	-5.66	40.95	797	867	9	34188	3	3
608	ES1450A	SANTA CLARA	-5.95	37.4	29	940	12	34112	2	2
609	ES1453A	II-SANTA COLOMA DE GRAMENET	2.21	41.45	56	921	25	34118	1	2
610	ES1472A	ITURRAMA	-1.65	42.81	449	1963	64	33037	3	3
611	ES1479A	AVDA. MARCONI	-6.27	36.51	4	1265	22	33777	4	4
612	ES1480A	IJ-BARCELONA (GRACIA-SANT GERVASI)	2.15	41.4	75	426	3	34611	1	3
613	ES1488A	IZKI	-2.5	42.65	833	1323	48	33693	5	4
614	ES1489A	VALDEREJO	-3.23	42.88	911	1399	143	33522	5	4
615	ES1490A	DURANGO	-2.64	43.17	113	1766	129	33169	1	3
616	ES1491A	MUNDAKA	-2.7	43.41	116	1254	59	33751	4	4
617	ES1492A	TRES MARZO	-2.67	42.86	518	1106	115	33843	3	3
618	ES1496A	RENTERIA	-1.9	43.31	23	2255	216	32593	1	3
619	ES1498A	TOLOSA	-2.08	43.13	90	1796	289	32955	1	2
620	ES1499A	BEASAIN	-2.19	43.05	153	2231	134	32699	1	2
621	ES1501A	AZPEITIA	-2.27	43.18	110	1052	56	33956	1	3
622	ES1502A	AVENIDA GASTEIZ	-2.68	42.85	517	2919	98	32047	3	3
623	ES1516A	RIO SAN PEDRO	-6.22	36.52	1	1886	168	33010	4	4
624	ES1517A	ALCUDIA I	3.15	39.84	15	1554	9	33501	4	4
625	ES1518A	CAN LLOMPART	3.04	39.84	25	2616	9	32199	4	4
626	ES1519A	SAN JERÓNIMO	-5.98	37.43	21	590	25	34449	2	2
627	ES1521A	BARRIO DEL PILAR	-3.71	40.48	673	501	36	32439	3	3
628	ES1529A	TETUÁN	-3.79	43.47	30	679	13	34372	3	3
629	ES1530A	REINOSA	-4.14	43	850	358	12	34694	4	4
630	ES1531A	LOS TOJOS	-4.26	43.15	651	787	13	34264	5	4
631	ES1535A	ALBACETE	-1.96	38.98	686	1339	42	33635	4	3
632	ES1536A	AZUQUECA DE HENARES	-3.26	40.57	662	945	23	34096	2	2
633	ES1537A	GUADALAJARA	-3.17	40.63	700	1104	30	33930	4	2
634	ES1542A	SANT JORDI	0.37	40.55	181	1356	13	33695	4	4
635	ES1543A	ZORITA	-0.17	40.73	619	1138	6	33920	4	3
636	ES1544A	AGURAIN	-2.48	42.85	594	1070	60	33934	4	3
637	ES1549A	EL EJIDO	-2.82	36.78	97	1203	39	33822	4	3
638	ES1560A	GRANADA - NORTE	-3.61	37.2	689	2035	29	33000	2	2
639	ES1563A	ALCALÁ DE HENARES	-3.38	40.48	595	283	9	34772	2	2
640	ES1564A	ALCOBENDAS	-3.64	40.54	688	290	26	34748	2	2
641	ES1565A	FUENLABRADA	-3.8	40.28	699	352	21	34691	2	2
642	ES1567A	LEGANÉS	-3.74	40.34	676	279	20	34765	1	2
643	ES1568A	MÓSTOLES	-3.88	40.32	660	547	21	34496	2	2
644	ES1572A	PURIFICACIÓN TOMAS	-5.87	43.37	286	613	5	34446	3	4

	station ID	station name	lon.	lat.	alt., m	N mis.	N flag.	N valid	CL, 1CA	CL, 2CA
645	ES1576A	ESTACIÓN DEL MEDITERRANEO	-3.84	43.41	16	721	13	34330	3	3
646	ES1577A	PARQUE DE CROSS	-3.84	43.42	10	626	11	34427	3	3
647	ES1578A	CASTRO URDIALES	-3.22	43.38	20	344	9	34711	3	4
648	ES1579A	LOS CORRALES DE BUELNA	-4.06	43.26	88	590	15	34459	1	3
649	ES1588A	BB-PONTS	1.19	41.91	370	879	11	34174	2	2
650	ES1589A	LEÓN 3	-5.56	42.61	838	3931	15	31118	3	3
651	ES1593A	SAN FERNANDO	-6.2	36.46	35	1195	37	33832	5	4
652	ES1595A	SANGRONIZ	-2.93	43.3	21	2130	60	32874	3	3
653	ES1596A	ENERGYWORKS-VA 1	-4.71	41.67	694	2726	7	32331	3	2
654	ES1597A	ENERGYWORKS-VA 2	-4.74	41.68	753	645	3	34416	3	3
655	ES1598A	ZALLA	-3.13	43.21	62	1818	41	33205	3	3
656	ES1599A	PAGOETA	-2.15	43.25	225	2231	142	32691	5	4
657	ES1601A	BADAJOZ	-7.01	38.89	390	1814	18	33232	4	3
658	ES1602A	LA CIGÜEÑA	-2.43	42.46	386	1340	22	33678	3	3
659	ES1604A	CASTILLO DE BELLVER	2.62	39.56	117	4707	47	30310	5	4
660	ES1611A	ARANJUEZ	-3.59	40.04	501	258	16	34790	2	2
661	ES1612A	MAJADAHONDA	-3.87	40.45	730	362	16	34686	4	3
662	ES1613A	COLMENAR VIEJO	-3.77	40.67	905	289	18	34757	4	3
663	ES1615A	CACERES	-6.36	39.47	389	1339	7	33718	4	3
664	ES1616A	MONFRAGÜE	-5.94	39.85	376	2438	35	32591	4	3
665	ES1619A	VALÈNCIA-VIVERS	-0.37	39.48	11	1910	7	33147	1	3
666	ES1620A	CARTUJA	-6.11	36.66	49	1254	21	33789	4	3
667	ES1623A	ALCOI - VERGE DELS LLIRIS	-0.47	38.71	534	3696	44	31324	4	4
668	ES1627A	ALCANTARILLA	-1.23	37.98	80	742	13	34309	2	2
669	ES1630A	ALJARAFE	-6.04	37.34	50	525	16	34523	4	3
670	ES1632A	VEGA SICILIA	-4.75	41.62	690	381	1	34682	3	2
671	ES1633A	SAN BASILIO	-1.14	37.99	40	2239	19	32806	2	2
672	ES1635A	ALACANT-EL PLÁ	-0.47	38.36	45	3214	32	31794	3	3
673	ES1638A	BERMEJALES	-5.98	37.35	26	1599	10	33455	2	2
674	ES1640A	ALCALÁ DE GUADAIRA	-5.83	37.34	68	887	12	34165	4	3
675	ES1641A	RENOVALES	-0.89	41.64	220	2315	21	32728	3	3
676	ES1642A	BD-VIC (ESTADIE MUNICIPAL D'ATLETISME)	2.24	41.94	498	1344	15	33705	2	2
677	ES1643A	SORIA	-2.47	41.77	1090	1178	20	33866	4	4
678	ES1644A	CENTRO	-5.99	37.39	19	552	16	34496	2	2
679	ES1648A	E2: ALCORNOCALES	-5.66	36.23	189	1338	11	33715	4	4
680	ES1649A	ALFARO	-1.74	42.18	365	638	5	34421	4	3
681	ES1650A	LEMONA	-2.78	43.21	49	1406	100	33558	1	2
682	ES1651A	JARDINES DE JUAN XXIII	-5.77	43.25	206	688	13	34363	1	3
683	ES1653A	DOS HERMANAS	-5.91	37.28	49	1001	26	34037	4	3
684	ES1654A	SIERRA NORTE	-5.67	38	573	3028	62	31974	4	3
685	ES1656A	RONDA DEL VALLE	-3.78	37.78	480	2015	50	32999	4	3
686	ES1657A	MARBELLA	-4.98	36.5	39	2336	58	32670	4	4
687	ES1658A	CAMPUS DEL CARMEN	-6.92	37.27	48	2401	17	32646	4	3

	station ID	station name	lon.	lat.	alt., m	N mis.	N flag.	N valid	CL, 1CA	CL, 2CA
688	ES1660A	CTCC-ARGUEDAS	-1.59	42.21	475	785	31	34248	5	4
689	ES1661A	CTCC-TUDELA	-1.63	42.07	383	829	22	34213	4	3
690	ES1662A	CTCC-FUNES	-1.81	42.31	460	939	21	34104	5	4
691	ES1666A	BE-TARRAGONA (PARC DE LA CIUTAT)	1.24	41.12	14	924	24	34116	3	3
692	ES1670A	CAUDETE DE LAS FUENTES	-1.28	39.56	804	925	22	34093	4	3
693	ES1671A	VILLAR DEL ARZOBISPO	-0.83	39.71	430	2134	17	32913	4	3
694	ES1675A	BENIDORM	-0.15	38.57	44	3259	16	31789	5	4
695	ES1677A	ORIHUELA	-0.85	38.08	32	4144	125	30795	3	3
696	ES1679A	IL-CIUTADELLA	2.18	41.39	5	1191	18	33855	1	3
697	ES1684A	BF-RUBA (CA N'ORIOL)	2.04	41.49	200	1412	21	33631	2	2
698	ES1685A	ALCORA	-0.19	40.05	160	1949	14	32933	3	3
699	ES1688A	BURRIANA	-0.07	39.89	37	2109	18	32937	3	3
700	ES1689A	CIRAT	-0.47	40.05	466	2011	21	33032	4	3
701	ES1690A	TORRE ENDOMENECH	-0.08	40.27	259	2349	34	32681	3	3
702	ES1691A	VIVER	-0.6	39.93	616	3463	19	31582	4	3
703	ES1696A	PUYO	-1.98	43.3	88	1719	158	33187	1	3
704	ES1709A	BENIGANIM	-0.44	38.93	195	4166	74	30824	4	3
705	ES1710A	L'ELIANA	-0.52	39.57	101	4081	31	30952	3	2
706	ES1711A	ONTINYENT	-0.7	38.79	510	4927	22	30115	4	4
707	ES1713A	PARQUE EUROPA	-2.9	43.26	76	1807	103	33154	1	3
708	ES1740A	PLAZA DE LA CRUZ	-1.64	42.81	455	1683	43	33338	1	4
709	ES1746A	GALILEA	-2.23	42.34	584	1856	39	33169	4	4
710	ES1747A	ROTXAPEA	-1.65	42.83	418	1195	37	33832	4	3
711	ES1750A	CARRANQUE	-4.45	36.72	36	1121	20	33923	4	3
712	ES1751A	EL ATABAL	-4.46	36.73	86	1550	21	33493	4	4
713	ES1752A	TORREJON DE ARDOZ II	-3.48	40.45	597	801	36	34227	2	2
714	ES1753A	PRADEJÓN	-2.06	42.34	402	2142	39	32883	4	4
715	ES1754A	BC-LA SÈNIA	0.29	40.65	428	164	11	34889	5	4
716	ES1765A	SAGUNT-NORD	-0.28	39.68	54	2897	14	32153	3	3
717	ES1779A	ARRÚBAL	-2.25	42.44	336	1787	23	33254	3	3
718	ES1783A	SA VINYETA - INCA	2.92	39.72	118	1933	4	33127	4	3
719	ES1786A	EL BOTICARIO	-2.39	36.87	55	1000	30	34034	5	4
720	ES1790A	PONFERRADA 4	-6.58	42.54	541	960	9	34095	1	3
721	ES1793A	EL ARENOSILLO	-6.73	37.1	31	2090	9	32965	4	4
722	ES1800A	ASOMADILLA	-4.78	37.9	152	1317	14	33733	4	3
723	ES1801A	ARGANDA DEL REY	-3.46	40.3	596	415	20	34629	2	2
724	ES1802A	EL ATAZAR	-3.47	40.91	940	905	19	34140	5	4
725	ES1803A	COLLADO VILLALBA	-4.01	40.63	873	293	20	34751	3	2
726	ES1804A	GETAFE	-3.71	40.32	638	295	17	34752	1	2
727	ES1805A	GUADALIX DE LA SIERRA	-3.7	40.78	853	188	16	34860	3	2
728	ES1806A	ORUSCO DE TAJUÑA	-3.22	40.29	800	342	19	34703	5	4
729	ES1807A	RIVAS-VACIAMADRID	-3.54	40.36	608	321	23	34720	2	2
730	ES1808A	SAN MARTIN DE VALDEIGLESIAS	-4.4	40.37	549	427	26	34611	4	4

	station ID	station name	lon.	lat.	alt., m	N mis.	N flag.	N valid	CL, 1CA	CL, 2CA
731	ES1809A	VALDEMORO	-3.68	40.19	610	172	15	34877	3	2
732	ES1810A	VILLA DEL PRADO	-4.27	40.25	512	467	18	34579	3	3
733	ES1811A	VILLAREJO DE SALVANES	-3.28	40.17	764	243	6	34815	4	3
734	ES1812A	BI-ALCOVER	1.18	41.28	243	937	31	34096	4	4
735	ES1813A	BJ- GUIAMETS	0.76	41.1	220	1097	14	33953	5	4
736	ES1814A	EA-MOLLET	2.21	41.55	476	1591	20	33453	1	2
737	ES1815A	EB-VILAFRANCA DEL PENEDÈS	1.69	41.35	200	1433	26	33605	3	3
738	ES1816A	EC-MATARÓ	2.44	41.55	40	1429	17	33618	4	3
739	ES1817A	ED-SANTA PERPETUA DE MOGODA	2.19	41.53	68	969	15	34080	1	2
740	ES1818A	TOLEDO2	-4.02	39.87	500	2535	49	32432	2	2
741	ES1819A	MERIDA	-6.34	38.91	214	1968	10	33086	4	3
742	ES1820A	ZAFRA	-6.39	38.43	551	2424	18	32622	5	4
743	ES1822A	PRADO REY	-5.53	36.79	390	2080	11	32973	5	4
744	ES1824A	LAS FUENTEZUELAS	-3.81	37.79	376	1574	27	33463	5	4
745	ES1827A	HOSPITAL JOAN MARCH	2.69	39.68	172	3604	21	31439	5	4
746	ES1828A	CIUTADELLA DE MENORCA	3.86	40.01	30	4402	29	30633	4	4
747	ES1832A	CEMENTOS PORTLAND 1	-4.47	41.93	721	2496	19	32549	2	3
748	ES1833A	CEMENTOS PORTLAND 2	-4.47	41.95	732	1961	27	33076	4	3
749	ES1834A	CASTELLÓ-PATRONAT D'ESPORTS	-0.03	39.99	18	4760	88	30216	3	3
750	ES1836A	LAS FUENTES	-0.86	41.64	198	1445	22	33597	1	2
751	ES1837A	CENTRO	-0.88	41.65	210	271	6	34787	1	2
752	ES1838A	ALGETE	-3.5	40.59	800	287	18	32575	4	3
753	ES1848A	CASPE	-0.03	41.23	152	4021	110	30741	4	3
754	FI00368	Evo (Lammi)	25.13	61.22	132	896	14	34154	3	4
755	FI00428	Ilomantsi	31.05	63.14	235	1093	14	33957	4	4
756	FI00425	Kallio 2	24.95	60.19	21	399	6	34659	3	4
757	FI00363	Kasarmipuisto	27.67	62.89	112	1793	9	33262	3	4
758	FI00208	Luukki	24.69	60.31	64	490	101	34473	3	4
759	FI00564	Mannerheimintie	24.94	60.17	5	1452	80	33532	1	4
760	FI00293	Metsäkangas	25.59	60.98	150	365	9	34690	3	4
761	FI00431	Palokka 2	25.71	62.29	143	1519	15	33530	1	4
762	FI00357	Raja-Jooseppi	28.3	68.48	262	2195	13	32856	4	4
763	FI00460	Ruissalo Saaronniemi	22.1	60.43	6	2172	67	32825	3	4
764	FI00226	Tikkurila 2	25.04	60.29	21	350	19	34695	3	3
765	FI00349	Utö	21.37	59.78	7	785	47	34232	4	4
766	FI00351	Virolahti	27.67	60.53	4	599	45	34420	3	4
767	FI00372	Ähtäri 2	24.19	62.59	180	1014	35	34015	4	4
768	FR24013	ADRECHAS	7.53	44.11	1826	3738	15	31311	5	4
769	FR31032	AGEN	0.62	44.19	36	848	2	34214	3	3
770	FR03029	AIX CENTRE ECOLE ART	5.44	43.53	188	779	14	34271	3	2
771	FR03048	AIX PLATANES	5.46	43.56	293	732	6	34326	3	2

	station ID	station name	lon.	lat.	alt., m	N mis.	N flag.	N valid	CL, 1CA	CL, 2CA
772	FR41001	AJACCIO CANETO	8.74	41.92	43	778	13	34273	4	3
773	FR41007	AJACCIO SPOSATA	8.76	41.95	60	734	18	32680	4	3
774	FR12026	ALBI DELMAS	2.15	43.93	165	270	3	34791	3	3
775	FR31034	AMBES 2	-0.53	45.01	3	921	2	34141	3	3
776	FR33211	ANNEMASSE	6.24	46.2	441	287	6	34771	3	2
777	FR24007	ANTIBES JEAN MOULIN	7.09	43.6	77	559	1	34504	3	2
778	FR04018	AUBERVILLIERS	2.39	48.9	42	1852	33	33179	1	2
779	FR03080	AVIGNON MAIRIE	4.81	43.95	16	674	10	34380	3	3
780	FR09008	AYTRE	-1.12	46.14	10	961	30	34073	4	3
781	FR08022	Agathois-piscénois	3.47	43.31	20	880	15	34169	4	4
782	FR33121	Albertville	6.39	45.67	352	419	4	34641	1	2
783	FR36004	Annonay Urb centre	4.67	45.25	200	1018	27	32099	3	3
784	FR11022	Armentieres Centre	2.89	50.69	13	530	4	34530	1	3
785	FR18039	Arrest	1.61	50.13	30	2293	8	32763	3	4
786	FR07014	Aurillac Aerodrome	2.42	44.9	640	880	11	34173	4	4
787	FR07017	Aurillac Mairie	2.45	44.93	641	448	5	34611	4	4
788	FR12024	BALMA	1.49	43.61	138	1408	17	33639	3	3
789	FR31007	BASSENS	-0.51	44.9	36	1134	12	33918	3	3
790	FR41002	BASTIA GIRAUD	9.45	42.7	60	1902	16	33146	5	4
791	FR12031	BELESTA EN LAURAGAIS	1.82	43.44	260	697	8	34359	4	4
792	FR12030	BERTHELOT	1.44	43.59	150	702	15	34347	3	3
793	FR14010	BETHENY	4.05	49.28	90	343	7	34714	3	2
794	FR31018	BIARRITZ	-1.55	43.46	65	888	47	33865	4	4
795	FR31013	BILLERE	-0.39	43.31	195	1139	15	33910	3	3
796	FR24024	BRIANCON	6.64	44.9	1210	1111	3	33950	3	3
797	FR03067	BRIGNOLES	6.08	43.4	274	928	8	34128	4	3
798	FR35004	BRIVE - Dalton	0.82	45.16	121	1269	34	33761	3	2
799	FR30020	Bar Le Duc	5.16	48.78	200	740	22	34302	1	2
800	FR18036	Beaumont Beauvais	2.1	49.44	93	1497	39	33528	3	3
801	FR02001	Berre l'Etang	5.17	43.49	6	1234	7	33823	4	3
802	FR07023	Besse et St Anastais	2.93	45.51	1050	683	7	34374	5	4
803	FR28028	Bethune Stade	2.64	50.52	20	2549	9	32506	3	3
804	FR08023	Biterrois-Narbonnais	3.19	43.41	71	990	16	34058	5	4
805	FR34062	Blois centre	1.33	47.59	70	451	9	34604	3	3
806	FR34061	Blois nord	1.3	47.59	115	565	14	34485	3	3
807	FR27007	Bourgoin-Jallieu	5.27	45.61	157	1757	42	33265	3	2
808	FR19012	Brest Mace	-4.49	48.39	48	450	16	34598	4	4
809	FR07020	Busset	3.52	46.06	495	538	2	34524	4	4
810	FR16060	C.C.3 Frontières	7.57	47.59	247	457	13	34594	1	2
811	FR04008	CACHAN	2.33	48.8	63	796	23	34245	1	2
812	FR03031	CADARACHE/DURANCE	5.76	43.7	294	1354	6	33536	2	2
813	FR24020	CAGNES LADOUMEGUE	7.16	43.66	21	1060	7	33997	3	2
814	FR24009	CANNES BROUSSAILLES	7.01	43.56	79	1559	7	33498	3	3
815	FR12017	CANTEPAU ALBI	2.16	43.93	165	254	1	34809	3	3

	station ID	station name	lon.	lat.	alt., m	N mis.	N flag.	N valid	CL, 1CA	CL, 2CA
816	FR14022	CHALONS	4.36	48.96	80	494	16	34554	1	2
817	FR33102	CHAMBERY LE HAUT	5.92	45.6	383	1042	10	34012	3	2
818	FR33120	CHAMONIX	6.87	45.92	1038	685	20	34287	1	2
819	FR04101	CHAMPIGNY-SUR-MARNE	2.52	48.82	74	1109	18	33937	1	2
820	FR24014	CIANS	6.99	44.09	1484	1404	4	33656	5	4
821	FR23172	CLAIRAIS	-1.43	47.27	17	268	5	34791	3	3
822	FR23175	CLOS DES BEAUVAIS	-0.61	47.43	55	189	7	34868	4	3
823	FR09017	COGNAC	-0.32	45.69	29	579	8	34477	3	3
824	FR12001	COLOMIERS	1.35	43.62	154	345	10	34709	4	3
825	FR03083	COMTAT VENAISSIN	5.04	44.1	69	1408	5	33651	3	2
826	FR20047	COTIERE AIN	4.95	45.82	180	777	11	34204	3	2
827	FR29421	COUBERTIN	4.39	45.47	480	839	36	34189	3	2
828	FR06009	Cambrai Gambetta	3.23	50.18	100	821	3	34168	3	3
829	FR25043	Centre Hospitalier	1.1	49.4	11	812	6	34246	3	3
830	FR04023	Cergy pontoise 95	2.04	49.05	85	821	21	34222	3	3
831	FR34003	Chambord	1.57	47.63	76	571	10	34051	3	3
832	FR15013	Champ sur Drac	5.73	45.08	267	512	11	34541	3	2
833	FR15012	Champagnier	5.73	45.11	363	856	15	34193	3	2
834	FR32002	Champforgueil	4.84	46.82	187	541	10	34513	1	2
835	FR15001	Charavines	5.52	45.43	491	721	17	34326	3	3
836	FR19003	Chartres de Bretagne	-1.71	48.05	40	636	6	34422	3	3
837	FR09010	Chasseneuil	0.38	46.66	74	540	11	34513	3	3
838	FR34051	Chateauroux Sud	1.69	46.8	155	429	2	34633	3	3
839	FR21001	Chemin Vert CAEN	-0.39	49.19	56	1024	22	34018	3	3
840	FR16053	Colmar Est	7.36	48.08	188	391	10	34663	3	2
841	FR16064	Colmar Sud	7.33	48.06	200	381	21	34662	3	2
842	FR13012	DAMBENOIS Citoyen	6.87	47.54	365	452	9	34603	3	2
843	FR31036	DAX	-1.04	43.7	3	442	11	34611	3	3
844	FR23152	DELACROIX	-1.44	46.66	72	171	5	34888	3	3
845	FR17009	DOLE CENTRE	5.5	47.1	223	1031	18	34015	3	3
846	FR07008	Delille	3.09	45.78	398	467	8	34589	3	3
847	FR06011	Denain Villars	3.4	50.33	80	568	3	34493	3	3
848	FR06003	Douai Theuriet	3.08	50.37	26	1281	3	33780	1	3
849	FR34044	Dreux Nord	1.37	48.75	130	555	7	34502	3	3
850	FR36005	Drôme Rurale Sud	5.09	44.52	460	1237	20	33807	5	4
851	FR34052	Déols	1.7	46.83	145	393	12	34659	3	3
852	FR12004	ECOLE M.JACQUIER	1.42	43.58	143	709	23	34332	3	3
853	FR23128	EMILE OUTTIER	-2.34	47.27	9	413	6	34645	4	4
854	FR23157	EPINETTES	-1.69	47.15	19	241	4	34819	3	3
855	FR09019	Ecole Jules Ferry	-0.46	46.33	65	268	19	34777	3	3
856	FR30019	Epinal	6.45	48.17	325	692	15	34357	3	3
857	FR25036	Espace du Palais	1.09	49.44	17	586	7	34471	1	2
858	FR25039	Evreux Centre	1.15	49.02	65	814	8	34242	3	3
859	FR25038	Evreux SDIS	1.14	49.04	130	891	9	31956	3	3

	station ID	station name	lon.	lat.	alt., m	N mis.	N flag.	N valid	CL, 1CA	CL, 2CA
860	FR29425	FIRMINY	4.28	45.39	467	354	11	34627	3	3
861	FR34054	Faverolles	1.41	47.17	128	585	6	34473	3	3
862	FR33303	Ferney-Voltaire	6.11	46.26	417	345	5	34714	3	2
863	FR23163	Fillé	0.15	47.92	41	451	7	34606	3	3
864	FR30021	Fléville	6.19	48.62	250	703	15	34346	1	3
865	FR15017	Fontaine Les Balmes	5.69	45.19	210	1058	11	33995	1	2
866	FR02013	Fos Les Carabins	4.93	43.46	5	1008	14	34042	4	3
867	FR19091	Fougeres DSTE	-1.2	48.35	110	1202	5	33857	3	3
868	FR34041	Fulbert	1.51	48.44	145	439	7	34618	3	3
869	FR33212	GAILLARD	6.21	46.19	426	327	7	34730	3	2
870	FR04145	GARCHES	2.19	48.85	134	377	11	34676	3	3
871	FR12029	GAUDONVILLE	0.84	43.88	222	461	6	34597	4	4
872	FR20045	GENAS	4.98	45.73	235	1131	18	33915	1	2
873	FR04002	GENNEVILLIERS	2.29	48.93	28	1307	27	33730	1	2
874	FR20017	GERLAND	4.83	45.74	172	1926	12	33126	1	2
875	FR31001	GRAND PARC	-0.58	44.86	3	1130	11	33923	3	3
876	FR24015	GRASSE CLAVECIN	6.92	43.66	356	846	14	34204	4	4
877	FR35005	GUERET - Nicolas	1.87	46.17	437	1035	54	33975	4	4
878	FR08204	Gard Rhodanien1	4.64	43.84	15	640	18	34406	4	3
879	FR08209	Gard Rhodanien2	4.68	43.94	85	534	11	34519	4	3
880	FR08614	Gauzy	4.37	43.83	40	510	16	34538	4	3
881	FR30022	Gerardmer	6.87	48.07	660	751	21	34292	3	3
882	FR07006	Gerzat	3.14	45.82	332	463	6	34595	3	3
883	FR34031	Gibjoncs	2.41	47.1	164	707	7	34350	3	3
884	FR15043	Grenoble Les Frenes	5.74	45.16	214	1681	80	33303	1	2
885	FR31014	HAMEAU	-0.32	43.31	227	862	17	34185	3	3
886	FR20049	HAUT BEAUJOLAIS	4.47	45.96	540	1446	13	33605	4	4
887	FR12034	HOPITAL CASTRES	2.24	43.6	520	767	35	34262	3	3
888	FR03069	HYERES	6.13	43.12	33	967	5	34092	4	3
889	FR11026	Halluin Cailloux	3.14	50.77	36	602	10	34452	1	3
890	FR28010	Harnes Serres	2.9	50.45	20	2500	10	32554	1	3
891	FR18040	Hirson	4.09	49.92	192	3431	35	31598	3	3
892	FR30016	Hotel Districal	6.18	48.69	210	1383	42	33639	1	2
893	FR21019	IFS Caen sud	-0.35	49.15	22	669	6	34389	3	3
894	FR31027	IRATY	-1.04	43.03	1400	2099	52	32913	5	4
895	FR02012	Istres	4.98	43.51	10	898	8	34158	4	3
896	FR07009	Jardin Lecoq	3.09	45.77	398	526	10	34528	3	3
897	FR30033	Jonville en Woevre	5.79	49.07	225	739	17	34308	3	3
898	FR34024	Joué lès Tours	0.65	47.34	85	544	2	34518	3	3
899	FR35012	LA NOUAILLE - MERA	2.06	45.81	810	1308	27	33729	5	4
900	FR23124	LA TARDIERE	-0.74	46.66	143	799	6	34259	4	4
901	FR14031	LA TOUR	4.08	48.3	105	994	3	34067	3	3
902	FR31021	LABASTIDE CEZERACQ	-0.54	43.38	125	819	13	34232	1	3
903	FR31008	LE TEMPLE	-0.94	44.87	43	1936	10	33118	3	3

	station ID	station name	lon.	lat.	alt., m	N mis.	N flag.	N valid	CL, 1CA	CL, 2CA
904	FR31030	LEOGNAN	-0.58	44.72	49	557	3	34504	3	3
905	FR23110	LEON BLUM	-2.25	47.26	25	234	3	34827	4	4
906	FR04049	LES ULIS	2.17	48.68	159	944	26	34094	3	3
907	FR35003	LIMOGES - Présidial	1.26	45.83	301	849	13	34202	3	3
908	FR09014	LIsle dEspagnac	0.2	45.66	55	640	27	34397	3	3
909	FR04098	LOGNES	2.64	48.84	80	622	12	34430	1	2
910	FR17013	LONS PERIPHERIE	5.57	46.68	300	910	8	34074	3	3
911	FR12042	LOURDES LAPACCA	-0.04	43.1	405	512	6	34546	3	3
912	FR33201	LOVERCHY	6.12	45.9	453	491	4	34569	1	2
913	FR20062	LYON Centre	4.85	45.76	160	955	12	33425	3	2
914	FR34025	La Bruyère	0.68	47.42	92	1139	9	33916	3	3
915	FR08617	La Calmette	4.27	43.93	75	1320	45	33699	4	3
916	FR09016	La Couronne	0.1	45.61	51	1084	36	33944	3	3
917	FR34012	La Source	1.93	47.84	106	739	12	34313	3	3
918	FR15031	Le Casset2	6.47	45	1750	1509	20	33535	5	4
919	FR32007	Le Creusot Molette	4.42	46.8	350	590	5	34469	3	3
920	FR05074	Le Havre Ec. Herriot	0.1	49.49	5	474	8	34582	3	4
921	FR07012	Le Puy Centre	3.88	45.04	644	534	11	34519	3	3
922	FR34032	Leblanc	2.4	47.08	109	423	7	34634	3	3
923	FR28002	Lens Service Tec	2.84	50.43	20	2876	18	32170	1	3
924	FR08714	Les Carmes	2.9	42.72	25	1062	26	33976	4	3
925	FR09015	Les Couronneries	0.36	46.59	119	851	16	34197	3	3
926	FR11033	Lesquin Centre	3.12	50.59	10	279	2	34783	1	3
927	FR21021	Lisieux	0.23	49.15	46	969	15	34080	3	3
928	FR26005	Local Espaces verts	5.07	47.31	255	738	17	34309	3	3
929	FR01001	Longlaville-Ecole	5.8	49.53	265	2381	3	32680	3	3
930	FR19032	Lorient B. Bissonnet	-3.39	47.74	50	1452	18	33594	4	4
931	FR19021	Lorient CTM	-3.38	47.75	25	711	14	34339	4	4
932	FR34042	Lucé	1.47	48.44	115	429	7	34628	3	3
933	FR04063	MANTES-LA-JOLIE	1.7	49	32	2110	15	32939	3	3
934	FR03043	MARSEILLE 5 AVENUES	5.4	43.31	64	791	5	34268	3	3
935	FR12021	MAZADES	1.44	43.62	139	970	14	34080	3	3
936	FR23123	MAZAGRAN	-0.77	48.07	54	400	8	34656	3	3
937	FR04069	MELUN	2.66	48.54	56	444	17	34603	1	2
938	FR13011	MONTANDON Baresans	6.83	47.3	746	992	6	34066	4	4
939	FR12046	MONTAUBAN	1.42	44.01	133	1671	12	33381	4	3
940	FR13002	MONTBELIARD Coteau J	6.79	47.5	343	835	35	34194	3	2
941	FR17023	MONTFAUCON	6.08	47.23	489	704	26	34334	4	4
942	FR04149	MONTGERON	2.46	48.71	68	361	17	34686	1	2
943	FR32006	Macon Paul Bert	4.84	46.32	190	635	15	34414	3	2
944	FR24018	Manosque04	5.79	43.84	371	2319	5	32740	4	3
945	FR11016	Marcq CTM	3.08	50.67	17	1611	6	33447	1	3
946	FR34017	Marigny-les-usages	2.01	47.96	127	587	8	34469	3	3
947	FR02004	Martigues P. Central	5.04	43.42	107	806	15	34243	4	3

	station ID	station name	lon.	lat.	alt., m	N mis.	N flag.	N valid	CL, 1CA	CL, 2CA
948	FR06007	Maubeuge Joyeuse	3.97	50.28	107	881	6	34177	3	3
949	FR25040	Mesnil Esnard	1.16	49.41	160	359	2	34703	3	3
950	FR01012	Metz-Borny	6.22	49.11	204	1816	8	33240	3	2
951	FR01011	Metz-Centre	6.18	49.12	192	737	8	34319	1	2
952	FR34018	Montargis	2.72	48	97	441	5	34618	3	3
953	FR32005	Montceau-les-Mines	4.37	46.67	280	411	15	34638	3	3
954	FR07004	Montferrand	3.11	45.8	340	375	5	34684	3	3
955	FR05079	Montivilliers	0.19	49.55	20	403	4	34657	3	3
956	FR07013	Montlucon Chateau	2.6	46.34	215	529	17	34518	3	3
957	FR07016	Montlucon Hippodrome	2.6	46.32	205	377	4	34683	3	3
958	FR16065	Mulhouse Est	7.34	47.72	330	256	5	34803	3	3
959	FR16066	Mulhouse Sud 2	7.31	47.74	250	805	17	34242	3	2
960	FR05084	NDGravenchon Pasteur	0.57	49.49	35	228	11	34825	3	3
961	FR04017	NEUILLY-SUR-SEINE	2.28	48.88	36	655	26	34383	1	2
962	FR24011	NICE OUEST BOTANIQUE	7.21	43.69	110	1089	4	33947	4	3
963	FR33202	NOVEL	6.14	45.92	461	1397	14	33653	3	2
964	FR30034	Nancy-Charles III	6.19	48.69	200	1201	43	33820	1	2
965	FR28020	Noeux S. Sports	2.66	50.48	20	2453	14	32597	3	3
966	FR18019	Nogent sur Oise	2.48	49.28	24	1635	36	33393	1	2
967	FR16017	Nord-Est Alsace	8.16	48.92	114	992	59	33965	3	2
968	FR10032	Outreau	1.58	50.69	15	2841	19	32204	4	4
969	FR34043	Oysonville	1.96	48.39	150	1448	11	33605	3	3
970	FR18008	P. Bert St Quentin	3.31	49.86	111	1515	53	33496	3	3
971	FR35007	PALAIS S/ V.- Garros	1.31	45.87	333	1160	23	33881	4	4
972	FR04037	PARIS 13eme	2.36	48.83	57	1554	16	33494	1	2
973	FR04004	PARIS 18eme	2.35	48.89	60	1166	17	33881	1	2
974	FR04055	PARIS 1er Les Halles	2.35	48.86	35	1155	30	32967	1	2
975	FR04160	PARIS 6eme	2.34	48.85	41	362	10	34692	1	2
976	FR33220	PASSY	6.71	45.92	594	543	12	34509	1	2
977	FR33101	PASTEUR	5.93	45.56	280	286	2	34776	1	2
978	FR12027	PAUL BERT TARBES	0.08	43.23	311	857	9	34198	3	3
979	FR03037	PENNE SUR HUVEAUNE	5.51	43.27	72	768	2	34294	3	2
980	FR31033	PERIGUEUX	0.73	45.19	142	1315	5	33744	3	3
981	FR12020	PEYRUSSE	0.18	43.63	175	1167	19	33878	4	4
982	FR03027	PLAN AUPS/STE BAUME	5.72	43.33	701	393	6	34665	5	4
983	FR17004	PLANOISE	5.97	47.22	271	846	23	34195	3	3
984	FR17018	PONTARLIER	6.36	46.92	871	990	22	32540	3	3
985	FR07022	Paray le Fresil	3.6	46.65	233	678	4	34382	3	3
986	FR25045	Phare d Ailly	0.96	49.92	80	409	9	34646	4	4
987	FR09009	Place du Marche	0.34	46.58	112	357	10	34697	1	3
988	FR22010	Porcelette(10)	6.65	49.16	210	1376	33	33247	3	3
989	FR34011	Prefecture	1.91	47.9	111	457	8	34599	3	3
990	FR08016	Prés Arènes	3.89	43.59	8	1010	26	34028	4	3
991	FR08018	Périurbaine Nord	3.8	43.69	80	478	8	34578	4	3

	station ID	station name	lon.	lat.	alt., m	N mis.	N flag.	N valid	CL, 1CA	CL, 2CA
992	FR08017	Périurbaine Sud	3.92	43.57	30	750	17	34297	4	3
993	FR19051	Quimper Ferry	-4.1	48	40	590	14	34364	3	4
994	FR14008	REVIN	4.59	49.92	395	540	8	34516	4	4
995	FR29423	ROANNE	4.07	46.04	259	1113	24	33927	3	3
996	FR27003	ROCHES DE CONDRIEU	4.77	45.45	152	2676	26	32362	3	2
997	FR27002	ROUSSILLON	4.81	45.37	157	2982	22	32060	1	2
998	FR07031	Rageade	3.28	45.1	1040	621	4	34439	5	4
999	FR30018	Remiremont	6.59	48.02	380	1064	41	33959	3	3
1000	FR19006	Rennes ENSP	-1.7	48.1	34	504	2	34558	3	3
1001	FR07032	Riom	3.12	45.89	340	325	7	34732	3	3
1002	FR02020	Rognac les Brets	5.22	43.51	45	1167	11	33886	4	3
1003	FR07001	Royat	3.05	45.76	520	290	5	34769	4	4
1004	FR18045	Roye	2.8	49.7	2	1662	11	33391	3	3
1005	FR04038	Rur S-O/Foret RAMB	1.88	48.58	152	1000	12	34052	3	3
1006	FR04048	Rurale Nord	2.34	49.1	140	560	8	34496	3	3
1007	FR29424	SAINT ETIENNE SUD	4.4	45.42	552	543	9	34512	3	3
1008	FR20048	SAINT EXUPERY	5.07	45.75	217	1016	18	34030	3	3
1009	FR23078	SAINT EXUPERY	-0.89	47.05	90	343	1	34720	3	3
1010	FR33111	SAINT JEAN	6.35	45.27	555	432	5	34627	3	2
1011	FR21040	SAINT LO EGLISE	-1.08	49.12	45	836	3	34225	3	4
1012	FR29426	SAINT-CHAMOND	4.52	45.48	366	446	18	34600	1	2
1013	FR31016	SAINT-CROUTS	-1.49	43.48	35	697	19	34348	3	3
1014	FR31031	SAINT-SULPICE	-0.38	44.91	16	836	7	34221	3	3
1015	FR12041	SICOVAL	1.57	43.46	170	939	14	34111	4	3
1016	FR35002	ST JUNIEN - Fontaine	0.9	45.89	206	1571	14	33479	3	3
1017	FR20004	ST JUST	4.82	45.76	250	1135	24	33905	3	2
1018	FR14021	ST MEMMIE	4.38	48.95	90	540	9	32211	1	2
1019	FR14032	ST PARRES AUX TERTRE	4.12	48.3	110	215	3	34846	3	3
1020	FR20036	ST PRIEST	4.91	45.7	195	1757	32	33275	3	2
1021	FR14033	STE SAVINE	4.05	48.3	110	573	7	34484	3	3
1022	FR16038	STG Est	7.78	48.57	139	885	13	34166	1	2
1023	FR16029	STG Nord	7.78	48.61	136	363	7	34694	1	2
1024	FR16001	STG Ouest	7.71	48.61	148	418	8	34638	3	2
1025	FR27005	Sablons	4.77	45.32	138	740	26	34298	3	2
1026	FR19061	Saint Brieuc Balzac	-2.75	48.52	80	813	10	34169	3	4
1027	FR18044	Saint Leu Amiens	2.3	49.9	24	868	11	34113	1	3
1028	FR11030	Salome Ecoles	2.84	50.53	10	883	9	34172	3	3
1029	FR02016	Salon de Provence	5.09	43.64	75	1146	30	33888	3	3
1030	FR18035	Salouel	2.24	49.87	29	904	17	34143	1	3
1031	FR10025	Sangatte	1.86	50.95	20	1036	16	34012	3	4
1032	FR02021	Sausset les Pins	5.12	43.33	7	1162	22	33880	4	3
1033	FR30028	Schlucht	7.01	48.05	1200	1013	15	34036	5	4
1034	FR01018	Scy-Chazelles	6.12	49.11	170	926	10	34128	3	2
1035	FR07029	Sembadel	3.69	45.27	1040	1204	7	33853	5	4

	station ID	station name	lon.	lat.	alt., m	N mis.	N flag.	N valid	CL, 1CA	CL, 2CA
1036	FR22014	Spicheren(14)	6.96	49.2	338	1992	31	33041	3	3
1037	FR09103	Square Pablo Casals	0.17	45.65	83	1851	38	33175	3	3
1038	FR08712	St Estève	2.84	42.72	50	717	20	34327	5	4
1039	FR34014	St Jean	1.97	47.92	100	442	12	34610	3	3
1040	FR15038	St Martin d'Heres	5.75	45.18	219	924	32	34108	1	2
1041	FR02023	St Remy de Provence	4.83	43.79	20	1422	16	33626	4	3
1042	FR05010	St Romain de Colbosc	0.36	49.53	117	366	10	34688	3	4
1043	FR30023	St-Nicolas	6.3	48.63	210	983	16	34065	1	2
1044	FR24017	StAuban04	6	44.09	110	1604	27	33433	4	3
1045	FR19081	StMalo Courtoisville	-1.99	48.65	10	864	2	34198	4	4
1046	FR26019	Station AUXERRE	3.57	48.8	250	1119	26	33919	3	3
1047	FR26007	Station BALZAC	5.05	47.34	251	1021	6	34037	3	2
1048	FR26010	Station DAIX	5	47.35	350	842	2	34220	4	3
1049	FR26012	Station MORVAN	4.09	47.27	620	3378	23	31663	4	4
1050	FR26017	Station NEVERS ISAT	3.17	47	200	1386	19	33659	3	3
1051	FR26016	Station SENS	3.28	48.19	250	733	8	34323	3	3
1052	FR26002	Station TARNIER	5.03	47.31	241	1113	28	33923	3	2
1053	FR02024	Ste Maries de la Mer	4.43	43.46	2	1087	12	33965	4	4
1054	FR31002	TALENCE	-0.59	44.8	20	722	10	34332	3	3
1055	FR17014	TAVAUX	5.4	47.04	192	2448	15	30873	3	2
1056	FR33260	THONON les Bains	6.48	46.37	425	288	3	34773	3	3
1057	FR14009	TINQUEUX	3.99	49.25	90	649	6	34409	3	3
1058	FR03063	TOULON ARSENAL	5.93	43.12	2	1220	7	33837	3	3
1059	FR04319	TREMBLAY-EN-FRANCE	2.58	48.96	65	1013	13	34038	1	2
1060	FR35006	TULLE - Hugo	1.76	45.26	236	694	7	34363	1	2
1061	FR01020	Thionville-Centre	6.16	49.36	154	1253	4	33807	1	2
1062	FR01021	Thionville-Garche	6.2	49.39	151	446	2	34616	3	3
1063	FR01019	Thionville-Piscine	6.16	49.37	156	837	7	34220	3	2
1064	FR30024	Tomblaine	6.22	48.69	217	986	29	34049	3	3
1065	FR05082	Touques	0.11	49.35	45	236	3	34825	4	4
1066	FR13008	VALDOIE Centre	6.84	47.67	372	542	16	32370	3	2
1067	FR09002	VAUGOIN	-1.19	46.16	13	1128	38	33898	4	4
1068	FR20046	VAULX EN VELIN	4.92	45.78	156	1538	53	33473	3	2
1069	FR13014	VESOUL Pres CAILLET	6.16	47.62	217	484	13	34567	3	2
1070	FR12025	VICTOR HUGO	0.07	43.23	305	338	10	34716	3	3
1071	FR20061	VILLEFRANCHE Village	4.72	45.99	204	864	21	34179	1	2
1072	FR04100	VILLEMOMBLE	2.51	48.88	85	628	11	34425	1	2
1073	FR04034	VITRY-SUR-SEINE	2.38	48.78	95	1483	17	33564	1	2
1074	FR36001	Valence Périurb. Sud	4.88	44.87	125	1008	17	34039	2	2
1075	FR36002	Valence Urb. Centre	4.89	44.93	125	848	25	34191	2	2
1076	FR07018	Vals pres le Puy	3.88	45.03	650	271	5	34788	3	3
1077	FR19031	Vannes Roscanvec	-2.76	47.66	30	904	6	34154	3	4
1078	FR27004	Vienne Centre	4.88	45.53	160	1890	40	33134	1	2
1079	FR34034	Vierzon	2.07	47.22	115	383	6	34675	3	3

	station ID	station name	lon.	lat.	alt., m	N mis.	N flag.	N valid	CL, 1CA	CL, 2CA
1080	FR34021	Ville aux Dames	0.76	47.38	49	387	5	34672	3	3
1081	FR02019	Vitrolles	5.24	43.46	110	2311	20	32397	4	3
1082	FR22017	Volmunster	7.38	49.13	349	2555	29	32480	3	3
1083	FR15044	Voreppe Volouise	5.64	45.28	191	557	25	34482	1	2
1084	FR16031	Vosges du Nord	7.32	48.86	340	432	4	34628	4	3
1085	FR04066	Zone rurale Sud	2.24	48.36	134	429	14	34621	3	3
1086	FR21035	Cherbourg doumer	-1.63	49.64	18	1927	5	33132	3	4
1087	FR09003	place de VERDUN	-1.15	46.16	10	1133	29	33902	3	4
1088	FR04142	Zone Rurale N-E -MONTGE-GOEL	2.75	49.03	162	914	6	34144	3	3
1089	FR04158	Zone Rurale N-O – FREMAINVILL	1.87	49.06	122	621	18	34425	3	3
1090	GB0031R	ASTON HILL	-3.33	52.5	370	2477	17	32570	4	4
1091	GB0681A	BARNSLEY GAWBER	-1.51	53.56	100	1514	21	33529	1	4
1092	GB0567A	BELFAST CENTRE	-5.93	54.6	10	2488	13	32563	1	4
1093	GB0032R	BOTTESFORD	-0.81	52.93	32	335	7	34722	3	4
1094	GB0033R	BUSH ESTATE	-3.21	55.86	180	574	17	34473	4	4
1095	GB0580A	CARDIFF CENTRE	-3.18	51.48	12	578	2	34484	1	4
1096	GB0673A	DERRY	-7.33	55	32	1798	3	33263	3	4
1097	GB0002R	ESKDALEMUIR	-3.21	55.32	269	1204	6	33854	4	4
1098	GB0051A	GIBRALTAR BLEAK HOUSE	-5.35	36.11	50	1587	16	33461	4	4
1099	GB0641A	GLASGOW CENTRE	-4.26	55.86	5	622	21	34421	1	4
1100	GB0034R	GLAZEBURY	-2.47	53.46	21	3550	16	31498	1	3
1101	GB0035R	GREAT DUN FELL	-2.45	54.68	847	4344	43	30677	4	4
1102	GB0036R	HARWELL	-1.33	51.57	137	1938	8	33118	3	4
1103	GB0037R	LADYBOWER	-1.75	53.4	420	1197	8	33859	4	4
1104	GB0643A	LEAMINGTON SPA	-1.53	52.29	175	864	20	34180	1	3
1105	GB0584A	LEEDS CENTRE	-1.55	53.8	78	818	14	34232	1	4
1106	GB0597A	LEICESTER CENTRE	-1.13	52.63	65	2617	9	32438	1	3
1107	GB0566A	LONDON BLOOMSBURY	-0.12	51.52	20	2108	8	32948	1	3
1108	GB0586A	LONDON ELTHAM	0.07	51.45	60	934	20	34110	1	3
1109	GB0638A	LONDON HARINGEY	-0.13	51.59	30	3944	8	31112	1	3
1110	GB0642A	LONDON HILLINGDON	-0.46	51.5	34	668	6	34390	1	3
1111	GB0682A	LONDON MARYLEBONE ROAD	-0.15	51.52	35	1349	16	33699	1	3
1112	GB0006R	LOUGH NAVAR	-7.9	54.44	130	1071	14	33979	3	4
1113	GB0613A	MANCHESTER PICCADILLY	-2.24	53.48	45	1832	41	33191	1	4
1114	GB0583A	MIDDLESBROUGH	-1.22	54.57	10	2448	24	32592	3	4
1115	GB0568A	NEWCASTLE CENTRE	-1.61	54.98	45	1692	17	33355	1	4
1116	GB0615A	SHEFFIELD CENTRE	-1.47	53.38	35	1088	14	33962	1	4
1117	GB0598A	SOUTHAMPTON CENTRE	-1.4	50.91	7	2101	10	32953	1	4
1118	GB0015R	STRATH VAICH	-4.78	57.73	266	2972	21	32071	5	4
1119	GB0013R	YARNER WOOD	-3.72	50.6	119	2173	12	32879	4	4
1120	GR0002A	ATHINAS	23.73	37.98	100	2003	10	33051	1	2

	station ID	station name	lon.	lat.	alt., m	N mis.	N flag.	N valid	CL, 1CA	CL, 2CA
1121	GR0039A	Agia PARASKEVI	23.82	38	290	850	15	34199	5	4
1122	GR0038A	Elefsina	23.54	38.05	20	2357	8	32699	4	3
1123	GR0027A	LIOSIA	23.7	38.08	165	2659	15	32390	2	3
1124	GR0035A	LYKOVRISI	23.78	38.07	210	1423	15	33626	4	2
1125	GR0022A	MAROUSI	23.79	38.03	170	1447	22	33595	4	2
1126	GR0031A	NEA SMIRNI	23.71	37.93	50	2201	14	32849	4	3
1127	GR0028A	PERISTERI	23.69	38.02	80	5262	28	29774	4	3
1128	GR0030A	PIREAUS-1	23.65	37.94	20	3340	41	31683	1	2
1129	GR0037A	THRAKOMAKEDONES	23.76	38.14	550	4126	34	30904	5	4
1130	GR0029A	VOTANIKOS	23.71	37.98	40	3712	12	31340	3	2
1131	HU0037A	Ajka	17.56	47.11	248	2307	13	32744	4	3
1132	HU0022A	Budapest Gilice	19.18	47.43	153	1086	16	33962	2	2
1133	HU0042A	Budapest Korakas	19.15	47.54	122	2138	27	32899	2	2
1134	HU0036A	Budapest Pesthidegkut	18.96	47.56	265	747	21	34296	3	2
1135	HU0023A	Debrecen Kalotaszeg	21.62	47.51	111	1371	31	33662	3	2
1136	HU0033A	Dunaujvaros	18.94	46.98	215	2251	6	32807	4	3
1137	HU0039A	Esztergom	18.75	47.79	122	430	12	34622	1	2
1138	HU0025A	Gyor Ifjusag	17.65	47.68	101	282	7	34775	3	2
1139	HU0002R	K-puszta	19.55	46.97	125	1153	13	33898	4	3
1140	HU0026A	Kazincbarcika	20.62	48.25	155	815	41	34208	2	2
1141	HU0029A	Pecs Boszorkany	18.21	46.08	200	5228	17	29819	4	3
1142	HU0038A	Sajoszentpeter	20.7	48.22	135	896	33	34135	2	2
1143	HU0040A	Sarrod	16.84	47.67	113	743	14	34307	3	3
1144	HU0035A	Sopron	16.58	47.69	241	470	35	34559	3	3
1145	HU0032A	Szazhalombatta	18.92	47.31	99	2354	8	32702	3	2
1146	HU0031A	Tatabanya Sagvari	18.42	47.56	199	232	6	34826	3	2
1147	HU0034A	Veszprem	17.9	47.09	274	1866	81	33117	3	2
1148	IE0111A	Emo Court	-7.2	53.11	20	1399	28	33637	3	4
1149	IE0091A	Glashaboy	-8.38	51.92	75	3928	8	31128	3	4
1150	IE0090A	Kilkitt	-6.88	54.07	170	1357	20	33687	4	4
1151	IE0031R	Mace Head	-9.9	53.33	8	292	2	34770	5	4
1152	IE0107A	Old Station Road	-8.47	51.9	10	2089	3	32972	1	4
1153	IE0028A	Rathmines	-6.28	53.35	25	562	43	34459	3	4
1154	IE0001R	Valentia	-10.23	51.93	10	1986	10	33068	5	4
1155	IT1288A	ABBADIA CERRETO 309801	9.59	45.31	64	2719	15	31754	2	1
1156	IT0545A	ACQUEDOTTO 1908964	15.27	37.08	62	2989	140	31623	5	4
1157	IT1830A	AL_6003_AL_VOLTA 100611	8.62	44.92	91	1640	14	33410	2	1
1158	IT0980A	AOSTA (MONT FLEURY) 200701	7.3	45.73	576	502	1	34561	2	2
1159	IT0983A	AOSTA (PIAZZA PLOUVES) 200703	7.32	45.74	581	555	11	34498	2	2
1160	IT1856A	AQ - Amiternum 1306601	13.38	42.36	710	3285	68	31663	3	3
1161	IT1681A	AR-CASA-STABBI 905108	11.9	43.66	650	3948	64	31052	4	4
1162	IT0950A	AR-VIA-ACROPOLI 905103	11.89	43.46	260	1661	19	33384	2	1

	station ID	station name	lon.	lat.	alt., m	N mis.	N flag.	N valid	CL, 1CA	CL, 2CA
1163	IT1203A	ARCONATE 301504	8.85	45.55	184	2136	28	32900	2	1
1164	IT1644A	LU-CARIGNANO 904611	10.45	43.87	120	3886	153	31025	4	3
1165	IT1523A	AT_5005_DACQUISTO 10501	8.21	44.91	149	1962	16	33086	2	1
1166	IT1065A	BASSANO DEL GRAPPA 502401	11.74	45.76	114	1019	38	34007	2	1
1167	IT1088A	BERGAMO - VIA GOISIS 301609	9.69	45.71	290	1299	14	33751	2	1
1168	IT1247A	BI_2012_BIELLA1 109602	8.06	45.56	405	1364	16	33684	2	1
1169	IT1246A	BI_2046_COSSATO 109603	8.19	45.57	273	1644	17	33403	2	1
1170	IT1245A	BI_2149_PONZONE 109604	8.19	45.65	485	848	17	34199	2	1
1171	IT1594A	BL - Città 502505	12.22	46.14	401	2625	39	32400	2	1
1172	IT0703A	BORGO VAL 402201	11.45	46.05	380	1727	8	33329	2	1
1173	IT0908A	BORMIO 301401	10.37	46.47	1225	1512	51	33501	4	4
1174	IT1848A	BOSCOCHIESANUOVA 502314	11.04	45.59	824	1864	60	32804	5	4
1175	IT0508A	BR1 Brunico 402102	11.94	46.8	830	1167	28	33869	1	1
1176	IT1465A	BRESCIA - VIA ZIZIOLA 301723	10.22	45.51	70	858	24	34182	2	1
1177	IT1835A	BUFALOTTA 1205884	12.53	41.95	41	1367	30	33667	1	1
1178	IT0507A	BX1 Bressanone 402101	11.65	46.72	564	550	42	34472	1	1
1179	IT0503A	BZ1 Via Amba Alagi 402104	11.34	46.5	266	842	65	34157	2	1
1180	IT1618A	Brindisi VIA TARANTO 1607178	17.95	40.64	10	3397	57	31610	5	4
1181	IT1876A	CALUSCO 301623	9.47	45.68	273	851	14	33695	2	1
1182	IT1152A	CARPI 2 803603	10.88	44.79	25	1147	10	33907	2	1
1183	IT1112A	PORCIA 609305	12.62	45.96	29	1964	59	33041	2	2
1184	IT0952A	CASTEL DI GUIDO 1205803	12.27	41.89	61	1153	23	33888	3	3
1185	IT1397A	CENAS8 2009204	9	39.23	9	2664	32	32368	4	3
1186	IT1233A	CENGIO - CAMPO DI CALCIO 700901	8.2	44.39	400	3160	34	31870	2	1
1187	IT1427A	CENNU2 2009102	9.33	40.32	511	3596	111	31357	4	4
1188	IT1377A	CENOR2 2009502	8.59	39.91	3	3105	30	31929	4	3
1189	IT1576A	CENPS7 2009222	8.39	39.2	25	3217	101	31746	5	4
1190	IT1380A	CENS11 2009018	8.57	40.72	220	3657	106	30581	3	4
1191	IT1243A	CENS12 2009015	8.55	40.71	192	4814	109	30141	4	4
1192	IT1270A	CENSA1 2009210	9.01	39.08	15	2094	49	32921	4	4
1193	IT1269A	CENSA2 2009211	9.02	39.07	22	2640	32	32392	3	4
1194	IT1373A	CENSA9 2009212	9.02	39.07	20	2576	26	32462	4	4
1195	IT1347A	CENSS3 2009001	8.36	40.81	15	3624	68	31348	4	3
1196	IT1662A	CHIAPPA - LA SPEZIA 701174	9.8	44.12	54	5941	11	29112	4	3
1197	IT0459A	CHIARAVALLE2 1104206	13.34	43.6	15	3812	61	31191	1	1
1198	IT1836A	CIPRO 1205883	12.45	41.91	31	908	51	34105	1	1
1199	IT1478A	CLAUT - LOCALITA PORTO PINEDO 609308	12.47	46.26	558	3087	115	31862	2	2
1200	IT1524A	CN_4003_ALBA 10407	8.03	44.7	164	1577	22	33465	2	1
1201	IT1529A	CN_4078_CUNEO 10402	7.54	44.38	551	1077	7	33980	4	3
1202	IT1519A	CN_4201_SALICETO 10401	8.17	44.41	390	877	8	34179	2	2

	station ID	station name	lon.	lat.	alt., m	N mis.	N flag.	N valid	CL, 1CA	CL, 2CA
1203	IT0888A	COLLEFERRO OBERDAN 1205806	13	41.73	219	851	17	34196	1	1
1204	IT0842A	CORTE DEI CORTESI 301903	10.01	45.28	61	2823	58	32183	2	1
1205	IT1180A	CORTONESE 1005401	12.37	43.1	290	2605	93	32366	2	2
1206	IT0839A	CREMA - VIA XI FEBBRAIO 301905	9.71	45.37	79	2150	38	32876	2	1
1207	IT1739A	CREMONA VIA FATEBENEFRATELLI 301915	10.05	45.14	45	1944	37	33083	2	1
1208	IT1796A	Civitanova IPPODROMO S. MARONE 1104305	13.67	43.34	110	5125	127	29740	5	4
1209	IT1385A	DARFO_2 301721	10.18	45.87	226	2910	34	32120	2	1
1210	IT1474A	DOBERDO DEL LAGO 603103	13.54	45.84	125	3271	25	31768	5	4
1211	IT0988A	DONNAS 200708	7.76	45.6	371	3064	7	31993	2	2
1212	IT0979A	ETROUBLES 200709	7.24	45.82	1330	653	9	34402	5	4
1213	IT1672A	FEBBIO 803515	10.43	44.3	1020	4780	49	30235	5	4
1214	IT1873A	FERNO 301218	8.75	45.62	215	385	11	34668	2	1
1215	IT0948A	FI-BOBOLI 904810	11.25	43.77	75	1840	7	33217	2	1
1216	IT1656A	FI-CALENZANO-GIOVANNI 904821	11.18	43.85	40	3008	39	32017	2	1
1217	IT0880A	FI-MONTELUPO-VIA-ASIA 904818	11.02	43.73	48	2141	15	32908	1	1
1218	IT1551A	FI-SCANDICCI-BUOZZI 904819	11.19	43.76	45	2752	26	32286	2	1
1219	IT0883A	FI-SETTIGNANO 904816	11.32	43.79	195	2969	29	32066	4	3
1220	IT0992A	FONTECHIARI 1206005	13.67	41.67	388	696	13	34355	4	3
1221	IT0741A	GAMBARA 301705	10.3	45.25	51	1445	34	33585	2	1
1222	IT1179A	GHERARDI 803805	11.96	44.84	-2	1763	13	33288	2	1
1223	IT0892A	GIARDINI MARGHERITA 803708	11.36	44.48	73	3132	135	30429	2	1
1224	IT1593A	GR-VIA-URSS 905301	11.12	42.78	10	2392	6	32666	4	3
1225	IT1587A	Gorizia 603105	13.62	45.94	50	2065	24	32975	2	2
1226	IT1679A	Grottaglie 1607389	17.42	40.54	200	4047	92	30901	5	4
1227	IT0977A	LA THUILE 200710	6.98	45.73	1640	1548	17	33499	5	4
1228	IT0499A	LA1 Laces 402106	10.86	46.62	641	1229	42	33745	3	2
1229	IT1176A	LARGO PERESTRELLO 1205875	12.54	41.89	37	733	25	34306	2	1
1230	IT1535A	LEGNAGO 502313	11.31	45.18	25	1634	30	33400	2	1
1231	IT0989A	LEONESSA 1205701	12.96	42.57	948	2661	23	32380	5	4
1232	IT1236A	LI-GABBRO 904904	10.41	43.5	240	2441	62	32561	5	4
1233	IT1239A	LI-VIA-GUIDO-ROSSA 904901	10.47	43.39	27	3064	122	31878	3	3
1234	IT1550A	LI-VILLA-MAUROGORDATO 904907	10.35	43.51	65	3030	44	31990	4	4
1235	IT0743A	LONATO 301706	10.48	45.46	188	1390	32	33642	2	1
1236	IT1696A	LS1 Laives 2102123	11.34	46.43	270	1263	40	33737	2	1
1237	IT0869A	LT-V.TASSO 1205906	12.91	41.46	21	1005	18	34041	3	3
1238	IT1089A	LU-PORCARI 904607	10.62	43.84	10	3397	58	31609	2	1
1239	IT1216A	LUCINICO 603101	13.57	45.93	84	1481	7	33576	2	2

	station ID	station name	lon.	lat.	alt., m	N mis.	N flag.	N valid	CL, 1CA	CL, 2CA
1240	IT1728A	Le Grazie 1005515	12.65	42.55	138	2435	18	32587	2	2
1241	IT1010A	MAGENTA VF 301525	8.89	45.47	138	1281	51	33732	2	1
1242	IT1393A	MANTOVA - LUNETTA 302011	10.82	45.16	25	1071	3	33942	2	1
1243	IT1480A	MARANELLO 803621	10.88	44.53	110	366	10	34688	2	1
1244	IT1188A	MARMIROLO - BOSCO FONTANA 302001	10.74	45.21	29	3752	11	31229	2	1
1245	IT1335A	ME1 Merano 402112	11.16	46.66	297	1680	36	33324	1	1
1246	IT1697A	ME2 Merano 2102122	11.17	46.65	292	415	23	34578	1	1
1247	IT0611A	MELILLI 1908962	15.13	37.18	300	3959	187	30606	5	4
1248	IT1017A	MILANO - P.CO LAMBRO 301530	9.25	45.5	122	2015	13	33036	2	1
1249	IT1812A	MOGGIO 309702	9.3	45.55	1192	1815	9	33240	5	4
1250	IT1538A	MONFALCONE 603104	13.53	45.81	5	2370	45	32649	4	3
1251	IT1418A	MONTANASO 309806	9.45	45.34	83	2005	47	32988	2	1
1252	IT1191A	MONTE GAZA 402203	10.96	46.08	1601	3547	39	31478	5	4
1253	IT0659A	MONTECCHIO MAGGIORE 502403	11.43	45.5	63	1038	129	33897	2	1
1254	IT1743A	MONZA via MACHIAVELLI 301569	9.27	45.58	162	2928	43	32093	2	1
1255	IT1190A	MORBEGNO2 301403	9.57	46.13	262	2191	52	32821	2	1
1256	IT1174A	MOTTA VISCONTI 301529	8.99	45.28	100	711	11	34342	2	1
1257	IT1795A	Macerata COLLEVARIO 1104304	13.43	43.28	225	2403	131	32530	4	3
1258	IT1598A	Manfredonia VIA DEI MANDORLI 1607176	15.91	41.63	20	4956	66	30042	4	4
1259	IT1680A	Martina Franca 1607388	17.33	40.7	400	3734	150	31180	3	4
1260	IT1602A	Molfetta ASM 1607275	16.56	41.2	10	3265	125	31674	4	3
1261	IT0553A	NARNI SCALO 1005505	12.52	42.54	94	2790	36	32214	3	3
1262	IT1518A	NO_3106_VERDI 10311	8.62	45.44	159	1125	9	33930	2	1
1263	IT1515A	NO_3118_PIEVEVERGONTE 10308	8.27	46.01	232	1855	21	33188	2	2
1264	IT1510A	NO_3156_VERBANIA 10303	8.57	45.93	197	2920	17	32127	2	1
1265	IT1259A	OSOPPO PROVI 603008	13.07	46.22	167	3831	48	31185	3	2
1266	IT1282A	OSPEDALE V. EMANUELE 1908508	14.23	37.07	40	3560	51	31453	4	4
1267	IT1182A	P.S.GIOVANNI 1005403	12.44	43.09	250	3212	110	31742	2	2
1268	IT0856A	PARCO ACQUASOLA - GENOVA 701026	8.94	44.41	45	2714	166	32184	4	4
1269	IT1030A	PARCO BUCCI 803911	11.87	44.28	35	852	10	34202	2	1
1270	IT1771A	PARCO FERRARI 803624	10.93	44.65	34	746	8	34310	2	1
1271	IT1048A	PARCO RESISTENZA 804009	12.05	44.22	29	4789	138	30113	2	1
1272	IT0912A	PAVIA - VIA FOLPERTI 301801	9.16	45.19	77	2699	17	32348	2	1
1273	IT1423A	PE - TEATRO D'ANNUNZIO 1306809	14.23	42.46	3	1134	53	33877	2	1
1274	IT1149A	PI-MONTECERBOLI-BIS 905007	10.88	43.25	353	2113	28	32923	5	4
1275	IT1110A	PI-PASSI 905008	10.4	43.74	5	2178	46	32840	2	1

	station ID	station name	lon.	lat.	alt., m	N mis.	N flag.	N valid	CL, 1CA	CL, 2CA
1276	IT1067A	PI-PONTEDERA 905009	10.64	43.66	15	551	2	34511	1	1
1277	IT1654A	PO-ROMA 904805	11.09	43.87	54	3926	134	31004	2	3
1278	IT1866A	PORTO MANTOVANO 302071	10.8	45.19	30	2878	7	32179	2	1
1279	IT0614A	PRIOLO 1908963	15.19	37.16	35	3808	112	30832	4	3
1280	IT1555A	PT-MONT-VIA-MERLINI 904703	10.77	43.88	21	3402	30	31632	2	1
1281	IT1553A	PT-MONTALE 904705	11.01	43.92	48	2724	39	32301	2	1
1282	IT0858A	QUARTO - GENOVA 701016	8.99	44.4	85	1349	22	33693	4	4
1283	IT1144A	QUILIANO 700909	8.41	44.29	16	2815	58	32191	4	4
1284	IT0505A	RE1 Renon 402109	11.43	46.59	1770	1339	53	33672	5	4
1285	IT0867A	RIETI 1 1205702	12.86	42.4	397	1856	30	33178	2	1
1286	IT0753A	RIVA GAR 402204	10.84	45.89	73	606	7	34451	2	1
1287	IT1214A	RO - Borsea 502902	11.79	45.04	3	1709	29	33326	2	1
1288	IT1215A	RO - Centro 502901	11.78	45.07	7	1801	90	33173	2	1
1289	IT0591A	ROVERETO LGP 402206	11.04	45.89	200	927	28	34109	2	1
1290	IT0940A	S. LAZZARO 803508	10.66	44.69	50	2299	73	32692	2	1
1291	IT1168A	S.GIOVANNI AL NATISONE 603010	13.39	45.97	62	2872	17	32175	4	3
1292	IT1170A	S.OSVALDO 603005	13.23	46.03	100	3530	40	31302	2	2
1293	IT0740A	SAREZZO - VIA MINELLI 301713	10.2	45.66	274	2995	61	32008	2	1
1294	IT1650A	SARONNO - SANTUARIO 301216	9.02	45.63	212	492	6	34566	2	1
1295	IT0620A	SCALA GRECA 1908910	15.27	37.1	60	3061	95	31596	3	4
1296	IT1865A	SCHIVENOGLIA 302072	11.07	45	16	3065	66	31933	2	1
1297	IT0506A	ST1 Vipiteno 402111	11.43	46.89	959	677	35	34352	1	2
1298	IT0957A	TENUTA DEL CAVALIERE 1205817	12.66	41.93	48	944	19	34101	1	1
1299	IT1801A	TERMOLI2 1407074	14.99	42	31	1561	6	33497	4	3
1300	IT0822A	TORVISCOSA 603014	13.28	45.82	3	3331	49	31684	2	2
1301	IT1121A	TO_1099_MANDRIA 100122	7.56	45.18	337	3357	21	31686	2	1
1302	IT1120A	TO_1171_ORBASSANO 100126	7.55	45.01	268	1256	7	33801	2	1
1303	IT0554A	TO_1272_TO_LINGOTTO 100106	7.65	45.02	220	2238	43	32783	2	1
1304	IT1125A	TO_1309_VINOVO 100132	7.64	44.96	232	1982	11	33071	2	1
1305	IT1037A	TRENTO PSC 402209	11.13	46.06	203	654	11	34399	1	1
1306	IT1466A	TREZZO D'ADDA 301555	9.51	45.62	187	2162	34	32868	2	1
1307	IT1636A	TUVIXEDDU 2009233	9.1	39.23	90	2023	9	33032	4	4
1308	IT1590A	TV - Via Lancieri di Novara 502608	12.24	45.67	15	2177	35	32852	2	1
1309	IT1061A	VALDAGNO 502406	11.31	45.64	240	1394	41	33629	2	1
1310	IT1734A	VALMADRERA 309701	9.35	45.84	237	491	3	34570	2	1
1311	IT1883A	VARALDO - SAVONA 700971	8.49	44.32	55	3243	57	31764	4	4
1312	IT0732A	VARESE - VIA VIDOLETTI 301213	8.8	45.84	382	254	4	34806	2	1
1313	IT1532A	VC_2016_BORGOSESIA 10203	8.28	45.71	345	1001	8	34055	2	1

	station ID	station name	lon.	lat.	alt., m	N mis.	N flag.	N valid	CL, 1CA	CL, 2CA
1314	IT0963A	VE - Parco Bissuola 502701	12.26	45.5	1	2307	50	32707	2	1
1315	IT0448A	VE - Sacca Fisola 502717	12.31	45.43	1	2025	198	32841	2	1
1316	IT1573A	VIA REDIPUGLIA 1104103	13.01	43.84	18	2437	176	31923	1	1
1317	IT0813A	VIA VENEZIA 1908513	14.26	37.07	15	2975	147	31942	3	3
1318	IT1735A	VOGHERA - VIA POZZONI 301813	9.01	45	90	3004	13	32047	2	1
1319	IT1343A	VR - Cason 502305	10.91	45.46	91	2267	65	32732	2	1
1320	IT1635A	piazza Sant'Avendrace 2009223	9.1	39.23	10	2288	10	32766	1	4
1321	LI0002A	Vaduz Austraße	9.52	47.12	450	651	44	34369	3	3
1322	LT00051	Aukstaitija	26	55.46	180	2430	57	32577	3	4
1323	LT00052	Dzukija N	24.29	54.09	130	3774	68	31222	3	3
1324	LT00041	Kaunas - Petrasiunai	23.99	54.9	31	1958	15	33091	3	3
1325	LT00043	Kedainiai	23.96	55.28	44	3161	27	31876	3	4
1326	LT00033	Klaipeda - Silutes	21.18	55.69	12	687	30	34347	1	4
1327	LT00023	Mazeikiai	22.33	56.31	67	4331	138	30595	3	4
1328	LT00054	Preila	21.03	55.38	5	1309	5	33750	4	4
1329	LT00022	Siauliai	23.31	55.94	122	2108	113	32843	1	4
1330	LT00002	Vilnius - Lazdynai	25.21	54.69	170	2809	114	32141	3	4
1331	LT00003	Vilnius - Zirmunai	25.29	54.72	119	788	23	34253	1	3
1332	LT00053	Zemaitija	21.89	56.01	155	1178	42	33844	3	4
1333	LU0105A	Beidweiler	6.31	49.72	319	1496	26	33542	3	3
1334	LU0102A	Esch/Alzette	5.98	49.51	292	1866	57	33141	1	2
1335	LU0101A	Luxembourg Bonnevoie	6.14	49.6	280	2327	76	32661	1	2
1336	LU0100A	Luxembourg Centre	6.13	49.61	280	2239	62	32763	1	3
1337	LU0103A	Mont St. Nicolas	6.18	49.94	515	2726	69	32269	4	4
1338	LV00010	Rucava	21.17	56.16	18	6781	21	28262	3	4
1339	MK0038A	Bitola 2 Strezevo	21.34	41.03	600	4770	164	30130	4	3
1340	MK0034A	Kocani	22.42	41.91	349	2866	6	32192	3	3
1341	MK0041A	Tetovo	20.97	42	84	3925	134	31005	4	3
1342	MT00005	Msida	14.49	35.9	2	4247	17	30800	3	4
1343	MT00004	Zejtun Station	14.54	35.85	56	2462	30	32572	5	4
1344	NL00520	Amsterdam-Florapark	4.92	52.39	4	5280	929	28855	1	3
1345	NL00544	Amsterdam-Prins Bernhardplein	4.92	52.35	0	2885	290	31889	1	3
1346	NL00918	Balk-Trophornsterweg	5.57	52.92	0	1656	342	33066	3	4
1347	NL00641	Breukelen-Snelweg	4.99	52.2	-1	3276	225	31563	1	3
1348	NL00620	Cabauw-Zijdeweg	4.93	51.97	-1	853	1658	32553	1	3
1349	NL00444	De Zilk-Vogelaarsdreef	4.51	52.3	4	3622	55	31387	3	3
1350	NL00404	Den Haag-Rebecquestraat	4.29	52.08	2	1861	253	32950	1	3
1351	NL00722	Eibergen-Lintveldseweg	6.61	52.09	19	609	338	34117	1	2
1352	NL00236	Eindhoven-Genovevalaan	5.47	51.47	17	1688	198	33178	1	3
1353	NL00938	Groningen-Nijensteinheerd	6.61	53.25	0	1447	95	33522	3	3
1354	NL00537	Haarlem-Amsterdamsevaart	4.65	52.38	1	1380	76	33608	1	3
1355	NL00137	Heerlen-Deken Nicolayestraat	5.98	50.89	115	2366	108	32590	1	3
1356	NL00807	Hellendoorn-Luttenbergerweg	6.4	52.39	7	631	708	33725	1	3
1357	NL00235	Huijbergen-Vennekenstraat	4.36	51.44	18	3605	429	31030	1	2

	station ID	station name	lon.	lat.	alt., m	N mis.	N flag.	N valid	CL, 1CA	CL, 2CA
1358	NL00934	Kollumerwaard-Hooge Zuidwal	6.28	53.33	1	1077	98	33889	3	3
1359	NL00318	Philippine-Stelleweg	3.75	51.3	5	653	460	33951	1	3
1360	NL00107	Posterholt-Vlodropperweg	6.04	51.12	32	1058	459	33547	1	2
1361	NL00418	Rotterdam-Schiedamsevest	4.48	51.92	3	3091	1568	30405	1	3
1362	NL00929	Valthermond-Noorderdiep	6.93	52.88	10	1036	470	33558	1	3
1363	NL00433	Vlaardingen-Floreslaan	4.33	51.91	-1	1244	1896	31924	1	2
1364	NL00131	Vredepeel-Vredeweg	5.85	51.54	28	1729	1220	32115	1	2
1365	NL00738	Wekerom-Riemterdijk	5.71	52.11	18	537	557	33970	1	2
1366	NL00437	Westmaas-Groeneweg	4.45	51.79	0	1292	114	33658	1	3
1367	NL00538	Wieringerwerf-Medemblikkerweg	5.05	52.8	-4	734	57	34273	3	3
1368	NL00133	Wijnandsrade-Opfergeltstraat	5.88	50.9	96	1255	254	33555	1	3
1369	NL00633	Zegveld-Oude Meije	4.84	52.14	-2	962	146	33956	1	3
1370	NL00301	Zierikzee-Lange Slikweg	3.92	51.64	-1	3121	138	31805	3	3
1371	NO0081A	Bærum	9.64	59.95	80	1838	86	33140	1	3
1372	NO0039R	Kårvatn	8.88	62.78	210	340	22	34702	3	4
1373	NO0043R	Prestebakke	11.53	59	160	330	9	34725	4	4
1374	NO0052R	Sandve	5.2	59.2	40	1110	21	33933	4	4
1375	NO0015R	Tustervatn	13.92	65.83	439	159	6	34899	5	4
1376	PL0028A	DsCzer02	15.31	50.91	645	1156	16	33892	5	4
1377	PL0189A	DsJgCiepA	15.68	50.86	341	1088	27	33949	3	2
1378	PL0058A	DsSnie04	15.56	50.78	1490	3302	44	31718	5	4
1379	PL0003R	DsSniezka	15.74	50.74	1603	1483	1	33580	5	4
1380	PL0192A	DsWalbWysA	16.27	50.77	436	2754	24	32286	3	3
1381	PL0194A	DsWrocKorzA	17.03	51.13	121	1634	47	33383	1	2
1382	PL0064A	KpBydgWarszawska	18	53.13	40	3204	10	31850	1	2
1383	PL0002R	LbJarczew	21.97	51.81	180	850	21	34193	3	3
1384	PL0094A	LdGajewWIOSAGajew	19.23	52.14	177	720	20	34324	3	3
1385	PL0096A	LdLodzWIOSACzernik	19.53	51.76	235	62	5	34997	3	3
1386	PL0105A	LdParzniWIOSAParznie	19.52	51.29	166	1587	43	33434	3	3
1387	PL0209A	LuGorzowWIOS_AUT	15.23	52.74	22	1707	245	33112	1	3
1388	PL0211A	LuSmobytWIOS_AUT	15.21	52.17	77	2369	166	32529	3	3
1389	PL0213A	LuZgoraWIOS_AUT	15.52	51.94	150	1752	115	33197	3	3
1390	PL0121A	MpSzymbaWIOS0507	21.12	49.63	327	3207	74	31783	3	3
1391	PL0014A	MzBelskIGPAN	20.79	51.84	180	581	22	34461	3	3
1392	PL0128A	MzGranicaKPN	20.45	52.29	81	2095	23	32946	3	3
1393	PL0129A	MzLegionZegIMGW	20.96	52.41	95	1013	51	34000	3	3
1394	PL0138A	MzRadomTochter	21.15	51.4	173	633	34	34397	1	3
1395	PL0139A	MzTluszczJKiel	21.43	52.43	108	849	48	34167	3	3
1396	PL0044A	MzWarPodIMGW	20.96	52.28	98	2800	3	32261	1	2
1397	PL0010A	MzWarszKrucza	21.02	52.22	112	1615	36	33413	1	2
1398	PL0150A	PdBorsuWiejska	23.64	53.22	180	4895	42	30127	3	3
1399	PL0171A	Pm.63.wDSAa	17.05	54.46	25	3262	100	31702	3	3
1400	PL0048A	Pm.a04a	18.49	54.56	70	634	11	34419	3	4
1401	PL0052A	Pm.a08a	18.62	54.38	40	723	4	34337	1	3

	station ID	station name	lon.	lat.	alt., m	N mis.	N flag.	N valid	CL, 1CA	CL, 2CA
1402	PL0004R	Pm08LEBAiEMEPa	17.53	54.75	4	111	0	34953	4	4
1403	PL0234A	SlBielbBiel_kossa	19.03	49.81	365	2807	189	32068	3	3
1404	PL0184A	SlCzestCzes_baczy	19.13	50.84	265	3117	182	31765	1	2
1405	PL0237A	SlDabroDabr_1000L	19.23	50.33	293	2345	175	32544	1	2
1406	PL0240A	SlTychyTych_tolst	18.99	50.1	252	4352	203	30509	1	2
1407	PL0241A	SlWodziWodz_galcz	18.46	50.01	271	1908	159	32997	1	2
1408	PL0243A	SlZlotyJano_lesni	19.46	50.71	291	2507	180	32377	4	3
1409	PL0175A	WmOlsztyWIOS_Puszkin	20.49	53.79	120	4756	80	30228	3	3
1410	PL0005R	WmPuszcz_IOS_Borecka	22.04	54.13	157	2779	6	32279	4	4
1411	PL0245A	WpWKP002	16.88	52.42	84	1271	39	33754	1	2
1412	PL0246A	WpWKP003	16.3	51.89	94	3329	58	31677	3	2
1413	PL0247A	WpWKP004	17.77	52.5	122	942	36	34086	3	3
1414	PL0182A	ZpGryfWiduchowa003	14.38	53.12	15	1083	96	33885	4	4
1415	PL0248A	ZpSzczecin001	14.66	53.38	17	1588	85	33391	3	3
1416	PT03082	Alfragide/Amadora	-9.21	38.74	109	405	12	34647	3	3
1417	PT03098	Alto do Seixalinho	-9.06	38.65	9	951	8	31729	3	4
1418	PT01028	Antas	-8.59	41.16	146	864	16	34184	1	3
1419	PT03093	Arcos	-8.89	38.53	2	343	9	34712	4	4
1420	PT01022	Baguim	-8.55	41.19	93	740	4	34320	1	3
1421	PT03070	Beato	-9.11	38.73	56	937	9	34118	3	3
1422	PT01045	Calendário	-8.53	41.4	120	2402	6	32584	1	3
1423	PT03092	Camarinha	-9.05	38.45	15	825	14	34225	4	4
1424	PT01044	Paços de Ferreira	-8.38	41.28	300	3815	6	31243	3	3
1425	PT03096	Chamusca	-8.28	39.21	43	857	9	34198	5	4
1426	PT01021	Custóias	-8.65	41.2	100	931	13	34120	3	3
1427	PT03072	Entrecampos	-9.15	38.75	86	1096	7	33961	3	3
1428	PT01023	Ermesinde	-8.55	41.21	140	707	16	34341	3	3
1429	PT02019	Ervedeira	-8.67	40.59	32	448	12	34604	4	3
1430	PT03095	Escavadeira II	-9.07	38.65	30	1830	45	33189	4	4
1431	PT02021	Fornelo do Monte	-8.1	40.64	741	2236	38	32790	5	4
1432	PT02020	Fundão	-7.18	40.14	473	848	5	34211	4	3
1433	PT01042	Horto	-8.46	41.57	51	2224	2	32838	1	2
1434	PT02016	Instituto Geofísico de Coimbra	-8.24	40.12	147	145	3	34916	3	3
1435	PT01048	Lamas de Olo	-7.8	41.37	1086	4614	72	30330	5	4
1436	PT03083	Laranjeiro	-9.16	38.66	20	2545	16	32455	4	4
1437	PT03085	Loures	-9.17	38.83	100	2845	37	32182	4	3
1438	PT03089	Mem Martins	-9.21	38.48	173	1226	28	33810	4	4
1439	PT04001	Monte Chãos	-8.83	37.97	103	2558	4	32502	4	4
1440	PT03097	Odivelas	-9.18	38.8	124	535	12	34253	4	4
1441	PT03071	Olivais	-9.11	38.77	34	2014	12	33014	3	3
1442	PT03063	Paio Pires aut.	-9.08	38.63	3	784	11	34269	3	3
1443	PT01025	Perafita	-8.42	41.14	25	537	12	34515	3	3
1444	PT03091	Quinta do Marquês	-9.19	38.42	48	354	11	34699	4	4
1445	PT03084	Reboleira	-9.23	38.75	30	435	18	34611	4	4

	station ID	station name	lon.	lat.	alt., m	N mis.	N flag.	N valid	CL, 1CA	CL, 2CA
1446	PT03087	Restelo	-9.21	38.71	20	467	14	34583	4	4
1447	PT04003	Sonega aut.	-8.72	37.87	195	879	17	34168	3	4
1448	PT04006	Terena	-7.4	38.61	187	1475	9	33532	3	4
1449	PT01024	Vermoim	-8.62	41.24	90	254	5	34781	1	3
1450	PT01031	Vila Nova da Telha	-8.66	41.26	88	1267	8	33789	3	3
1451	PT02018	Alhavo	-8.4	40.35	32	188	9	34867	3	3
1452	RO0066A	B2 Titan	26.18	44.41	30	3876	45	31143	1	2
1453	RO0069A	B5 Drumul Taberei	26.05	44.41	30	5286	59	29719	1	2
1454	RO0071A	B7 Magurele	26.03	44.35	30	4171	53	30840	1	3
1455	RO0081A	ROMANIA DJ-4	23.73	44.39	98	5362	252	29450	1	2
1456	RO0082A	ROMANIA DJ-5	23.72	44.34	128	3271	160	31633	3	3
1457	RO0086A	ROMANIA IS-4	27.55	47.2	165	5047	202	29815	4	4
1458	SE0012R	Aspvreten	17.38	58.8	25	1526	18	33520	4	4
1459	SE0026A	Borås	12.94	57.72	170	2268	145	32651	3	4
1460	SE0005R	Bredkälen	15.34	63.85	380	595	7	34462	4	4
1461	SE0013R	Esrange	21.07	67.88	524	407	3	34654	5	4
1462	SE0004A	Femman	11.97	57.71	30	344	1	34719	3	4
1463	SE0039R	Grimsö	15.47	59.73	132	266	2	34796	3	4
1464	SE0054A	Lund	13.2	55.7	20	2548	56	32460	4	4
1465	SE0066A	Norr Malma	18.63	59.83	20	198	8	34858	3	4
1466	SE0032R	Norra Kvill	15.56	57.81	263	672	13	34379	4	4
1467	SE0001A	Rådhuset	13	55.61	25	475	14	34575	3	4
1468	SE0014R	Råö	11.91	57.39	10	151	3	34910	4	4
1469	SE0022A	Södermalm	18.06	59.32	20	1262	6	33796	3	4
1470	SE0011R	Vavihill	13.15	56.03	163	845	12	34207	4	4
1471	SE0035R	Vindeln	19.77	64.25	271	626	16	34422	3	4
1472	SI0001A	Celje	15.27	46.24	240	2407	242	32415	1	2
1473	SI0037A	Hrastnik	15.09	46.14	290	2603	170	32291	3	2
1474	SI0008R	Iskrba	14.86	45.56	540	1870	257	32193	3	2
1475	SI0038A	Koper	13.72	45.54	56	2088	222	32754	4	3
1476	SI0032R	Krvavec	14.54	46.3	1740	2739	278	32047	5	4
1477	SI0003A	Ljubljana Bezigrad	14.52	46.07	299	2263	260	32541	2	1
1478	SI0002A	Maribor	15.66	46.56	270	2078	336	32650	1	2
1479	SI0033A	Murska Sobota-Rakican	16.2	46.65	188	2338	161	32565	3	2
1480	SI0034A	Nova Gorica	13.66	45.96	113	2695	191	32178	2	2
1481	SI0036A	Zagorje	15	46.13	240	2308	414	32342	1	2
1482	SK0048A	Bratislava - Jeséniova	17.12	48.17	287	223	11	34830	4	3
1483	SK0001A	Bratislava - Mamateyova	17.13	48.13	138	899	45	33688	3	2
1484	SK0002R	Chopok - EMEP/O3	19.59	48.94	2008	484	18	34562	5	4
1485	SK0041A	Ganovce	20.25	49.07	694	194	4	34866	4	4
1486	SK0037A	Humenné - Nám. slobody	21.91	48.93	160	640	14	33834	3	3
1487	SK0025A	Jelsava - Jesenského	20.24	48.63	289	716	9	34099	3	2
1488	SK0042A	Kojsovska Hola	20.99	48.78	1244	1481	12	33571	5	4
1489	SK0006R	Starina - Vodná nádr. EMEP/O3	22.26	49.04	345	882	13	34169	4	3

	station ID	station name	lon.	lat.	alt., m	N mis.	N flag.	N valid	CL, 1CA	CL, 2CA
1490	SK0004R	Stará Lesná - AÚ SAV EMEP/O3	20.29	49.15	808	136	11	34917	4	4
1491	SK0007R	Topolniky - Aszód/EMEP	17.86	47.96	113	474	31	34559	4	3
1492	SK0020A	Zilina - Obezná	18.77	49.21	356	235	3	34826	3	2

List of figures

List of tables

Abbreviations

abs	absolute
alt.	altitude
CA	cluster analysis
CL	cluster
CI	confidence interval
CTM	Chemistry-Transport Model
EMEP	European Monitoring and Evaluation Program database
EEA	European Environmental Agency
EMD	Earth Mover's Distance
GAW	Global Atmosphere Watch program
lon.	longitude
lat.	latitude
MOZART	Model for Ozone and Related Tracers
MACC	Monitoring Atmospheric Composition and Climate project
nmol mol^{-1}	nmole gas per mole of air
NMVOC	non-methane volatile organic compounds
norm	normalized
PAES	Pollution Atmosphérique à Echelle Synoptique
ppb	parts per billion
PR	property
STE	stratosphere-troposphere exchange
SSD	sum of squared distances
UBA	Umwelt Bundesamt
WDCGG	World Data Centre for Greenhouse Gases

Acknowledgements

I would like to thank my direct supervisor Martin Schultz for giving me the opportunity to start this work. This was jointly decided with Director of IEK-8, Prof. Andreas Wahner, so I am grateful to him as well for accepting me here on PhD position.

For the completion of my thesis I am thankful first of all to Martin Schultz, for his assistance nearly always when I needed. He had the initial scientific idea, which then became a topic of my work and developed into this thesis. During all the time I have had many useful discussions with Martin, which motivated me to proceed. I am thankful for his significant help in writing part as well.

I am very grateful to my supervisor from Bonn University, Prof.Andreas Hense, for his essential support and many good advices for statistical part of this work, for suggestion of k-means as a method for classification, and some other special methods like EMD and bootstrapping for data analysis, for his help in data interpretation and many useful comments.

Further I would like to thank also the members of our "Global modelling" group of IEK-8 for the nice atmosphere around and positive attitude. I am especially thankful to Snehal Waychal for creation of databases on the local server and for conversion of Martin's data filtering code into Python programming language. Besides, I am appreciative to Olaf Stein for his comments and corrections, and Sabine Schroeder for preparing the MACC data set.

Separate thanks to the European Topic Centre on Air Pollution and Climate Change and Mitigation (ETC/ACM) on behalf of the European Environment Agency for managing Airbase. Many thanks to MACC-II project team for designing and operating the MACC forecasting system and running the reanalysis and to EU for funding MACC-II under the grant no. 283576. I thank all data centers and networks (Airbase, EMEP, UBA, WDCGG, PAES), which made the data available. The Helmholtz REKLIM initiative is acknowledged for funding and for good possibility to take part in the conferences, where I could present and discuss my results with scientific public.

This thesis is primarily done on the Python programming language. Hence, I am thankful to creators of this project and related libraries, which made my work easier.

At last, I have special gratitude to my close friends Rena and David, who were able to understand me and support in difficult situations.

Band / Volume 251
Long Term Aerosol Composition Measurements at the CESAR Tower at Cabauw, NL
P. Schlag (2015), iii, 228 pp
ISBN: 978-3-95806-037-1

Band / Volume 252
Modellbasierte Spezifikationsmethodik zur effizienten Systementwicklung von Brennstoffzellenantrieben
R. Biurrun Sotelo (2015), 255 pp
ISBN: 978-3-95806-038-8

Band / Volume 253
Three-dimensional ray-tracing simulations of convective gravity waves
S. Kalisch (2015), iii, 183 pp
ISBN: 978-3-95806-040-1

Band / Volume 254
First-Principles Study on Pyrites and Marcasites for Photovoltaic Application
T. Schena (2015), 206 pp
ISBN: 978-3-95806-041-8

Band / Volume 255
Glass-Ceramic Sealant Reinforcement for High-Temperature Applications
B. Cela Greven (2015), xi, 119 pp
ISBN: 978-3-95806-042-5

Band / Volume 256
Entwicklung planarer $Ba_{0,5}Sr_{0,5}Co_{0,8}Fe_{0,2}O_{3-\delta}$-Membranmodule zur Sauerstoffabtrennung und Analyse ihres Transportverhaltens
P. Niehoff (2015), VIII, 134 pp
ISBN: 978-3-95806-044-9

Band / Volume 257
Extension of the Reactor Dynamics Code MGT-3D for Pebble-bed and Block-type High-Temperature-Reactors
D. Shi (2015), x, 162 pp
ISBN: 978-3-95806-045-6

Band / Volume 258
Failure Analysis of Thin Film Solar Modules using Lock-in Thermography
M. Siegloch (2015), XIII, 131 pp
ISBN: 978-3-95806-047-0

Band / Volume 259
Relation between growth rate, material quality, and device grade condition for intrinsic microcrystalline silicon:
From layer investigation to the application to thin-film tandem solar cells
S. Michard (2015), vi, 184 pp
ISBN: 978-3-95806-048-7

Band / Volume 260
Quantitative analysis of spatially resolved electroluminescence of Cu(In,Ga)Se_2 and a-Si:H thin-film solar cells and modules
T. Tran (2015), iii, 161 pp
ISBN: 978-3-95806-050-0

Band / Volume 261
Influence of the surface composition and morphology on the reflectivity of diagnostic mirrors in a fusion reactor
M. Matveeva (2015), 158 pp
ISBN: 978-3-95806-051-7

Band / Volume 262
Very High Cycle Fatigue Behavior of Riblet Structured High Strength Aluminum Alloy Thin Sheets
S. Stille (2015), XII, 123 pp
ISBN: 978-3-95806-054-8

Band / Volume 263
The role of soil heterogeneity on field scale evapotranspiration: 3D integrative modelling and upscaling of root water uptake
K. Huber (2015), xii, 128 pp
ISBN: 978-3-95806-057-9

Band / Volume 264
Strontium-Diffusion in Cer-Gadolinium-Oxid als Degradationsmechanismus der Festoxid-Brennstoffzelle
T. Mandt (2015), iii, 160 pp
ISBN: 978-3-95806-058-6

Band / Volume 265
Cluster analysis of European surface ozone observations for evaluation of MACC reanalysis data
O. Lyapina (2015), 187 pp
ISBN: 978-3-95806-060-9

Energie & Umwelt /
Energy & Environment
Band / Volume 265
ISBN 978-3-95806-060-9